Investigating Cerebrovascular Health and Functional Plasticity using Quantitative FMRI

By

Catherine Foster

A Thesis

Submitted to the School of Graduate Studies

in Partial Fulfillment of the Requirements

for the Degree

Doctorate of Philosophy

Cardiff University

Doctor of Philosophy (2017)

(Psychology)

Cardiff University,
Cardiff, Wales

Title: Investigating cerebrovascular health and functional plasticity using quantitative fMRI

Author: Catherine Foster

Supervisors: Prof. Richard G. Wise, Dr. Valentina Tomassini

Number of pages: 292

Declaration Form

The following declaration is required when submitting your PhD thesis under the University's regulations.

Declaration

This work has not previously been accepted in substance for any degree and is not concurrently submitted in candidature for any degree.

. . . .

Candidate Date

Statement 1

This thesis is being submitted in partial fulfillment of the requirements for the degree of PhD.

. . . .

Candidate Date

Statement 2

This thesis is the result of my own independent work/investigation, except where otherwise stated. Other sources are acknowledged by explicit references.

. . . .

Candidate Date

Statement 3

I hereby give consent for my thesis, if accepted, to be available for photocopying and for inter-library loan, and for the title and summary to be made available to outside organisations.

. . . .

Candidate Date

Statement 4: Previously approved bar on access

I hereby give consent for my thesis, if accepted, to be available for photocopying and for inter-library loans after expiry of a bar on access previously approved by the Graduate Development Committee.

. . . .

Candidate Date

Abbreviations for Frequently Used Terms	
AF	Aerobic fitness
ASL	Arterial spin labelling
BOLD	Blood oxygen-level dependent
BP	Blood pressure
CASL	Continuous arterial spin labelling
CBF	Cerebral blood flow
CBV	Cerebral blood volume
CSF	Cerebrospinal fluid
$CMRO_2$	Cerebral metabolic rate of oxygen consumption
CNS	Central nervous system
CVR	Cerebrovascular reactivity
EDSS	Expanded Disease Status Scale
EPI	Echo planar imaging
FSL	FMRIB's software library
FSPGR	Fast spoiled gradient echo recalled
FMRI	Functional magnetic resonance imaging
GM	Grey matter
Hb	Haemoglobin
HR	Heart rate
MNI	Montreal Neurological Institute
MS	Multiple Sclerosis
MRI	Magnetic resonance imaging
MTI	Multiple inversion time
OEF	Oxygen extraction fraction
PASL	Pulsed arterial spin labelling
PCASL	Pulsed continuous arterial spin labelling
PICORE	Proximal control for off resonance effects

Abbreviations for Frequently Used Terms	
PO_2	Oxygen pressure
PtO_2	Tissue oxygen pressure
QUIPSS II	Quantitative imaging of perfusion using a Single Subtraction II
SNR	Signal to noise ratio
SRT	Serial reaction time
TE	Echo time
TI	Inversion time
TR	Repetition time
VBM	Voxel based morphometry
$\dot{V}O_{2max}$	Maximal volume of oxygen uptake
$\dot{V}O_{2peak}$	Peak oxygen uptake volume
WM	White matter

Acknowledgements

I would like to acknowledge several people who contributed to the work in this thesis. Firstly, a huge thanks to my supervisor Richard Wise who guided the conception, design and analysis of each chapter and for being extremely supportive throughout my PhD and post-PhD grant applications and career planning. I would also like to thank Kevin Murphy for assisting with the analysis using Afni in Chapter 3 but also for the valuable advice on many things throughout my time in CUBRIC.

Thanks also to Jessica Steventon who made it possible to conduct the two exercise studies and collect the data in Chapter 7. These studies involved many hours of set-up and data collection which would not have been possible without Jessica's presence and guidance. Thanks to Hannah Chandler and Rachael Stickland who assisted data collection for Chapter 8 and, collected almost all the data in Chapter 9 as well as processing the patient data due to unforeseeable delays with study approval. Many thanks also to my second supervisor Valentina Tomassini for informing the design of the MS study and assisting with patient recruitment.

Data collected in the new centre (Chapters 5, 8 and 9) would not have been possible without the MR sequences developed by Michael Germuska, who also developed the MR processing and analysis pipeline for these chapters.

I would like to thank Esther Warnert for developing the analysis pipeline used in Chapter 4, and Joe Whittaker for helping to improving my code over the years. Also thanks to Ian Driver for his valuable input on data acquisition and analysis.

A huge thank you also to Ilona Lipp for her support with analysis of the SRT task data, and all things Matlab related.

Table of Contents

Thesis Summary

A healthy cerebrovasculature is necessary to maintain optimal levels of blood flow and oxygen metabolism required for overall brain health. Cerebrovascular health also promotes functional plasticity which facilitates lifelong adaptation with experience and recovery following injury. In diseases such as Multiple Sclerosis (MS), there is known vascular and metabolic dysfunction, however, patients retain variable levels of functional plasticity which aids recovery following acute bouts of inflammation. Physical exercise interventions, aimed at improving cerebral blood flow and oxygen metabolism, present a potential avenue for improving patient outcomes and slowing the progression of disability. However, there is a lack of mechanistic understanding of i) brain energetic processes underlying plasticity and ii) how aerobic fitness (AF), which is linked to increased brain plasticity, benefits brain vascular and metabolic function. The work presented in this thesis uses arterial spin labelling (ASL) functional magnetic resonance imaging (fMRI) to quantitatively characterise the vascular and metabolic processes associated with functional brain plasticity, and the effects of AF on the brain's functional capacity in healthy adults.

This thesis begins with an overview of the neurobiological processes of interest and fMRI techniques that can quantify these processes. Next, a comparison of common ASL acquisition and analysis procedures is made to establish the most appropriate methods for subsequent experimental work. Chapters 4 and 5 investigate the effects of AF on cerebrovascular function in healthy adults. Chapter 6 then gives an overview of existing functional motor plasticity work, before Chapters 7 and 8 which quantify vascular and metabolic adaptations following motor training in the healthy brain. Chapter 9, presents preliminary work in an MS cohort, applying methods from previous chapters to quantify vascular and metabolic differences between patients and controls. The general discussion in Chapter 10 summarises the main findings and contributions of this work and key areas for future research are outlined.

Research Background and Rationale

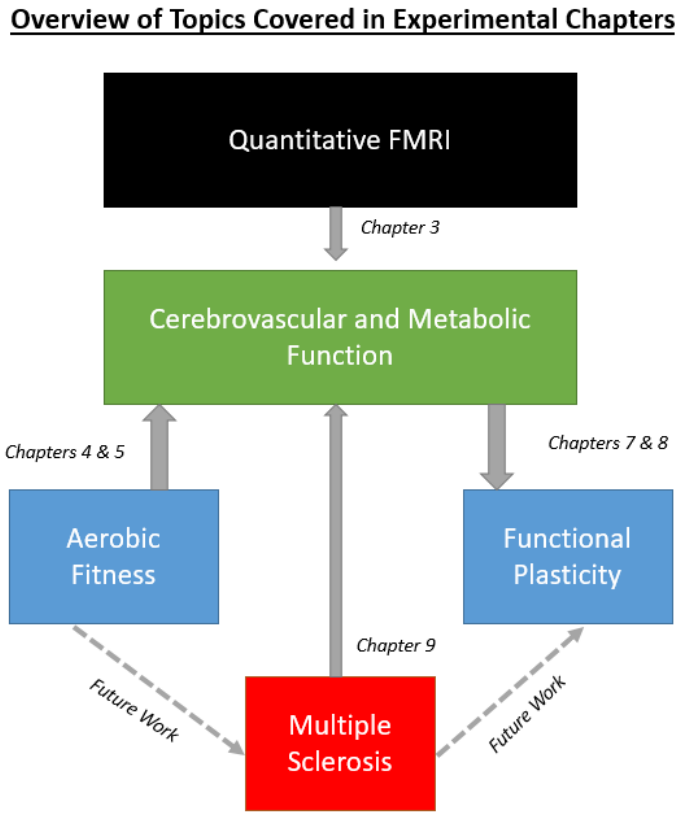

Figure 1 Overview of topics covered in each experimental chapter. For example, chapter 3 evaluates quantitative fMRI methods of measuring cerebrovascular function and chapters 4 & 5 investigate the effects of aerobic fitness on vascular and metabolic function. Additional future studies are needed to extend the current body of work, such as using aerobic fitness as a method to improve cerebrovascular health in Multiple Sclerosis.

The overall objectives of this thesis were to;

- Characterise the effect of aerobic fitness on cerebrovascular and metabolic function in healthy young adults using quantitative fMRI
- Identify cerebrovascular and metabolic mechanisms of functional motor plasticity in the healthy brain
- Map differences in blood flow and oxygen metabolism in people with MS and healthy controls

The above objectives were chosen to address gaps in the literature regarding lifestyle and behavioural interventions which may maintain or improve brain health in ageing and disease. Figure 1 outlines areas of investigation of each chapter as well as areas not covered which future studies informed by the outcomes of the current experimental work can address. This body of research is motivated by the need to develop novel treatment interventions for diseases such as MS, which work to improve the foundation of brain function; a plentiful supply of oxygenated blood to tissue, and efficient extraction and metabolism of nutrients such as oxygen.

The past few decades have seen an increasing body of evidence supporting the beneficial role of aerobic fitness (AF) in cerebrovascular health, and this is discussed in detail in Chapter 4, which along with Chapter 5, investigates the links between AF, vascular and metabolic function using quantitative fMRI. AF is believed to increase the capacity for plasticity in the brain, in both healthy ageing and disease (Colcombe et al., 2004; M. W. Voss, Vivar, Kramer, & van Praag, 2013) as plasticity is dependent on an adequate energy supply. A separate body of work shows that training on a motor sequence learning task for people with MS can improve performance which is accompanied by altered patterns of activation (Tomassini, Johansen-Berg, et al., 2012). This suggests retained capacity for plasticity in patients which could be exploited by targeted training of affected functions. However, physical rehabilitation strategies vary in efficacy between patients (Lipp & Tomassini, 2015) and this may be explained by varying levels of plasticity, which in turn may be dependent on brain energetic function. Brain energetics are affected in MS (Juurlink, 2013) and in future, combined interventions using exercise training to improve AF, along with task-specific training, may improve cerebrovascular function with subsequent increases in plasticity and recovery of function.

However, it is not known whether AF and task-specific training interventions also benefit oxygen extraction and metabolism; therefore, the extent to which such rehabilitation strategies may slow disease progression is also unknown. Further, the neural energetics underlying plasticity are not yet well established even in the healthy brain. To address this, Chapters 7 and 8, again employing quantitative imaging, investigate $CMRO_2$ changes during motor learning, and sustained cerebral blood flow (CBF) changes in task and resting state networks following motor learning, respectively. The work in this thesis, therefore, investigates both the effects of AF on cerebrovascular function and metabolism, and the energetic processes underlying motor plasticity in the healthy brain.

Chapter 9 moves towards clinical translation of this work, applying quantitative fMRI techniques used in Chapter 5 to characterise vascular and metabolic dysfunction on a regional basis. Further, this ongoing work will look at the effects of baseline blood flow and oxygen metabolism on motor plasticity, using a motor training task employed in Chapters 7 and 8. This work is ongoing, however, preliminary results demonstrate the feasibility of quantifying regional oxygen extraction and metabolism in people with MS.

Below, specific objectives related to each chapter are listed.

Chapter 3

- Assess differences in cerebral blood flow (CBF) and cerebrovascular reactivity (CVR) values obtained in the same imaging session using single and multiple inversion time ASL
- Assess the effects of partial volume correction (PVC) on CBF and CVR values and data variability
- Compare CBF and CVR results quantified using different implementations of the general kinetic model (GKM) in FSL and AFNI, two commonly software packages widely used for analysis of ASL data
- Determine the most appropriate methods for acquisition and analysis of ASL data and the limitations where the gold-standard is not available

Chapter 4

- Investigate whether young, healthy adults with greater aerobic fitness (AF) have higher CBF and CVR
- Test whether subjects with greater fitness achieve higher cognitive test performance

Chapter 5

- Building on chapter 4, investigate whether similar relationships between CBF and CVR are observed
- Investigate the metabolic effects of AF in young adults, specifically differences in capillary cerebral blood flow (CBVcap), baseline oxygen extraction fraction (OEF_0) and the cerebral metabolic rate of oxygen consumption ($CMRO_2$) which correlate with fitness level

Chapter 7

- Using calibrated fMRI, characterise neuroenergetic responses to a motor sequence training task
- Measure energetic changes over time associated with task adaptation and functional plasticity

Chapter 8

- Investigate whether sustained CBF changes, indicative of functional plasticity are observed in task-relevant networks following motor sequence training
- Use ASL resting state functional connectivity (RSFC) analysis to examine whether M1 connectivity is altered following motor sequence training, and if so, measure changes in CBF in these regions.

Chapter 9

- Examine differences in CBF and oxygen metabolism, as well as CBV between people with MS and healthy controls

Quantitative FMRI as a Tool to Study Human Brain Function

The ultimate goal of quantitative brain imaging is to reach a detailed understanding of how energy is supplied to and utilised by the brain at rest and during neural activation. To understand brain dysfunction in disease, it is necessary to first quantify healthy brain activity at rest, and in response to stimulation and interventions.

Rapid technological advancement in the last 50 years means that we can now study brain function using a variety of minimally invasive and non-invasive methods. These include positron emission tomography (PET) which can measure CBF, glucose and oxygen metabolism by detecting the radiation given off by injected tracers. Although tracers contain a very low level of radioactive material, PET is not ideally suited to repeated use in basic neuroscience. Non-invasive techniques such as electroencephalography (EEG) which measures electrical activity in the brain through electrodes placed on the scalp, and magnetoencephalography (MEG) which records the magnetic fields produced by electrical signals from neuronal activity provide non-invasive alternatives. EEG and MEG provide excellent temporal resolution but relatively poor spatial resolution and detection of subcortical activity is often degraded. In contrast, fMRI has lower temporal resolution (~1s) than EEG or MEG (<1 ms) as it measures blood flow rather than electrical activity, but has excellent spatial resolution (typically 1-2mm, although sub-millimetre resolution is now possible). At present, fMRI is one of the most widely used imaging techniques due to it being widely available, non-invasive and suitable for studying the whole brain under almost all conditions from anaesthesia to complex cognitive processing. FMRI relies on changes in blood flow in response to neuronal activity and although it is an indirect measure of neuronal activity, there is high correlation with local field potentials (LFPs) (Nikos K Logothetis & Pfeuffer, 2004) and EEG signals (Mayhew, Macintosh, Dirckx, Domenico, & Wise, 2010; Singh, Kim, & Kim, 2003). The introduction of ASL and development of biophysical models of brain activity based largely on experimental animal models means that it is now possible to obtain absolute values of CBF, cerebral blood volume and oxygen metabolism through magnetic labelling of blood water, as opposed to intravenous tracers used in PET.

The relationship between CBF and brain function was experimentally linked by Charles Roy and Charles Sherrington in 1890, then Linus Pauling and Charles Coryell in 1936 discovered that oxyhaemoglobin is diamagnetic and repelled by magnetic fields, and deoxyhaemoglobin is paramagnetic, making it attracted to magnetic fields. MRI was being used to study brain structure up until 1990 when Seiji Ogawa and Kenneth Kwong independently published the

first fMRI work using blood oxygen level dependent (BOLD) contrast. Kwong and Ogawa are now jointly credited for discovering functional mapping of the brain using the deoxyhaemoglobin contrast which gives rise to the BOLD signal. BOLD is still the most common fMRI technique, however due to several limitations, discussed in later sections, most notably the inability to obtain quantitative information about the BOLD signal, the use of ASL imaging of brain perfusion (Williams, Detrett, Leight, & Koretsky, 1992) is growing and offers a quantitative alternative to BOLD. Dual-echo and dual-excitation (see section 2.10) ASL is used throughout this thesis to acquire CBF data, with BOLD-weighted data mainly used for calibration purposes or to identify regions of interest (ROIs) for analysis of metabolic activity changes. In Chapter 1 the biological processes which can be measured and modelled using BOLD and ASL are outlined, followed by an overview of the basis of the MR signal and techniques relevant to this thesis in Chapter 2.

Chapter 1

The Energetic Brain: Functional Processes in Health and Disease

1.1 Neuronal Activity

Neuronal cells are structured to comprise a nucleus, located in the cell body (soma), dendrites which extend from the soma and an axon coated in a myelin sheath. Dendrites conduct signals towards the soma and the axon carries signals away from the soma. The myelin sheath facilitates rapid signal transmission to other cells. Interconnected neurons possess synapses, where the axon of one neuron almost connects to the dendrites of another. Neurotransmitters are released from the synapse to the receiving neuron, therefore transferring the signal. This ability of neurons to transmit signals is based on the excitability or electrical potential of the neuron.

A neuron's resting potential, or charge, is around -70mV with a threshold potential around -40 to -55mV. Neuronal excitability, which determines signal generation, is generated from this negative electrical potential (-70mV) between intra and extra-cellular space. This is called the membrane potential and is dependent on a balance between sodium ions (Na+), calcium (Ca2+), potassium (K+) and chlorine (Cl-). Na+, Ca2+ and Cl- all have a greater concentration outside the cell, and K+ is greater inside. A stimulus will activate voltage-gated sodium channels causing them to open, flooding the cell with positive sodium ions and ramping up the voltage. The now positive charge within the cell causes an outflow of potassium ions. Potassium channels within the cell are now dampened so that further sodium entrance into the cell activates more sodium channels. Sodium influx depolarises the cell to establish its own equilibrium potential (+52mV) making the inside of the cell positive relative to the outside.

Signal, or an action potential, is generated because of transient depolarisation of the membrane potential i.e. the loss of a difference in charge between the inside and outside of the plasma membrane of a neuronal cell following a permeability change in the cell, and movement of sodium ions into the cell. Then, neurotransmitter signalling to the receiving neuron alters its resting potential. A positive excitatory potential exchange is created through

the neurotransmitter glutamate while γ-aminobutyric acid (GABA) generally causes negative or inhibitory changes. The net change in polarisation achieved from the total of the excitatory and inhibitory contributions determines the signal in the neuron receiving the signal, this is called the post-synaptic neuron. Once the signal transmission has been completed, synaptic recovery is necessary. Neurotransmitter molecules are taken back into the pre-synaptic and the membrane potential is brought back to equilibrium in both the transmitting and receiving neurons. This requires sodium ions to be transported against the gradient. This process is aided by astrocytes, which along with blood vessels are required for neurovascular coupling (NVC), the relationship between local neuronal activity and the subsequent vascular (blood flow) response. With fMRI, it is possible to measure this blood flow response, hence fMRI provides an indirect measure of neuronal activity.

The human brain has around a hundred billion neuronal cells which generate and transmit electrical signals across the brain. Neuronal signalling requires significant energy availability, and perhaps counter-intuitively, most resources are allocated to post-synaptic recovery (Buxton, 2013). Brain energy metabolism is therefore very closely related to neuronal spiking, as recovery has a high energetic cost. Inflowing blood to the brain carries the essential sources of brain energy, oxygen and glucose to meet neuronal demands. As the brain cannot store energy a constant adequate supply is required, and obstructing circulation to the brain for even seconds can result in permanent brain damage.

Chemical processes within brain cells convert glucose to adenosine triphosphate (ATP) the primary source of brain cellular energy. When energy is required, ATP is converted to adenosine diphosphate (ADP) and back to ATP molecules for energy storage. ATP and ADP constantly convert back and forth in response to energetic demand. Glucose is converted to usable energy, first by glycolysis where glucose is converted to pyruvate and then from pyruvate to water and carbon dioxide (CO_2). ATP is produced at both stages, however the latter cycle (also called the Krebs cycle) is slower and requires oxygen consumption but produces more ATP (~18 times more) than the process of glycolysis. During glycolysis, some of the pyruvate can be stored as lactate and shuttled back and forth between neurons and astrocytes in response to energetic demand. The close coupling between local neuronal energy metabolism and functional brain activity mean that neuroimaging techniques such as PET and fMRI, capable of quantifying rates of energy metabolism, as well as the percentage of oxygen extracted from blood, may provide a highly sensitive way to investigate neural processes in the healthy and diseased brain. This thesis uses BOLD and ASL fMRI, techniques that are sensitive

to the concentration of oxyhaemoglobin, which indirectly reflects neuronal activity. The next sections provide an overview of the brain's vascular network through which energy is supplied as well as the utilisation of oxygen in the brain.

1.2 Organisation of the Cerebrovasculature

The cerebral circulation is equipped with mechanisms to ensure an uninterrupted supply of oxygenated blood (Iadecola & Nedergaard, 2007), ensuring sufficient quantities of energy reach the site of functional activity, as well as maintaining adequate resting flow throughout the brain. Constant supply of blood flow and nutrient delivery in the brain is regulated by a complex network of large arteries (Figure 1.1) and smaller pial arteries, which are arterioles covering the brain's surface. Pial arteries then become penetrating arteries and arterioles within brain tissue. These arteries and arterioles have 3 layers; the innermost endothelial layer (tunica intima), a medial smooth muscle layer (tunica media) and the outer layer of leptomeningeal cells (tunica adventitia). The cerebrospinal fluid (CSF) filled Virchow-Robin space separates the penetrating vessels from the rest of the brain. Beyond the Virchow-Robin space, deeper in the brain the vascular basement membrane comes directly into contact with astrocytic end-feet (figure 1.2). Deeper again into brain tissue, arterioles become capillaries (figure 1.3) which do not possess the smooth muscle cell layer of arteries. Regional blood flow and metabolism varies throughout the brain, which is in part due to variation in the density of capillaries within the neurovascular unit (NVU) (Girouard & Iadecola, 2006).

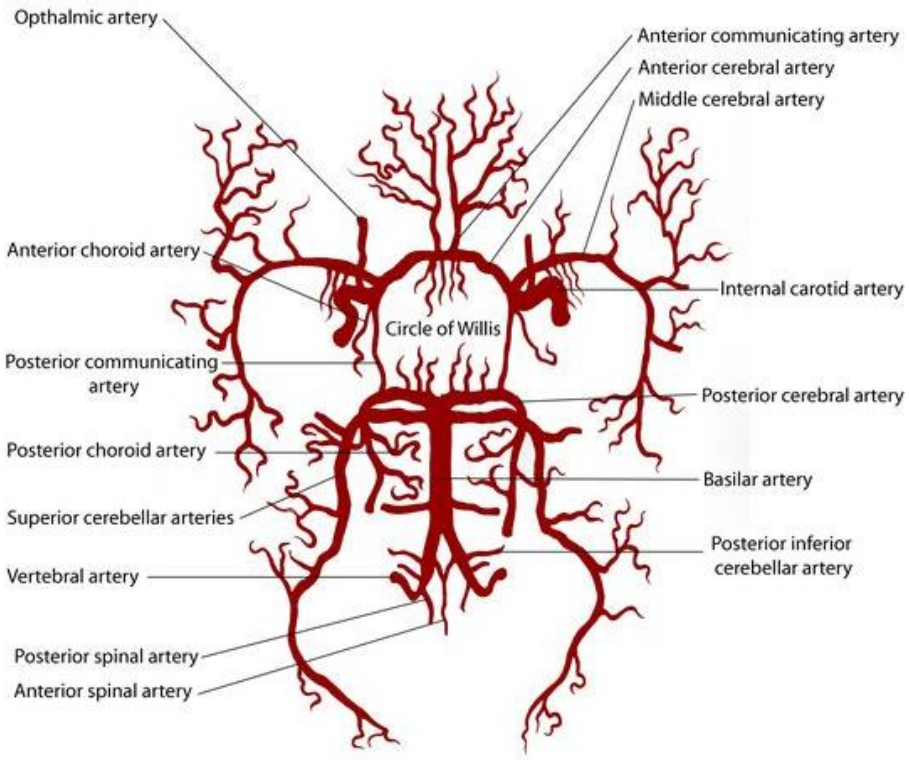

Figure 1.1 Organisation of the cerebral arteries. Anterior blood supply to the brain comes from the left and right internal carotid arteries (ICA) and posterior blood supply from the vertebral arteries (VA). The ICA arteries branch to form the middle cerebral artery (MCA) and the VA arteries converge to form the basilar artery. The VA and ICA arteries form the Circle of Willis (CoW). The ICA, anterior and posterior cerebral arteries along with the anterior and posterior communicating arteries are the main components of the CoW. The anterior, middle and posterior cerebral arteries branch from the CoW, each supplying blood to smaller connecting vessels distributed across the brain.

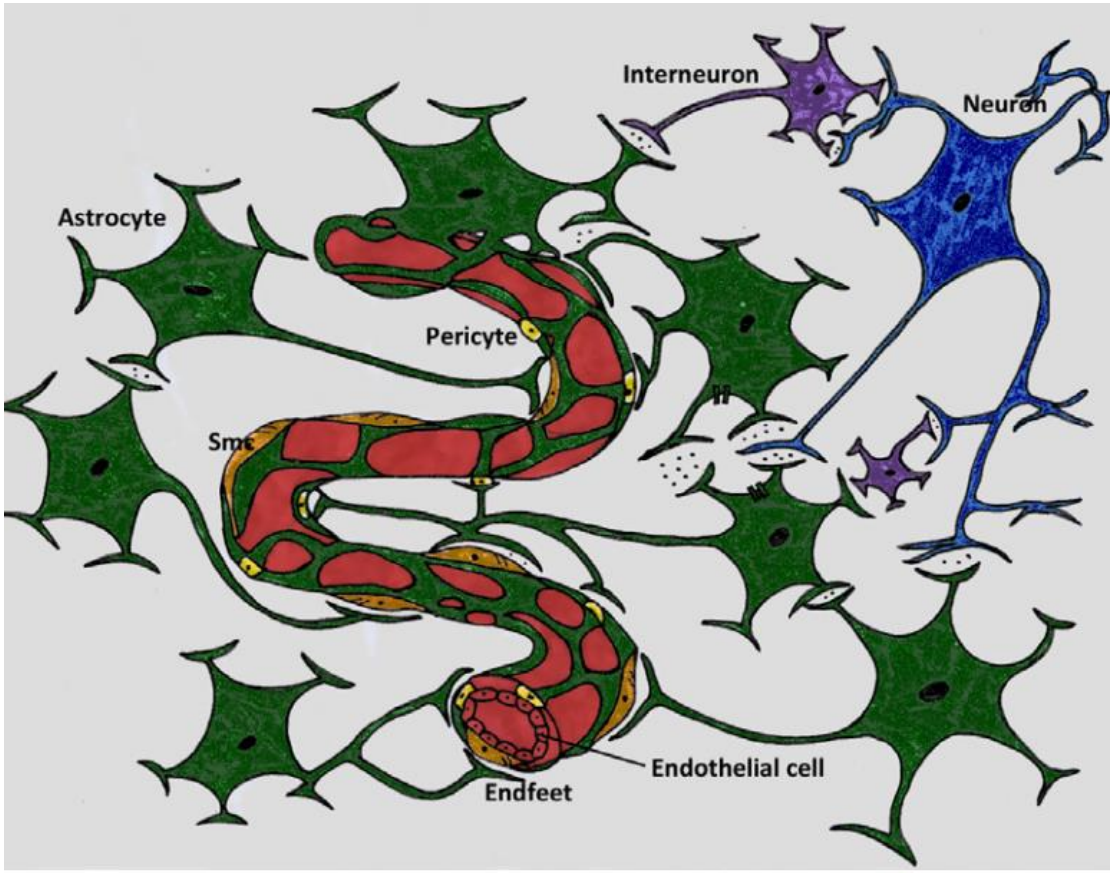

Figure 1.2 The neurovascular unit (NVU). Image taken from Muoio et al. (2014). Smc = Smooth muscle cells.

The NVU is comprised of vascular endothelial cells, myocytes (smooth muscle cells), glia (astrocytes, microglia, and oligodendrocytes) and pericytes in addition to neurons and inter-neurons (figure 1.2). Each of these cell types have specific functions and together make up the blood-brain barrier (BBB) which maintains the neuronal environment required for normal functioning, as well acting as the first line of defence against infection and injury (Paulson, 2002). Endothelial cells, for example, line the blood vessels forming the vessel wall which makes up the BBB, as well as producing nitric oxide (NO) which maintains vascular homeostasis, vasodilatory tone and stimulates cell growth. NO is also protective against injury. Smooth muscle cells control the contractile properties of the vessels which is mediated by $Ca2^{+}$. Glial cells maintain the ionic environment for neurons, modulate signal propagation and synaptic transmission, and importantly provide a protective barrier against injury and aiding recovery. Lastly, pericytes support endothelial cell function as well as having the ability to dilate and constrict to regulate vessel tone (Muoio, Persson, & Sendeski, 2014). Together, the components of the NVU provide dynamic regulation of the cerebral environment to meet energy needs during activation and protect the brain against injury.

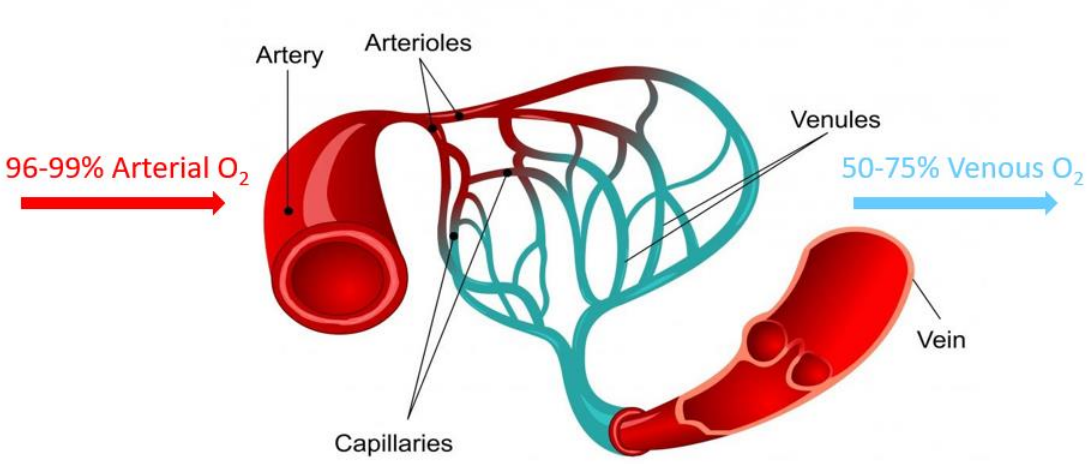

Figure 1.3 Organisation of blood vessels. Oxygenated haemoglobin is transported from the heart through arteries and arterioles to reach capillaries. From capillaries oxygen diffuses through the tissue to reach cells and mitochondria. Deoxygenated blood is then transported away from the brain through venules and veins.

1.3 Regulation and Modulation of Cerebral Blood Flow

In the healthy brain, the average CBF to grey matter (GM) tissue is approximately 50-60ml/100g/min, about 2.5 times that of white matter (WM) (Buxton, 2013). In GM, arterioles and capillaries carrying oxygenated blood, and veins and venules draining deoxygenated blood (figure 1.3), also occupy a proportion of the tissue. This is referred to as the cerebral blood volume (CBV) and is estimated to be ~4 ml/100g of tissue (Traystman, 2017).

As discussed earlier in the chapter, CBF is primarily driven by neuronal energy demand. The CBF response is extremely fast and initiated by NVC, a process that is not completely understood. NVC involves interactions between neuronal firing, molecular signalling factors, astrocytes, pericytes and endothelial cells, triggering a rapid increase in local CBF, CBV and tissue oxygenation as well as $CMRO_2$ (Girouard & Iadecola, 2006), all of which decline when the stimulus is removed. Astrocytes surround arterioles and influence their diameter, pericytes control vasodilation and constriction of arteries and arterioles and endothelial cells are responsible for the release of factors that cause vasodilation (e.g. NO) and constriction (insulin, endothelin). These components of the NVU work in collaboration to maintain homeostasis in the brain, in terms of perfusion, oxygenation and clearance of waste products (e.g. CO_2), and disruption to the function of any of these cell types can impair blood flow, and therefore brain oxygenation.

Cerebral vascular resistance is a key mediator of CBF, and is determined by the smooth muscle cell layer (see figure 1.2) which regulates the internal diameter of arteries and arterioles. Vasoactive substances such as CO_2 and O_2 decrease and increase vascular resistance respectively, which in turn is regulated by Ca^{2+} concentration in cells. Membrane potential is affected by vasoactive agents which act on ion channels to alter Ca^{2+} concentration and muscle contraction and relaxation activity. Arterial concentrations of CO_2 and O_2 can be modulated to increase CBF and tissue oxygenation in fMRI experiments through administration of appropriate gas mixtures. This effect forms the basis of calibrated fMRI experiments where vasodilatory capacity, also called cerebrovascular reactivity (CVR), oxygen extraction and metabolism can be quantified to study functional processes in the healthy brain as well as developing markers of disease-related dysfunction (Hoge, 2012; Marshall et al., 2014; Merola et al., 2017).

1.4 Cerebrovascular Reactivity

The vasodilatory effect of CO_2 can be observed as a global BOLD and/or CBF increase within seconds. Brain perfusion is highly responsive to changes in the partial pressure of carbon dioxide ($PaCO_2$) and partial pressure of oxygen (PaO_2) (Kety & Schmidt, 1947), although most notably, changes in $PaCO_2$. Hypercapnia, where $PaCO_2$ is raised by administration of enhanced inspired CO_2 concentration, is an effective vasodilator which decreases vascular resistance as well as the OEF. The brain's response to changes in arterial blood gases serves to maintain cardiovascular and respiratory autonomic control in the brainstem. Cerebral autoregulation counteracts increased CO_2 in tissue by increasing CBF, likewise during hypocapnia CBF is decreased to offset the reduction in tissue CO_2 and maintain optimal gas ratios. Many studies have measured the blood velocity response and assumed a homogeneous reactivity level throughout the brain (Bailey et al., 2013a; Barnes, Taylor, Kluck, Johnson, & Joyner, 2013). This approach may over or underestimate regional differences in CVR to CO_2 occurring in the healthy brain or through vascular dysfunction not apparent at the global level. With fMRI, all CVR measurements are based on either BOLD signal changes or direct CBF measurements rather than blood velocity changes. CVR measures vascular regulation of CBF in response to vasoactive stimuli through temporary adjustments in cerebral arterial resistance. CVR is an autoregulatory process and therefore plays a role in NVC. In recent years, the measurement of CVR using vasoactive stimuli during fMRI has been developed for use in basic and clinical research to assess cerebrovascular health (Cantin et al., 2011; Marshall et al., 2014) as CVR provides an index of the brain's capacity to increase CBF in response to increased demand for

oxygenated blood. CVR is typically calculated as the ratio between BOLD or CBF changes and the end-tidal CO_2 ($P_{ET}CO_2$) response and reported as percentage CVR (percentage change in BOLD or CBF per mmHg change in $P_{ET}CO_2$). Breath-holding, which causes a build-up of CO_2 in the vasculature can be used as an alternative approach to estimate CVR where gas administration is not practical or tolerable. Measurement of CVR during fMRI, as well as its use for BOLD signal calibration is discussed in sections 2.13 and 2.14.

1.5 Oxygen and Carbon Dioxide Transport in the Brain

Oxygen is transported via red blood cells (RBCs), which contain the protein haemoglobin (Hb), and each molecule of Hb binds four oxygen molecules to form oxyhaemoglobin. Oxygen molecules diffuse from capillaries to individual cells requiring oxygen for energy production. Diffusion alone is not sufficient to meet energy requirements, therefore oxygen exerts a partial pressure (pO_2), also referred to as oxygen tension, as it travels from capillaries. The pO_2 determines how much oxygen is bound to Hb, and the concentration of Hb determines the oxygen carrying capacity of blood. When oxygen is bound to all Hb molecules, the blood reaches 100% saturation. The transport of oxygen in blood can be described using the oxygen dissociation curve (Brown, Wade, & Marshall, 1985), which relates oxygen saturation (SO_2) to pO_2 (see figure 1.4). Oxygen travelling from the lungs to the tissue via capillaries diffuses down a relatively large pressure gradient, from around 100mmHg in lungs to 35-50mmHg in capillaries. This gradient causes highly oxygen saturated blood which has reached the capillaries from the lungs, to be released to the tissue. Active tissue has a greater energy (oxygen) demand, and this oxygen usage causes a drop in pO_2, and thus a larger pO_2 gradient which allows more oxygen to be delivered to active tissue (Wittenberg & Wittenberg, 2007).

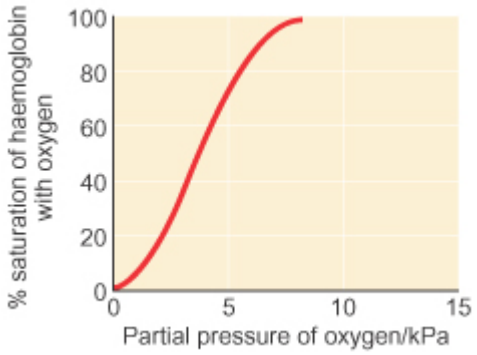

Figure 1.4 The oxygen dissociation curve relates oxygen saturation (SO_2) to pO_2 and is determined by haemoglobin's (Hb) affinity for oxygen, how easily Hb acquires and releases oxygen from the surrounding tissue. Left shifts indicate increased affinity for oxygen and right shifts indicate reduced affinity for oxygen. Image taken from Rsc.org. (2017). Chemistry for Biologists: Transport of oxygen in

the blood. [Online] Available at: http://www.rsc.org/Education/Teachers/Resources/cfb/transport.htm [Accessed 13 Sep. 2017].

Hb concentrations are ~130-170 g/L in healthy males and ~120-150 g/L in healthy females (Bain et al., 2006). However, variations due to age or disease will affect the CBF and BOLD signal due to the dependence on blood oxygenation in the baseline state (Levin et al., 2001; Tuunanen & Kauppinen, 2006). In order to account for Hb differences between individuals, peripheral Hb samples can be obtained from the capillary and used to inform model estimations of neurophysiological parameters. Peripheral and central Hb are not equivalent, however, peripheral measures should help to control for relative differences between subjects or groups.

Tissue oxygen pressure (ptO_2) is heterogeneous due to the complex organisation of vessels, therefore the longitudinal oxygen pressure gradient varies between capillaries and is referred to as capillary transit time heterogeneity (CTTH). CTTH is dependent on multiple factors including vascular geometry, $CMRO_2$, capillary density and capillary oxygenation (Østergaard et al., 2014). Leithner & Royl (2014) used the Krogh-Erlang model (1919) to show that where inter-capillary distances are short, i.e. there is a high capillary density, a smaller tissue oxygen gradient is sufficient for adequate oxygen delivery as the density tends to decrease CTTH. Where capillary density is lower, CTTH becomes more variable which can lead to reductions in maximum OEF (OEF_{max}) during CBF increases, leaving tissue vulnerable to hypoxia.

Jespersen & Østergaard (2012), incorporated CTTH into a simplified version of the Krogh-Erlang model (Krogh, 1919) to show the potential impact of CTTH on CBF-$CMRO_2$ coupling. Model predictions show that CTTH reductions with constant CBF result in $CMRO_2$ increases, as do CBF increases with a constant CTTH. Importantly, CTTH reduction and ptO_2 increases improve oxygen availability to tissue by counteracting OEF reductions which inherently occur with CBF increases. During hyperaemia (excess of blood in the vessels), low CTTH maintains adequate oxygenation, thus protecting the brain from potential activation-induced hypoxia. Lower CTTH is thought to protect tissue under conditions of hypoperfusion by increasing OEF_{max} and therefore lower CTTH is considered to be a favourable physiological state (Jespersen & Østergaard, 2012). At present, ptO_2 and CTTH is not easily measured using non-invasive ASL. However, deviations from normal values in these factors will affect the accuracy of estimated OEF and $CMRO_2$ in physiological models which rely on assumptions regarding oxygen kinetics. Therefore, it is important to consider potential changes in ptO_2 and CTTH when interpreting the output of physiological models of oxygen metabolism. This point is discussed further in Chapter 5.

Carbon dioxide (CO_2) is produced in the mitochondria by cell metabolism, and is a waste product of respiration. CO_2 is not transported in the form it is created, but reacts with water to form bicarbonate ions that dissolve easily in blood plasma for removal. This accounts for ~25% of CO_2 removal. The formation of bicarbonate is slow in plasma, but enzymes (carbonic anhydrase) in RBCs, speed up this process turning CO_2 into hydrogen and hydrogencarbonate ions. The process through which carbonic acid dissociates into hydrogen and hydrogencarbonate decreases blood pH. Hydrogen ions then react with oxyhaemoglobin which releases Hb bound to RBCs and reduces the acidity of the blood. This process could be described as a buffering effect which allows large amounts of carbonic acid carrying CO_2 to be transported in the blood without dangerous alterations in pH. In active cells respiration is high, so that Hb releases oxygen. Hb which has released oxygen increases its binding to CO_2. CO_2 concentration in the cell is then reduced and carried back to lungs as a continual process.

Impaired ventilation can affect the transport of O_2 and CO_2 to and from tissue, which must be taken into consideration in fMRI studies. For example, a reduction in the CO_2 gradient in the lungs can cause an increase in vascular CO_2 concentrations. As CO_2 has a vasodilatory effect, this could lead to an increased BOLD or CBF signal which is non-neural in origin. This is one of several reasons, discussed in section 2.7, why BOLD must be used with caution in groups where the vasculature may be abnormal.

As arterial gas concentrations are manipulated in fMRI experiments to modulate BOLD and CBF signal, it is necessary to sample respiratory fluctuations. In order to sample arterial gas concentrations an arterial puncture is required. This is invasive and not practical in imaging, therefore the end-tidal concentrations of CO_2 and O_2 are sampled instead. Expired gas can be recorded non-invasively using a nasal cannula or mask and represent the alveolar gas levels. Due to rapid diffusion of O_2 and CO_2 across the tissue, the arterial and alveolar partial pressures are almost equivalent (Young, Prohovnik, Ornstein, Ostapkovich, & Matteo, 1991), therefore end-tidal measures are a valid proxy for arterial gas levels.

1.6 Cerebral Blood Flow and Oxygen Metabolism

ATP production declines almost instantly once the flow of oxygenated blood stops or is interrupted, therefore the central role of CBF is to provide cells with the oxygen and other nutrients required for survival and function. As mentioned in the previous section, oxygen diffuses from the capillary to tissue down a concentration gradient. One of the most crucial

determinants of oxygen consumption is the OEF. The OEF refers to the fraction of oxygen extracted from oxyhaemoglobin by tissue and is around 0.3-0.5 in the healthy brain under resting conditions (Leithner & Royl, 2014). OEF can be calculated from arterial and venous oxygen saturation:

$$OEF = \frac{CaO_2 - CvO_2}{\mathrm{CaO_2}}$$

where CaO_2 is the arterial oxygen content and CvO_2 is the venous oxygen content. OEF is generally homogenous across the brain, therefore areas of variation could indicate pathology.

$CMRO_2$ can be calculated by combining OEF with measures of CBF and arterial oxygen concentration (Zheng et al., 2002) using the formula given below:

$$CMRO_2 = CaO_2 * OEF * CBF$$

where OEF relates to the concentration of deoxyhaemoglobin in blood. From previous investigations, it is known that the average rate of $CMRO_2$ in the healthy adult brain at rest is 160 µmol/100g/min, around 80% of $CMRO_{2max}$, and therefore deviations from normal values can, like OEF, indicate abnormal brain physiology. As neuronal energy consumption is closely connected to oxygen metabolism, optimisation of imaging approaches to quantify absolute $CMRO_2$ has been of interest for the development of brain markers of pathophysiology and physiological responses to treatment (Bulte et al., 2012; Gauthier & Hoge, 2013a; Wise, Harris, Stone, & Murphy, 2013b). In Chapters 5 and 9, the application of a recently developed optimised physiological model to quantify, OEF_0 and absolute $CMRO_2$ is demonstrated in a healthy and clinical population respectively.

Upon neuronal activation, the CBF response is much greater than the increase in $CMRO_2$ (Fox & Raichle, 1986). A number of models have been proposed to explain this effect. Buxton & Frank (1997) described a model which assumed constant oxygen diffusion in the absence of capillary recruitment and 100% metabolism of oxygen in brain tissue. With mean transit time (MTT) decreases accompanying CBF increases, OEF is therefore reduced, and CBF increases must be large to provide adequate tissue oxygenation. Another model by Vafaee & Gjedde (2000) predicted nonlinear CBF-$CMRO_2$ responses based on an assumption of low oxygen tension in mitochondria; if the oxygen gradient between the capillary and mitochondria can only be increased by a rise in capillary pO_2, which necessitates a reduction in OEF as OEF becomes less efficient with greater oxygen tension gradients, then an increase in CBF must occur, to ensure sufficient oxygen delivery. A recent model proposed by Jespersen &

Østergaard (2012) is an extension of the Krogh-Erlang model (Krogh, 1919) which describes the oxygen diffusion process. The Krogh-Erlang equation relates the radius of a capillary and radius of the tissue cylinder supplied by that capillary, tissue oxygen diffusion properties and oxygen metabolism, to the oxygen gradient from the capillary to tissue. The Krogh-Erlang model permits calculation of the minimum oxygen gradients required to support $CMRO_2$, but as this model was developed for muscle, where capillaries can be described as cylindrical tubes, it is not directly accurate for calculating oxygen gradients in the brain where capillary geometry is less ordered. Jespersen & Østergaard (2012) included CTTH changes into this model to show the effects of CTTH on the relationship between CBF and $CMRO_2$ changes. Briefly, the model predicts that where CBF is constant, and where CTTH is decreasing, $CMRO_2$ increases. Conversely, CBF increases with constant CTTH leads to $CMRO_2$ decreases. The model allows for a degree of variation in CTTH and CBF changes without a decrease in brain oxygen metabolism. CTTH reduction allows for greater OEF, creating a more homogenous flow rate and allowing oxygen to be extracted more easily. However a state of malignant CTTH can occur where capillary flow is impaired; high CBF causes a reduction in MTT and OEF, when combined with a high CTTH which reduces OEF_{max}, tissue oxygenation is reduced, despite high levels of CBF (Angleys, Østergaard, & Jespersen, 2015). This model demonstrates that CBF alone does not deliver a complete picture of tissue oxygenation and potential ischemia. Additional measures of OEF and $CMRO_2$ can provide more detail on the health of tissue, this is especially important for disease studies where CBF may appear similar to controls.

Finally Leithner & Royl (2014) suggest that excess CBF evolved as a safety mechanism to ensure adequate oxygen delivery, which in most cases is not needed. The authors present previous experimental evidence where $CMRO_2$ was constant in the presence of CBF decreases (Mathiesen et al., 2011), or apparent increases with constant CBF (Offenhauser, Thomsen, Caesar, & Lauritzen, 2005; Vanzetta, 1999) and argue that this effect shows that large CBF increases evolved as a buffer against transient reductions in oxygen supply. In addition, Leithner & Royl (2014) also suggest that factors other than oxygen supply may regulate $CMRO_2$ such as rapid ATP production required for neural signalling. It is argued that the evolutionary mechanism to increase ATP production to support neuronal activity is unlikely to have been via a slow increase in CBF followed by a $CMRO_2$ increase, instead $CMRO_2$ dynamic adjustment of $CMRO_2$ is followed by an overcompensation in CBF to ensure sufficient oxygenation of tissue when energy demands cannot be predicted. In summary, the exact mechanisms determining the regulation of relative changes in CBF and $CMRO_2$ during activation are still unknown as it is difficult to study *in-vivo*. It is known that in the healthy brain CBF increases much more than

$CMRO_2$, and the coupling varies between brain regions, and potentially depending on task demands. In disease, the coupling between CBF and $CMRO_2$ is likely to be altered (Blicher et al., 2012; Iannetti & Wise, 2007b) due to a number of vascular and neuronal factors which must be considered when interpreting relative changes in brain activity.

1.7 Impaired Oxygen Availability and Metabolism in Disease

As outlined in previous sections, inadequate oxygen availability to cells, will quickly lead to irreversible brain damage (see figure 1.5, below). Dysregulation of the brain's vascular and metabolic network occurs gradually with normal ageing (Aanerud et al., 2012) and is exacerbated in neurological diseases such as MS, where hypoperfusion (D'haeseleer, Cambron, Vanopdenbosch, & De Keyser, 2011) as well as reductions in OEF and $CMRO_2$ have been reported (Fan et al., 2014; Ge et al., 2012).

Although chronic reductions in metabolic activity are prevalent in disease, changes in blood flow and vascular reserve can lead to initial compensatory increases in OEF, which has been reported in acute stroke (Park et al., 2014), and $CMRO_2$, as observed in Parkinson's disease (Powers, 2009). Changes in OEF and $CMRO_2$ may also occur before measurable CBF changes. For example, OEF may increase where CBF cannot be adjusted to meet energy demands which may be higher in early disease stages than in healthy tissue (Sperling et al., 2010). In the healthy brain, OEF is highly homogenous, however, in order to maintain optimal oxygenation, OEF increases to counteract perfusion reductions. Beyond a certain point, OEF cannot be further increased (Jespersen & Østergaard, 2012) and eventually, with chronic or severe transient CBF reductions, diminished energy supply will lead to cellular dysfunction and death.

Absolute $CMRO_2$ and the coupling between CBF and $CMRO_2$ during activation are also informative indicators of cellular metabolic function. The fractional increase in CBF is generally 1.5-4 times higher than the change in $CMRO_2$ as the coupling ratio varies from rest to activation, as well as by brain region. Alterations in CBF-$CMRO_2$ ratios can indicate flow reductions where $CMRO_2$ is increased to sustain metabolic demand, however this flow reduction will reduce metabolic capacity and neuronal function in the long-term. Alternatively, reduced $CMRO_2$ may indicate metabolic dysfunction in the presence of adequate flow, where oxygen extraction and/or metabolic efficiency is impaired. In such cases, CBF alone would not be representative of metabolic health. OEF and $CMRO_2$ may provide more sensitive indicators of early disease-related brain dysfunction capable of identifying areas of at-risk tissue prior to ischemia.

Whether vascular dysfunction is a primary cause of brain damage and disability in MS, or secondary to neuronal loss caused by inflammatory activity, is not yet known. Regardless, impaired oxygen availability is likely to limit brain plasticity and functional recovery following relapses and may accelerate disease progression. Treatments which maintain, or restore healthy CBF and oxygen metabolism are of interest and may complement anti-inflammatory drugs such as interferon-beta (IFN-beta) which currently used to manage MS. FMRI techniques capable of quantifying oxygen metabolism which are used in this thesis can identify the efficacy of behavioural and pharmacological interventions in promoting healthy vascular function.

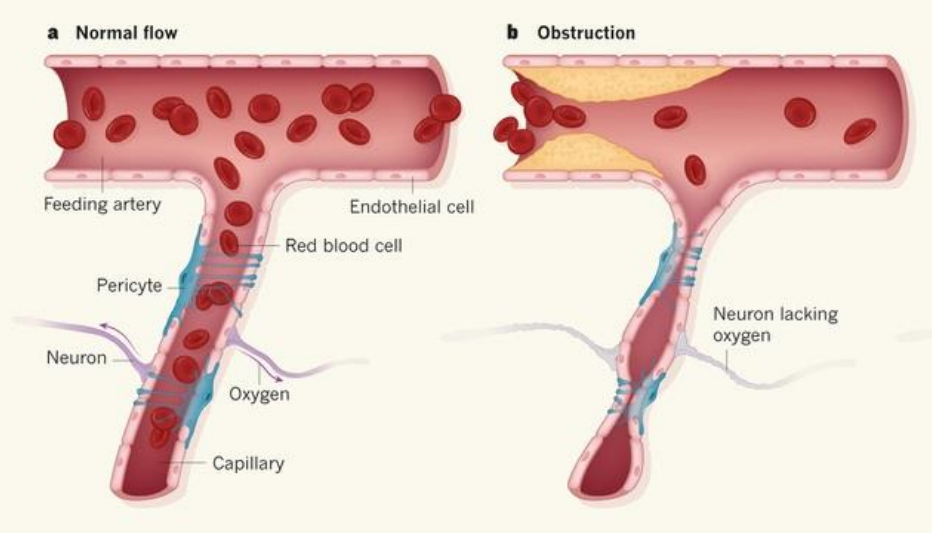

Figure 1.5 Healthy (a) and impaired (b) energy supply to neurons. Even brief interruptions to oxygen supply will result in cell death due to hypoxia. Image adapted from Greif and Eichmann (2014), *Nature*.

Healthy Resting Brain Values	
CBF	50-60 ml/100g/min
Inspired CO_2	0.04 %
Inspired O_2	20.9%
$CMRO_2$	160 µmol/100g/min
OEF	30-50%
CBV	4 ml/100g

Table 1.1 Typical concentrations and rates of physiological parameters of interest in fMRI research.

1.8 Multiple Sclerosis

MS is a chronic, progressive autoimmune disease, where inflammation leads to white matter demyelination and axonal loss, as well as lesions in the grey and white matter. In later disease stages, brain atrophy can occur because of cumulative inflammatory damage. Increasingly, vascular and metabolic dysfunction such as hypoperfusion (De Keyser, Steen, Mostert, & Koch, 2008; Miguel et al., 2013; Ota et al., 2013), reductions in cerebrovascular reactivity (CVR) (Marshall et al., 2014), and reduced $CMRO_2$ (Ge et al., 2012) are also being identified. Symptoms of MS include vision, balance, motor and cognitive impairment as well as depression, bladder problems and extreme fatigue. The first stage of MS is relapsing-remitting MS (RR-MS), where acute bouts of inflammation cause a flare-up of symptoms, followed by periods of remission which can last weeks, months or years. Disease modifying therapies (DMTs) can help to reduce the number and severity of relapses but are not a cure, and have little effect on cognitive and behavioural symptoms. Physiotherapy is also often used for specific motor problems and can help to restore function. The majority of patients are diagnosed with RR-MS before disease progression leads to primary-progressive (PP-MS) and secondary-progressive (SP-MS) disease stages. The Expanded Disability Severity Scale (EDSS) is used to categorise the disease stage, and this can increase or decrease depending on treatment response, which is highly variable. Other lifestyle factors can help to manage MS such as physical exercise. For example, exercise can benefit people with MS by improving certain disease symptoms such as fatigue (Andreasen, Stenager, & Dalgas, 2011) and higher AF has been linked to increased cortical plasticity in MS (Prakash et al., 2007). Brain plasticity, the ability to adapt or reorganise following injury is believed to influence treatment response (Lipp & Tomassini, 2015).

Vascular dysfunction in MS has received considerably less research focus than structural damage, however, without a healthy energetic system, the brain will not be capable of repair. The work in this thesis is focused on understanding the normal vascular and metabolic adaptations involved in plasticity, and investigating potentially beneficial effects of AF on vascular and metabolic function. Ongoing work presented in the final chapter then maps regional differences in vascular and metabolic function between patients and controls, and this quantification of resting brain function will be used to investigate the effect of baseline function on motor plasticity. In future, interventions which include physical exercise training to increase AF may be an effective way to boost functional plasticity and improve disease management.

1.9 What is Functional Brain Plasticity?

The brain retains a lifelong capacity to adapt and reorganise in response to new experiences or following injury. However, this plasticity which can be both structural and functional, is reduced by the ageing process and by disease, as neuroinflammation limits neuronal and non-neuronal cell survival and adaptation (Yirmiya & Goshen, 2011). Impaired plasticity then leads to behavioural and cognitive dysfunction, including learning and memory failures and motor impairments; the specific functions affected may depend on the location and extent of damage. Residual adaptive neuroplasticity in MS can work to promote recovery following disease modifying treatments to reduce inflammation (Tomassini, d'Ambrosio, et al., 2016). However, treatment response is variable and may be dependent on vascular reserve and energy availability to tissue.

Imaging studies of plasticity frequently investigate motor plasticity (Zeller & Classen, 2014) as motor impairment is a common disease feature. Functional adaptation to motor task training occurs quickly, in the form of BOLD and CBF response increases, and motor paradigms can easily be conducted during fMRI (see Chapter 6 for a review of imaging studies of motor plasticity). In Chapters 7 and 8, the energetic changes during and following motor training are investigated in the healthy brain both to assess the feasibility of quantifying the energetics of plasticity using ASL, and to characterise blood flow and oxygen metabolism changes during motor learning in the healthy brain.

1.10 The Role of Aerobic Fitness in Cerebrovascular Function

Aerobic fitness (AF), or cardiovascular fitness is measured as the amount of oxygen transported in the blood to working muscles, and the ability of the muscle to use transported oxygen. High AF means that the cardiovascular system has a greater capacity to supply oxygen and other nutrients carried by blood around the body, and the brain. Higher levels of AF reduce the risk of all-cause mortality (Kodama et al., 2009) and AF is associated with greater cerebrovascular health in ageing (Brown et al., 2010; Gauthier et al., 2015).

Experimental animal models of exercise have shown that sustained periods of aerobic exercise increases neurogenesis and survival of new neurons as well as increasing angiogenesis, the formation of new blood vessels (Pereira et al., 2007; R. A. Swain et al., 2003; van Praag, Kempermann, & Gage, 1999). Upregulation of neurotrophic factors including brain-derived neurotrophic factor (BDNF), insulin-like growth factor (IGF-1) and vascular-endothelial growth factor (VEGF) (Cotman & Berchtold, 2002; Cotman, Berchtold, & Christie, 2007) is believed to

play a role in the beneficial effect of exercise on the brain. IGF-1 blockage, for example, mitigates the beneficial effect of exercise on brain health and behaviour following injury (Carro, Trejo, Busiguina, & Torres-Aleman, 2001). In humans, neurogenesis and brain concentrations of growth factors cannot be studied directly. However, cross-sectional evidence suggests a neuroprotective effect of AF against ageing effects on brain volume (Chaddock-Heyman et al., 2016), CBF (Thomas et al., 2013) and blood flow velocity (Ainslie et al., 2008); see Chapter 4 for a more in-depth discussion.

More recent evidence suggests a similarly protective role of AF in MS; as mentioned above greater AF is associated with cortical plasticity (Prakash et al., 2007) as well as greater regional brain volume and white matter integrity (Prakash, Snook, Motl, & Kramer, 2010). However, taking all available literature, the evidence for a modifying effect of physical activity in MS is mixed, and future studies would benefit from an improved understanding of several areas; the mechanisms through which exercise benefits cerebral health and plasticity, whether the level of AF achieved through exercise mediates the extent of benefits, or whether regular physical activity is enough, and the extent to which AF benefits the brain and behaviour. For example, it is unclear whether lifelong benefits are observed, or whether the effect is merely neuroprotective when the brain becomes vulnerable to damage. Further, whether AF can restore cerebrovascular and metabolic health, or merely protect against further decline is of clinical interest and the potential vascular and metabolic mechanisms underlying brain effects of AF are investigated in healthy adults in Chapters 4 and 5.

Cerebrovascular function may be improved by AF, and is necessary for optimal brain plasticity. Therefore, increasing AF may facilitate plasticity and offer a route to improving brain health and functional ability in patient groups and older adults. However, before a full-scale intervention to test whether increases in AF affect both cerebrovascular function and plasticity in clinical or ageing groups, the neurophysiological processes which facilitate adaptive plasticity must be better understood, as well as the effects of AF on cerebrovascular and metabolic function.

FMRI is arguably the best available tool for studying brain haemodynamics *in-vivo* and assessing the efficacy of interventions to improve brain health due to its superior ability spatial resolution and ability to quantify a number of markers of function, including CBF and absolute $CMRO_2$ without the need for contrast, as in PET. The following chapter details the basis of BOLD and ASL imaging, the range of image acquisition options available, and the strengths and

limitations of each technique. This is not intended to be an exhaustive review of all available methods, focus is given to methods used in the experimental work presented in later chapters.

Chapter 2

Functional Magnetic Resonance Imaging: Basis and Application in Cerebrovascular Research

2.1 Nuclear Spin

Hydrogen is the most abundant atom in the human brain, found in water molecules which are arranged as two atoms of hydrogen and one of oxygen (H_2O). Each atom contains a nucleus and orbiting electrons and fundamentally, MRI relies on the spinning motion of specific nuclei in biological tissues. Although nuclei with an even mass number (equal neutrons and protons) have no net spin, when nuclei have an odd mass number, spin directions are not in equal opposition so the nucleus does have a net spin, otherwise known as angular momentum. When these nuclei are placed in a static magnetic field (B_0) their axis of rotation comes into alignment with the magnetic field as the positively charged protons possess electrical charge. According to the Faraday law of electromagnetic induction (Faraday, 1931), as hydrogen nuclei have motion (spin) and electrical charge they acquire a magnetic moment and can therefore align with a static magnetic field. In the absence of a magnetic field they are randomly oriented. Some nuclei align in parallel with the field, a smaller proportion align anti-parallel.

B_0 (always referred to as the z-direction in MR convention) produces additional motion (as regarded in the classical model) of the hydrogen magnetic moments around B_0 in a circular path, this is called precession. So, there are many low energy parallel (spin up) nuclei and a smaller number of high energy anti-parallel (spin down) nuclei. The precessional frequency, or Larmor frequency, is given by the Larmor equation which states that the precessional frequency is proportional to the magnetic field strength (see equation 1.1), which is 128MHz at 3 Tesla. As B_0 increases or decreases, so does the precessional frequency.

$$\omega_0 = \gamma B_0$$

Equation 1.1 The Larmor Equation where ω_0 is the precessional frequency, B0 is the magnetic field strength and γ is the gyromagnetic ratio.

Resonance occurs when the hydrogen nuclei in tissue gain energy from a radiofrequency (RF) pulse delivered at the same precessional frequency as the nuclei in question. In simple terms, an RF pulse is a magnetic field, referred to as the field, which is temporarily applied in order to cause excitation of hydrogen atoms. For resonance of hydrogen to occur, RF pulses at the same Larmor frequency as hydrogen need to be applied. Non-hydrogen nuclei which may have aligned to B_0 will not resonate as they have a different gyromagnetic ratio and Larmor frequency to hydrogen. The application of a RF (excitation) pulse causes energy absorption and an increase in the number of high energy spins as some of the low energy spins become high energy spins due to resonance. When resonance occurs, the net magnetisation vector (NMV) moves out of alignment with B_0 (see figure 2.1) into the transverse B_1 field.

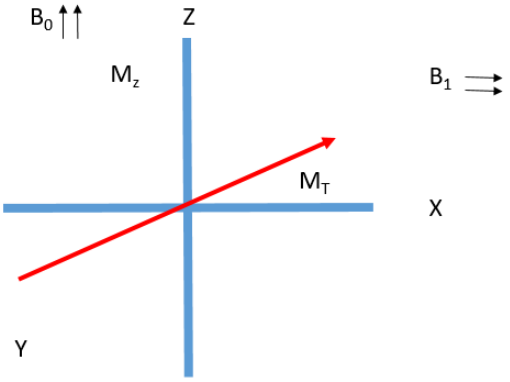

Figure 2.1 Schematic of the net magnetisation. Mz = longitudinal magnetisation, Mt = transverse magnetisation

Transverse magnetisation is produced by the net magnetic moment of hydrogen and represents the balance between high and low energy nuclei. The NMV moving into B_1 is caused by low energy spins joining the high-energy population. The NMV then lies at an angle to B_0 rather than parallel as it did before the RF pulse was applied to excite the tissue. This angle is referred to as the flip angle and its magnitude is dependent on the RF pulse amplitude and duration. Flip angles between 0-90° are used for gradient echo sequences, spin echo sequences use a series of 180° pulses. Flip angle determines the signal intensity and image contrast.

Following RF excitation, the magnetic moments of hydrogen move into phase, meaning that they are in the same place on the precessional path. The MR signal results from in-phase magnetisation which is detected by the receiver coil in the scanner. The transverse magnetisation (flip angle) causes magnetic field fluctuations within the coil, and the phase and magnetisation induce an electrical voltage (see Faraday's law) which produces the measured

MR signal, the magnitude of which depends on the amount of transverse magnetisation. When the temporarily applied magnetic field (RF pulse) is switched off the NMV returns to its resting state (B_0) and this causes a signal, or radio wave, to be emitted and detected by the RF receiver coil. This signal is used to create the resultant MR image, following digitisation and filtering of the signal to obtain frequency and phase information contained within the signal (see 2.4 Signal Processing in K-space).

RF pulse timings and magnitudes can be used in various combinations to create pulse sequences which generate the required contrast in MRI. For reference, the transverse magnetisation is dictated by the x and y direction and rotates around the z axis (figure 2.1).

2.2 Relaxation and Decay

When the RF pulse is switched off, the NMV attempts to realign with B_0 as the hydrogen nuclei lose the energy transferred to them by the RF pulse, a process known as relaxation. As relaxation occurs, magnetisation in the longitudinal plane (M_z) recovers, this is called T1 recovery. At the same time, there is a loss of magnetisation in the transverse plane, this is called T2 decay.

T1 recovery is the process of hydrogen nuclei losing thermal energy to the surrounding environment or lattice, hence the term spin-lattice relaxation. Energy released to the lattice results in nuclei recovering their magnetisation in the longitudinal direction. This recovery time is an exponential with a recovery time constant; the T1 relaxation time. This is the time it takes 63% of the longitudinal magnetisation to recover i.e. realign to B_0 with most nuclei in a low energy state. The spin-lattice relaxation time determines what delay between pulses should be used. The nuclear spin system must be allowed to relax back to equilibrium before the next pulse is applied and this time is determined by T1 relaxation.

T2 decay is caused by the magnetic fields of proximal nuclei interacting with each other and deviating from the Larmor frequency, also called spin-spin relaxation. In addition, static magnetic field inhomogeneities, such as those found near the boundaries of different tissue types (e.g. water and bone) cause additional dephasing of hydrogen nuclei which mimics T2 decay. Like T1 recovery, T2 decay is exponential so the T2 recovery time constant is the time it takes 63% of the transverse magnetisation to decay.

Decay caused by field inhomogeneities can be reversed with a 180° refocusing pulse. Following a RF pulse, a free induction decay (FID) curve is present and the FID has an exponential T2*

decay. The application of a 180° pulse can reverse the T2* effects, however, signal decay still occurs due to irreversible T2 decay.

2.3 Slice Selection and Image Formation

The next step in acquiring an image of the object of interest, in this case the brain, is to spatially select the relevant area within the magnetic field. For this purpose, MR scanners have additional gradient coils which serve to manipulate the static magnetic field, creating a spatial variation of the Larmor frequency. MR images of the brain are made up of a series of slices (or a single slice), usually a few mm in thickness. A slice selection gradient is applied to isolate the desired imaging plane. Each slice is selected through the presence of a linear gradient in the B_0 field induced in the scanner's gradient coil. Each slice has a different Larmor frequency based on its location in the field. The B_1 field must precess at the same frequency as the selected slice for successful spatial selection.

The next step is to encode the transverse magnetisation in the x any y planes. Two additional coils are used for this, one for frequency encoding in the x plane and a second for phase encoding in the y plane. These gradient coils make the frequency and phase of the signal relate to position within the image. Stronger gradients allow better spatial specificity and therefore resolution.

The effect of the frequency encode gradient is that hydrogen spins take on frequency variations depending on their position along the x-axis. The phase encode gradient causes phase differences depending on the y position of the spin. Following signal encoding, each spin has a frequency and phase specific to the location of the slice it lies within.

The signal which is then read out is the transverse magnetisation from the spins within each slice which results in a map with spatially varying intensities depending on the amplitude, or spin densities, within the brain slices. The frequency and phase encoding gradients determine the signal frequencies just as the amplitude is determined by the spin densities.

To reconstruct the final MR image, the signal must be converted from the time domain in which it is stored, called k-space, to the spatial frequency domain using the Fourier transform (FT).

2.4 Signal Processing in K-space

K-space is the FT of the MR image; in simple terms, k-space is a matrix of numbers relating to the spatial frequencies contained within an MR image. Points in k-space are displayed on a

grid with axes k_x and k_y which correspond to the horizontal (k_x) and vertical (k_y) axes of the acquired image. The axes x and y axes in k-space represent spatial frequencies, not positions, in the x and y axes of the image. Importantly, each point in k-space contains spatial frequency and phase information relating to the full image.

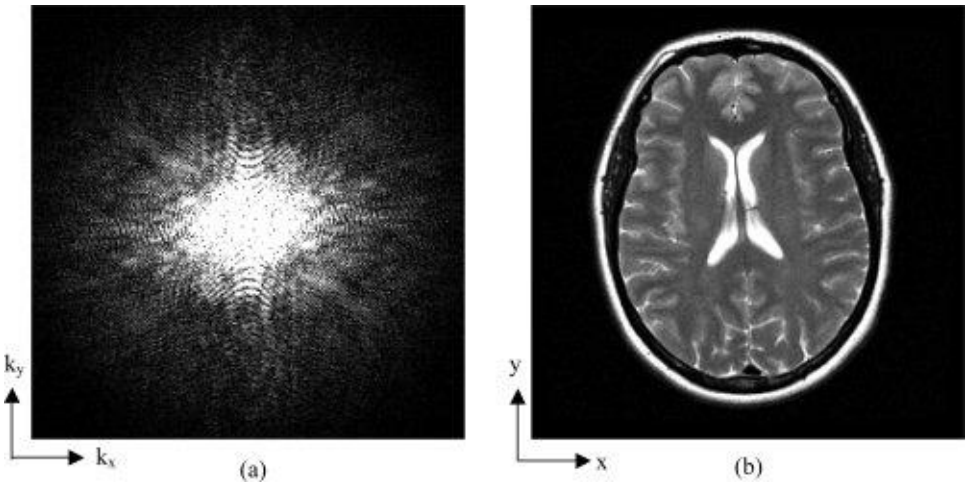

Figure 2.2 Spatial information in k-space (a) is transformed into conventional MR image space (b) via the Fourier transform. Image adapted from Paschal & Moris (2004).

K-space can be sampled in multiple ways, however only two trajectories, Cartesian and spiral, are relevant to this thesis. Echo planar imaging (EPI) refers to spin echo and gradient echo sequences where k-space is filled in either one or a small number of excitations (single shot and multi-shot EPI respectively) by rapidly switching gradients so that the k-space trajectory scans back and forth across the entirety of the space (Buxton, 2009). Cartesian EPI ('blipped EPI') (Mansfield, 1977) is currently the most widely used fMRI acquisition technique. It has been a useful method in terms of acquisition speed and ease of reconstruction but there is a trade-off as image resolution is low compared to slower techniques where k-space is acquired line by line after one excitation pulse. Cartesian has the benefit of a fast readout which reduces the blurring and distortion seen in spiral data. However, Cartesian trajectories have a longer encode duration than spiral which can result in image warping and motion artifacts. Off-resonance[1] effects can create ghosting effects and pulsatile motion from flow can result in

[1] Off-resonance effects are any signal which has a different than expected precessional Larmor frequency in a nucleus. The pulse sequence relates spatial position to precession frequency so off-resonance effects result in problems such as signal loss, ghosting, image distortion/blurring and spatially specific areas of high or low signal which is not a true tissue signal.

variable phase errors depending on the readout time with respect to the brain pulsatility (Glover, 2013).

Spiral acquisitions in contrast, cover k-space in an Archimedean trajectory using either a spiral in or spiral out pattern to or from the centre of k-space respectively. Spiral-out is an even faster, efficient method of filling k-space compared to Cartesian read-outs as it can skip the corners of images where there is very low unusable signal. However, spiral does require more complex reconstruction and is harder on the gradient system. An advantage of spiral schemes is that they do not require gradient loading at the start of the acquisition, therefore allowing very short TEs (~2.7ms) to be used. The time efficiency allows the centre of k-space to be oversampled in a short amount time. This translates to reduced pulsatile and motion artifacts which affect signal at the centre of k-space more than the periphery as high spectral energy (present near the k-space origin) is more susceptible to the effects of phase changes (Glover & Lee, 1995).

Another factor to consider in terms of SNR is bandwidth. Bandwidth controls the frequency range in RF excitation (transmit bandwidth) and the MR signal received (receiver bandwidth). Larger receiver bandwidths decrease SNR but speed up imaging time. Slice thickness is proportional to the transmit bandwidth, lowering the bandwidth allows reduced slice thickness but can increase distortion.

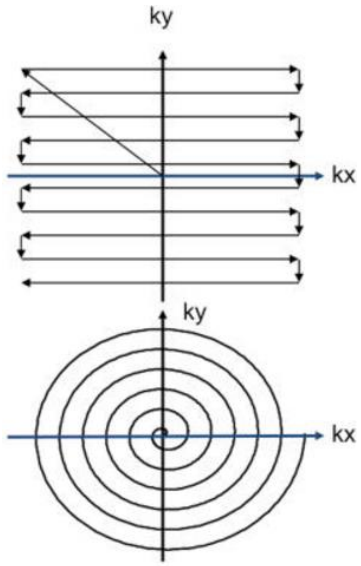

Figure 2.3 Example of a Cartesian readout (top) and spiral-out trajectory (bottom). Image adapted from Glover (2013), Neuroimage.

Partial k-space acquisition is also possible and is extremely useful in terms of significantly reducing acquisition time. 50-70% of k-space can be filled, filling the remaining space with zeroes and exploiting the symmetry of the FT to reconstruct the full image. Phase variations due to off-resonance and motion effects across the image effect SNR, however, due to the general smoothness of phase variations, this can be overcome by generating a low-resolution map of the phase distribution which is then used to correct the full image (Buxton, 2009, Chapter 10).

2.5 MR Contrast Mechanisms

Contrast between the process of interest and surrounding tissue is necessary in every MR scan. Contrast arises from a number of sources; the hydrogen spin density *p* of tissue or fluid, T1, T2, or T2* which is T2 decay plus the additional magnetic field inhomogeneities which are always present.

In practice, MR contrast comes from a mixture of all of these mechanisms, but, one contrast mechanism can be emphasised over the others by designing the pulse sequence with the appropriate repetition time (TR), echo time (TE), inversion time (TI) and flip angle.

For example, a high-resolution structural brain image with good contrast between grey matter (GM), white matter (WM) and cerebrospinal fluid (CSF) is achieved using T1 weighting. In such images GM appears darker than white matter as GM has a longer T1 than WM. CSF appears

black as it has the longest T1 of the three tissue types (see table 2.1 for relaxation times of tissue at 3T) and image volumes are acquired before longitudinal magnetisation has recovered in GM or WM. This is achieved using a short TR and short TE (~8 and 3ms respectively) so that the signal does not have time to fully recover between excitations and steady state longitudinal magnetisation can be achieved.

The most common contrast in functional imaging is T2*, where contrast arises from T2* decay differences between tissue types. In T2* a long TR and long TE (~3s/30ms) is used so that contrast is not affected by differences in longitudinal magnetisation between tissue types. T2* is central to BOLD imaging which exploits the dephasing phenomenon caused by inhomogeneities in the magnetic field. T1 provides the contrast mechanism for ASL, hence the benefit of moving to higher field strengths for perfusion imaging. In addition to a signal to noise (SNR) increase, due to the higher magnetic signal, the T1 of tissue is lengthened meaning the labelling time of tissue is extended which increases the ASL signal (Ferré et al., 2013).

It is also possible to use exogenous paramagnetic chemical contrast agents in MR. However, due to the risk of toxicity, MR contrast agents tend to be used mainly for clinical applications. There are current efforts in MRI research to develop non-invasive alternatives to contrast MRI, for example, PET is the gold-standard for measuring oxygen metabolism, however optimisation of dual-calibrated ASL, as used in Chapters 5 and 9, may provide a clinical alternative to PET.

Relaxation Times at 3T				
	T1 (ms)	**T2 (ms)**	**T2* (ms)**	**PD**
Grey Matter	1820	100	50	0.69
White Matter	1080	70	50	0.61
CSF	3817	1442	n/a	1.00
Arterial Blood	1932	275	46	0.72

Table 2.1 Relaxation times for tissue types at 3T (MacIntosh & Graham, 2013). PD = Proton Density.

2.6 Spin Echo and Gradient Echo Imaging

Spin echo can be used to obtain, T1, T2/T2* or PD weighted images with parameter adjustments. In the spin echo sequence, a 90° RF pulse tips the NMV into the transverse plane. A voltage is induced in the receiver coil caused by precession in the transverse plane. Once the 90° pulse is switched off a FID begins causing T2* decay. A 180° RF pulse is then applied to reverse T2* dephasing, flipping the out of phase spins through 180°. This momentarily puts

the slow (trailing) spins in phase with the fast (leading) spins putting all the spins on the same precessional path. At this point the maximum signal is induced in the receiver coil as the transverse magnetisation is in phase. This is how the spin echo is formed. As T2* dephasing has been reduced, T1 and T2 information is prolonged due to the extended time for relaxation to occur. In spin echo, the TR is the time between the 90° RF pulse for each slice and TE is the time between the RF and the peak of the spin echo signal.

The basic spin echo sequences can be adapted further such as in fast turbo spin echo and multiple echo acquisitions. In multi-echo acquisitions, multiple 180° refocusing pulses are applied to create separate images for each echo. Turbo spin echo reduces the overall imaging time by applying numerous 180° pulses which each fill separate lines in k-space. For example, imaging time is reduced by a factor of 6 where 6 spin echoes are used (Buxton, 2009).

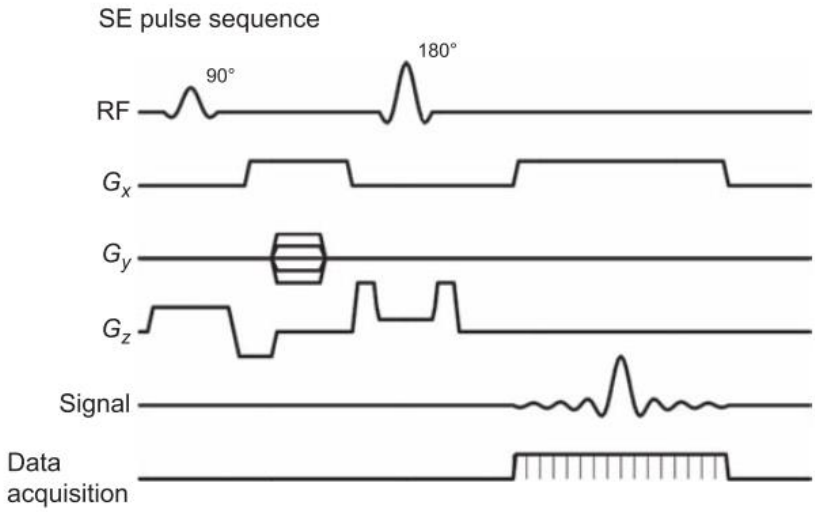

Figure 2.4 Spin echo pulse sequence. Image adapted from "Introduction to Functional Magnetic Resonance Imaging" Figure 10.1.

Although spin echo and gradient echo sequences use gradient echoes, spin echo includes a second refocusing pulse whereas gradient echo sequences do not. This 180° refocusing pulse is what separates the two classes of sequence. The gradient echo sequence uses a variable RF pulse (0-90°) to tip the NMV into the transverse plane. When flip angles <90° are used, longitudinal magnetisation is only partially converted to transverse magnetisation, this has the advantage of allowing shorter TR. As in spin echo, as soon as the RF pulse is removed, the FID induces T2* dephasing. A gradient is then applied in the opposite direction to the RF pulse which rephrases the spins. The gradient induces a change in the magnetic field strength which

causes an increase or decrease in the precessional frequency of spins (as stated by the Larmor equation) at different locations along the linear gradient. Gradients cause hydrogen nuclei to speed up or slow down depending making it possible to rephrase or dephase spins depending on their position.

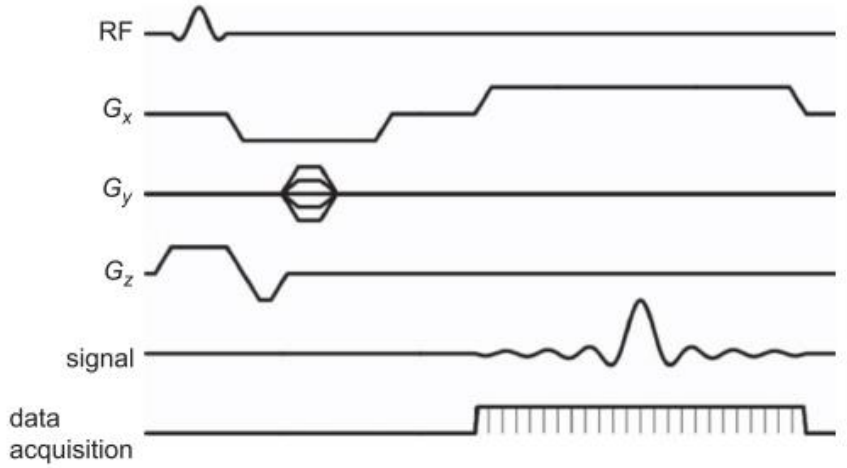

Figure 2.5 Gradient echo pulse sequence. Image adapted from "Introduction to Functional Magnetic Resonance Imaging" Figure 9.7.

Comparison of Spin and Gradient Echo Sequences		
Echo Type	**Pros**	**Cons**
Spin Echo	Better tissue contrast, reduced sensitivity to artifacts	Longer acquisition time
Gradient Echo	Fast acquisition, shorter possible TR and TE	T2* cannot be eliminated, magnetic susceptibility and chemical shift artifacts

Table 2.2 Comparison of spin echo and gradient echo sequences

2.7 The Blood Oxygen Level Dependent (BOLD) Signal

To recap from section 2.2, the transverse relaxation rate T2, is the time constant for phase coherence loss among spins oriented at a given angle to the static magnetic field due to spin-spin interaction. This process causes a loss of transverse magnetisation and MRI signal decay. T2* accounts for the additional signal loss due to magnetic field inhomogeneity and this process is exploited in BOLD-weighted imaging. Note, T2 is always greater than T2*.

Sensitivity to blood oxygenation arises in T2*-weighted MRI because the image intensity is generally subject to attenuation caused by deoxyhaemoglobin (dHb), a paramagnetic relaxation enhancer introduced into venous blood vessels as tissues extract oxygen during aerobic metabolism. Increasing the concentration of oxygenated blood in tissue leads to dilution of venous dHb, reducing the attenuation of the T2*-weighted signal. The subsequent increase in signal intensity is referred to as the BOLD response. However, increases in CBF also cause compliant venous vessels to dilate and increase the tissue volume fraction occupied by dHb. This partially counteracts the diluting effect of the CBF increase. If the rise in CBF is due to neuronal activity, as assumed in the explanation above, then the rise in the cerebral metabolic rate of oxygen consumption $CMRO_2$ and oxygen extraction fraction (OEF) of tissue will accelerate the production of dHb and further counteract the dilution effect (Hoge et al., 1999). The BOLD signal is reliant on the fact that the CBF increase following a neural stimulus is typically over twice the increase in $CMRO_2$ (Fox & Raichle, 1986). As neural activity and CBF increase, the fraction of oxygen extracted by tissue decreases, and this phenomenon forms the basis of BOLD. The dHb reduction with higher regional venous oxygenation due to OEF reductions leads to an increase in the BOLD signal (Buxton, 2013). BOLD is an indirect measure of neuronal activity, but has been a key tool in studying functional networks due to its superior ability to localise resting state functional connectivity and evoked responses.

In comparison to ASL, BOLD has a much higher SNR, making it easier to detect very small changes, especially in sub-cortical and frontal regions which can suffer from signal dropout and blurring (Detre & Wang, 2002). A main limitation of BOLD is that it is not possible to quantify activity changes due to its reliance on the relative mismatch between CBF and $CMRO_2$ upon neuronal activation. The BOLD signal is a complex interaction between changes in haematocrit, cerebral blood volume (CBV), CBF, OEF and $CMRO_2$, and contrast is dependent on signal decay resulting from changes in the amount of deoxyhaemoglobin present in the vasculature (Blockley, Griffeth, Simon, & Buxton, 2013). Signal dependence on the interplay between these physiological variables means that it is challenging to interpret the exact meaning of the BOLD signal in terms of brain function. If neuronal or vascular physiology is abnormal, then the BOLD signal is not reliable in determining group differences and the signal can be misleading where baseline physiology is altered (Iannetti & Wise, 2007). For example, a study is designed to compare BOLD responses in young versus older adults to a visual stimulus. CBF is known to decline with age so a significantly reduced BOLD signal may occur in the older group despite potentially unchanged neural activity. Alternatively, declining neural function may require

increased energy resources in this older group resulting in a similar or higher BOLD signal compared with the younger group. Either way, it is unclear from the BOLD signal alone whether electrical activity, vascular responses or both are causing the between group differences. Therefore, when investigating brain function in any group with suspected or known abnormal vascular physiology or neuronal function, it is helpful to acquire additional data to calibrate the BOLD signal and make meaningful conclusions about data.

Another limitation of BOLD is the effect of the draining of dhb from capillaries to veins on spatial specificity. This issue is most pronounced in studies which elicit a large BOLD response as a portion of the blood draining into large vessels downstream of activation will have originated in the activated area and combine with blood draining from other activated regions, meaning that there will be a measured BOLD response from both the site of activation and larger downstream vessels. When the true area of activation is small, dhb is diluted with blood from non-activated areas quite quickly which reduces the non-specific signal (Kim & Ogawa, 2012). To overcome this problem, a high statistical threshold can be used in analysis to select the most strongly activated areas, or predefine regions of interest (ROIs). Alternatively, where simultaneous BOLD and ASL data have been acquired (see 2.10), the overlap of responses can be selected as the ROI, as the ASL signal does not suffer from this draining vein contribution. Lastly, the susceptibility to physiological noise (see 2.17) and thermal noise caused by the motion of free electrons in the system, makes BOLD non-specific in terms of neuronal activity (Ugurbil, 2016).

Despite these limitations, BOLD is a useful tool in quantitative fMRI, as demonstrated in this thesis, where calibrated fMRI (see 2.13) can be used alongside ASL to determine relative changes in $CMRO_2$, as well as determining the baseline OEF (OEF_0) and CBV. These applications are discussed in the following sections.

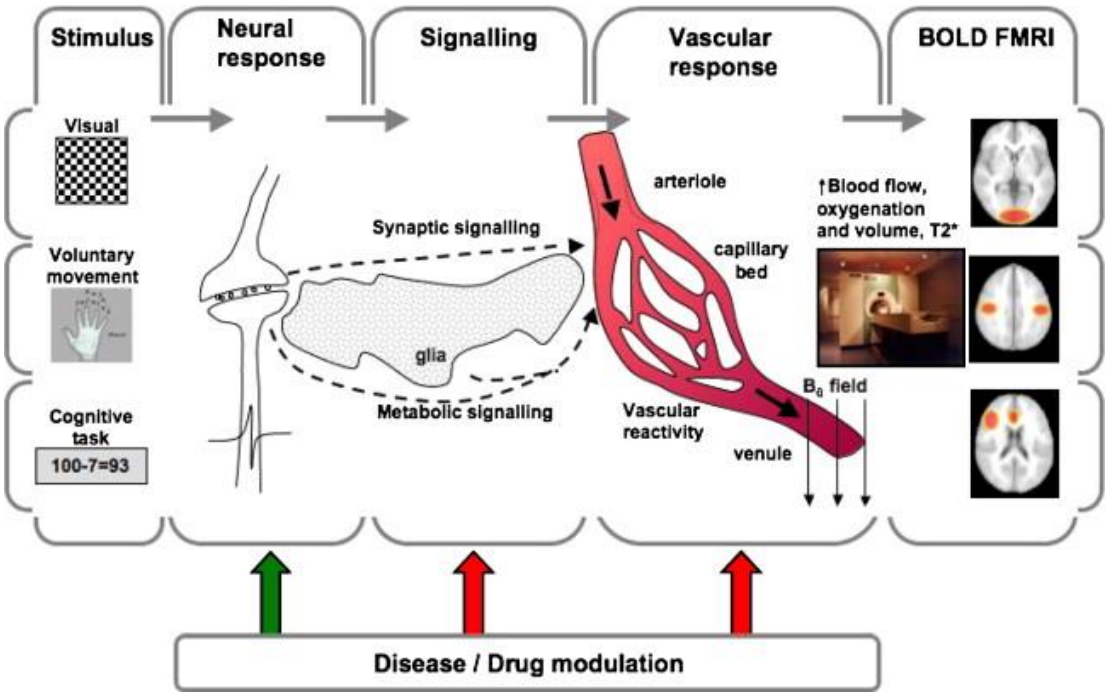

Figure 2.6 Diagram showing the components of the BOLD signal. Image taken from: Iannetti & Wise (2007).

2.8 Arterial Spin Labelling

CBF, which is quantified using ASL, is a direct measure of the amount of arterial blood delivered to a tissue element (Buxton, 2013). ASL permits quantitative measurement of CBF, non-invasively, using a diffusible endogenous tracer, arterial blood water. Water molecules in tissue constantly exchange with molecules in inflowing blood to capillaries. Magnetic labelling proximal to the tissue of interest is used to invert magnetisation of hydrogen protons in arterial water. After the labelled protons flow into the tissue through the capillaries the net magnetisation of the region is altered. Image intensity of the tissue is then altered as signal is proportional to the magnetisation present. A modified Bloch equation (Williams, Detrett, Leight, & Koretsky, 1992) can be used to explain the tissue magnetisation:

$$\frac{dM_b}{dt} = \frac{M_b^0}{T_{1b}} + \mathrm{p}_b f(M_a - M_v)$$

where M_b, M_a, and M_v represent magnetisation of brain tissue, arterial blood and venous blood respectively. M_b^0 is the equilibrium magnetisation in the absence of a RF pulse, T_{1b} is brain T1 (MR decay constant which is a function of magnetic field strength and tissue structure) and f is the perfusion. P_b is the density of the brain tissue and is relevant because perfusion or CBF is defined as the volume of blood being delivered to a tissue unit per minute, CBF is

conventionally denoted in ml/100g/min. As T_{1b} cannot be calculated precisely, absolute CBF is not calculated from the temporal dynamics of the signal alone. Rather, average difference images are calculated by subtracting images where magnetic inversion has been applied (tag images) from images acquired directly before or after the tagged image without magnetic inversion (control images). This subtraction improves the temporal stability of the images and is necessary for quantification of CBF. Relative CBF changes can be calculated if the magnetisation of tissue and arterial blood is different, for quantification, the magnetisation of arterial blood must be different between the tag and control images.

In ASL, the measured perfusion signal in the region of interest is extremely small relative to static background tissue, on the order of 1-4% (Shen & Duong, 2011). Although receiver coil development and moving to higher field strengths has improved ASL sensitivity, ASL still has lower SNR than BOLD, especially in populations where motion is difficult to minimise, i.e. patient groups. Coupled with noise arising from physiological fluctuations over time, background suppression of static tissue is an important consideration in ASL protocols and can substantially increase the sensitivity to dynamic changes in CBF (Petcharunpaisan, Ramalho, & Castillo, 2010).

Despite SNR limitations, ASL is more closely coupled to neuronal activity than BOLD as it directly reflects capillary blood. ASL is also more resistant to scanner drift than BOLD making it a superior technique for measuring changes in activity over long time scales (Olson et al., 2006) or between different physiological states separated in time e.g. drug vs. placebo activity (Wise & Tracey, 2006).

2.9 Types of ASL

There are two main ASL acquisition schemes, pulsed ASL (PASL) and continuous ASL (CASL), a variation of the latter, pseudocontinuous ASL (PCASL) now being more widely used. In PASL, labelling is achieved by applying a single pulse covering a slab of tissue (i.e. 10-20 cm) in the neck region so that all spins are excited instantaneously (figure 2.9). Arterial blood water is magnetically labelled below the lowest imaging slice using a 180° RF inversion pulse. This causes inversion of the net magnetisation of the water molecules in the labelled arterial blood. After a specified labelling duration and inversion time (TI), the magnetically labelled blood water flows into the slice of interest where it exchanges with tissue water. The inflowing blood water containing the inverted spins reduces overall tissue magnetisation and therefore signal intensity is also reduced. An image is acquired at this point, referred to as the tag image. A

control image without magnetic labelling is acquired before or after the tag image. The resulting dataset contains pairs of tag and control images which are then subtracted from each other to give the difference images which are perfusion weighted. Averaging the timeseries of images is carried out to obtain a mean perfusion map. The perfusion weighted image or images represents the amount of arterial blood delivered to voxels in the slice of interest within the TI, also called the post-labelling delay (PLD) time. In other words, the magnetisation difference between the tag and control images is proportional to the CBF in a voxel in the PLD period. Label timing dynamics have a considerable effect on the ASL signal amplitude. In PASL, techniques such as QUIPSS II (GE) and Q2TIPS (Siemens) are used to fix the bolus duration and reduce inaccuracies associated with changes in the label duration. QUIPSS II renders the labelled bolus time-dependent such that more spins are labelled when blood flow becomes faster (Wong, Buxton, & Frank, 1998). This is done by applying two extra saturation pulses to the labelled bolus to destroy any remaining inverted spins after the chosen TI. The TI effectively determines the label duration, i.e. following the TI, no more inverted spins leave labelled bolus.

This scheme is effective so long as the trailing edge of the tagged bolus does not exit the tagging region before saturation pulses are applied. However, the bolus may exit the tag region earlier during flow increases, such as with hypercapnia, as increased flow increases flow velocity in feeding arteries in the brain (Tancredi et al., 2012). This would result in QUIPSS II/Q2TIPS pulses becoming ineffective; CBF being underestimated during hypercapnia, where flow velocity increases occur, and is one potential limitation of QUIPSS II and Q2TIPS.

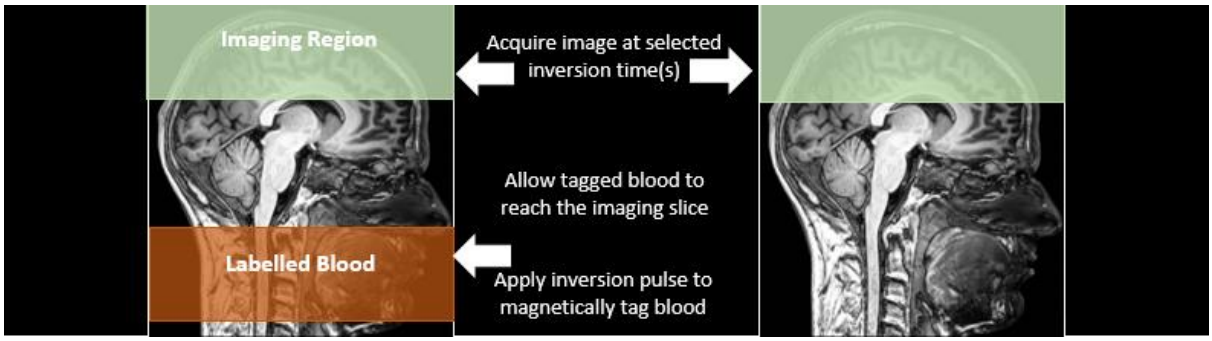

Figure 2.7 Schematic showing PASL acquisition scheme. With PASL a large slab of static and moving spins are tagged in one go before the image is acquired after the selected TI(s).

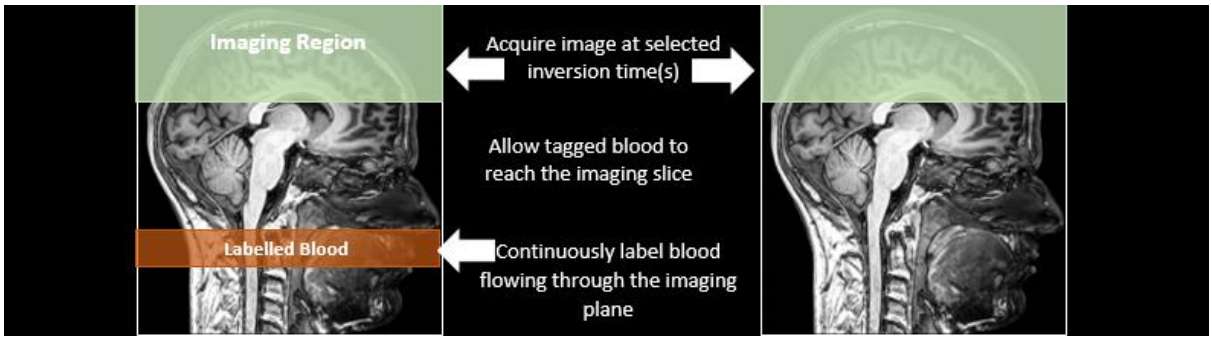

Figure 2.8 Schematic of CASL/PCASL acquisition where a narrow plane of blood is continuously tagged for a chosen duration and images collected after the selected TI(s).

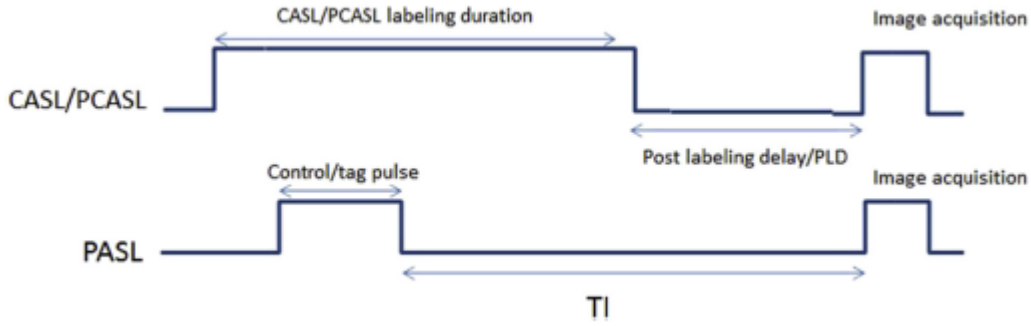

Figure 2.9 Pulse sequence designs for PCASL and PASL acquisitions. Figure adapted from Wong et al. (2016).

PASL is the most widely available ASL technique due to its relatively straightforward implementation and compatibility with existing MRI hardware. PCASL however, can offer some advantages over PASL. PCASL is an advancement of CASL where spins are continuously labelled as they flow through a narrow tagging band. The labelling scheme can be problematic due to the long RF duration (1-2s), putting high demand on the hardware and causing high specific absorption rates (SAR). To overcome this, PCASL was implemented which involves multiple short RF pulses in place of the single long pulse, making the label duration longer than in PASL.

PCASL may be beneficial for CBF quantification during hypercapnia as label duration is inherently controlled. The temporal duration of bolus labelling is longer in PCASL than PASL, meaning that a larger volume of labelled blood is delivered to tissue which increases SNR. PCASL also has higher flow contrast compared to PASL, providing increased temporal SNR (Tancredi et al., 2012) but as fewer images are acquired, power is reduced. A potential drawback of PCASL is that labelling efficiency is affected by flow velocity making CBF estimations under conditions with expected velocity changes less reliable. In PASL the

instantaneous labelling pulse reduces the sensitivity to velocity changes in the labelled plane (Aslan et al., 2010). However, a study by Tancredi et al., (2012) compared PASL and PCASL during CO_2 induced hypercapnia, visual stimulation and rest. Resting and visually-evoked CBF responses were comparable, however PCASL led to significantly higher estimates of cerebrovascular reactivity (CVR) to CO_2. The authors concluded that PCASL may be more sensitive to flow changes during hypercapnia, as label duration is controlled to a greater extent than PASL, where arterial velocity changes may affect the efficacy of QUIPSS II/Q2TIPS implementation. A greater number of voxels in GM were active for PCASL also; in sum, these results suggest that experiments using PCASL may benefit from higher SNR and labelling timing control. However, a degree of magnetisation transfer (MT) may have led to an overestimation of CBF rather than higher CBF being due to increased sensitivity of PCASL to measure flow.

A second limitation of PCASL, which can be overcome, is the potential for MT effects which arises from the repeated short RF pulses saturating protons in water macromolecules. These pulses, off-resonance to the tissue volume, cause spins to transfer saturation to water protons in the imaging slice which decreases the tissue signal in the labelled images. This would cause an overestimation of perfusion as signal from labelled images would be contaminated by MT-related signal reduction. To overcome this, gradients with higher amplitudes than used in CASL are necessary during labelling (Saba, 2016) which make the resonance offset of the RF pulses larger relative to the imaging region. This is an imperfect solution but MT effects are reduced to the point that they are not a systematic source of error in PCASL (Wong, 2014). Lastly, arrival times are longer in PCASL due to the greater distance from the labelling plane to the brain tissue which must be taken into consideration when comparing results achieved using PASL and PCASL. Table 2.3 summarises the strengths and limitations of each labelling scheme. In this thesis, both PASL and PCASL are used. Halfway through the thesis data collection, a move to a new imaging centre and vendor (GE to Siemens) means that PASL was used in 2 experiments, Chapters 3, 4 and 7, and PCASL in the remainder (Chapters 5, 8 and 9) as sequences analogous to those used in were no longer available. See figure 2.10 for example raw images and calibrated CBF maps from each scanner.

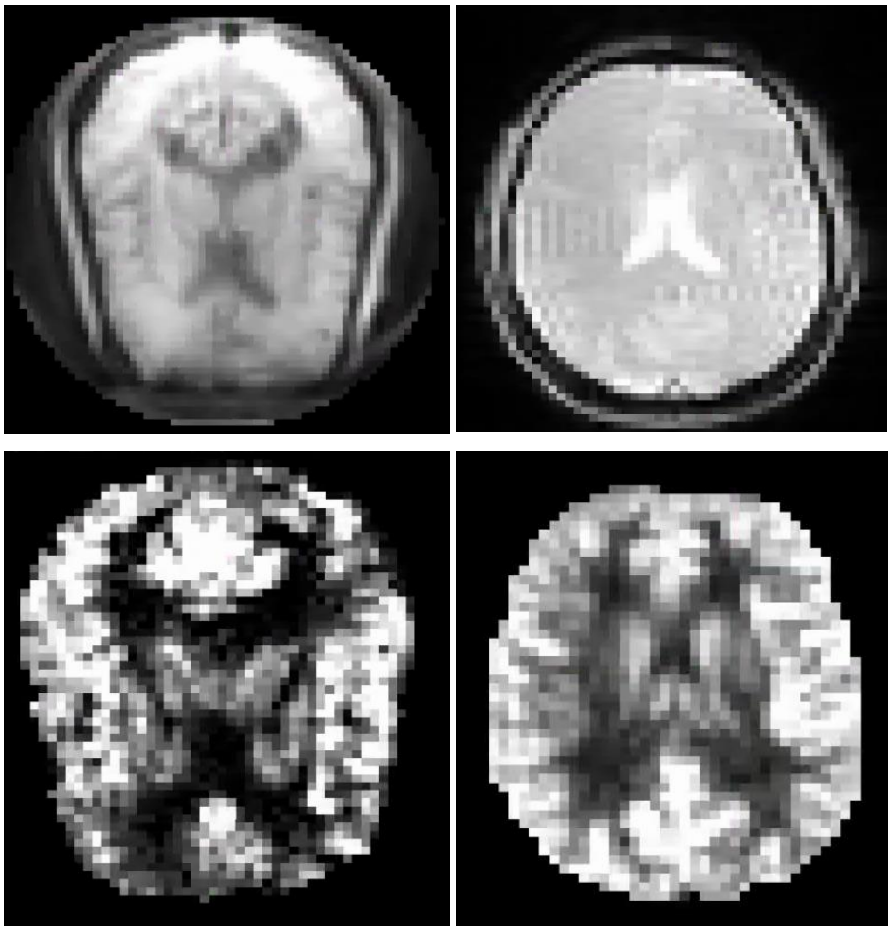

Figure 2.10 Raw first echo images from the dual-echo sequence used on the GE scanner (top left) and dual excitation sequence used on the Siemens scanner (top right). The bottom left image shows a CBF map from the GE scanner following pre-processing and on the right, a processed CBF map from the Siemens scanner. Details of the acquisition and processing of images are detailed in Chapters 4 (GE) and 5 (Siemens).

Comparison of ASL Strategies		
	Strengths	**Limitations**
PASL	Less sensitive to velocity changes	Lower labelling efficiency, missed perfusion
PCASL	Higher SNR and labelling efficiency.	Sensitive to velocity changes, some MT effects
CASL	Greater SNR vs. PASL, higher flow contrast and shorter TT delay	Higher SAR, lower inversion efficiency (80-95 %), MT effects

Table 2.3 MT = Magnetisation Transfer, RF = Radio Frequency, TT = transit time

Within PASL sequences there are three main methods of creating the tag and control images; Echo-Planar Imaging and Signal Targeting with Alternating Radio frequency (EPISTAR) (Edelman & Chen, 1998), Flow-sensitive Alternating Inversion Recovery (FAIR) (Kim & Tsekos, 1997) and Proximal Inversion with a Control for Off-Resonance Effects (PICORE) (Wong, Buxton & Frank, 1997). In EPISTAR, a wide inversion band is applied proximal to the lowest imaging slice prior to label image acquisition and the control image is acquired after the same band is inverted but this time distal to the imaging volume. In FAIR, there is a non-selective inversion pulse is applied to all spins (global inversion) for the tag image and the control image is acquired after a selective RF pulse is applied to the imaging slice. This means that during tag image acquisition, all hydrogen spins are inverted and all spins are fully relaxed during control image acquisition. In PICORE, the label image is acquired as in EPISTAR but the control is subsequently acquired with the same inversion pulse but without the slice selective gradient turned on. In PICORE, no spins are inverted above the imaging slice, making PICORE sensitive only in ascending flow, therefore, it is ideal for axial imaging where all labelled blood comes from the neck. For this reason, where PASL is used in this work, PICORE is the chosen labelling method. PCASL also uses PICORE, where tagging is applied proximal to the imaging plane and control images are acquired with the same pulse, but without the slice selective gradient.

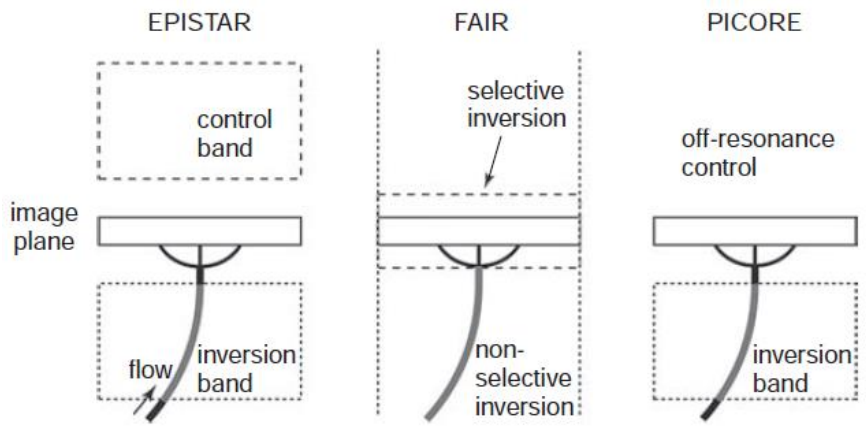

Figure 2.11 Labelling schemes for PASL. Image adapted from Introduction to Functional Magnetic Resonance Imaging by R.B. Buxton, Figure. 13.3.

2.10 Dual echo and Dual Excitation

In experiments where both BOLD and CBF data is required, such as calibrated fMRI studies, there are several acquisition options. BOLD and CBF data can be acquired separately using optimal parameters for each contrast, however this is not ideal as the data is not acquired

simultaneously which can introduce variability in data quality and physiological responses can change over short periods of time. The second option is to acquire data using a single-echo or single-excitation sequence where CBF and BOLD contrast is gained from one acquisition (Olson et al., 2006). In this approach, it is not possible to achieve both optimal CBF and BOLD contrast, so there will be a trade off in quality for either BOLD or CBF. Short TE will maximise CBF signal at the cost of BOLD image weighting but the longer TE required for BOLD will attenuate the perfusion signal. Dual-echo or dual-excitation approaches where the first short TE (9-13ms) generates CBF images and a second longer TE (29-35ms) yields BOLD-weighted images, provide better overall data quality where simultaneous BOLD and CBF signal is needed. As this results in longer acquisition times per slice, later acquired slices have a lower signal due to T1 relaxation. Whole brain coverage with high SNR is therefore difficult with dual-echo sequences but acquisition strategies such as spiral read-outs and partial-Fourier, where data is sampled from only a portion of k-space and used to reconstruct the full image, speed up image acquisition and can partially overcome this issue.

As an alternative to double-echo, double excitation methods have been developed where CBF data is collected at short TE followed immediately by a second excitation where BOLD data is collected at a longer TE. This means that CBF for all slices can be collected quickly following the inversion time and helps to overcome signal loss due to relaxation. One issue with double excitation ASL is the possibility of saturation from the CBF excitation affecting the BOLD excitation. Many initial studies using dual-excitation also had limited coverage (Kastrup, Kru, Neumann-haefelin, Glover, & Moseley, 2002) however, Schmithorst et al. (2014) introduced a whole brain coverage method using PCASL with a RF body coil for transmission and a 32-channel head coil for echo detection and sensitivity encoding (SENSE) reconstruction. Schmithorst et al. (2014) reported that the double-excitation method provided better SNR in the later acquired slices vs. the dual-echo method as well as BOLD signal sensitivity. Fernandez-Seara et al. (2016), in agreement with these findings, reported that dual-excitation provided superior temporal SNR (tSNR) for CBF data. BOLD tSNR was comparable to dual-echo but resulted in 30% lower t-scores on activation maps. However, for calibrated fMRI where high perfusion tSNR is necessary, the double-excitation method was preferable. A dual-excitation PCASL sequence developed in-house was used to acquire the data in Chapters 5, 8 and 9, which were acquired on the Siemens Prisma scanner.

2.11 Single and Multiple Inversion Time ASL

Most frequently, ASL data is acquired at a single inversion time (TI), usually within 1500-2000ms post labelling, when labelled blood will have reached tissue but significant signal decay has not yet occurred. This approach permits quantification of CBF using a single compartment kinetic model (Buxton et al., 1998) and generally yields reliable approximations of tissue CBF. However, arrival time of labelled blood to tissue may vary, due to age, disease, experimental conditions, or vascular geometry. In this case, imaging at a single delay time may over or underestimate perfusion. By acquiring perfusion images at multiple inversion times (MTIs) the kinetic curve of CBF can be fit to the data resulting in more accurate estimations of CBF as well as permitting estimation of arterial and tissue arrival times and the arterial cerebral blood volume (aCBV), providing short TIs are included in the protocol (Chappell et al., 2010). MTI data however, requires longer acquisition times to achieve sufficient images at each TI for acceptable SNR. For this reason, MTI imaging is best suited to resting state CBF estimates as task timings, other than visual stimulation or motor tapping, are unlikely to be compatible with MTI runs. In Chapter 3, CBF and CVR values achieved using single and MTI acquisitions are compared to determine differences in values achieved using each approach.

2.12 Quantification of Cerebral Haemodynamics

Tag and control ASL images, following subtraction, must be appropriately scaled to convert the perfusion signal to absolute CBF units (ml/100g/min). The general kinetic model (GKM) developed by Buxton and colleagues (Buxton et al., 1998) models the kinetics of CBF through vessels and tissue. Both PASL and PCASL can be quantified using this model with several modifications to the mathematical implementation. The GKM describes the amount of perfusion in a given voxel, based on 3 components; the delivery function, c(t) describes the amount of tagged blood arriving in a voxel at a time *t*, the residue function r(t) which is the amount of tagged blood remaining in a voxel at time t, and the relaxation function m(t) which is the remaining longitudinal relaxation of tagged blood after time *t*. The original GKM assumes that all signal arises from a single compartment, i.e. tissue, which is not always the case. Tagged blood must flow through the intravascular compartment, arteries, before reaching the extravascular compartment, tissue, which is where the signal of interest generally lies.

In using MTI imaging, a dual compartment model can be fit to the data which makes it possible to model signal arising from both arterial and tissue sources. Chappell et al. (2010) extended the GKM of Buxton et al. (1998) to allow fitting and removal of an arterial signal component

from perfusion estimates. Two-compartment models can provide more accurate estimates of perfusion, as single compartment models can either under or overestimate perfusion at high and low flow rates, respectively (Parkes, 2005). However, MTI imaging is not always appropriate, or available, as discussed above. Where calibrated fMRI is performed, separate MTI acquisitions can be acquired to achieve the most accurate estimates of baseline perfusion.

2.13 Calibrated FMRI

The BOLD signal arises from the mismatch between CBF and $CMRO_2$ increases as discussed in 2.7, therefore relative changes in $CMRO_2$ in response to a task can be calculated from BOLD and CBF CVR, measured during hypercapnia or hyperoxia, as well as during the task or stimulus of interest (Davis, Kwong, Weisskoff, & Rosen, 1998a; Hoge et al., 1999). Hypercapnic calibration, which is most widely used, provides an estimate of the theoretical maximum BOLD signal *M*, assuming a full washout of dhb, for the measured baseline state. This calibration factor can also help to account for between-subject differences in baseline physiology.

Hypercapnia is achieved by increasing the inspired level of CO_2, as blood flow is sensitive to changes in arterial CO_2; CBF and CBV will increase to maintain optimal gas concentrations. Calibrated fMRI is based on the premise that CVR to CO_2 is isometabolic and elicits a purely vascular response through a reduction in dhb, and although this assumption has been challenged (Driver, Wise, Murphy, & Driver, 2017), Bulte et al. (2012) have previously shown only small changes in $CMRO_2$ at the mild levels of hypercapnia (typically raising the partial pressure of end-tidal CO_2 ($P_{ET}CO_2$) by 5-7 mmHg) generally used in calibrated fMRI which had no meaningful effect on end results.

Estimates of BOLD and CBF CVR and task responses as well as *M* can then be entered into a BOLD signal calibration model originally developed by Davis, Kwong, Weisskoff, & Rosen (1998a) to interpret the BOLD signal in terms of the oxygen metabolism changes in response to a task or neuronal stimulus. This thesis uses the calibrated fMRI approach originally proposed by Davis et al. (1998), with optimised parameters for grey matter at 3T in Chapter 7 to estimate relative $CMRO_2$ ($rCMRO_2$) changes during a motor sequence learning task. In this method, CBV is not known, therefore CBV changes are estimated from CBF changes using the Grubb equation (Grubb, 1974) with a constant exponent representing the CBF-CBV relationship.

The main limitations of standard calibrated fMRI approaches are the reliance on relative changes and the sensitivity of the model to noise. Interpreting relative changes in $CMRO_2$ can be problematic, as with standard BOLD, where the baseline $CMRO_2$ is affected by drugs or disease, however calibrated fMRI still provides additional information to BOLD alone as the vascular (CBF) and metabolic ($rCMRO_2$) responses can be separated to infer physiological meaning of the direction of BOLD signal change.

Propagation of noise is a more difficult problem to overcome; errors in CVR calculations feed forward into inaccurate *M* values and affect end results. Despite these limitations, the original calibration model has proved to be robust and accurate under most applications where good quality CVR estimates can be obtained.

To overcome the limitations of standard calibrated fMRI, dual-calibrated fMRI which uses hypercapnia and hyperoxia to modulate CBF and venous oxygenation was introduced (Bulte et al., 2012;Gauthier & Hoge, 2013; Wise et al., 2013). With hypercapnia, the CBF and BOLD signal is increased with an assumed constant $CMRO_2$, whereas in hyperoxia the increase in venous oxygenation increases BOLD signal, leaving CBF and $CMRO_2$ relatively unchanged.

Biophysical modelling (Bulte et al., 2012; Gauthier & Hoge, 2013; Germuska et al., 2016) of BOLD and CBF data acquired during blocks of interleaved hypercapnia and hyperoxia as well as a normocapnic baseline, thus permits detailed quantification of cerebral haemodynamics and oxygen utilisation. Using dual-calibrated (hyperoxia and hypercapnia), dual-excitation ASL, as demonstrated in Chapters 5 and 9, baseline CBF, OEF, CVR, CBVcap and **absolute** $CMRO_2$ can be estimated using the physiological forward model developed by Germuska et al. (2016). The model also uses an optimised BOLD signal model which is sensitive to the capillary blood flow compartment (Merola et al., 2016) so that capillary blood flow (CBVcap) can also be estimated.

These measures may be particularly useful for detecting subtle differences in cerebrovascular function, for example where there is adequate blood supply to tissue but the ability to efficiently extract and use oxygen from blood is affected. In this thesis, measures of OEF, CBVcap and absolute $CMRO_2$ are used as measure of brain function in addition to CBF and CVR, first in healthy subjects and later to investigate functional changes in MS. Cerebral metabolic dysfunction may contribute to disease progression and clinical disability as neurons require a constant supply of energy to survive, therefore regional mapping of metabolic function may identify specific regions of pathology, an advancement on previous methods estimating global metabolism through venous oxygenation (Ge et al., 2012).

2.14 Measurement of Cerebrovascular Reactivity

In situations where only arterial CO_2 is being manipulated, breath-hold tasks (Murphy, Harris, & Wise, 2011) are commonly used as a convenient and fast way to measure CVR. Participants are instructed to hold their breath for multiple 15-20 second periods followed by recovery blocks where breathing is paced. This process is typically repeated for 5-10 breath-hold periods to accurately model the peak $P_{ET}CO_2$. It is vital that participants exhale at the end of the breath-hold so that this can be measured. As a result, breath-hold tasks rely on the participant being well trained and having the capacity to carry out the task as instructed. The breath-hold method can lead to poor estimates of CVR or loss of data in non-compliant groups. It is also impossible to control the increase in $P_{ET}CO_2$ which may not be enough to cause a measurable CBF increase, especially if the breath-hold is not properly performed. However, in healthy well instructed cohorts breath-holding is feasible and repeatable (Lipp, Murphy, Caseras, & Wise, 2013).

CO_2 administration, however, is the preferred method as direct manipulation of inspired gases means that it is possible to achieve tighter control of $P_{ET}CO_2$ modulation and there is less reliance on the participant's ability to comply with instructions. Throughout this thesis gas challenges are used instead of breath-holding. Gas challenges can be carried out in several ways (Tancredi & Hoge, 2013). The first method is to use manual flow-meters where a researcher can dynamically adapt gas flow rates to achieve the required end-tidal values e.g. a 7 mmHg increase in $P_{ET}CO_2$. This works well as there is individual variation in the response to CO_2. However, inconsistencies in the timing of gas administration can occur making it difficult to accurately model periods of hypercapnia and normocapnia. Second, this method is only feasible where either hypercapnia or hyperoxia is induced as attempting to control the switch between conditions would be lengthy and imprecise. Alternatively, gases can be delivered

using the fixed-inspired (FI) method where pre-programmed gas mixtures are delivered at specified timings and flow rates. While this method ensures correct block timings, it can result in greater individual differences in $P_{ET}CO_2$ and fMRI responses due to differences in sensitivity to CO_2 or O_2. However, in experiments which use dual-calibration techniques automatic gas delivery systems allow rapid switching between hypercapnia and hyperoxia using additional gas mixtures which speed transitions e.g. during hyperoxia blocks, 50% O_2 is administered to participants, but short periods of 100% O_2 following hypercapnia speed the transition to hyperoxia.

Although gas challenges provide a more reliable vasoactive stimulus, they are not trivial to do. Gas experiments involve a high cost, considerable set up time and many sites require a trained physician present during experiments. In addition, a portion of individuals will not tolerate hypercapnia as it can cause feelings of anxiety and breathlessness. However, as demonstrated in Chapter 9, some patient groups will be able to tolerate hypercapnia. In situations where gas challenges are not feasible, breath-holding or hyperventilation are useful alternatives.

In several experiments in healthy controls (Chapters 4 and 7) manual flowmeters were used to control gas mixtures as achieving similar $P_{ET}CO_2$ levels across subjects was prioritised. Other experiments (Chapters 5 and 9) using dual-calibration with hypercapnia and hyperoxia necessitated the use of the FI method to achieve quick and smooth transitions between hypercapnia and hyperoxia.

2.15 Signal Contamination in BOLD and ASL

Although BOLD and ASL provide detailed insight into brain function, several sources of noise can contaminate the fMRI signal and confound results, especially where noise has a similar spatial or temporal pattern to the signal of interest. As well as artefacts caused by head motion, BOLD baseline drift and magnetic susceptibility near bone and air cavities (Kim & Ogawa, 2012). It is known that fluctuations in respiratory and cardiac cycles and arterial CO_2 can heavily influence the fMRI signal; this is true for BOLD and CBF data (Bright & Murphy, 2015; Murphy, Birn, & Bandettini, 2013; Wise, Ide, Poulin, & Tracey, 2004). Vasomotion due to low-frequency oscillations (< 0.1Hz) (Murphy et al., 2013) exists throughout the body and can influence the resting state signal and lead to spurious correlations with task paradigms. Blood pressure fluctuations and cerebral autoregulation processes can introduce similar confounds (Murphy & Fox, 2017). Methods to correct for physiological noise have been implemented including retrospective image correction (RETROICOR) of physiological motion effects (Glover, Li, & Ress,

2000). RETROICOR regresses out cardiac and respiratory phase information and is now a standard step in BOLD pre-processing. RETROICOR has less effect on ASL signal quality, and if used, is best applied to data before subtraction (Chen, Jann & Wang, 2015). Alternative noise removal techniques are available, such as global signal regression (Desjardins, Kiehl, & Liddle, 2001) developed for resting state data, however, global signal will likely contain neuronal as well as physiological signal and may bias BOLD and CBF measures (Murphy & Fox, 2017). Any physiological noise correction method should be used with caution and with regard to the signals of interest as it is likely that both neuronal and physiological information will be removed due to common frequencies.

Simpler approaches which carry less risk of removing neural signal, include using the CO_2 trace only, which has the most significant effect on the fMRI signal, as a nuisance regressor in a GLM analysis. Alternatively, data can be normalised using CO_2 which may reveal effects masked by CO_2 differences, for example average CO_2 may change following motor training and lead to inaccurate interpretations of CBF differences. This latter approach was used in Chapter 8 where CBF changes following motor sequence learning were investigated, although RETROICOR was used in earlier experiments (Chapters 3, 4 and 7).

2.16 Summary Comparison of BOLD and ASL

Table 2.4 summarises the relative advantages and limitations of BOLD and ASL which have been outlined in this chapter. BOLD and ASL are complementary techniques and when used together with physiological and mathematical models, provide quantitative estimates of oxygen extraction and metabolism, not possible with BOLD or CBF-weighted imaging alone. The focus of this thesis was to quantify cerebrovascular and metabolic processes, either in relation to aerobic fitness levels or motor plasticity, although certain paradigms necessitate the use of relative estimates of flow and metabolism, such as in Chapter 7. As the work in this thesis was conducted with intentions for clinical applications, quantitative or semi-quantitative (standard calibrated fMRI) measurements were used to overcome difficulties in interpreting standalone measure of relative BOLD changes. While CBF is the main quantitative measure of brain health, additional investigation of vascular reserve, blood volume and oxygen metabolism may provide more sensitive measures of function which may help to determine both the mechanisms underlying the proposed benefits of physical fitness on brain health, and which facilitate plasticity. Establishing neurobiological effects of physical fitness, and motor training in relation to plasticity in the healthy brain will help to identify informative markers of dysfunction, capacity for plasticity and functional recovery in MS.

Overview of BOLD and ASL		
	BOLD	**ASL**
Signal Source	CBF, CBV, $CMRO_2$	CBF
Vascular Specificity	Venules, draining veins	Capillaries, arterioles
Contrast Parameter	T2*	T1
Intersubject Variability	High	Low
Advantages	Good spatial resolution Widely available Whole brain coverage achieved more easily	Quantitative More direct measure of neural activity High repeatability, suited to longitudinal studies Good spatial specificity and signal stability
Limitations	Qualitative Interpretation complicated by vascular dysfunction Baseline drift over longer periods Susceptibility artefacts, lower spatial specificity	Lower spatial resolution and SNR than BOLD Vascular (arterial) artefacts due to TT differences Whole brain coverage challenging

Table 2.4 Summary of the relative advantages and disadvantages of BOLD and ASL. Adapted from Detre & Wang (2002). TT = transit time.

2.17 Overview of Statistical Approaches

2.1.1 Sample Sizes

A-priori sample size calculations were not carried out but were instead based on previous sample sizes used in studies of a similar nature, as well as necessary considerations of time and cost involved. As the studies, were addressing novel questions, the expected effect size was not known, thus a-priori calculations were not carried out. However, the observed effect sizes can be used to inform future a-priori calculations for similar studies.

2.1.2 Multiple Comparison Corrections

To correct for multiple comparisons, several approaches were used throughout the experimental chapters based on the type of data in question and software being used for statistical analysis.

For voxelwise data, multiple comparisons were corrected for using the false discovery rate (FDR), which is automatically applied within FSL's FEAT (https://www.fmrib.ox.ac.uk/fsl) package. FDR limits the number of false positives found across the brain, and as it is sensitive to the p-value distribution across all voxels, depends on the level of signal present making it a widely used strategy in voxelwise imaging analysis.

For investigating correlations between fMRI ROI data and behavioural, demographic or other physiological measures such as VO_2peak in Chapters 4 and 5, permutation testing was used when multiple correlations between potentially related variables were being compared. The rationale for this approach was that Bonferroni is extremely conservative when variables are likely to co-vary. FSL's Randomise (https://www.fmrib.ox.ac.uk/fs) was used in Chapters 4 and 5 for voxelwise data, and as it uses a permutation approach, similar corrections were used within these chapters for ROI and behavioural data.

Paired t-tests with bootstrapping (95% CIs, 1000 samples) were used when comparing data from the same subjects at two timepoints. Bootstrapping, like permutation testing aids appropriate data interpretation where sample sizes are small, and is robust where data does not follow a normal distribution. Where more than two conditions or variables where being tested for significant differences, ANOVAs were chosen as the most appropriate test. Bonferroni corrections were used for ANOVAs carried out within SPSS as this is an accepted correction approach for this test. Further, errors can occur using permutation testing with factorial ANOVAs as it is not always clear what data should be permuted.

For parametric tests, normality was assessed using the Shapiro-Wilk test. Mauchley's test for sphericity was carried out to test for variance homogeneity and degrees of freedom were corrected using the Greenhouse-Geisser method where the data did not meet the assumption of homogeneity of variances.

Although multiple comparison correction methods differed throughout this thesis, approaches were not mixed within the same analysis and appropriate methods were chosen for each test, with the intention of choosing the most sensible approach for each analysis.

2.1.3 Outliers

As the observed data variability was physiologically plausible in most cases (see Chapter 7, discussion), it was decided that the typical approach of discarding data >3 standard deviations from the mean was not appropriate here, and variability in parameters such as CBF and oxygen metabolism with fitness and during learning is not well established in young adults. An exception to this strategy was made for CVR data in Chapter 3, where 1 subject was removed for this reason. As CVR is relatively homogenous at 5% hypercapnia in healthy subjects, the data was considered a true outlier.

Elsewhere, data not considered physiologically plausible was removed, such as in Chapter 7 where a subject with a large BOLD calibration factor of 40%, this value is typically under 12% in healthy controls.

Chapter 3

Evaluation of the effects of partial volume correction and kinetic model parameters on PASL estimates CBF and CVR

Abstract

There are several potential pitfalls in ASL experiments which if not addressed could lead to incorrect quantification of CBF and CVR. These include; partial volume (PV) effects, selection of post-labelling delays and kinetic model implementation. The aim of this investigation was to establish the most appropriate ASL acquisition and analysis approaches for the studies in this thesis.

To summarise, this investigation was motivated by three main questions;

- **Does partial volume correction (PVC) improve CBF estimates in healthy cohorts and what effect does PVC have on data variability? Do the data support the use of PVC in healthy control studies?**
- **Is there a meaningful difference between multiple inversion time (MTI) and single inversion time (SiTI) estimates of CBF and CVR? What are the implications of using SiTI acquisitions where MTI is not available or practical?**
- **How different are results obtained from the same dual-compartment ASL kinetic model with Bayesian probabilistic fitting vs. a frequentist non-linear least squares (NLLS) fitting?**

The outcomes suggest that MTI should be used where feasible to obtain the most accurate perfusion estimates in healthy controls. PVC was not included in analysis of healthy subject data due to increased variability and noise introduced by registration error. The comparison between MTI and SiTI demonstrated that while SiTI yielded higher estimates of CBF, estimates were moderately to strongly correlated between the acquisitions. Given that MTI acquisitions are not feasible in dual-echo or task acquisitions in many cases, SiTI data must be acquired. Finally, a Bayesian framework rather than strict lower and upper limits on data is likely to result in more accurate estimations and reduce experimenter bias and uncertainty which could be introduced by setting limits arbitrarily.

3.1 Introduction

Arterial spin labelling (ASL) functional magnetic resonance imaging (fMRI) has a wide variety of applications in healthy individuals and patients as it permits non-invasive quantitative measures of cerebral blood flow (CBF). Cerebrovascular reactivity (CVR) is commonly estimated with the administration of CO_2 which has a vasodilatory effect on cerebral arteries, resulting in a global increase in CBF without, or with little change in oxygen metabolism. The cerebral rate of oxygen metabolism ($CMRO_2$) will be addressed in later chapters, as this chapter focuses on quantification of CBF and CVR.

CVR has been shown to be a reliable indicator of vascular reserve (Mark & Chen., 2015) and can be used to identify areas of damaged or at-risk tissue (Bouvier et al., 2014; Cantin et al., 2011; Richiardi et al., 2015) giving the technique direct clinical application. However, there are several potential pitfalls in ASL experiments which if not addressed could lead to incorrect quantification of CBF and CVR. These include; partial volume (PV) effects and the use of appropriate post-labelling delays, so that CBF and tissue arrival times of the labelled bolus are correctly estimated. As well as carefully choosing acquisition parameters, some thought should also be given to the implementation of the ASL kinetic model to ensure a good fit to the data. Each of these points are discussed below.

3.1.1 Single vs. Multiple Postlabelling delay sequences

ASL data can be acquired at a single delay time, also called single inversion time (herein referred to as SiTI), or using multiple inversion time (MTI) sequences which collect image volumes at a range of CBF inflow times. MTI sequences provide more detailed haemodynamic information, such as estimations of arterial cerebral blood volume (aCBV) and tissue arrival time (TAT) of the labelled blood bolus. In SiTI acquisitions, a single bolus arrival time must be assumed across the brain, although TAT is known to vary across the brain (Gallichan & Jezzard, 2009; MacIntosh et al., 2010). MTI acquisitions are recommended where absolute perfusion is of interest, as variations in TAT can lead to errors in CBF estimation. To establish the most appropriate acquisitions and analysis for further work in this thesis, this chapter compares SiTI and MTI ASL acquisitions. It was expected that MTI data would provide more accurate CBF and CVR estimation for the reasons mentioned above. However, as MTI acquisitions are not suited to certain study designs, and MTI imaging is not always available, CBF and CVR data were acquired for the same participants in the same session using MTI and SiTI acquisitions and were compared to investigate the relationship between values obtained using each method.

3.1.2 ASL Partial Volume Correction

ASL acquisition must be fast to image signal from the labelled blood before it returns to equilibrium. This speed comes at a cost to signal in later acquired slices and coupled with the large voxels required in ASL, overall image quality is compromised. Large voxels introduce PV effects which reduces the accuracy of CBF quantification. PV effects occur where multiple tissue types are present in a single voxel. As CBF is ~2-4 times lower in white matter (WM) than grey matter (GM) (Van Osch et al., 2009), CBF can be underestimated in voxels near boundaries between GM and WM (or CSF which has no true ASL signal). For example, a binary mask used to calculate CBF is typically thresholded to include all voxels with 50% GM probability and above and typically no correction is applied to account for other tissue types in voxels which will result in lower measured CBF. It should also be noted that as tissue flow is different between GM and WM, apparent flow may actually be tissue variability and not true blood flow (Borogovac & Asllani, 2012).

PV effects are more pronounced in subjects with brain atrophy. In older adults or patients with atrophy, compensatory hyperperfusion to the remaining tissue often occurs. Due to PV effects, this process may not be detected. CBF may then be inaccurately estimated as lower than controls because there is less overall tissue, not because there is less perfusion to remaining tissue. PV effects can also affect TAT estimations as the labelled blood takes ~2.5 times longer to reach WM than GM (MacIntosh et al., 2010).

Several partial volume correction (PVC) methods have been proposed for single and multiple inversion time ASL data. A local linear regression (LLR) method was proposed by Asllani et al. (2008). In this method, probability maps for GM and WM are created from a T1-weighted anatomical scan which is segmented and co-registered to the ASL image. Perfusion signal is then modelled as the sum of GM, WM and CSF contributions using linear regression with spatial regularisation. A criticism of this method is that it introduces spatial blurring due to the assumption of constant CBF over a specified region (Petr, Schramm, Hofheinz, Langner, & Van Den Hoff, 2013). This reduces spatial boundaries and is therefore not sensitive to regions of abnormal perfusion. Liang et al. (2013) developed a modification of this method using a least trimmed squares (LTS) regression to reduce spatial blurring. The authors used a sorting-based algorithm based on a prior that assumes all neighbouring voxels should have similar perfusion. Any sudden, large deviations in perfusion cause the voxel to be rejected from the regression model. In this method, voxels are selected based on the squared residuals of the voxel as opposed to a random with replacement approach making the LTS method more efficient and

reducing spatial blurring. Both LLR and LTS were developed for single delay data, but can in theory be applied to MTI data. An alternative correction method for MTI ASL was developed by Chappell et al. (2011) which uses Bayesian non-linear regression in an effort to reduce the blurring observed in LLR methods. PV estimates of GM, WM and CSF along with differences in GM and WM kinetics are used to determine the contribution of each tissue type in a voxel, with CSF signal always set to zero. Spatial smoothing is adaptive and defined from the data. In simulated as well as real data the method of Chappell et al. (2011) preserved spatial boundaries more effectively than LLR. The two methods were found to be comparable in terms of CBF estimation with a tendency for the Bayesian method to overestimate CBF.

However, the Bayesian non-linear regression method proposed by Chappell et al. (2011) is computationally intensive. In addition, the model uses several adaptive spatial priors which could result in over-fitting of the model and produce artificially high estimates of CBF. In this chapter, CBF and CVR estimates obtained using the CBF kinetic model proposed by Chappell et al. (2010) were compared following analysis without PVC and with the Bayesian PVC method (Chappell et al., 2011). To assess whether the Bayesian method may be prone to overfitting, a simplified PVC approach was also applied to the uncorrected data. This method assumes signal from CSF and WM to be 0 and a GM PV estimate map is used to scale CBF values. A second objective of the PVC comparison was to determine whether PVC increases data variability as it relies on accurate segmentation and registration of the T1 image used to create the tissue probability maps. As ASL SNR is low, an analysis method which increases variability would be counterproductive.

3.1.3 Quantification of CBF

CBF quantification can be carried out using single or dual-compartment models. Single compartment models (Buxton et al., 1998; Davis, Kwong, Weisskoff, & Rosen, 1998), as discussed in Chapter 2, model tissue and intravascular blood (IV) as one well mixed signal, whereas dual-compartment models (Chappell et al., 2010; Parkes & Tofts, 2002) consider tissue signal and the IV signal, comprising arterial blood, separately. One of the most commonly used dual-compartment models is that of Chappell et al. (2010) which is incorporated into Oxford ASL within the BASIL toolkit in FSL (www.fmrib.ox.ac.uk/fsl/basil). In its typical usage, this Bayesian model sets a mean prior value for aCBV, TAT, and a fixed bolus duration, typically 700ms. CBF is determined from the data with no prior assumptions, and the IV parameter is only fit where it is justified by the data. IV signal is then discarded from the estimated tissue perfusion value. This prior is set to have a mean of zero, as it assumes most

voxels will not have an IV signal component. The data itself determines whether an IV component is fit to each voxel; where variance is large or "non-informative", an arterial component can be included in the signal from that voxel. Where variance is small, or the data is physiologically "informative", only a tissue compartment is fit to the voxel. This data-driven approach to fitting an IV component contrasts with other dual-compartment models which automatically fit an IV component to each voxel.

The model described by Chappell et al. (2010) was used here to obtain quantitative CBF maps from SiTI and MTI data; Oxford ASL was developed primarily for MTI data but can be adapted for single delay data. The MTI data were then analysed using a dual-compartment model within Afni. Afni is an open source package for analysis and visualisation of fMRI data using C code and can be used instead of, or in combination with FSL tools for fMRI data analysis. Both models use the general kinetic model (GKM) of (Buxton et al., 1998) extended to include an arterial component, the main difference is that Afni fits an IV component to every voxel whereas the FSL toolkit only does this for voxels which display a large variance from the surrounding voxels. The output from each model was compared to determine the agreement between CBF and CVR values when similar values were used with different model implementations.

To summarise, this investigation was motivated by three main questions;

1. Does PVC improve CBF estimates in healthy cohorts and what effect does PVC have on data variability? Do the data support the use of PVC in healthy control studies?

2. Is there a meaningful difference between MTI and SiTI estimates of CBF and CVR? What are the implications of using SiTI acquisitions where MTI is not available or practical?

3. How different are results obtained from the same dual-compartment ASL kinetic model with Bayesian probabilistic fitting vs. a frequentist[2] non-linear least squares (NLLS) fitting?

[2] The main difference between Bayesian and frequentist non-linear parameter estimation is that frequentist methods produce best fit parameter estimates by sampling over the range of possible datasets defined by the given range of parameter values. Bayesian approaches use prior probability distributions to estimate the parameter (or posterior) probability distribution directly.

3.2 Methods

3.2.1 Participants

20 (11 females, mean age 25±4.6) healthy adults were recruited from advertisements placed around Cardiff University. The study was approved by the Cardiff University School of Psychology Research Ethics Committee and performed in accordance with the guidelines stated in the Cardiff University Research Framework (version 4.0, 2010). All participants were non-smokers, with no cardiac, neurological or respiratory diagnoses.

3.2.2 MRI Acquisition

Images were acquired on a 3T whole body MRI system (GE Excite HDx, Milwaukee, WI, USA) using an eight-channel receive-only head coil. Heart rate and cardiac traces were recorded using a pulse oximeter and respiratory bellows. A sampling line connected to the face mask of the breathing circuit was used to monitor end-tidal CO_2 and O_2 concentrations. The MEDRAD system (MEDRAD, Pittsburgh, PA) was used to monitor O_2 saturation throughout the experiment.

A T1-weighted 3D fast spoiled gradient echo (FSPGR) was acquired for registration of functional data and segmentation of tissue probability maps; TR/TE = 7.8/2.9ms, 1x1x1mm isotropic resolution.

3.2.3 MTI Image Acquisition

A single subtraction pulsed arterial spin labelling (PASL) PICORE QUIPSS II sequence (Wong et al., 1998) with a dual-echo gradient-echo readout (Liu et al., 2002) and spiral k-space acquisition (Glover, 1999) (non-commercial) was used. MTI data were collected at 8 inversion times; 400, 500, 600, 700, 1100, 1400, 1700 and 2000ms. QUIPSS-II cut-off at 700ms required that short and long inversion times be acquired in separate runs. 16 and 8 tag-control pairs were acquired for each short and long inversion time respectively. A variable TR was used for efficiency, minimum of 1100ms for short TIs and minimum of 1600ms for long TIs. Other acquisition parameters were; TE = 2.7ms, voxel size/gap = 7mm with 1.5mm gap, 3.1mm^2 in-plane resolution, matrix size 64x64mm, FOV = 198mm, flip angle = 90°, slice delay 55ms, 15 slices. Label thickness = 200mm with 10mm gap between the end of the label and the most proximal imaging slice.

A calibration image without labelling was acquired before the MTI with matched acquisition parameters, except TR = 4s; this was to obtain the equilibrium magnetisation of cerebrospinal

fluid (M_0, CSF), needed for the quantification of CBF. A minimal contrast image was acquired to correct for coil inhomogeneities with TR/TE = 2s/11ms. This protocol was performed twice, first during rest, then while volunteers were hypercapnic. The hypercapnia modulation was carried out using the prospective control method described by Tancredi & Hoge (2013). A gas mixing chamber had three feeding lines coming in for the delivery of medical air, 5% CO_2, and medical oxygen, the latter incorporated as a safety backup but not used during experimentation, the circuit is described in detail by Tancredi, Lajoie, & Hoge (2014). A target $P_{ET}CO_2$ elevation of 7mmHg using 5% CO_2 diluted in medical air was set and scanning began once participants reached the target elevation.

3.2.4 SiTI Acquisition

The SiTI sequence was performed following the FSPGR to allow end-tidal traces to return to baseline. This scan was a block design comprising 3x2 minutes of baseline, normal air inspiration, and 2x2 minutes of hypercapnia (see figure 3.1). A 7mmHg end-tidal CO_2 increase was targeted as before. The same dual-echo sequence described above was used but with imaging parameters adjusted to obtain acceptable BOLD weighted images from the second echo. BOLD data was acquired for a separate research question and is not used here. Imaging parameters were; TR = 2400ms, TE1/TE2 = 2.7/29ms, TI1/TI2 = 700/1500ms.

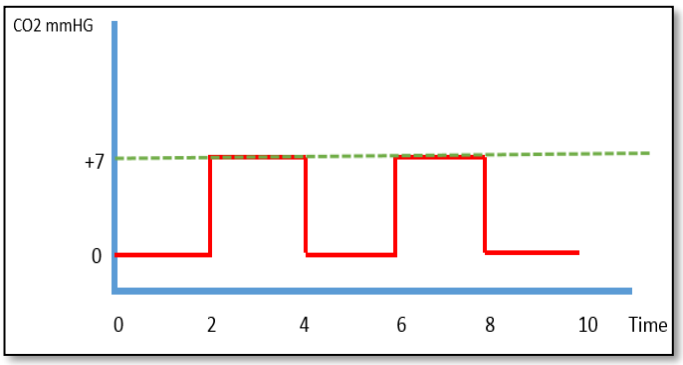

Figure 3.1 Hypercapnia protocol for the SiTI acquisition. Heart rate and oxygen saturation (O_2 sat) were monitored and recorded throughout the session.

3.3 Data Analysis

3.3.1 General Image Preprocessing

Physiological noise correction was carried out using a modified RETROICOR technique (Glover et al., 2000) to remove cardiac and respiratory noise components from the BOLD and CBF task

data. First and second harmonics of the respiratory and cardiac cycle along with the interaction term were regressed from the raw fMRI signal (before tag and control subtraction) in a GLM framework. In addition, slower variability related to respiration and heart rate (e.g. breath to breath variations in breathing depth and heart rate variability) were removed from the signal (Birn, Murphy, Handwerker & Bandettini, 2009). MTI data were motion corrected using MCFLIRT within FSL (FMRIB's Software Library, www.fmrib.ox.ac.uk/fsl, (Jenkinson, Bannister, Brady, & Smith, 2002). Interpolated surround subtraction of the first echo tag and control image time-series was performed to remove BOLD signal contamination. The interpolation method was chosen over pairwise subtraction as this method has been shown to perform better in block designs (Liu & Wong, 2005). Average difference images were obtained for each inversion time from tag-control subtraction of the CBF time series (Lu, Donahue, & Van Zijl, 2006). A total average image over all inversion times was created for MTI data at rest and separately for the hypercapnic acquisition. Average difference images were created for the SiTI data by averaging the 3 rest blocks and 2 hypercapnia blocks to create a resting CBF image and hypercapnic CBF image per subject.

3.3.2 MTI Analysis

MTI data were analysed using the dual-compartment ASL kinetic model, Oxford ASL, within FSL's BASIL toolkit (www.fmrib.ox.ac.uk/fsl/basil) (Chappell et al., 2010; Chappell, Groves, Whitcher, & Woolrich, 2009). As no coherent CSF signal should arise from the tag-control difference images the signal from CBF is assumed to be 0 in this model. IV signal was accounted for using an automatic relevancy determination (ARD) prior which removed the IV component from the model where the data did not support it. The perfusion images were corrected for coil sensitivity inhomogeneities using the minimal contrast images (Jinghua Wang, Qiu, & Constable, 2005) and converted to ml/100g/min using the CSF signal as a reference to estimate the fully relaxed magnetization of blood (Chalela et al., 2000).

Mean values for resting CBF and hypercapnic CBF were calculated for each subject by averaging the CBF time series over all time points and over all voxels within GM. CBF was calculated for whole brain GM using individual subject masks thresholded to include voxels with >50% GM probability.

This analysis was repeated with Bayesian PVC incorporated into the Oxford ASL kinetic model (Chappell, Groves, MacIntosh, et al., 2011). PVC is achieved through a multi-tissue component

model weighted by PV estimates of each tissue type and informed by the different kinetics of GM and WM. Spatial regularisation is applied based on the data to reduce spatial blurring.

A second simplified PVC method was applied to the SiTI and MTI perfusion maps from the first Oxford ASL analysis where the quantified perfusion map was scaled by the GM probability map. All voxels with GM probability of <50% were excluded from the GM map. This approach served as a comparison for the Bayesian PVC which incorporates WM CBF in the PVC algorithm.

To assess the robustness of the two PVC options, data were downsampled, the rationale being that lower resolution data would be more affected by PV effects, therefore the method which produced the lowest variance in results is likely to be more robust.

3.3.3 Kinetic model estimation using a non-linear framework

The MTI data, following pre-processing, were also analysed using a non-linear regression approach. This was carried out using the Afni NLfit programme (https://afni.nimh.nih.gov) using the same underlying kinetic model as that of Chappell et al. (2010). The NLfit model however, does not use a set of Bayesian priors, but instead fits the CBF model within a specified range of values for each parameter and an IV component is fit for all voxels. Unlike Oxford ASL, NLfit generates maps of the model fit (R^2) which can be used to evaluate the parameters used and discard data where the fit is poor, such as in areas of low signal. Two iterations of this model were carried out; the first used parameters as near to the Oxford ASL implementation as were achievable (referred to as NLfit A, see table 3.1), the second used a more liberal range of values (NLfit B) to assess the robustness of the model when parameters were free to vary to a greater degree.

Kinetic Model Parameters								
Model	CBF (ml/100g/min)	TAT (s)	aCBV (%)	AAT (s)	Bolus duration (s)	$T1_b$ (s)	Inversion efficiency	λ
Oxford ASL	Non-informative	0.7 (0.3)	0 - ARD	0.5 (0.3)	0.7	1.66	0.98	0.9
NLfit A	0 – 1000	0.4 – 1	0 – 3	0.2 – 0.8	0.7	1.7	0.98	0.9

NLfit B	0 – 1000	0 – 1.5	0 – 10	0 – 1.3	0.7	1.7	0.98	0.9

Table 3.1 Model parameters for each kinetic model implementation. Both models are two-compartment extensions of the original general kinetic model (Buxton et al., 1998). λ = Blood-brain partition coefficient. $T1_b$ = T1 of blood.

3.3.4 SiTI Analysis

SiTI data were analysed using Oxford ASL only which performs quantification on single delay data by assuming an arrival time of 0.7 seconds across the brain. Note that aCBV and variations in arrival time cannot be calculated for single delay data. PVC was applied in the same way as described for the MTI data.

3.3.5 CVR

For MTI data, CVR to CO_2 was calculated by dividing the percentage change increase in CBF during hypercapnia by the unit (mmHg) increase in $P_{ET}CO_2$ during hypercapnia. The CVR response for the SiTI acquisition was calculated using the CVR analysis method described by Bright & Murphy (2013) where the beta weight calculated for the CO_2 regressor derived from the end-tidal trace reflects the percentage CBF signal change caused by hypercapnia. This change is quantified in % signal change per mmHg unit increase in end-tidal CO_2. As the timing of the haemodynamic response is not uniform across the brain and there are delays in the physiological response to CO_2, the end-tidal CO_2 regressors were shifted per the best fit to the data, this was calculated by fitting 97 time shifts to the data.

3.3.6 Statistical Analysis

6 acquisition and analysis options with PASL were compared; 2 acquisition types (SiTI and MTI) and 3 PVC approaches; without PVC (woPVC), Bayesian PVC (bPVC) and simple PVC (sPVC) (figure 3.2). MTI and SiTI results were collapsed across acquisitions in (i the effects of each PVC on CBF ii) differences in MTI and SiTI CBF treated with the same PVC approach.

Coefficient of variance (CV) was calculated for group CBF and CVR values for each data type. The CV provides a metric to compare normalised variability between data types with significantly different means. To test whether the variance between any two methods was significantly different, *F*-tests of variance were performed. As there were many comparisons, the 2 groups with the largest CV difference per research question were compared first. If this difference was not significant no further *F*-tests were performed. If the difference was significant the groups with the next biggest CV difference were compared, and so on until the

F-test was not significant. The CV and *F*-test are slightly different measures, but, as both measure variance, the *F*-test was chosen to validate the CV values.

Statistical analysis was carried out using IBM SPSS Version 20.0, significant results are reported following Bonferroni corrections for multiple comparisons.

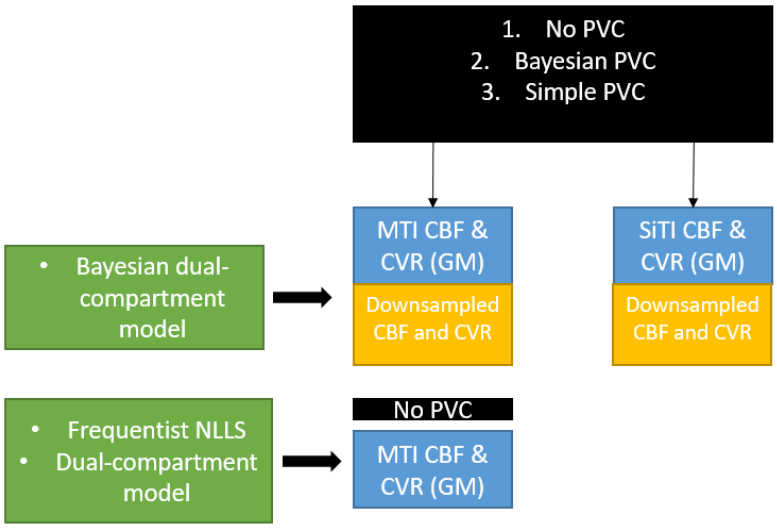

Figure 3.2 Diagram of PVC carried out for single and multiple delay data. This analysis was repeated on downsampled data to investigate how each PVC method handled the lower resolution data. Next MTI data without PVC were analysed using the same model implanted using a frequentist non-linear least squares approach.

3.4 Results

3.4.1 Effects of PVC and acquisition sequence on CBF and CVR

Data Type	rCBF ml/100g/min	rCBF CV %	hCBF ml/100g/min	hCBF CV %	CBF Change %	CVR %	CVR CV %
MTI woPVC	46.5 (8.6)	18.5	57.7 (10.2)	17.6	24.4 (8)	3.1 (0.9)	30.5
MTI bPVC	73 (15.6)	21.4	93.6 (22)	23.5	29 (18.1)	3.7 (2.3)	62.2
MTI sPVC	55.3 (10)	18	66.9 (15.69)	18.9	23.9 (10.24)	3.1 (1.2)	41.6
SiTI woPVC	60.9 (14.6)	23.40	72.1 (17.7)	23.92	18.5 (14)	3.3 (2)	58.2

Data Type	rCBF ml/100g/min	rCBF CV %	hCBF ml/100g/min	hCBF CV %	CBF Change %	CVR %	CVR CV %
SiTI bPVC	73.1 (19.3)	26.4	84.8 (22.4)	25.8	16.4 (9.3)	3 (1.4)	49.7
SiTI sPVC	87.3 (20.9)	24.0	103.5 (25.1)	23.6	15.1 (8.6)	3.3 (2)	58.8

Table 3.2 Group mean (sd) values for CBF and CVR derived from each acquisition and analysis method (CVR reported as % ΔCBF per unit Δend-tidal CO_2). r = rest, h = hypercapnia. CV = Coefficient of Variation. woPVC = without partial volume correction. bPVC = Bayesian partial volume correction. sPVC = Simple partial volume correction.

3.4.1.1 CBF and CVR differ per acquisition type and PVC method

For the 6 data types presented in table 3.2, there was a significant CBF increase during hypercapnia from rest; paired t-tests all significant at $p < 0.001$ (supplementary table 3.6). A repeated measures ANOVA (RM-ANOVA) revealed a significant effect of data type on rCBF Greenhouse-Geisser corrected $F(1.403, 26.652 = 57.3, p < 0.001)$.[3] Follow up comparisons revealed significant differences between all data types except MTI and SiTI CBF with bPVC ($p = 1.00$). MTI woPVC produced the lowest CBF values and SiTI with sPVC the highest (see table 3.2).

For hCBF, there was also a significant effect of data type, Greenhouse-Geisser corrected $F(1.834, 34.853, = 66.916, p < 0.001)$. Pairwise comparisons showed that again MTI woPVC produced significantly lower CBF values than any other method. SiTI with bPVC and sPVC were significantly higher than SiTI woPVC, both $p < 0.001$.

One outlier was removed from the SiTI CVR analysis as CVR was >3 standard deviations from the mean. A third RM-ANOVA revealed that CVR was not significantly different between any methods, $F(1.863, 35.404 = 0.731, p = 0.480)$.

[3] Greenhouse-Geisser correction was applied where Mauchley's test showed that the assumption of sphericity was violated.

3.4.1.2 Correlations

RCBF correlations were high within acquisition type (MTI or SiTI) but only moderate between acquisition types. For hCBF data, there were high, significant positive correlations between all data types (supplementary tables 3.7 and 3.8).

Moderate significant correlations were observed between MTI CVR estimates and strong significant correlations were found between SITI estimates (supplementary table 3.9). However, MTI and SiTI estimates were not correlated, despite no significant CVR differences between methods. The similar group average CVR disguised the fact that many subjects had very different CVR values when estimated using MTI vs. SiTI data (figure 3.3). This may have been due to data quality differences between acquisitions, as the SiTI data was acquired last in the protocol. Further, SiTI has been shown to overestimate CBF changes due to flow transit time changes upon neuronal activation which cannot be measured at a single inversion time (Van Osch, Hendrikse, Buchem, & Grond, 2007).

Although CO_2, is a primarily vascular stimulus, transit time changes occur as CBF increases regardless of neuronal activation. SiTI has less sensitivity to detect changes in activation as a result, however individual differences in vasculature may result in sensitivity differences between subjects. This would explain similar trends in some subjects across acquisitions but not others.

3.4.1.3 Variability

SiTI data were more variable than MTI, and bPVC had the highest CV for both MTI and SiTI in rCBF and hCBF. For rCBF, the largest CV difference between MTI bPVC and MTI sPVC was not significant, $F(19, 19 = 0.41, p = 0.06)$. Between SiTI methods, there was not a significant difference between SiTI woPVC and SiTI with bPVC, $F(19, 19 = 1.738, p = 0.237)$. The *F* statistics for MTI and SiTI data treated with the same PVC approach were computed. Significant differences in variance were observed for data woPVC, $F(19, 19 = 2.88, p = 0.025)$ and sPVC, $F(19, 19 = 4.41, p = 0.002)$ but not bPVC, $F(19, 19 = 1.528, p = 0.362)$.

For hCBF, variability between MTI woPVC and bPVC differed significantly, $F(19, 19 = 4.705, p = 0.001)$ and between bPVC and sPVC, $F(19, 19 = 2.88, p = 0.02)$ but not between MTI woPVC and sPVC, $F(19, 19 = 1.634, p = 0.294)$. For SiTI, there was not a significant difference between SiTI with bPVC and sPVC, $F(19, 19 = 0.79, p = 0.620)$. MTI and SiTI with bPVC data did not have significantly different variance $F(19, 19 = 1.03, p = 0.943)$, but SiTI had significantly more variance in bPVC data $F(19, 19 = 0.266, p = 0.005$ and data woPVC $F(19, 19 = 0.03, p = 0.019)$.

CV was much higher for CVR data than CBF, as expected due to the low SNR of ASL (table 3.2). For MTI data, bPVC data had a relatively high CV (62.2% vs. 41.6% and 30.5% for sPVC and woPVC) with significant variance between bPVC and sPVC $F(19, 19 = 3.25, p = 0.013)$ and woPVC $F(19, 19 = 5.817, p < 0.001)$. In SiTI data there were no significant differences in variability between PVC approaches, the largest difference between SiTI woPVC and sPVC was not significant, $F(19, 19 = 0.956, p = 0.923)$. Comparing MTI and SiTI data woPVC, MTI CVR had greater variance $F(19, 19 = 3.99, p = 0.004)$ as did MTI with bPVC $F(19, 19 = 2.508, p = 0.051)$. For sPVC, there was not a significant variance difference.

Based on these results, it was decided that MTI data woPVC should be used where possible given its lower variability for calculated CVR. However, the moderate to high CBF correlations between MTI and SiTI data and non-significant differences in % CVR suggest that SiTI acquisitions can provide adequate CBF and CVR estimates where absolute perfusion at the single subject level is not required.

3.4.2 Downsampled CBF and CVR with and without PVC

Downsampled Data	rCBF ml/100g/min	rCBF CV %	hCBF ml/100g/min	hCBF CV %	CBF Change %	CVR %	CVR CV %
MTI woPVC	32.8 (5.8)	17.9	40.5 (8.1)	19.7	23.5 (10.9)	3 (1.3)	42.5
MTI bPVC	52.9 (10.2)	19.3	65.4 (13.6)	20.8	23.7 (11.6)	3.1 (1.3)	43.7
MTI sPVC	47.9 (8.4)	17.6	59.1 (11.3)	19.2	23.6 (11.7)	3 (1.4)	44.6
SiTI woPVC	62.2 (15)	24.1	73.1 (14.3)	17.7	18 (11.4)	3.13(1.9)	49.1
SiTI bPVC	72.2 (17.9)	22.9	83.2 (20.7)	25	15.4 (8)	2.9 (1.4)	48.1
SiTI sPVC	103.3 (20.7)	20	123.4 (27)	22	19.1 (12)	3.3 (1.9)	54.2

Table 3.3 Mean (sd) shown. Data was downsampled by 1mm in each plane to compare the robustness of each PVC method. rCBF = Resting CBF. hCBF = Hypercapnic CBF

3.4.2.1 Effect of PVC on low resolution data

All images were resampled to a lower resolution, 4.5x4.5x8mm/1.5mm gap, to increase PV effects in GM. Paired t-tests were used to compare the original rCBF data with its downsampled counterpart. For MTI data, resampling resulted in significantly lower CBF (all $p < 0.001$). However, for SiTI data there was no significant difference between bPVC data before and after resampling ($p = 0.794$), however woPVC downsampled data was significantly lower, SiTI with sPVC was higher than data at the original resolution, both $p < 0.001$. For hCBF, downsampled CBF data was significantly lower, $p < 0.001$, except woPVC and sPVC SiTI data which was higher, $P < 0.001$. CVR did not differ between the original and downsampled data.

3.4.2.2 CV differences due to acquisition type and PVC

CV was generally lower for downsampled data. For MTI data CV was significantly higher for bPVC than woPVC, $F(19, 19 = 3.039, p = 0.019)$ but the difference was not significant between bPVC and sPVC $F(19, 19 = 2.072, p = 0.120)$. In SITI data the largest CV difference between SiTI woPVC and sPVC was not significant $F(19, 19 = 1.921, p = 0.163$. Comparing CV for MTI and SiTI, SiTI woPVC was significantly higher $F(19, 19 = 6.528, p < 0.001)$ as was sPVC $F(19, 19 = 6.052, p < 0.001$ and bPVC, $F(19, 19 = 3.08, p = 0.018)$.

MTI hCBF showed significantly greater variance in bPVC vs. uncorrected data $F(19, 19 = 2.876, p = 0.026)$ but not for bPVC vs. basic PVC $F(19, 19 = 2.017, p = 0.135)$. HCBF showed significantly higher variance for bPVC vs. sPVC in the SiTI data $F(19, 19 = 5.622, p < 0.001$, but not between bPVC and woPVC, $F(19, 19 = 2.409, p = 0.062)$. Comparing MTI and STI data, SiTI variance was significantly greater for data woPVC $F(19, 19 = 4.895, p < 0.001)$ and sPVC, $F(19, 19 = 5.667, p < 0.001$, but not bPVC data, $F(19, 19 = 2.337, p = 0.071)$.

For CVR, the CV was lower in downsampled datasets, except for MTI data woPVC correction (see tables 3.1 and 3.3). MTI CV was not significantly different between the data types with the biggest CV difference, bPVC and sPVC $F(19, 19 = 0.939, p = 0.892)$. SiTI CVs did not differ significantly, $F(19, 19 = 0.536, p = 0.184)$ between bPVC and sPVC. Comparing the CV between MTI and SiTI CVR, the biggest difference between SiTI with sPVC and MTI woPVC, the variance was not significantly different $F(19, 19 = 1.915, p = 0.165)$.

Downsampling the data showed that MTI data woPVC had less variance in most cases, but PVC had little effect on variance for SiTI CBF and CVR, and contrary to our predictions, downsampling the data did not identify the most robust PVC method of the two.

3.4.3 Buxton Model with IV component implemented using Oxford ASL and NLfit

Model	CBFr ml/100g/min	CBFr CV %	CBFh ml/100g/min	CBFh CV %	Change r to h %	CVR %	CVR CV %
Oxford ASL	46.5 (8.6)	18.5	57.7 (10.2)	17.6	24.4 (8)	3.1 (0.9)	30.5
NLfit A	60.8 (9.9)	16.2	76.6 (13.3)	17.3	19.6 (12.6)	1.8 (1)	59
NLfit B	63.5 (9.2)	14.5	79.7 (13.5)	16.8	20.2 (14.2)	1.8 (1.2)	70.3

Table 3.4 Mean(sd) CBF and CVR values for each kinetic model implementation. NLfit A was generated using values as close as achievable to the default implementation in Oxford ASL. NLfit B was generated using a wider range of parameter values for aCBV, TAT and AAT.

3.4.3.1 ANOVAs

There was a significant difference in rCBF between the 3 models, with Oxford ASL producing significantly lower values (all pairwise comparisons $p < 0.001$ following RM-ANOVA). For hCBF, significant differences were also found between Oxford ASL and NLfit A, $p = 0.026$, Oxford ASL and NLfit 3, $p < 0.001$, and NLfit A and NLfit B, $p < 0.001$. There were significant CVR differences; Oxford ASL produced the highest CVR values, Oxford ASL vs. NLfit A ($p = 0.003$), and vs. NLfit B ($p = 0.010$). NLfit A and B CVR did not differ significantly, $p = 0.580$.

3.4.3.2 Correlations

Moderate to high significant correlations were observed for all 3 models in rCBF and hCBF data with Oxford ASL and NLfit B having the highest correlation for both conditions, $r = .787$, $p < 0.001$ for rCBF, $r = .752$, $p < 0.001$ for hCBF (supplementary tables 3.10 and 3.11). In the CVR data, NLfit A and B were highly correlated, $r = .973$, $p < 0.001$, but Oxford ASL showed inverse non-significant correlations with NLfit A and B (supplementary table 3.12).

3.4.3.3 Variability

There was not a significant difference in variance between Oxford ASL and NLfit B, $F(19, 19 = 1.13$, $p = 0.78)$ for rCBF or hCBF, $F(19, 19 = 2.4, 0.060)$. For CVR, NLfit A and B CV was 1.9 and 2.3 times higher than Oxford ASL CV respectively. However, the variance differences were not

significant between Oxford ASL CVR and NLfit A CVR, $F(19, 19 = 0.816, p = 0.66)$ or NLfit B CVR, $F(19,19 = 0.653, p = 0.361)$.

3.4.4 Individual model parameter differences

Finally, the model fit (R^2) and AAT were compared between NLfit A and B, as Oxford ASL does not produce this information, aCBV and TAT were compared between all three models to investigate parameter differences affecting CBF values (table 3.5).

Model	rCBF	rTAT	raCBV %	rAAT	rR2	hCBF	hTAT	haCBV %	hAAT	hR2
Oxford ASL	46.5 (8.6)	0.8 (.03)	0.2 (0.06)	n/a	n/a	57.7 (10.2)	0.7 (.04)	0.2 (.09)	n/a	n/a
NLfit A	60.8 (9.9)	0.7 (.03)	1.4 (0.1)	0.39 (.02)	0.7 (.06)	76.6 (13.3)	0.6 (.04)	1.4 (.13)	0.4 (.02)	0.7 (.09)
NLfit B	63.5 (9.2)	0.7 (.07)	4.9 (0.3)	0.47 (.05)	0.76 (.05)	79.7 (13.4)	0.7 (.07)	5.1 (.4)	0.42 (.05)	0.8 (.09)

Table 3.5 Mean (SD) for each model parameter. NLfit A was generated using values as close as achievable to the default implementation using BASIL oxford ASL. NLfit B was generated using a wider range of model parameters.

There was a significant difference between all 3 models for resting aCBV (raCBV) and hypercapnic aCBV (haCBV), pairwise comparisons all $p < 0.001$ following RM-ANOVAs. Oxford ASL produced the lowest aCBV and where aCBV parameters were set within a wide range, values reached 5%, which is notably higher than literature values for GM.

RTAT and hTAT was also significantly different between the 3 models, all $p < 0.05$, Oxford ASL TAT estimates were longer at rest and during hypercapnia.

R^2 estimates of model fit were significantly lower for NLfit A where parameters were more tightly constrained, $p < 0.001$ for rest and hypercapnia. RAAT and hAAT were significantly longer for NLfit B, rest, $p < 0.001$, hypercapnia, $p < 0.004$.

3.4.5 Summary of main findings

There were three main aims of the data exploration presented here. First, to evaluate the effect of PVC on CBF and CVR estimates, second, to compare CBF and CVR estimates acquired using single vs. multiple delay ASL acquisitions and third, to compare CBF and CVR values

obtained using two software packages which use the same dual-compartment ASL kinetic model, but which implement the model differently.

- PVC increased CBF estimates for both MTI and SiTI data, and all CBF estimates were highly correlated for MTI and SiTI. Further, bPVC increased variability in MTI data in line with the greater variability seen in the SiTI data. Mean CVR was not affected by PVC, but PVC did increase variance in the MTI CVR data.
- Estimates of CBF produced by the SiTI data were significantly higher than MTI data with greater variability. However, values were highly correlated, suggesting reliable relative difference estimates between participants. SiTI and MTI CVR differences were not statistically significant, but CVR estimates were not correlated between the two acquisitions which may be due to differences in sensitivity to activation or data quality.
- Choice of model had a significant effect on CBF and CVR. Oxford ASL produced CBF estimates around ~30% lower and CVR estimates ~70% higher than a similar set of parameters in NLfit, and when NLfit was given a more liberal parameter range. CBF values were highly correlated between each implementation, indicating that where relative differences between subjects or groups are of interest, choice of model and exact parameters are less important. Group-level CVR estimates calculated from Oxford ASL were significantly higher than NLfit values and CVR did not correlate between the two models. Higher CBF values obtained with NLfit may explain the lower CVR overall, but not the lack of correlation. This may be due to much greater data variability (see table 3.4) introduced by the NLfit model.
- TAT was longer and aCBV was lower with Oxford ASL than both NLfit models. AAT was shorter with NLfit A and R^2 was higher with NLfit B where there was greater flexibility in the model fit.

3.5 Discussion

3.5.1 PVC

CBF is defined in terms of the volume of arterial blood delivered to a voxel of tissue in a unit time divided by the volume of the voxel (Buxton, 2013). Typical GM CBF in the human brain is approximately 40-60ml/100g/min at rest. Ml/100g/min is the standard unit used to report CBF but can be misleading as it assumes a mean brain density across all voxels (Petersen et al., 2006). This could introduce bias where brain volume and density differences are present,

therefore PVC methods aim to correct for differences in tissue types per voxel. While PVC does not correct directly for density differences, if a voxel contains only 50% GM due to atrophy for example, PVC will reflect this in the CBF calculation. PVC increased GM CBF in the data presented here, as expected (Asllani et al., 2008; Chappell et al., 2011; Liang et al., 2013), as WM, when classified as GM, lowers perfusion estimates. Also, as WM CBF is lower than in GM, if voxels with low CBF are falsely identified as grey matter it has the effect of inflating the CVR value. This effect could have led to false high CVR values, however in this sample CVR was not significantly different following PVC.

Here, mean rCBF without PVC and with sPVC fell within expected values for uncorrected data, and bPVC CBF was significantly higher than both. The same trend was present for hCBF, and the % CBF increase in the bPVC data was higher leading to slightly higher CVR. However, as CBF had higher variance, this had a notable effect on CVR calculated with this method, doubling the CV from the uncorrected data. PVC may reveal true variability in CBF not obvious in uncorrected data. It is also possible however, that errors in co-registration of segmented tissue maps to ASL data, coupled with the correction algorithm which also attempts to calculate WM CBF present in predominantly GM voxels, leads to overestimation of CBF. The sPVC method, which gives all WM CBF a value of 0, increased CBF to a lesser degree and may be more appropriate where GM CBF is of interest or where there is a low or unreliable WM signal.

In SiTI data, PVC again increased CBF, but sPVC produced higher values than bPVC. CV was higher for bPVC CBF but lowest for bPVC CVR. Interestingly, bPVC CBF was almost identical for SiTI and MTI data, whether this is by chance or to do with the algorithm used for PVC should be investigated further.

Downsampling the data was not as helpful as expected in terms of identifying which, if either, PVC method introduced more variance into low resolution data. Downsampling led to overall CBF reductions and reduced variability. The larger voxels may have blurred CBF differences and led to the data appearing more homogeneous, an issue which should be considered where spatial resolution is poor.

Until further PVC simulations and methodological comparisons are conducted, when calculating perfusion in healthy brains where atrophy and perfusion abnormalities are not expected, there is good reason to omit PVC from the analysis. PVC may add errors in the analysis due to registration imperfections, as the PVC is only as good as the co-registration and segmentation of T1 images. In several subjects in this analysis it was not possible to achieve

excellent registration. Alternative PVC methods which use only low resolution ASL data such as that proposed by Ahlgren, Wirestam, Petersen et al. (2014) could overcome reliance on exact co-registration. PVC should be explored further in groups with atrophy, as the benefits of PVC may outweigh the increased variability where perfusion is being compared to controls without atrophy. However, in studies with young healthy groups only, results suggest that PVC does not benefit the overall results.

3.5.2 Choice of post-labelling delay scheme

The difference between CBF and CVR values estimated using SiTI and MTI acquisitions was of interest as MTI sequences are not always available and it takes longer to acquire multiple averages, to achieve acceptable SNR. CBF values produced from SiTI ASL data were significantly higher, as expected. This is because using a single delay time can lead to arterial blood being modelled as tissue perfusion if the delay time is not long enough for all labelled blood to reach the tissue. Alternatively, where longer delay times are used, there is a risk of underestimating perfusion due to low SNR. The higher rCBF observed here for SiTI resulted in lower CVR estimates, although this difference was not statistically significant. The smaller increase in CBF during hypercapnia however, suggests that single delay methods have lower SNR and less sensitivity to detect CBF changes.

The arrival time of tagged blood to tissue, varies across the brain, and with ageing and disease. Imaging at a single time-point is not optimal for accurate perfusion quantification across the whole brain and in groups with heterogeneous perfusion abnormalities (Buxton et al., 1998). Imaging at multiple timepoints means that the kinetic curve can be sampled at a range of times which ideally will capture early and delayed perfusion, as well as estimating TAT. Changes in transit time of blood tissue can occur with activation, in this case during hypercapnia, meaning that the relative change between baseline and hypercapnic perfusion is less reliable when measured at only a single inversion time. In this study, the percentage increase in CBF during activation was not significantly different between the SiTI estimation of 19.3% and non-PVC MTI estimation of 24.4% $p > 0.05$. However, the degree of variability in the SiTI changes was much higher than in the MTI data, in studies with only small activation changes this could have a more serious impact on results.

To summarise, SiTI data produced higher CBF values with greater variability between subjects and a smaller CBF increase was detected during hypercapnia. This suggests that MTI acquisitions provide more accurate CBF estimates, however as SiTI and MTI data were highly correlated, SiTI likely provides a useful indication of relative CBF differences between subjects

or longitudinally. CVR did not correlate between the acquisitions however, which is problematic and suggests the lower SNR and higher variance in SiTI data may mean that it is not a reliable method to calculate CVR. An alternative explanation is that the different methods used to calculate CVR led to the lack of correlation. The method used for SiTI CVR shifted the CO_2 and CBF data to find the best fit whereas a less sophisticated method of dividing the percentage CBF change by the unit CO_2 change was used for the MTI data.

Where MTI is not feasible, SiTI should still provide a good indicator of cerebrovascular activity. Results from SiTI ASL should be interpreted with caution where arrival times may be altered as this could lead to errors in quantification.

3.5.3 Kinetic Model Differences

The kinetic models used here were both dual-compartment extensions of the GKM proposed by Buxton et al. (1998), with different implementations; Oxford ASL uses probabilistic Bayesian inference (Chappell et al., 2010) to fit the model to the data whereas NLfit uses a typical non-linear regression approach, fitting the model within a specified range of values. As NLfit assumes IV signal in all voxels this model could be predicted to underestimate CBF if it falsely identifies tissue perfusion as arterial signal. However, NLfit produced significantly higher rCBF and hCBF values than Oxford ASL, but significantly lower and more variable estimates of CVR much like the trend seen in SiTI data. Oxford ASL does not assume any IV signal in tissue voxels but uses ARD to remove arterial signal where there is evidence to do so. A possible explanation for the lower CBF with Oxford ASL is that it may overfit this component and discard tissue signal. This possibility needs more in-depth investigation using simulated data as there is no clear evidence for this argument from the current data.

In terms of other kinetic model components contributing to CBF estimation, GM aCBV values were significantly lower in the Oxford ASL data, < 0.5% aCBV per voxel, where a mean aCBV of 0% was set as signal from arterial blood is expected to flow through tissue to its intended destination elsewhere in the brain (Chappell et al., 2010) This is in keeping with other GM aCBV values obtained using PASL and Oxford ASL (E. A. H. Warnert et al., 2014), but aCBV values using this method are scarce. In NLfit, the importance of prior information about physiological values was highlighted by the very different aCBV values produced by each model implementation. A lower limit of 0 was set in NLfit A and B and while an upper limit of 3% produced a 1.4% rCBF mean, the NLfit upper limit of 10% aCBV produced mean GM value of 4.9%. Literature aCBV values in GM tend be around 1-3% using multiple ASL techniques

(Brookes, Morris, Gowland, & Francis, 2007; Bulte et al., 2012; Yan, Li, Kilroy, Wehrli, & Wang, 2012).

TAT and AAT were also significantly affected by choice of model but all were within expected physiological ranges of ~0.6-0.8s for TAT and ~0.3-0.6s for AAT. Similarly, although R^2 estimates of fit were significantly different between the NLfit models, all were within 0.7-0.77 with standard deviations of 0.05-0.09. NLfit B had a better fit for rCBF and hCBF, due to the more liberal parameter limits giving the data a greater range to vary within. This may be because whole GM was used as the ROI, and as physiological parameters vary throughout the brain, a better fit was achieved overall by letting model parameters vary. Unfortunately, it was not possible to produce the same R^2 maps for Oxford ASL due to the hard-coded nature of the software. As this analysis was carried out to determine the CBF analysis for research questions about whole GM, regional ROIs were not investigated but would be useful to better understand the optimal kinetic model design. In summary, the results from this model comparison suggest that prior physiological information coupled with CBF and aCBV determined from the data itself may improve the accuracy of the kinetic model and reduce the variability seen in CVR estimates where limits are set based on researcher expectations of the data alone. However, this may become problematic in patient studies where physiology is unknown, for example delayed TAT, and priors or limits are not of a sufficient to capture differences between or within groups.

3.5.4 Limitations

A limitation of this work is that CBF and CVR values were calculated as a mean over whole brain GM as the following chapter looks at global CBF and CVR. While this approach is less sensitive to PVC errors in small regions where registration may not have been excellent, CBF and CVR are not uniform throughout the brain and this analysis may have failed to identify brain regions where PVC made an important difference.

A second limitation is that as SiTI hypercapnic data was collected in a block design and MTI in separate rest and hypercapnic scans, CVR was calculated in different ways (see methods). Interestingly, CVR was not significantly different despite the difference in analysis but this may have had on effect on variance.

A third limitation is that this was a post-hoc exploratory analysis, conducted to determine the most fitting method to analyse data that was already collected to answer other research

questions. In future, MTI and SiTI data should be collected using the same timings for hypercapnia challenges or tasks and *in-vivo* data should be compared with simulations.

3.6 Conclusions

The current data provide a useful insight into the impact of PVC on data variability as well as the potential CBF and CVR differences obtained with SiTI vs. MTI ASL. The kinetic model comparison also highlights the differences in CBF and CVR achieved using Bayesian and frequentist implementations of the kinetic model and demonstrates the importance of accurate prior knowledge of physiology when defining the model.

Lastly, quantitative fMRI aims to overcome the limitations of relying on relative BOLD or CBF changes. However, acquisitions must fully capture blood flow kinetics and analysis not be biased by limits placed on models. Otherwise, although values are converted to physiological units, they are essentially qualitative, only capturing relative differences between subjects.

In this thesis, MTI without PVC is used where feasible to obtain the most accurate perfusion estimates. PVC was not included in analysis of healthy subject data as increased variability and noise introduced by registration error, likely outweighs the benefits of PVC. The high correlations between non-PVC and PVC data justify this choice when relative differences are of interest. The comparison between MTI and SiTI demonstrated that while SiTI yielded higher estimates of CBF, estimates were moderately to strongly correlated between the acquisitions. Given that MTI acquisitions are not feasible in dual-echo or task acquisitions in many cases, SiTI data must be acquired. Oxford ASL was chosen as the preferred tool to quantify CBF. A Bayesian framework rather than strict lower and upper limits on data is likely to result in more accurate estimations and reduce experimenter bias and uncertainty which could be introduced by setting limits arbitrarily.

Chapter 3 Supplementary Information

Paired Samples Test between resing and hypercapnic CBF for each data acqisition and PVC treatment									
		Paired Differences					t	df	Sig. (2-tailed)
		Mean	Std. Deviation	Std. Error Mean	95% Confidence Interval of the Difference Lower	Upper			
Pair 1	MTI No PVC	-11.170500	3.9115759	.8746550	-13.001174	-9.3398261	-12.771	19	.000
Pair 2	MTI KM PVC	-20.751500	13.2254903	2.9573095	-26.941220	-14.561780	-7.017	19	.000
Pair 3	MTI Basic PVC	-13.160000	5.9671778	1.3343015	-15.952725	-10.367275	-9.863	19	.000
Pair 4	SiTI NO PVC	-11.22450	7.51550	1.68052	-14.74186	-7.70714	-6.679	19	.000
Pair 5	SiTI KM PVC	-11.76050	6.32552	1.41443	-14.72093	-8.80007	-8.315	19	.000
Pair 6	SiTI Basic PVC	-16.23350	10.90638	2.43874	-21.33784	-11.12916	-6.657	19	.000

Table 3.6 Paired t-tests showing significant rest vs. hypercapnia CBF increase.

Resting CBF Correlations							
Resting CBF Data Type		MTI no PVC	MTI KM PVC	MTI basic PVC	SiTI no PVC	SiTI KM PVC	SiTI basic PVC
MTI no PVC	Pearson Correlation	1	.873**	.999**	.688**	.681**	.692**
	Sig. (2-tailed)		.000	.000	.001	.001	.001
MTI KM PVC	Pearson Correlation	.873**	1	.868**	.521*	.530*	.538*
	Sig. (2-tailed)	.000		.000	.018	.016	.014
MTI basic PVC	Pearson Correlation	.999**	.868**	1	.697**	.692**	.701**
	Sig. (2-tailed)	.000	.000		.001	.001	.001
SiTI no PVC	Pearson Correlation	.692**	.538*	.701**	.996**	.991**	1
	Sig. (2-tailed)	.001	.014	.001	.000	.000	
SiTI KM PVC	Pearson Correlation	.681**	.530*	.692**	.985**	1	.991**
	Sig. (2-tailed)	.001	.016	.001	.000		.000
SiTI basic PVC	Pearson Correlation	.688**	.521*	.697**	1	.985**	.996**
	Sig. (2-tailed)	.001	.018	.001		.000	.000

**. Correlation is significant at the 0.01 level (2-tailed).

*. Correlation is significant at the 0.05 level (2-tailed).

Table 3.7 Correlations between resting CBF data acquired with single and multiple TIs and analysed with and without PVC

Correlations between estimated CBF during hypercapnia							
Data Type		MTI no PVE	MTI KM PVC	MTI basic PVC	SiTI no PVC	SiTI KM PVC	SiTI basic PVC
MTI no PVC	Pearson Correlation	1	.953**	.963**	.699**	.783**	.705**
	Sig. (2-tailed)		.000	.000	.001	.000	.001
MTI KM PVC	Pearson Correlation	.953**	1	.931**	.745**	.825**	.758**
	Sig. (2-tailed)	.000		.000	.000	.000	.000
MTI basic PVC	Pearson Correlation	.963**	.931**	1	.726**	.789**	.729**
	Sig. (2-tailed)	.000	.000		.000	.000	.000
SiTI no PVC	Pearson Correlation	.699**	.745**	.726**	1	.954**	.997**
	Sig. (2-tailed)	.001	.000	.000		.000	.000
SiTI KM PVC	Pearson Correlation	.783**	.825**	.789**	.954**	1	.961**
	Sig. (2-tailed)	.000	.000	.000	.000		.000
SiTI basic PVC	Pearson Correlation	.705**	.758**	.729**	.997**	.961**	1
	Sig. (2-tailed)	.001	.000	.000	.000	.000	

**. Correlation is significant at the 0.01 level (2-tailed).

Table 3.8 Correlations for CBF data during hypercapnia for each data type

Correlations between each CVR estimation							
CVR Estimations		MTI No PVC	MTI KM PVC	MTI basic PVC	SiTI no PVC	SiTI KM PVC	SiTI basic PVC
MTI No PVC	Pearson Correlation	1	.552*	.629**	.047	-.053	.050
	Sig. (2-tailed)		.012	.003	.845	.825	.834
MTI KM PVC	Pearson Correlation	.552*	1	.581**	.093	.099	.087
	Sig. (2-tailed)	.012		.007	.696	.677	.715
MTI basic PVC	Pearson Correlation	.629**	.581**	1	.055	-.007	.052
	Sig. (2-tailed)	.003	.007		.817	.978	.827
SiTI no PVC	Pearson Correlation	.047	.093	.055	1	.870**	.999**
	Sig. (2-tailed)	.845	.696	.817		.000	.000
SITI KM PVC	Pearson Correlation	-.053	.099	-.007	.870**	1	.864**
	Sig. (2-tailed)	.825	.677	.978	.000		.000
SiTI basic PVC	Pearson Correlation	.050	.087	.052	.999**	.864**	1
	Sig. (2-tailed)	.834	.715	.827	.000	.000	

*. Correlation is significant at the 0.05 level (2-tailed).

**. Correlation is significant at the 0.01 level (2-tailed).

Table 3.9 Correlations between CV estimates from each data acquisition and analysis.

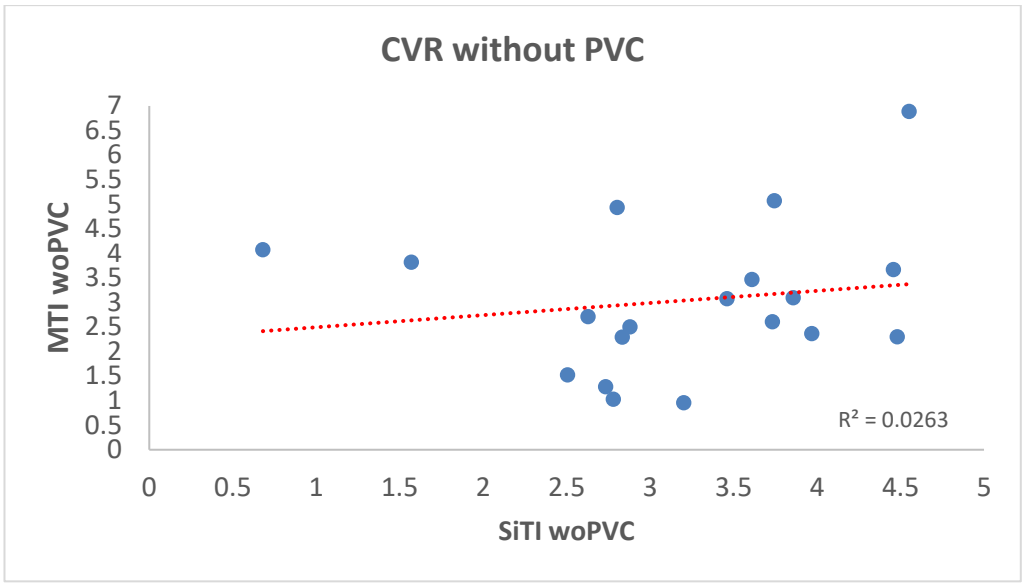
CVR without PVC
MTI woPVC
SiTI woPVC
R² = 0.0263
0
0.5
1
1.5
2
2.5
3
3.5
4
4.5
5
0
0.5
1
1.5
2
2.5
3
3.5
4
4.5
5
6
6.5
7

A

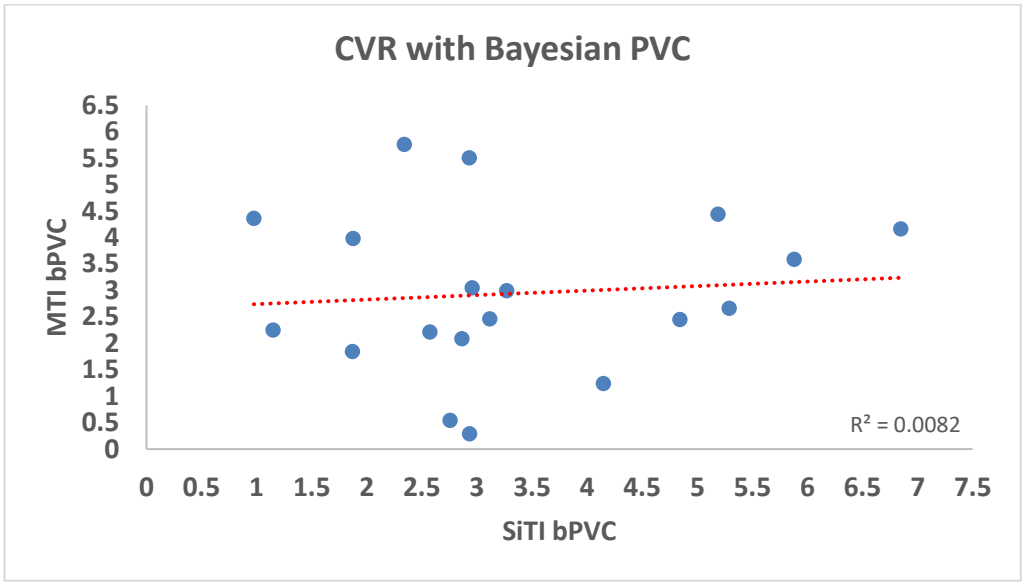
CVR with Bayesian PVC
MTI bPVC
SiTI bPVC
R² = 0.0082
0
0.5
1
1.5
2
2.5
3
3.5
4
4.5
5
5.5
6
6.5
7
7.5

B

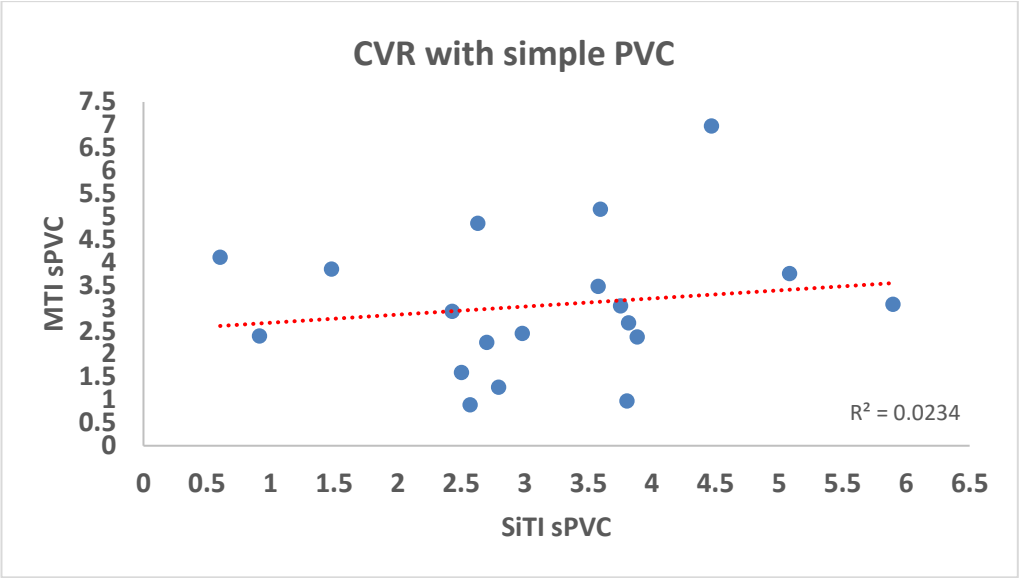

C

Figure 3.3 Correlations plots for MTI and SiTI CVR estimates

Correlations between rCBF values from each kinetic model

		Oxford ASL	NLfit A	NLfit B
Oxford ASL	Pearson Correlation	1	.547*	.787**
	Sig. (2-tailed)		.013	.000
	N	20	20	20
NLfit A	Pearson Correlation	.547*	1	.652**
	Sig. (2-tailed)	.013		.002
	N	20	20	20
NLfit B	Pearson Correlation	.787**	.652**	1
	Sig. (2-tailed)	.000	.002	
	N	20	20	20

*. Correlation is significant at the 0.05 level (2-tailed).

**. Correlation is significant at the 0.01 level (2-tailed).

Table 3.10 RCBF correlations for each model implementation

Correlations between hCBF values from each kinetic model

		Oxford ASL	NLfit A	NLfit B
Oxford ASL	Pearson Correlation	1	.587**	.752**
	Sig. (2-tailed)		.007	.000
	N	20	20	20
NLfit A	Pearson Correlation	.587**	1	.547*
	Sig. (2-tailed)	.007		.013
	N	20	20	20
NLfit B	Pearson Correlation	.752**	.547*	1
	Sig. (2-tailed)	.000	.013	
	N	20	20	20

**. Correlation is significant at the 0.01 level (2-tailed).

*. Correlation is significant at the 0.05 level (2-tailed).

Table 3.11 HCBF correlations for each model implementation

Correlations for CVR values produced by each kinetic model

		Oxford ASL	NLfit_A	NLfit_B
Oxford ASL	Pearson Correlation	1	-.169	-.200
	Sig. (2-tailed)		.475	.397
	N	20	20	20
NLfit_A	Pearson Correlation	-.169	1	.973**
	Sig. (2-tailed)	.475		.000
	N	20	20	20
NLfit_B	Pearson Correlation	-.200	.973**	1
	Sig. (2-tailed)	.397	.000	
	N	20	20	20

**. Correlation is significant at the 0.01 level (2-tailed).

Table 3.12 CVR correlations for each model implementation

Chapter 4

Assessment of the Effects of Aerobic Fitness on Healthy Adults using Multiple Inversion Time ASL fMRI

Abstract

Neurodegenerative diseases are a global health burden and despite extensive research there are no cures or effective long-term management solutions. Neuroimaging studies have provided evidence of a neuroprotective effect of aerobic fitness (AF) in older adults, linking higher AF with greater cognitive performance, brain volume (Erickson et al., 2011), cerebral blood flow (CBF) (Thomas et al., 2013) and cerebrovascular reactivity (CVR) (Bailey et al., 2013; Barnes et al., 2013). However, there is a lack of knowledge regarding the cerebrovascular effects of AF in early adulthood which is necessary to establish the mechanisms of effect across the lifespan.

This study used multiple inversion time (MTI) arterial spin labelling (ASL) fMRI to measure cerebral perfusion at normocapnia and hypercapnia in 20 young, healthy adults (25±4.6) who completed a $\dot{V}O_2$peak test to determine AF and a battery of cognitive tests. In a voxelwise analysis, subjects with a higher $\dot{V}O_2$peak had significantly lower CBF in portions of the thalamus, brainstem, visual cortex, precuneus and cerebellum. Region of interest analysis revealed greater grey matter (GM) CVR to CO_2. There was no significant relationship between cognitive performance and AF, or GM volume and AF.

The results demonstrate an effect of AF on cerebrovascular function in early adulthood indicative of increased metabolic efficiency. Additional work is needed to extend these results to determine the effects of AF on cerebral blood volume and oxygen metabolism.

4.1 Introduction

Neurodegenerative diseases are a global health burden and despite extensive research there are no cures or effective long-term management solutions. The cost to the healthcare system of dementia alone was estimated at $818 billion worldwide in a 2015 World Alzheimer's Report (https://www.alz.co.uk/research/world-report-2015), and this cost is predicted to rise due to an ageing population. Aerobic fitness (AF) has emerged as a modifiable lifestyle factor which reduces the risk of all-cause mortality (Kodama et al., 2009), cardiovascular events and obesity (Haskell, Lee, Pate, Powell, & Blair, 2007; Lee et al., 2010; Roque, Hernanz, Salaices, & Briones, 2013) and protects the brain against age and disease-related decline (Hayes, Alosco, & Forman, 2014; Hillman, Erickson, & Kramer, 2008; Nishijima, Torres-Aleman, & Soya, 2016).

Neuroimaging studies have provided evidence of a neuroprotective effect of AF in older adults, linking higher AF with greater brain volume (Erickson et al., 2011) and cerebral blood flow (CBF) (Thomas et al., 2013), discussed in more detail in the following paragraphs. AF has also been associated with greater cerebrovascular reactivity (CVR) assessed using transcranial Doppler (TCD) ultrasound, an index of vascular reserve (Bailey et al., 2013a; Barnes, Taylor, Kluck, Johnson, Joyner, et al., 2013). CVR reflects the ability of the cerebral vessels to dilate and maintain adequate brain perfusion, and as a result CVR is a useful indicator of vascular reserve independent of neuronal activity. CVR is typically calculated as the percentage CBF change in response to an increase in partial pressure of end-tidal carbon dioxide ($P_{ET}CO_2$) concentration. However, the findings of Bailey et al. (2013) are in conflict with the MRI results of Thomas et al. (2013) who reported lower CVR in Masters Athletes (MA) vs. sedentary young and age-matched controls. These conflicting results regarding CVR and AF represent a bigger problem of inconsistent findings regarding AF and its benefits for brain function.

If AF training is to be systematically delivered as a clinical intervention to reduce age and disease-related brain decline, a full understanding of the mechanisms through which AF delivers its apparent benefits is needed. To do this, the role of AF in protecting or potentially restoring brain function must be investigated across the lifespan and health spectrum. At present, it is unclear whether AF influences cerebrovascular function in the healthy brain, or whether it serves to maintain function where the brain is vulnerable to damage.

In addition, brain structure and function are closely linked; to maintain healthy brain tissue, adequate energy must be supplied. Many studies have investigated the link between AF and structure; cerebrovascular function has not been extensively studied in humans. The work presented here focuses on how AF impacts the cerebrovascular processes which maintain delivery and circulation of brain nutrients.

The current study was designed to investigate the effects of AF on the healthy brain. The objective was to quantify variations in CBF and CVR, two widely used indices of cerebrovascular function, in a sample of young, healthy adults within a normal range of fitness levels (i.e. sedentary and active, but not athletes in structured training). Based on the extant TCD and fMRI evidence, we predicted a positive relationship between fitness and resting grey matter (GM) CBF. We also expected to see a positive correlation between CVR to CO_2 and $\dot{V}O_2$peak in line with the findings of Bailey et al. (2013). Cognitive tests chosen to measure a number of cognitive domains were included to test a secondary hypothesis that higher $\dot{V}O_2$peak would be associated with better cognitive performance. If CBF and CVR differences due to fitness were evident, then demonstrating additional cognitive benefits would provide evidence for functionally relevant effects of neurobiological differences.

This study used multiple inversion time (MTI) arterial spin labelling (ASL) fMRI to measure cerebral perfusion at normocapnia and hypercapnia. A key benefit of ASL is that unlike BOLD fMRI, it is possible to quantify baseline activity and changes in response to a stimulus, making it an ideal technique to study groups with compromised cerebrovascular function as well as healthy populations.

A brief review of the evidence for AF exerting beneficial effects on cerebrovascular function is first presented along with potential mechanisms of effect.

4.1.1 Experimental Models of Exercise and Aerobic Fitness

Experimental models have provided much of our current knowledge about the potential mechanisms underlying the neuroprotective and neuromodulatory effects of exercise and AF on the brain. One of the first studies to demonstrate exercise-induced brain changes was conducted by van Praag et al. (1999). This study showed that mice exposed to 43 days of either voluntary wheel running or an enriched environment (EE) had double the number of surviving newborn neurons compared with controls undergoing either water maze training or forced swimming. Although enriched environments and aerobic exercise provided similar benefits,

results show that physical activity resulted in enhanced neurogenesis. Stress, which has negative effects on neurogenesis may have offset the benefits of swimming as animals were forced to do this. A later study by (Kobilo et al., 2011), extended these findings showing that neurogenesis and cell survival in rodents housed in an EE was only increased when access to running was available suggesting that the running component of an EE underlies its neurogenic effects. In terms of cerebrovascular function, Swain et al. (2003) reported reduced proton signal intensity in the motor cortex of rats following 30 days of wheel running. The authors attributed this change to greater capillary perfusion and/or cerebral blood volume (CBV) following exercise. In a second experiment, also by Swain et al. (2003), measuring CBF during normocapnia and hypercapnia, a greater CBF response to hypercapnia was observed in the running group, although no baseline differences were evident. This result was explained as an increase in the vascular reserve of capillaries due to exercise training (ET). In agreement with these results, Pereira et al. (2007) demonstrated that mice subjected to wheel running had increased cerebral blood volume (CBV) in the dentate gyrus (DG) of the hippocampus compared to non-exercised controls, and the degree of CBV increase correlated with levels of neurogenesis in the DG. Building on the evidence for cerebrovascular adaptations to exercise, Cahill et al., (2017) reported increases in normocapnic and hypercapnic CBF in mice following 4 weeks of voluntary wheel running vs. non-exercised controls. In addition, greater CBF changes correlated with volume changes in the hippocampus. CBF changes were not detected in motor cortex, suggesting that flow changes may have been driven by vascular remodelling in response to increased neuronal density or metabolic demand. However, this short intervention study is unlikely to show the full extent of the effects of long-term physical activity on the brain as imaging studies have demonstrated greater CBF in trained subjects in regions other than the site of neurogenesis in the hippocampus (Macintosh, Swardfager, Crane, Ranepura, & Saleem, 2014; Robertson et al., 2015; Thomas et al., 2013).

A constant adequate supply of blood delivering oxygen and other nutrients such as glucose is required for optimal cerebral function. Results from experimental models suggest vascular adaptations to exercise, such as increased angiogenesis and CBF, increases the availability of nutrients necessary to support neurogenesis and cell survival. This in turn facilitates molecular signalling for efficient brain communication and plasticity at the synaptic level. Exercise-driven brain changes are thought to be underpinned by increased availability of a number of growth factors including insulin-like-growth-factor (IGF-I), brain-derived-neurotrophic-factor (BDNF) and vascular endothelial-derived growth factor (VEGF) (Cotman et al., 2007). Nitric oxide (NO), a free radical, is a signalling molecule with both neuroprotective and neurotoxic effects (Kro,

Fehsel, & Kolb-bachofen, 1997). NO has a vasodilatory effect in vessels and is necessary for maintaining vascular endothelial function (Vallance & Hingorani, 1999). NO bioactivity is increased with exercise training, and this increase has been demonstrated in humans with cardiovascular disease (Walther, Gielen, & Hambrecht, 2004) and metabolic syndrome (Gomes, Casella-Filho, Chagas, & Tanus-santos, 2008). Endothelial dysfunction which is associated with vascular disease may be exacerbated by free radical production which interferes with NO production. Increasing NO bioactivity through exercise may counteract the effects of free radical damage and therefore improve vascular endothelial function (Green, Maiorana, O'Driscoll, & Taylor, 2004).

These molecular factors are likely to play a key role in the cerebrovascular benefits linked to AF, however these factors can only be measured peripherally in humans, and it is unknown whether peripheral concentrations reflect levels in the brain, preventing researchers from making causal associations. Human imaging studies focus on changes at the macroscopic level such as changes in CBF and CVR as well as microstructural white matter (WM) and cortical volume differences between trained and sedentary groups. The two bodies of work are important in understanding fully how the molecular adaptations lead to large scale vascular changes which maintain brain function.

4.1.2 Aerobic Fitness and Cerebrovascular Function: Evidence from Human Imaging

Acute exercise has been shown to increase CBF in tissue (MacIntosh et al., 2014), therefore long-term aerobic ET, leading to higher AF, may support maintenance of optimal cerebral energy supply and metabolism. This in turn may work to promote neuronal survival and adaptive plasticity in response to new experiences or injury, protecting against age and disease related functional decline.

Blood is supplied to the brain primarily through the internal carotid (IC) and vertebral arteries which interconnect with the middle cerebral artery (MCA) to form the Circle of Willis which connects with smaller branching arteries throughout the brain. The brain's capillary bed, is comprised of a single layer of endothelial cells which make up the entire blood vessel wall and control the passage of molecules through this protective layer, the blood-brain-barrier (BBB). The capillary bed is responsible for the transfer of nutrients such as oxygen (O_2) to neurons and removal of waste products including CO_2. Capillaries do not possess elasticity, unlike arteries. Arterial elasticity is therefore necessary for maintaining smooth blood flow into the capillaries. Ageing processes contribute to the stiffening of arteries slowing or reducing

nutrient delivery to neurons as arteries become less compliant to changes in CBF. There is evidence to suggest that where compliance is reduced, perfusion pressure is increased to maintain adequate energy supply to brain tissue, unlike in healthy arteries where vasodilation occurs to support increased CBF to meet neuronal activity requirements (Warnert, 2016). Sedentary lifestyles have been linked to arterial stiffening (Joyner, 2000; Tanaka et al., 2000), meaning that sustained aerobic activity is important in delaying the effects of ageing on arterial compliance (AC). Whether AF is limited to slowing AC reductions and CBF, or delivers cerebrovascular benefits from development, has had limited investigation, and future studies should address the effect of AF on cerebral arteries from early to late adulthood.

Only a small number of studies, most from the same lab, have looked at the relationship between brain function and AF in children and young adults. One study has linked higher AF with greater hippocampal perfusion (Chaddock-Heyman et al., 2016) and another with neural network efficiency during cognitive control tasks (Voss et al., 2012) in preadolescent children. Several other studies show small but positive effects of fitness on selective cognitive domains such as relational memory and executive function in children, see Khan & Hillman (2014) for a review.

In young adults (<30 years old), Bailey et al. (2013) showed that $\dot{V}O_2$max, the gold standard test of AF, displayed a positive linear relationship with MCA velocity and CVR to CO_2 inhalation measured using transcranial Doppler (TCD) imaging. This relationship was also observed in older adults in the same study. These results suggest that fitness may increase vascular reserve and AC which could help to maintain healthy blood pressure and efficient blood supply to neural tissue. However, Barnes et al. (2013), using the same technique, did not find a relationship between CVR and $\dot{V}O_2$max in younger adults despite observing the same trend as Bailey et al. (2013) in a cohort of older adults. This may be explained by differences in the study design or a smaller spread of fitness levels in the Barnes et al. (2013) study. Also, Bailey et al. (2013) compared CVR between two groups, sedentary vs. trained, whereas Barnes et al. (2013) used a single group with a range of fitness levels who did not participate in a structured training regime. Another TCD study in older women (A. D. Brown et al., 2010) reported positive correlations between $\dot{V}O_2$max and cerebrovascular conductance (CVC), an index of CBF, as well as between $\dot{V}O_2$max and mean arterial pressure (MAP). $\dot{V}O_2$max was also weakly correlated with global cognitive performance (r = .4), for cognitive domains including cognitive speed, verbal ability and executive functions, a consistent correlation of ~0.3 was reported. An interesting finding of the study was that CVC and MAP were stronger predictors of overall

cognitive performance across domains, highlighting the potential role of cerebrovascular health in cognition. A later study by Dupuy et al. (2015) using near infrared spectroscopy (NIRS) in young (19-34 years old) and older women (55-72) reported higher levels of prefrontal oxygenation and faster reaction times during the executive condition of the Stroop task in than their less fit counterparts. The authors did not find an age effect in this study; however the effects on cognition were extremely selective, only one of the ten domains revealed a performance or oxygenation effect related to fitness. Cerebral oxygenation differences during the Stroop were found only in the right inferior frontal gyrus (IFG). The prefrontal cortex is a key area involved in executive function, and is an area most vulnerable to age related perfusion reductions (Lu et al., 2011). The IFG may therefore be a region with visible perfusion differences in individuals with higher AF when energy requirements are increased, however it seems unlikely that effects would be so localised given that a network of brain regions are involved in any task. If AF increases AC to maintain CBF and CVR, a whole brain increase in oxygenated blood flow would be expected. Studies measuring CBF in the resting brain are necessary to clarify whether resting global differences are apparent in young people, such as in the current study, or whether effects only become measurable when local energy needs increase. Much more work is needed to better characterise the link between fitness and whole brain function in early adulthood. MRI is an ideal technique for this as TCD and NIRS offer limited spatial coverage and resolution.

Using gadolinium contrast T1-weighted imaging, Pereira et al. (2007) reported increases in DG cerebral blood volume (CBV) in untrained adults following a 3 month aerobic ET intervention, and CBV changes correlated with $\dot{V}O_2$max. Further, vascular adaptations have been shown following a 12-week intervention in sedentary young and older people designed to increase $\dot{V}O_2$max. Murrell et al. (2013) found a small but statistically significant increase in MCA CVR in both age groups, a promising result suggesting that cerebrovascular adaptations can be achieved in a relatively short time frame across the lifespan.

In the fMRI study from Thomas et al. (2013) mentioned in the introductory paragraph, CBF and CVR in a group of MA were compared to that of age-matched and young sedentary groups. The MA group had greater absolute CBF vs. age-matched controls in the precuneus and posterior cingulate cortex (PCC), part of the default mode network (DMN). The DMN is believed to be involved in alertness and action monitoring and its action is known to be downregulated in ageing and dementia. Further, relative perfusion was greater than that of the young and age-matched control group. Despite lower total brain volume, aerobically fit older adults had greater blood supply to these regions. In agreement with this finding,

Boraxbekk et al. (2015) reported that higher levels of current physical activity, and activity over a 10-year period, predicted PCC perfusion. Performance on a visuospatial task (block design) was also predicted by physical activity, however performance on other task was not, in keeping with the seemingly selective fitness-cognition relationship. Zimmerman et al. (2014), in agreement with the Thomas et al. (2013) study, reported that cardiorespiratory fitness was positively correlated with GM, but not WM, CBF in adults aged 55-85. A mediation analysis showed that fitness was responsible for offsetting the age-related CBF reduction, demonstrating a neuroprotective role for fitness in ageing.

In contrast to the TCD work, in the study by Thomas et al. (2013), a lower BOLD CVR response to CO_2 in MA vs. age-matched and young sedentary controls was also observed in temporal regions and the insula at a statistically significant level, although this trend was present throughout the brain. Thomas et al. (2013) attributed these results to a dampened CO_2 response as a result of lifelong exposure to elevated arterial CO_2. To add further complexity to these results, Gauthier et al. (2015) found that in older adults, $\dot{V}O_2$max was positively correlated with BOLD CVR in periventricular watershed areas but inversely related to CVR in regions of the frontal cortex. Taken together, these studies suggest regional variations in the effects of AF on CVR, which may explain the mostly consistent positive correlation between MCA CVR and AF in TCD studies which is spatially limited. An exception to the TCD findings comes from a study by Zhu et al. (2013), also comparing MA, sedentary older adults and young sedentary controls. Zhu et al. (2013) found a similar relationship to Thomas et al. (2013) in that cerebral vasomotor reactivity (CVMR) to hypocapnia was lowest in the MA group. However, CVMR to hypercapnia, was higher in both older groups with no difference between the MA and sedentary groups. Zhu et al. (2013) did not find a resting MCA flow velocity difference between the older groups at rest, hypocapnia or hypercapnia, however as expected, values were higher for the younger group across conditions. At present, therefore, it is difficult to come to a strong conclusion on how AF affects the brain at different stages of life, and what this means in terms of cognition and behaviour.

There are also suggestions that physical activity benefits patients with chronic neurological disorders such as Multiple Sclerosis (MS); improvements in fatigue, balance and ambulatory capacity (Motl & Pilutti, 2012) as well as greater functional connectivity (FC) between the hippocampus and frontal regions (Prakash, Patterson, Janssen, Abduljalil, & Boster, 2011) have been reported. In addition, Prakash et al. (2011) showed that higher physical activity was related to greater hippocampal-posteromedial cortex (PMC) coherence which in turn was

related to relational memory performance. Linking function to structure, greater volume of the hippocampus, thalamus and basal ganglia have been demonstrated in MS patients with higher $\dot{V}O_2$peak (Prakash et al., 2010), potentially due to maintained cerebrovascular function and therefore energy delivery to tissue. However, this has not been directly examined.

The relationship between AF and brain function is even more difficult to determine in patients, due to difficulties establishing whether patients are less impaired and/or have less cerebrovascular damage because they have higher AF, or whether they have higher AF because they are less impaired. Studies evaluating cerebrovascular function and AF pre and post ET interventions are crucial for establishing the therapeutic role of aerobic exercise training in patients. In support of the former, a TCD study in a cross-section of stroke patients demonstrated improvements in CVR of ~28% following a six month ET intervention which increased $\dot{V}O_2$peak by 19% (Ivey, Ryan, Hafer-macko, & Macko, 2011), providing evidence of functional recovery facilitated by increased AF. However it is still possible that participant selection was dictated by level of impairment.

To summarise, imaging studies of the relationship between brain function and AF report mixed evidence for AF protecting against cerebrovascular decline in ageing and disease or having lifelong functional benefit. The main reason for this is a small number of overall studies with varying methodologies and design. As TCD is limited to single arterial measurements and measures flow rather than perfusion, there is a gap in the literature for studies investigating global effects of AF, especially in younger adults free from age-related comorbidities. The current study seeks to address this gap.

4.2 Methods

4.2.1 Participants

20 healthy adults (11 females, mean age 25±4.6) were recruited from advertisements placed around Cardiff University. The study was approved by the Cardiff University School of Psychology Research Ethics Committee and performed in accordance with the guidelines stated in the Cardiff University Research Framework (version 4.0, 2010). All participants were non-smokers and educated to university level.

4.2.2 Study Procedures

The study consisted of 3 lab visits. In Visit 1, eligibility screening for MRI, respiratory modulations and intensive exercise was carried out. Contraindications to exercise were

assessed using the Physical Activity Readiness Questionnaire (PARQ). Sociodemographic information was recorded and estimations of weekly activity level were established using the International Physical Activity Questionnaire (IPAQ) Short Form (Craig et al., 2003). Elevated CO_2 inhalation can cause sensations of breathlessness, light headedness and anxiety in some individuals. For this reason, all volunteers took part in a gas modulation session in a simulation MR scanner to ensure the gas modulations were tolerable. A stepwise protocol was employed to allow participants time to become accustomed to CO_2 inhalation (see figure 4.1). No adverse effects were reported in this sample.

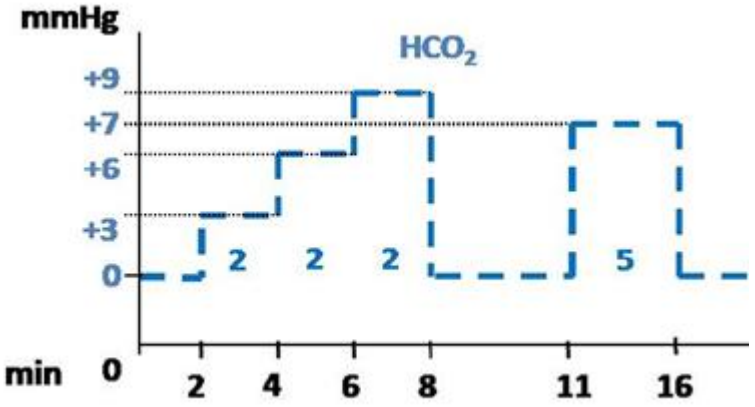

Figure 4.1 Protocol for the pre-MRI respiratory modulation test session. Heart rate and oxygen saturation were monitored and recorded throughout the session. Figure adapted from Merola, (2016).

In Visit 2, volunteers completed 7 cognitive tests, administered by the same researcher for all participants, prior to the fitness test. The tests covering a range of cognitive domains were chosen as they are validated for use in patient and control samples (see table 4.1).

Test	**Domain Measured**
Speed and Capacity of Language Processing (SCOLP) (Baddeley, Emslie, Nimmo-Smith, 1992)	Information processing, speed and language comprehension
Forward Digit Span	Working memory
Letter Fluency (Categories)	Verbal fluency
Conners Continuous Performance Test (Conners et al., 2000)	Sustained attention and response inhibition

Trail Making Test (Part B)	Processing speed and executive function
Symbol Digit Modalities Test	Information processing speed

Table 4.1 List of cognitive tests used in this study.

4.2.3 Fitness Test

The fitness test was also performed in Visit 2. The PAR-Q was conducted a second time to identify potential risk factors associated with exercise in the unlikely event of circumstance changes from Visit 1. The $\dot{V}O_2$peak test protocol used has previously been described by Collett et al. (2011) and Cooney et al. (2013). The test began with a 2-minute unloaded warm up at 50 revolutions per minute (rpm) on a Lode cycle ergometer (Lode, Groningen, Netherlands). During the test participants maintained a constant 50rpm and work rate was increased from 50 watts by 25 watts every 2 minutes. The protocol was designed so that exhaustion would be reached in under 20 minutes. The test was terminated if any of the following criteria were reached; work rate fell below 45rpm for > 10 seconds, RER was >1.15, or volitional exhaustion occurred. At the end of each 2-minute step Borg ratings of perceived exertion (RPE), on the CR10 scale (Borg & Kaijser, 2006) were used to record perceived heaviness of legs and breathing.

Blood lactate concentration was sampled from the earlobe using Unistik 3 1.8mm Safety Lancets (Williams Medical, Caerphilly, Wales) and tested using the Lactate Plus system (Nova Biomedical, Waltam, MA USA) at baseline, 2 minute intervals and at exhaustion. Respiratory gas exchanges were continuously monitored using breath by breath analysis with the Cortex Metalyser 3b (Cortex Biophysik Metalyzer, Germany). $\dot{V}O_2$peak was taken as the highest value over a 30 second block average at the maximum recorded work rate. Heart rate (HR) and work rate were also recorded at baseline and at 2 minute intervals and electrocardiography (ECG) was monitored for the duration of the test. Blood pressure (BP) was recorded at baseline and at the end of the test. Following termination of the $\dot{V}O_2$peak test participants were monitored for 10-minutes. In this 10-minute recovery period blood pressure, HR and blood lactate were sampled every 2 minutes to ensure values were within baseline levels before leaving the lab.

4.2.4 MRI Acquisition

In Visit 3 volunteers were underwent a MR scan. Images were acquired on a 3T whole body MRI system (GE Excite HDx, Milwaukee, WI, USA) using an eight-channel receive-only head coil. Heart rate and cardiac traces were recorded using a pulse oximeter and respiratory

bellows. A sampling line connected to the face mask of the breathing circuit was used to monitor end-tidal CO_2 and O_2 concentrations. The MEDRAD system (MEDRAD, Pittsburgh, PA) was used to monitor O_2 saturation throughout the experiment.

Pulsed arterial spin labelling (PASL) data were acquired using a single subtraction PICORE QUIPSS II (Wong et al., 1998) with a dual-echo gradient-echo readout (Liu et al., 2002) and spiral k-space acquisition (Glover, 1999) the first echo being used for CBF quantification. Data were acquired at 8 inversion times; 400, 500, 600, 700, 1100, 1400, 1700 and 2000ms. QUIPSS II cut-off at 700ms meant that short and long inversion times were acquired in separate runs. 16 and 8 tag-control pairs were acquired for each short and long inversion time respectively. A variable TR was used for efficiency, minimum of 1100ms for short TI data and minimum of 1600ms for long TIs. TR increased with TI e.g. TI of 800ms = TR 1600ms, TI of 1100ms = TR 1900ms. Other acquisition parameters were; TE = 2.7ms, voxel size = 3.5x3.5x7mm^3, 3.2mm in-plane resolution, matrix size 64x64mm, FOV = 19.8cm, flip angle = 90°, slice delay 55ms, 15 slices, slice gap 1.5mm for maximum brain coverage. Label thickness was 200mm with 10mm gap between the end of the label and the most proximal imaging slice.

A calibration image without any labelling was acquired before the perfusion images using the same acquisition parameters, except a long TR; this was used to obtain the equilibrium magnetisation of cerebrospinal fluid (M_0, CSF), needed for the quantification of CBF. A minimal contrast image was also acquired to correct for coil inhomogeneities with TE = 11ms, TR = 2s. This protocol was performed twice, first during rest, then while volunteers were hypercapnic. The hypercapnia modulation was carried out using the prospective control method described by Tancredi & Hoge (2013). A gas mixing chamber had three feeding lines coming in for the delivery of medical air, 5% CO_2, and medical oxygen, the latter incorporated as a safety backup but not used during experimentation, the circuit is described in detail by Tancredi, Lajoie, & Hoge (2014). $P_{ET}CO_2$ elevation of 7mmHg was targeted using 5% CO_2 (balance air) and the scan commenced once participants reached the target CO_2 level. MTI data acquisition time was ~15 minutes in total.

A T1-weighted 3D structural fast spoiled gradient echo (FSPGR) was also acquired for registration of functional data and voxel-based morphometry (VBM) analysis; TR/TE = 7.8/2.9ms, resolution = 1mm isotropic.

4.2.5 Data Analysis

4.2.5.1 $\dot{V}O_2$peak Calculation

$\dot{V}O_2$peak was calculated from the respiratory gas exchanges which were continuously monitored using breath-by-breath analysis and averaged over 10 second blocks. $\dot{V}O_2$peak was defined as the averaged value at maximum recorded work rate. HR, RER and blood lactate were recorded every 2 minutes and at termination of the fitness test to validate $\dot{V}O_2$peak criteria being reached. The test result was considered valid if heart rate exceeded 90% of age predicted maximum, RER = >1 and blood lactate concentration was greater than 8 mM at the end of the test (McArdle et al., 1996, Horton et al., 2011; Milani, Lavie, Mehra, & Ventura, 2006; Poole, Wilkerson, & Jones, 2008).

4.2.5.2 Cognitive Data Scoring

Cognitive data were scored by hand by the same researcher, the Conners Continuous Performance test is computer based and scored automatically. Demeaned scores were calculated for correlation analysis with $\dot{V}O_2$peak and MR data.

4.2.5.3 Imaging Analysis

Physiological noise correction was carried out using a modified RETROICOR (Glover et al., 2000) as described in Chapter 3. ASL data were motion corrected using MCFLIRT within FSL (FMRIB's Software Library, www.fmrib.ox.ac.uk/fsl, Jenkinson, Bannister, Brady, & Smith, 2002). Average difference images were obtained for each inversion time from tag-control subtraction of the CBF time series (Lu et al., 2006) and a perfusion map was created from the average over all inversion times. A two-compartment CBF kinetic model (Chappell et al., 2010) was used to obtain voxel-wise estimates of CBF, tissue arrival time (TAT) and arterial cerebral blood volume (aCBV) (see Chapter 3 for a detailed model description). The CBF timeseries for the normocapnia and hypercapnia scans were corrected for coil sensitivity inhomogeneities using the minimal contrast images (Jinghua Wang et al., 2005) and converted to ml/100g/min using the CSF signal as a reference to estimate the fully relaxed magnetisation of blood (Chalela et al., 2000). The mean resting CBF for each subject was calculated by averaging the CBF time series over all time points and over all voxels within the masked GM image.

CVR was calculated by dividing the percentage change in CBF from rest during hypercapnia by the mmHG change in $P_{ET}CO_2$ increase during hypercapnia.

4.2.5.4 ROI Analysis of Grey Matter CBF and CVR

Individual subject GM masks were created using FMRIB's Automated Segmentation Tool (FAST) and thresholded to include voxels with 50% and above probability of GM. ROI analysis of the relationship between GM CBF at rest, during hypercapnia and CVR and $\dot{V}O_2$peak was carried out using correlation analysis and permutation testing (100,000 permutations per comparison) in Matlab (Mathworks Inc., MA, USA). Permutation testing was used as an alternative to Bonferroni correction for multiple comparisons which is too conservative when related variables are tested. This approach was also applied to examine the associations between GM CBF and CVR and cognitive test scores.

4.2.5.5 Voxelwise Analysis of Grey Matter CBF and CVR

Follow up voxelwise analysis was conducted using FSL's Randomise tool (http://www.fmrib.ox.ac.uk/fsl/randomise/index.html) (Winkler, Ridgway, Webster, Smith, & Nichols, 2014) to examine the voxelwise correlation between i) CBF and $\dot{V}O_2$peak and ii) CVR and $\dot{V}O_2$peak. The individual subject masks described in the ROI Analysis section were used to confine this analysis to GM only. Randomise is a permutation testing method that uses threshold free cluster enhancement (TFCE) (Smith & Nichols, 2009) to correct for multiple comparisons across voxels. Significance was set at $p < 0.05$ (FDR corrected). TFCE identifies cluster-like regions of activation while the image remains inherently voxelwise. TFCE is a permutation method which produces images both corrected and uncorrected for multiple comparisons. TFCE is thought to be more sensitive than traditional voxelwise thresholding methods but potentially less spatially specific (Nichols, 2014).

4.2.5.6 Grey Matter Volume

T1-weighted structural data were analysed with FSL-VBM (Douaud et al., 2007; Good et al., 2001, http://fsl.fmrib.ox.ac.uk/fsl/fslwiki/FSLVBM). Structural images were brain extracted and segmented into grey and WM and CSF before being registered to the MNI 152 standard space template using non-linear registration (Andersson et al., 2007). The resulting images were averaged and flipped along the x-axis to create a left-right symmetric, group-specific GM template. Second, all native GM images were non-linearly registered to this study-specific template and modulated to correct for local expansion (or contraction) due to the non-linear component of the spatial transformation. The modulated GM images were then smoothed with an isotropic Gaussian kernel with a sigma of 3mm. Finally, voxelwise GLM was applied using permutation-based non-parametric testing, correcting for multiple comparisons across space to investigate whether GM volume and $\dot{V}O_2$peak were correlated.

4.3 Results

4.3.1 Demographics and Fitness Test Outcomes

Characteristics	Mean (sd) or % (n)
Age	25 (4)
Sex	55% female (11)
Weight (kg)	69.1 (8.8)
Height (cm)	173 (7)
BMI	23 (2.1)
VO2peak (L/min)	2.9 (0.6)
VO2peak (L/kg/min)	41.2 (8)
Baseline Lactate	0.96 (0.3)
PE Lactate	9.5 (2)
Baseline HR	79.2 (18.8)
Peak HR	185.35 (9.8)
Peak RER	1.1 (0.04)
Maximum Work Rate (watts)	205 (40)
Baseline Borg (legs)	0.075 (0.18)
Peak Borg (legs)	8.5 (1.7)
Baseline Borg (breathing)	0.075 (0.25)
Peak Borg (breathing)	7.55 (1.95)

Table 4.2 Group characteristics and fitness test outcomes including $\dot{V}$O2peak and secondary validation criteria.

All subjects completed the test until volitional exhaustion. Out of the 20 subjects 17 achieved an RER > 1.1 and 3 achieved RER > 1. 17 subjects exceeded the 90% HR maximum threshold and achieved a lactate peak >9, the remaining 3 exceeded 80% of HR maximum and achieved a lactate peak >6. As this was a $\dot{V}O_2$peak test all subjects satisfied test criteria by working to volitional exhaustion. However, based on typical $\dot{V}O_2$max criteria, 17 subjects fulfilled criteria for a maximal exercise test (Dupuy et al., 2015; Wilkinson, Leedale-brown, & Winter, 2009).

4.3.2 Correlations between CBF, CVR and $\dot{V}$O2peak

4.3.2.1 ROI Analysis

There was a non-significant inverse association between $\dot{V}O_2$peak and resting CBF (rCBF) in GM; r = -.4, p = .07, p' =.17 (figure 4.2) and hypercapnic CBF (hCBF); r = -.23, p = .33, p' =.58 (figure 4.3). There was a significant positive correlation between $\dot{V}O_2$peak and CVR; r = .62, p = .004, p' =.009 (figure 4.4). G*Power (v3.1.9.2) was used to investigate the statistical power of the significant correlation between $\dot{V}O_2$peak and CVR. With a power of 0.8 and significance threshold of 0.05, a power of 0.91 was achieved based on the effect size. This means we can be confident that there was sufficient power to detect an effect in this analysis (see supplementary table 4.5).

Neither baseline $P_{ET}CO_2$ nor the $P_{ET}CO_2$ response to hypercapnia was driven by $\dot{V}$O2peak; r = -.26, p = .27 (Figs. 5 & 6). The $P_{ET}CO_2$ response to hypercapnia was not driven by resting CBF; r = -.14, p = .55 (supplementary figure 4.8). There was a positive trend between resting CBF and baseline $P_{ET}CO_2$ (supplementary figure 4.9), however baseline $P_{ET}CO_2$ was not a predictor of CVR response ((supplementary figure 4.10).

TAT and aCBV did not show any strong trends in relation to fitness (supplementary figures 4.11-14).

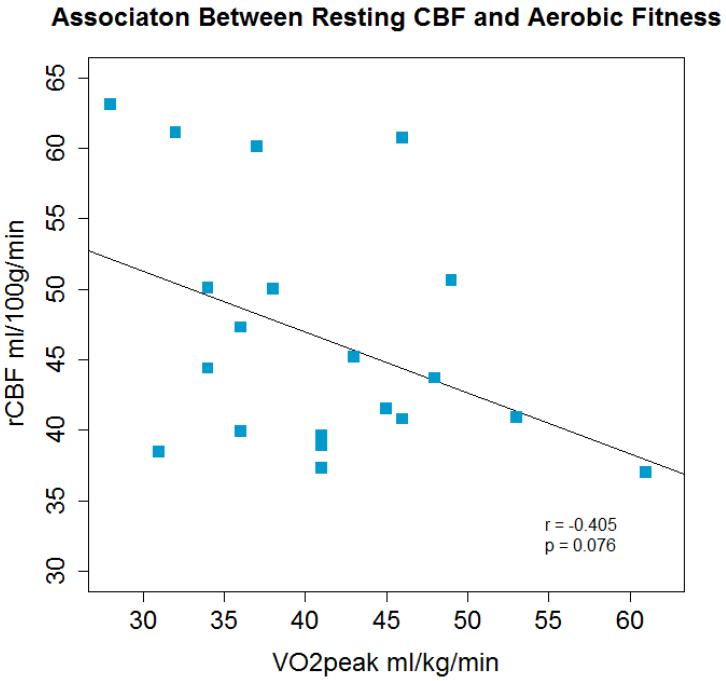

Figure 4.2 A non-significant inverse association between AF and CBF was observed

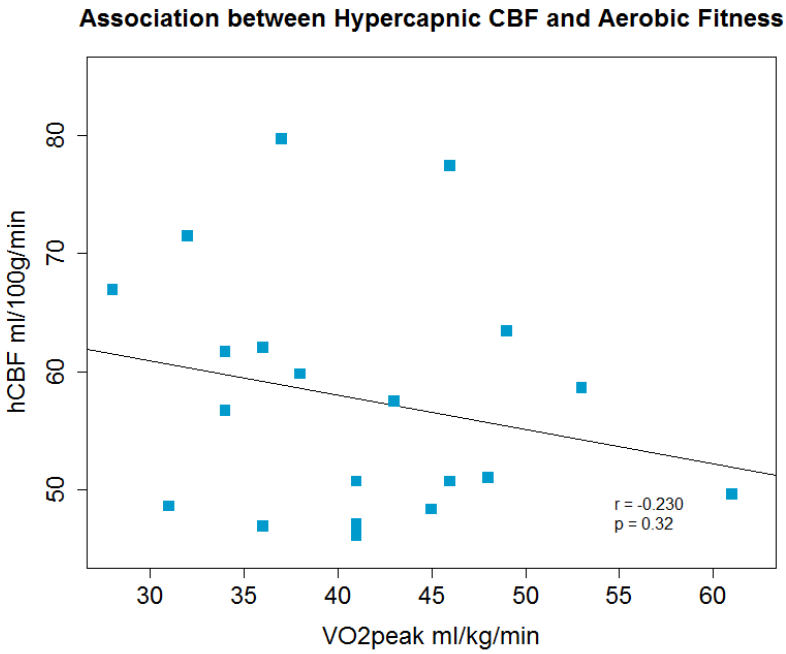

Figure 4.3 There was a trend towards AF being inversely associated with CBF during hypercapnia

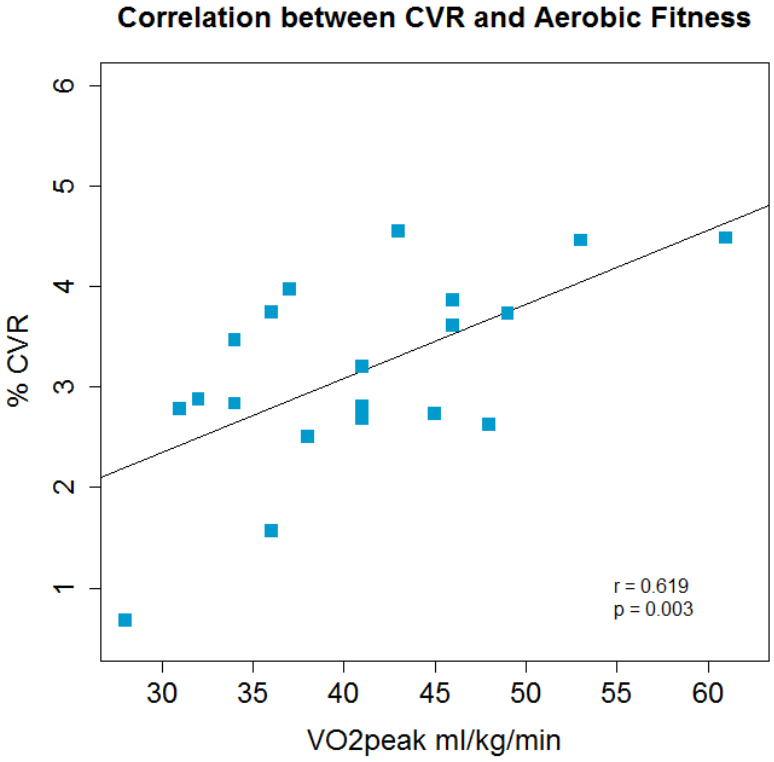

Figure 4.4 Across the group CVR and AF were positively correlated.

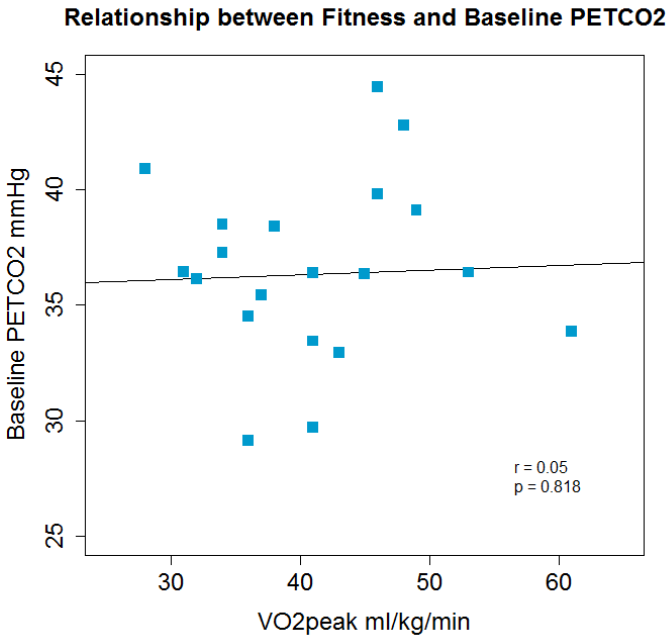

Figure 4.5 AF was not a predictor of baseline $P_{ET}CO_2$

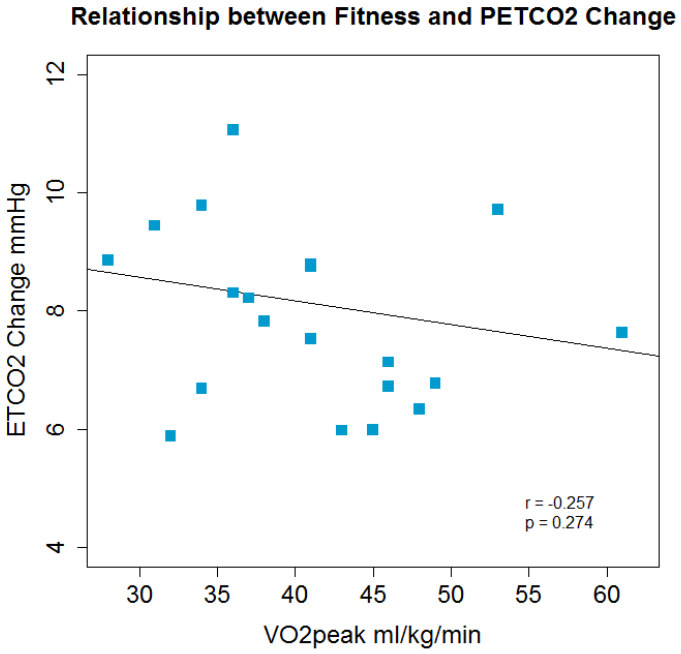

Figure 4.6 AF was not a strong predictor of $\Delta P_{ET}CO_2$ during hypercapnia

4.3.2.2 Voxelwise Analysis

Follow-up voxelwise analysis revealed a significant inverse association between $\dot{V}$O2peak and resting CBF in the left and right thalamus, brainstem, left V1, left precuneus cortex and

cerebellum; but only in the frontal pole for hypercapnic CBF (figure 4.7). Voxelwise CVR was not related to $\dot{V}$O2peak in any region.

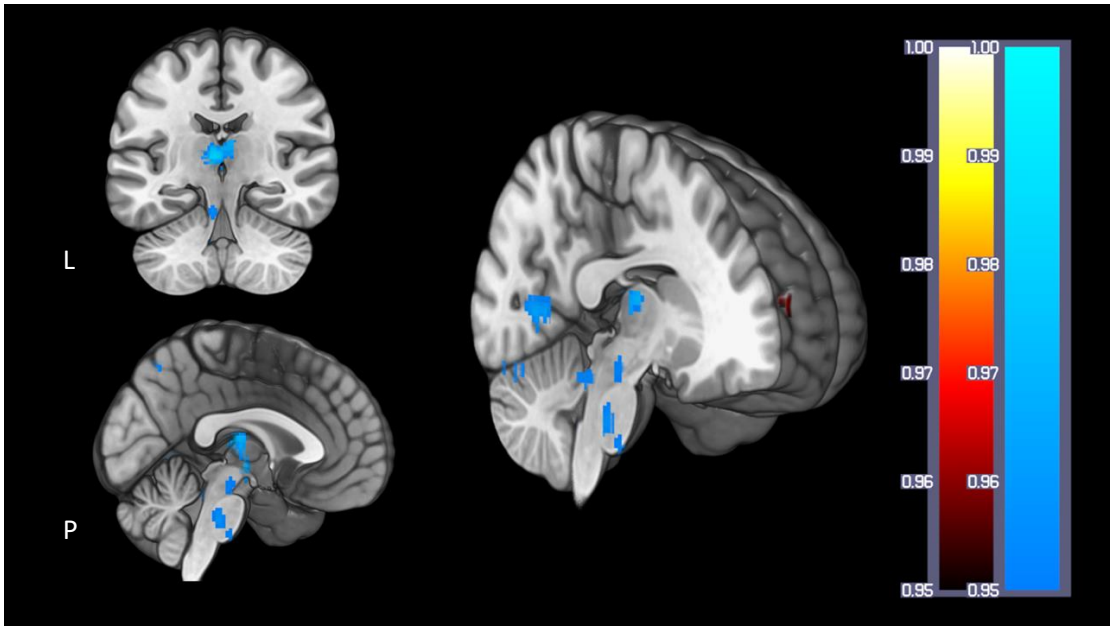

Figure 4.7 Regions of significantly lower CBF in subjects with higher aerobic fitness at rest (shown in blue) in the thalamus, brainstem, precuneus, visual cortex (V1) and lingual gyrus. During hypercapnia (shown in red), CBF in one cluster in the right frontal pole also displayed this inverse correlation. L = Left. P = Posterior.

4.3.2.3 $\dot{V}O_2$peak, Grey Matter Volume and Cognitive Performance

The FSL-VBM output showed no significant, or sub-threshold association between $\dot{V}$O2peak and GM brain volume.

Correlation analysis did not reveal any significant correlations between $\dot{V}O_2$peak and cognitive performance, or fMRI results following permutation testing to correct for multiple comparisons (Table 4.3). Average scores are shown in supplementary table 4.4.

Correlation Analysis				
Cognitive Test	**rCBF**	**hCBF**	**CVR**	**$\dot{V}$O2peak**
SCOLP	r = 0.06 p = 0.80, p' = 1.00	r = -0.01, p =0.96, p' = 1.00	r = 0.26, p = 0.27, p' = 0.832	r = -0.02, p = 0.95, p' = 1.00
Digit Span	r = 0.04, p = 0.88, p' = 1.00	r = 0.01, p = 0.97, p' = 1.00	r = -0.07, p = 0.76, p' = 1.00	r = -0.46, p = 0.04, p' = 0.233
Letter Fluency	r = -0.16,	r = 0.01,	r = 0.47,	r = 0.27,

Correlation Analysis				
Cognitive Test	**rCBF**	**hCBF**	**CVR**	**$\dot{V}$O2peak**
	p = 0.50, p' = 0.982	p = 0.99, p' = 1.00	p = 0.04, p' = 0.205	p = 0.25, p' = 0.808
Conners' Continuous Performance d'	r = -0.31, p = 0.18, p' = 0.675	r = 0.15, p = 0.52, p' = 0.985	r = 0.38, p = 0.10, p' = 0.46	r = 0.24, p = 0.31, p' = 0.878
Trail Making B	r = -0.02, p = 0.93, p' = 1.00	r = -0.06, p = 0.82, p' = 1.00	r = 0.01, p = 0.97, p' = 1.00	r = 0.20, p = 0.40, p' = 0.947
SDMT	r = 0.24, p = 0.32, p' = 0.889	r = 0.28, p = 0.99, p' = 1.00	r = 0.08, p = 0.75, p' = 0.999	r = -0.14, p = 0.56, p' = 0.991

Table 4.3 Correlations between cognitive task performance and fitness as well as CBF and CVR. RCBF = Resting CBF, hCBF = hypercapnic CBF. p' = corrected p value.

4.4 Discussion

4.4.1 Summary

In this study, we examined the effects of AF on two indices of cerebrovascular health, CBF and CVR, using MTI PASL. This is the first study to investigate CBF CVR as opposed to BOLD CVR in young adults, as well as being the first study to quantify whole GM CBF using ASL in young adults. Across the group, subjects with a higher $\dot{V}O_2$peak had lower GM CBF and greater CVR to CO_2. Second, the results did not support the hypothesis that $\dot{V}O_2$peak would be associated with better cognitive task performance.

4.4.2 $\dot{V}O_2$peak and CBF

The most striking result in this study was the inverse correlation between CBF and $\dot{V}O_2$peak, as the opposite was predicted based on findings from studies in children (Chaddock-Heyman et al., 2016), young adults (Bailey et al., 2013) and older adults (Ainslie et al., 2008; Brown et al., 2010; Thomas et al., 2013). However, with the exception of Thomas et al. (2013) and Chaddock-Heyman et al. (2016), previous studies have used TCD which measures blood flow velocity only as TCD cannot measure vessel diameter which would be required to calculate flow using this method. FMRI measures CBF directly through the labelling of inflowing blood

to tissue. Therefore, results should not be directly compared as they are measuring different, albeit related, vascular parameters. Second, MRI studies investigated groups undergoing neurodevelopment and older adults where the mechanistic relationships with AF may be different to adults not in stages of either development or decline.

In this study, CBF was not significantly lower across the brain, but was localised to regions of the thalamus, brainstem, visual cortex, cerebellum and precuneus. Regional variation in SNR may explain why these particular regions correlated with fitness. However, brainstem SNR is low for PASL (Brooks, Faull, Pattinson, & Jenkinson, 2013; Warnert et al., 2014), therefore if the results are SNR based, sensitivity to CBF differences in this region would not be expected. A study by Robertson et al. (2015) in stroke survivors, using single inversion time PCASL, similarly found an inverse correlation between precuneus CBF and AF, but also found a positive correlation between thalamic and posterior cingulate CBF and AF. Gauthier et al. (2015) found both positive and inverse correlations with AF in older adults, and the Robertson study adds to the evidence that AF may have complex, regionally varying effects on the brain. Although the direction of the correlation in stroke survivors contradicts the current results, the current study and that of Robertson et al. (2015) further suggests that AF may exert localised effects on CBF (Chaddock-Heyman et al., 2016; Thomas et al., 2013). Given that participants in each of these cited studies have differed in age and health status, the fact that consistent regions associated with AF have not been reported is unsurprising. The variance in the effects of AF on brain function with age needs further investigation through interventions in young and older groups.

There is a potential neurobiological explanation to explain the negative correlation between CBF and $\dot{V}O_2$peak in this study. Physical training which increases $\dot{V}O_2$max, leads to an increased ability of tissue to extract oxygen from blood (Kalliokoski et al., 2001; Ookawara et al., 2002). A higher oxygen extraction fraction (OEF) in fitter subjects would explain the inverse relationship between $\dot{V}O_2$peak and CBF as cerebral autoregulation ensures balance between CBF and OEF to maintain the optimum cerebral rate of oxygen metabolism. Usually, this means that in diseases where hypoperfusion has occurred, the OEF increases to maintain adequate oxygen supply to the brain (Derdeyn et al., 2002). However, in the healthy brain, fitness related OEF increases may result in the brain being able to extract the required energy from less blood, reducing CBF demand. Fitness may enhance oxygen extraction capacity in the healthy brain in early adulthood leading to observed reductions in CBF at rest. In later adulthood, this efficiency may serve to sustain optimal cerebrovascular function meaning that blood flow is higher in

trained than sedentary subjects, as the age-related CBF decrease is offset. This could explain the seemingly opposing effects of higher AF on CBF seen in this study in young adults and existing work in older adults. Further evidence for differential effects of AF with age comes from a recent study from Williams et al. (2017) which reported a positive correlation between cortical thickness and $\dot{V}O_2$peak in older adults but an inverse correlation between these measures in young adults. Future studies directly examining the relationship between AF, CBF and OEF would clarify whether the evidence supports this explanation.

Data from experimental models does however contradict the current results. Animals subjected to wheel running for several weeks had increased angiogenesis and therefore capillary density compared with sedentary animals (Pereira et al., 2007; R. . Swain et al., 2003). From this, in humans with higher levels of fitness, greater CBV and CBF could be predicted. However, the short duration of interventions and lifespan of rodents means that effects seen in these studies may not be comparable to work investigating effects of long term AF, gained through years of physical training.

Angiogenesis and capillary density cannot be studied *in*-vivo, instead CBV serves as an imaging correlate in humans. Although the gold standard method for CBV measurement using MRI is dynamic susceptibility contrast (DSC) MRI, CBV can be measured using VASO (Lu, Golay, Pekar, & Zijl, 2003) or respiratory gas challenges (D. Bulte, Chiarelli, Wise, & Jezzard, 2007) as contrast injection is not practical. Potential side-effects and adverse reactions to gadolinium contrast range from nausea and skin complaints to injection site pain and nephrotoxicity in extreme cases (Fraum, Ludwig, Bashir, & Fowler, 2017), therefore non-invasive alternatives are necessary. Non-invasive measurement of CBV is not trivial due to the difficulty of isolating blood volume from tissue (Lu, Hua, & van Zijl, 2013), however a number of methods do exist. VASO indirectly measures CBV changes through nulling signal from blood and measuring volume changes in the surrounding tissue, i.e., extravascular water signal. Using the latter method of hyperoxia as an intravenous contrast agent, combining hyperoxic and normoxic blocks, CBV can be estimated through the calculation of the signal difference during baseline and steady state "infusion" of oxygen which is then normalised using the parameter *M*. Future work should measure CBV to examine volume differences between trained and sedentary groups, as well as changes brought about by physical activity interventions as CBV more closely reflect angiogenesis than CBF. In this study, CBV values were much lower than literature averages (Paula, Emma, & Ian, 2015; Yan, Li, Kilroy, Wehrli, & Wang, 2012) and CBV was not strongly related to $\dot{V}O_2$peak (supplementary figures 4.13 and 4.14). This contrasts with the

work of Pereira et al. (2007) who used T1 signal differences before and after gadolinium contrast to infer CBV increases in the DG in both rodents and young adults following ET. However, as CBV was not a primary outcome measure, the ASL sequence used here was not optimised for CBV, but was estimated as part of the kinetic model fitting (Michael A. Chappell et al., 2010) as was tissue arrival time (TAT). TAT influences CBF estimation, as it is an index of dispersion of tagged blood throughout the brain. As such, TAT is affected by arterial function and is known to be affected in diseases such as MS (Paling et al., 2014). In this dataset, there was not a strong association between TAT and $\dot{V}O_2$peak (supplementary tables 4.11 and 4.12), possibly due to the fact that all subjects regardless of fitness were assumed to have healthy arterial function.

Upon neuronal activation, there is an increase in demand for energy; in the healthy brain this is met with an increase in CBF through dilation of upstream arteries. These arteries deliver blood to arterioles which in turn feed capillaries in the active tissue. The lower resting CBF observed here, although initially counterintuitive, is not problematic if there is an adequate vascular reserve to meet energy demands. The data support this argument as a greater CVR to CO_2 was observed in subjects with a higher $\dot{V}O_2$peak. If AF maintains CBF and metabolic efficiency, both of which naturally decline with age, then an increase in CBF would be expected when comparing trained versus sedentary older adults. Such an explanation would fit with the seemingly contradictory results found in the ageing literature and the current experimental data. AF enhances metabolic efficiency in young people leading to a reduced CBF but also maintains optimal energy supply and metabolism with advancing age, leading to higher CBF measures in fit versus sedentary older groups.

Although evidence to date is not in agreement with the current results, either different aspects of cerebrovascular function have been investigated, or the age ranges (children and older adults) mean that we may be observing different age-dependent cerebrovascular effects of AF. It should be noted that De Vis et al., (2015) showed that $P_{ET}CO_2$ accounted for age-related CBF differences almost entirely. In this study, there was a positive trend ($r = .4$, $p = 0.06$) between baseline $P_{ET}CO_2$ and CBF, but no strong association between $\dot{V}O_2$peak and baseline $P_{ET}CO_2$ or the $\Delta P_{ET}CO_2$ during hypercapnia. This suggests a cerebrovascular effect of fitness on CVR rather than an effect on $P_{ET}CO_2$ alone.

4.4.3 $\dot{V}O_2$peak and CVR

The ROI analysis showed a moderate statistically significant positive correlation between CVR and $\dot{V}O_2$peak in global GM which was not observed in a follow-up voxelwise analysis. CVR, as it is dependent on CBF, declines with age. In the literature, there are contradictory reports on the association between CVR and AF (Bailey et al., 2013; Barnes, Taylor, Kluck, Johnson, & Joyner, 2013; Gauthier et al., 2015; Thomas et al., 2013), as discussed in the introduction, and the positive association between $\dot{V}O_2$peak and CVR reported here is in agreement with the TCD findings by Bailey et al. (2013), whereby young trained adults had greater CVR than a sedentary comparison group. However, few studies have investigated the relationship between CVR and AF in healthy young adults, therefore much more work is needed to adequately understand this relationship. The literature to date suggests that ET and AF has complex and varying effects on brain regions with potential mechanistic differences across the lifespan. This complexity presents an exciting area of future research in different age groups, and a need to comprehensively map cerebrovascular function across the brain.

4.4.4 Cognitive Performance

In this study, cognitive performance scores were similar across the group (see Supplementary Information) and there were no strong associations with $\dot{V}O_2$peak nor with fMRI measures. It is likely that more sensitive cognitive tests are required to detect differences among high functioning groups. It is also possible that cognitive differences in young adults may only be visible at more extreme ends of the fitness spectrum.

The cognitive reserve hypothesis (Chodzko-Zajko & Moore, 1994) states that higher fitness in older age offsets age-related decline in cerebral circulation, enhancing oxygen delivery to support neural demand. Etnier, Nowell, Landers, & Sibley (2006) conducted a meta-regression on studies examining the effects of fitness on cognitive function. A discussion on the full findings is beyond the scope of this chapter but in summary, the authors did not find strong support for a beneficial effect of fitness in any age group once moderator variables were considered, and in fact found a negative association between fitness and cognition in studies using a pre-post design. Only a very small number of studies report a beneficial effect of fitness or physical activity on select cognitive domains in young people (Baym et al., 2011; Themanon, Pontifex & Hillman, 2009; Stroth, Hille, Spitzer, & Reinhardt, 2016) and other studies report significant effects in older but not young adults (Hayes, Forman, & Verfaellie, 2014).

Lastly, there was no variation in structural volume with fitness in this sample as evidenced by VBM. Region-specific increases in volume following exercise interventions have been reported (Erickson et al., 2011; Thomas et al., 2015) in older adults and cross-sectional studies have reported an inverse relationship between cortical volume and $\dot{V}O_2$peak (V. J. Williams et al., 2017) in young adults. Greater hippocampal (Chaddock, Erickson, Prakash & Kim et al., 2010) and basal ganglia volume in children with higher AF (Chaddock, Erickson, Prakash & VanPatter et al., 2010). In sum, more work is needed in young adults to determine both structural and functional effects of AF and their functional relevance in terms of health and cognition.

4.4.5 Limitations

This study had a number of limitations.

A 90° saturation pulse is applied to the imaged volume before labelling is applied. The purpose of this saturation pulse is to zero the longitudinal magnetisation of the imaged volume and eliminate the T_1 effect introduced by a variable TR. However, as this saturation pulse is not perfectly timed, the variable TR, and incomplete nulling of the longitudinal magnetisation can have some residual influence on the signal from the static brain tissue, contaminating the signal from the label. Unfortunately, it is not possible to quantify how accurate the saturation pulse is at cancelling longitudinal magnetisation, also, its accuracy may vary across the brain and between tissue types. In this study, there were originally 10 inversion times, however, notable signal dips were observed at the first short TI (300ms) and first long TI (800ms). Images at these TIs were removed due to the signal contamination. Hence, there is a large gap from 700-1100ms where CBF was not estimated.

A second limitation is that haemoglobin ([Hb]) levels were not measured. Blood [Hb] is a protein molecule in red blood cells responsible for transport of O_2 to tissue. [Hb] concentration affects exercise performance; reduced [Hb] means that blood can carry less oxygen (Calbet, 2006). [Hb] concentration also affects perfusion estimates as there is an inverse relationship between [Hb] and the T_1 of blood. Brain [Hb] cannot be measured directly *in-vivo*, however capillary samples may provide an indication of [Hb] differences between subjects or groups which could help to explain biological mechanisms driving CBF differences.

Like many fMRI studies, costs and time constraints limited the sample size. In this sample of 20 subjects, results with borderline statistical significance or in some cases only directional trends were observed. As more data becomes available, it will be more feasible to conduct detailed power analyses and inform priors for Bayesian analysis. This more rigorous approach

may help to clarify whether real differences exist between groups and how confident researchers can be about the validity of results.

Here, the voxelwise and ROI analyses were not in total agreement. While the voxelwise analysis of CBF revealed regions of significantly lower CBF with fitness, the ROI analysis showed a non-significant trend in the same direction for global GM. The ROI analysis of CVR however, showed a moderate significant association with fitness while the voxelwise analysis did not reveal a strong trend in any direction related to fitness. This work needs replication to be able to make any definitive conclusions about the results. ASL is an intrinsically low SNR technique compared to standard BOLD EPI. Although ASL offers significant benefits in terms of quantification of physiological parameters, the SNR may have prevented detection of greater voxelwise associations with $\dot{V}O_2$peak. An alternative possibility is that CBF is more heterogeneous throughout the brain than CVR which is more affected by low SNR; therefore greater averaging of data in the ROI analysis allowed CVR differences to be detected.

Lastly, there are known hormonal effects on exercise test performance (Jonge, 2003) and CBF (Brackley, Ramsay, Pipkin, & Rubin, 1999; Duckles & Krause, 2007). In this case, the CBF difference at baseline was not significantly different between groups; t(18)=-0.602, p = 0.094 but controlling for menstrual cycle phase or limiting individual studies to one sex only would reduce variability within cohorts. It is important to ensure both sexes are studied however, as hormonal differences are likely to play a role in mediating the effects of fitness on brain health. Moreover, intervention studies are necessary to determine sex-specific responses to exercise.

4.4.6 Future Directions

Pathological mechanisms such as inflammation and loss of vascular elasticity associated with ageing and disease are associated with alterations in CBF and energy metabolism. Numerous studies have demonstrated cerebrovascular changes with so-called healthy ageing (Aanerud et al., 2012; Lu et al., 2011; Martin, Friston, Colebatch, & Frackowiak, 1991) as well as dementia (Cantin et al., 2011; Daulatzai, 2017) and non age-related progressive neurological diseases such as MS (D'haeseleer, Cambron, Vanopdenbosch, & De Keyser, 2011a; Juurlink, 2013). The most consistent finding with regards to AF and brain function is that fitness appears to offset age-related CBF decreases. Studies measuring OEF and $CMRO_2$ in trained vs. sedentary older adults would be extremely informative to build on this work to characterise vascular and metabolic health benefits of AF. Lu et al. (2011) reported $CMRO_2$ increases with age, from

these results a lower $CMRO_2$ in trained older subjects vs. sedentary controls would be predicted if AF offsets ageing effects.

In young people, we know very little about how AF affects cerebrovascular function. In-depth mapping of multiple aspects of cerebrovascular function e.g. CBF, CBV, CVR, $CMRO_2$ and OEF in both young and older trained and sedentary adults will provide information necessary to move forward in developing ET protocols to increase the adoption of fitness training as a preventative health tool.

A clear narrative about the role AF plays in supporting brain function is lacking, despite accumulating evidence of its efficacy in both preventing cerebrovascular decline (Thomas et al. 2013; Zimmerman et al., 2014) and improving patient outcomes (Ivey et al., 2011). Contradictory results may be a major factor limiting the use of exercise to increase aerobic capacity as a clinical tool. With evidence-based examples of how AF benefits brain health, schools would be encouraged to place more emphasis on physical education and the importance of maintaining fitness from childhood to late adulthood. Research investigating the neurological effects of fitness across the lifespan is therefore extremely important, but a collaborative effort is required due to the conflicting results arising from small studies and methodological differences. Recent efforts to clarify differences between MRI and TCD measures of CVR (Burley et al., 2016) are valuable and will allow the methods to be complementary rather than contradictory.

Research over the next decade should work to establish whether it is exercise itself that delivers brain benefits or higher AF as a result of exercise. Answering this question will guide optimal dose-response recommendations and guide interventional studies. At present, mixed effects in the literature are likely due to interventions differing in intensity and duration and levels of fitness in fit vs. sedentary comparison groups.

The results of the current study suggest that fitness influences cerebrovascular function in young, healthy adults, however the modest effects observed need replication in larger samples. As mentioned in previous paragraphs, follow-up studies could extend the current investigations by directly examining whether higher $\dot{V}O_2$peak is associated with greater OEF, and whether the reduced CBF seen in this study can be replicated. Additionally, CBV quantification would provide evidence for increased capillary density due to chronic physical activity. This could be achieved using ASL with hyperoxia and hypercapnia challenges (D. Bulte

et al., 2007). This method, with optimisation, could also be used to estimate WM vascular parameters including CBV and CVR. Investigations in WM require careful MRI parameter planning due to the lower signal in WM, hence why existing studies have mostly limited investigations to GM.

Finally, this work has focused solely on AF. The importance of strength training should not be ignored. Resistance training increases bone density, has hormonal influences during development and adulthood as well as associations with psychological well-being (Westcott, 2011). However, it is sensible at present to separate resistance and AF training separately to determine mechanistic links with health.

Chapter 4 Supplementary Information

4.5 Cognitive Performance

Cognitive Test	Mean (sd)
Conners Continuous Performance (d')	43.6 (7.6)
SDMT	62 (10)
Trail Making B	51.3 (28.5) (s)
SCOLP (max 100)	81 (17)
Digit Span (LDSF)	6.8 (1.4)
Letter Fluency	45.1 (8.6)
HADS A	3.75 (2.2)
HADS D	0.7 (0.9)

Table 4.4 Group average cognitive test perfomrmance.

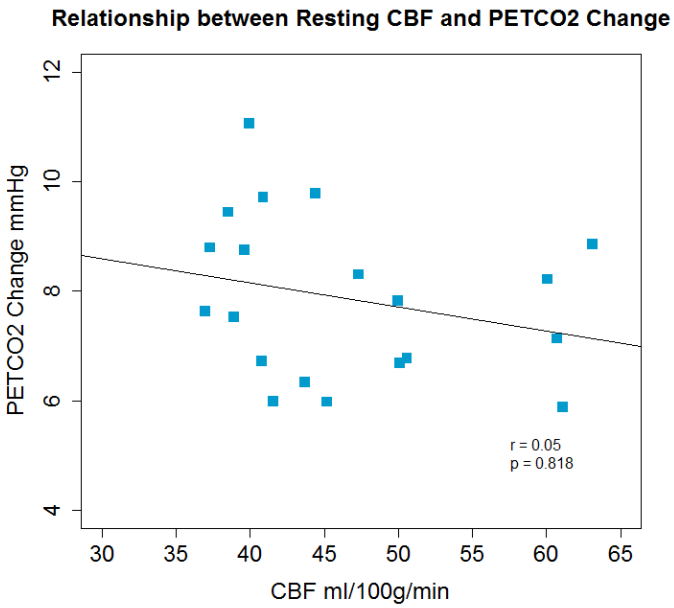

Figure 4.8 Baseline CBF was not strongly related to the ΔPETCO2 during hypercapnia

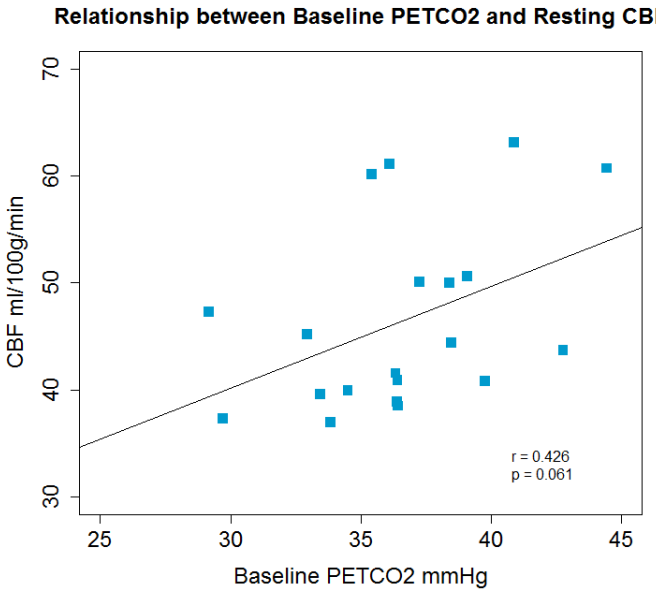

Figure 4.9 There was a non-significant positive association between resting CBF and baseline $P_{ET}CO_2$

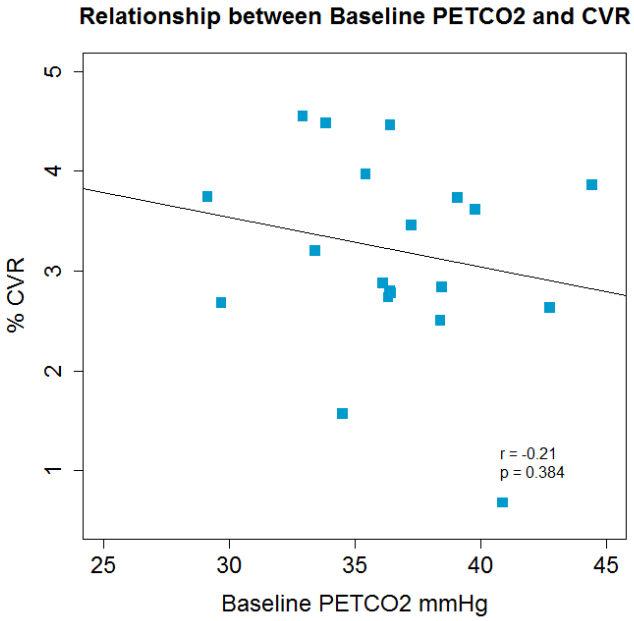

Figure 4.10 Baseline $P_{ET}CO_2$ was not a strong predictor of CVR

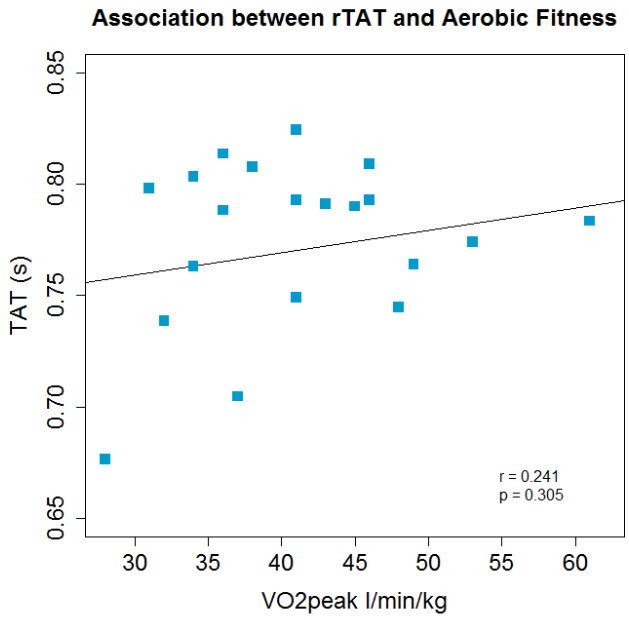

Figure 4.11 AF and TAT at rest were not strongly associated

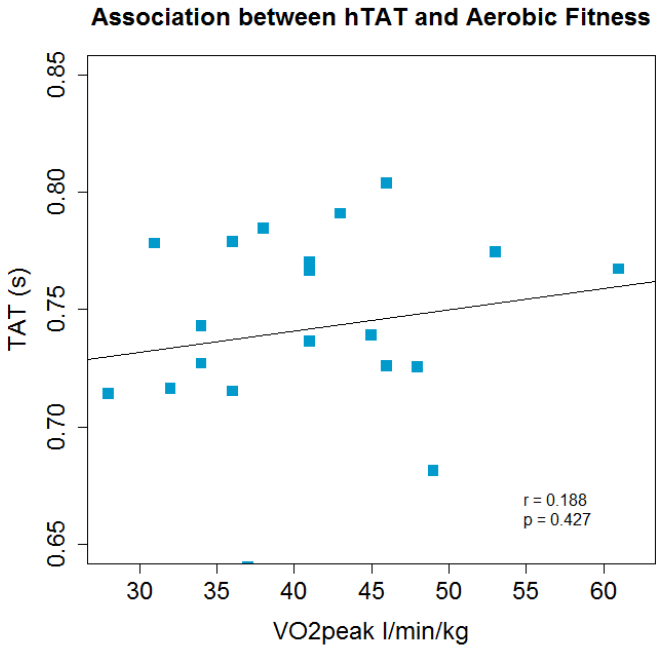

Figure 4.12 As above, AF and TAT during hypercapnia were not strongly associated

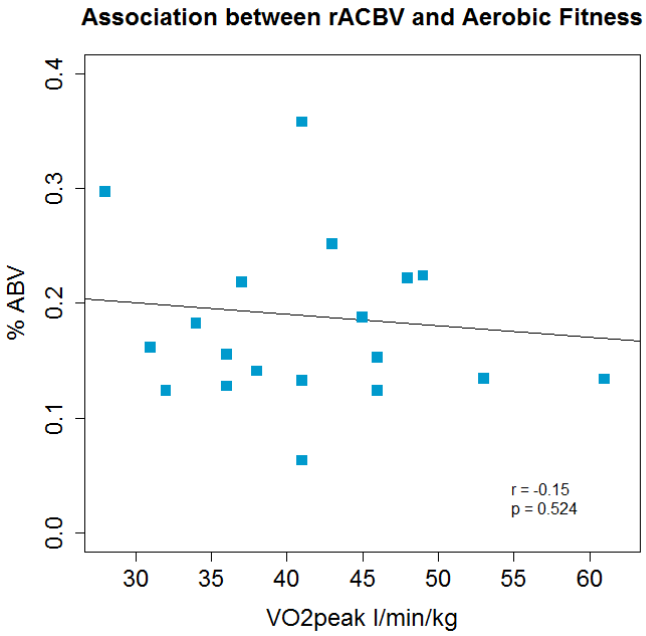

Figure 4.13 A weak inverse assocaiton between aCBV at rest and AF.

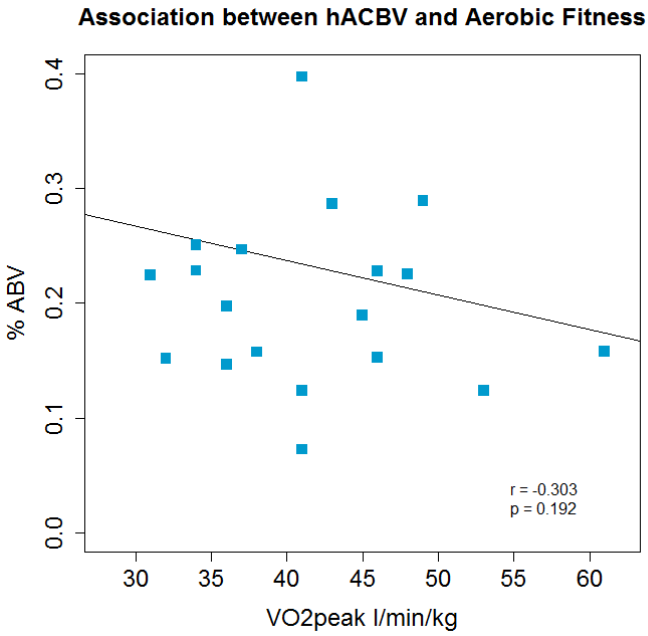

Figure 4.14 As above, a weak inverse assocaiton between aCBV during hypercapnia and AF.

4.6 Power Analysis

Power Analysis			
Post-Intervention Correlations with $\dot{V}O_2$peak	**Effect Size (r)**	**Power**	**Sample Size required for power of 0.8**
Resting CBF	0.405	0.45	44
Hypercapnic CBF	0.23	0.17	143
CVR	0.619	0.91	15

Table 4.5 Power analysis conducted post-hoc to determine power and sample sizes for future studies. All calculated using the correlation coefficient (r) in G*Power

Chapter 5

A Cross-Sectional and Interventional Study to Characterise the Cerebral Vascular and Metabolic Effects of Aerobic Fitness

Abstract

Introduction: To elucidate the proposed neuroprotective effects of aerobic fitness (AF) on cerebrovascular function, it is necessary to conduct cross-sectional and interventional studies. This study investigated, cross-sectionally, associations between $\dot{V}O_2$max and cerebral blood flow (CBF), cerebrovascular reactivity (CVR), capillary blood volume (CBVcap), baseline oxygen extraction fraction (OEF_0), and the cerebral metabolic rate of oxygen consumption ($CMRO_2$). Second, a 1-week intensive exercise training (ET) intervention was conducted to assess whether rapid brain vascular and metabolic adaptations occur with ET.

Methods: Dual-calibrated, dual-excitation PCASL fMRI was conducted at baseline and following 1-week of ET in 15 healthy males aged 23-43 years old. An estimated $\dot{V}O_2$max test to estimate AF was conducted at baseline using cycle ergometry and the Storer method to calculate $\dot{V}O_2$max. Exercise training consisted of 5 supervised sessions of stationary cycling at 55-75% of the age-predicted maximum heart rate for 25 minutes, followed by a circuit of resistance exercises on 3 of the 5 days.

Results: ROI analysis of the post-intervention data showed that CBVcap, $CMRO_2$ and OEF_0 were negatively correlated with estimated $\dot{V}O_2$max, before corrections for multiple comparisons. Voxelwise analysis of the post-intervention data showed significant negative correlations with estimated $\dot{V}O_2$max for CBVcap and OEF. CBVcap was negatively correlated with estimated $\dot{V}O_2$max in left primary motor cortex (M1), left precuneus, bilateral anterior and posterior cingulate gyrus, left intracalcarine cortex and left lateral occipital cortex. For OEF, the negative correlation with $\dot{V}O_2$max was confined to the left M1 and supplementary motor areas. No other correlations between pre-training or post-intervention data and estimated $\dot{V}O_2$max were statistically significant. The intervention did not result in significant changes in any parameter of interest. ***Discussion:*** The cross-sectional data suggest that AF leads to lower CBVcap and OEF_0 in numerous cortical regions including the precuneus and M1. However

further investigations are needed to rule out confounding effects of capillary transit time heterogeneity (CTTH), the oxygen tension of tissue (PtO_2). The intervention suggests that sustained cerebrovascular adaptations due to AF occur over longer periods of time, and are independent of acute cerebral responses to exercise.

5.1 Introduction

To elucidate the effects of aerobic fitness (AF) on cerebrovascular function, it is necessary to conduct cross-sectional and intervention studies. The previous chapter investigated cross-sectionally the relationship between $\dot{V}O_2$peak, baseline CBF (CBF_0) and CVR in young, healthy adults. Secondly, the links between $\dot{V}O_2$peak, brain function and cognition were explored. The results showed that greater $\dot{V}O_2$peak was associated with lower CBF and higher CVR in grey matter (GM). However, there was no association with cognitive performance.

The study described in this chapter follows on from the work reported in Chapter 4, to test the hypothesis that the lower CBF observed in more aerobically fit subjects was due to metabolic adaptations, whereby greater ability to extract oxygen from blood results in lower CBF requirements. Data from Chapter 4 was combined with measures of baseline oxygen extraction fraction (OEF_0), collected for a separate study by Merola et al. (2017), for common subjects (n=7) by Furby (2016) to assess whether AF is associated with increased brain tissue OEF. A trend towards a greater OEF with higher $\dot{V}O_2$peak was observed but did not reach statistical significance. A post-hoc power analysis conducted by Furby (2016) calculated a required sample size of 15 to detect an adequately powered effect.

The current study recruited 15 healthy males <45 years old, to further investigate the relationship between AF, CBF_0 and OEF_0. Previously, no correlation between the cerebral metabolic rate of oxygen consumption ($CMRO_2$) and OEF has been observed at rest (F. Xu, Ge, & Lu, 2009) and under neural activation OEF is decreased vs. rest as the fractional change in CBF is typically 2-4 times greater than the fractional $CMRO_2$ increase (Fox & Raichle, 1986). However, based on the hypothesis that higher baseline OEF (OEF_0) in subjects with higher AF is due to greater metabolic capacity, it is of interest to also investigate whether resting absolute $CMRO_2$ is also affected by AF. If oxygen supply, in the form of CBF, is altered with fitness level (Bailey et al., 2013; Chaddock-Heyman et al., 2016; Thomas et al., 2013), then oxygen demand would also be expected to differ. Age-related global increases in $CMRO_2$ have been reported (Lu et al., 2011), and as AF is thought to offset age-related vascular and metabolic decline, $CMRO_2$ could be predicted to be lower in individuals with greater AF. However, animal studies report increased neurogenesis with exercise training (Cotman & Berchtold, 2002; van Praag et al., 1999), which suggests that if similar processes occur in humans, then a higher $CMRO_2$ to sustain larger neuronal populations may be observed. As the

relationship between AF, OEF and $CMRO_2$ has not been reported in young adults, studies such as the current one are much needed to understand the role of AF in cerebral energy demand and supply, and the functional significance of this in terms of cognition and protection against age and disease related damage.

In Part 1 of this study, we expected CBF and OEF to show inverse and positive correlations with $\dot{V}O_2$max, respectively, along with a positive CVR and $\dot{V}O_2$max association, in line with the previous results, and the suggestion that fitness increases vascular reserve (Bailey et al., 2013; Bherer, Erickson, & Liu-Ambrose, 2013). The use of dual-calibrated[4], dual-excitation pulsed continuous arterial spin labelling (PCASL) also enabled estimation of capillary cerebral blood volume (CBVcap) from BOLD signal changes and estimation of OEF_0 (D. P. Bulte et al., 2012b; Germuska et al., 2016).

Animal models have reported greater angiogenesis, as well as neurogenesis, in the dentate gyrus (DG) of the hippocampus in exercised animals (Pereira et al., 2007; Swain et al., 2003a, 2003b), resulting in higher CBV. Pereira et al. (2007) found similar results in humans using T1-weighted gadolinium contrast imaging to acquire global CBV maps. Results showed that DG CBV increased following 3 months of exercise training, and CBV following the intervention was correlated with individual changes in $\dot{V}O_2$max, suggesting a direct link between fitness and CBV. This CBV increase was limited to the DG and entorhinal cortex, although CBV increases in the latter did not reach statistical significance. Pereira et al. (2007) investigated hippocampal subregions, specifically, rather than whole brain effects. The hippocampus is particularly affected by the ageing process along with default mode areas including the posterior cingulate and precuneus (Boraxbekk et al., 2015), and plays an important role in cognitive functions such as memory encoding, pattern separation (Deng, Aimone, & Gage, 2010) and spatial navigation (Ekstrom et al., 2003). AF is known to offset cognitive effects of ageing (Bherer, Erickson, & Liu-Ambrose, 2013; Voss et al., 2015), therefore, investigating and demonstrating increased CBV with AF in this region provides evidence for a mechanism through which exercise benefits hippocampal-mediated cognitive functions. Investigating whether increased $\dot{V}O_2$max and CBV

[4] Dual-calibrated fMRI uses hypercapnia and hyperoxia to modulate BOLD and CBF responses. Hyperoxia enables estimation of venous oxygen saturation from which baseline OEF and absolute $CMRO_2$ can be estimated, unlike calibration with hypercapnia alone where only relative $CMRO_2$ changes can be estimated.

were associated with cognitive performance, Pereira et al. (2007) found that $\dot{V}O_2$max after exercise training was related to better verbal learning performance and a trend was observed for verbal learning and CBV. Delayed recognition and source memory testing showed similar trends but did not each significance for $\dot{V}O_2$max or CBV. These selective effects on cognition are representative of effects seen elsewhere in healthy adults (Etnier, Nowell, Landers, & Sibley, 2006; Thomas et al., 2015) and it is possible that cognitive effects of AF are not observed in younger adults at the peak of lifetime cognitive ability. Cerebrovascular effects in young adults, such as CBV changes observed by Pereira et al. (2007) may indicate long-term neuroprotective processes, essentially laying down vascular reserve for later life. For this reason, the current study focuses on cerebrovascular rather than cognitive effects of AF. Further, it is important to elucidate the effects of AF across the brain, to determine whether the hippocampus is selectively responsive to exercise training, or whether AF can benefit global brain health. The DG may particularly benefit due to its capacity for neurogenesis, but AF may have benefits for cerebral arterial health maintaining a healthy energy supply and preserving function in the rest of the brain where neurogenesis does not occur across the lifespan. In the current study, we investigated associations between $\dot{V}O_2$max and cerebrovascular parameters in whole brain GM.

There is a lack of exercise training (ET) intervention studies in young adults aimed at establishing ET-related cerebrovascular changes, an exception being the Pereira et al. (2007) study discussed above, and a transcranial Doppler (TCD) ultrasound study by Murrell et al. (2013) which reported an increase in CVR at rest and during sub-maximal exercise following 12-weeks of ET in young and older adults. Thomas et al., (2015) conducted a 6-week intervention study in young adults and used a multi-modal approach to investigate hippocampal changes in volume, as well as myelination and total CBV, assessed using susceptibility-weighted imaging (SWI), quantitative susceptibility mapping (QSM), T1, T2 and direct CBV measurement using contrast agent. After 6 weeks, increased volume of the anterior hippocampus along with apparent myelination increases were observed. However, hippocampal volume returned to baseline 6 weeks post intervention where training was discontinued. The SWI, QSM and T2 imaging was suggestive of myelin changes rather than vascular adaptations, and the CBV imaging did not reveal any significant indications of blood volume changes. This result is intriguing as it is difficult to explain the mechanistic drivers of structural changes without accompanying metabolic adaptations. In the current study, cerebrovascular rather than structural adaptations with ET were of interest, therefore,

multiple indices of flow and metabolism, including OEF and $CMRO_2$ as well as capillary CBV, were calculated to differentiate between specific vascular and metabolic processes which may be altered through ET.

Regarding the timescale of changes, an intervention was conducted which reduced exercise, requiring Masters Athletes to cease training for 10 days (Alfini et al., 2016), which led to rapid perfusion reductions across the brain. This study suggests that rapid cerebrovascular adaptations occur in response to detraining, therefore equally rapid adaptations in response to ET may also occur. Intervention studies are necessary to rule out potential differences attributed to fitness, but which are actually driven by other behaviours that physically active people engage in, e.g. a healthy diet, and to determine the timescale of brain adaptations to physical training. For example, it is still not clear whether cerebral benefits of exercise are specifically due to greater AF in individuals who exercise regularly, or whether regular exercise participation is sufficient to gain benefits. Intervention studies will help to clarify this question and determine how long it takes to achieve neurophysiological and cognitive benefits, as well as the intensity of exercise required to have an effect on brain health.

Part 2 of the current study enrolled volunteers in a short ET intervention. To the best of our knowledge, no published studies have used ASL fMRI to investigate the effects of a short ET intervention in young adults. The timescale of exercise-related brain changes is unknown, however, short-term changes in brain microstructure have been demonstrated in non-exercise related training studies, for example after a 2-hour spatial learning task (Hofstetter, Tavor, Moryosef, & Assaf, 2013) and the same duration of virtual car racing (Sagi et al., 2012). Motor learning studies discussed in the following Chapter 6, show that resting brain activity is altered following motor training (Albert, Robertson, & Miall, 2009; Ma, Narayana, Robin, Fox, & Xiong, 2011), and although these changes may not reflect sustained brain changes, they show that even stationary training interventions can lead to short-term cerebrovascular alterations. In studies more directly related to the current work, acute exercise interventions have shown decreases in resting CBF following exercise (MacIntosh et al., 2014). The study by Macintosh et al. (2014) used single inversion time PCASL fMRI to assess perfusion before and after 20 minutes of moderate intensity cycling in healthy young adults (mean age = 26). Results showed global GM decreases at 10 minutes post-exercise and in an ROI analysis, decreases were observed over the same timescale in the hippocampus and insula. These reductions returned

to baseline by 40 minutes post-exercise where an increase in perfusion was observed in a voxel-wise analysis in left somatosensory cortex. However, a separate small study using multiple inversion time (MTI) PASL contradicts the results of Macintosh et al. (2014), reporting increases in global resting CBF following 30 minutes of moderate cycling (Carson-Smith, Paulson, Cook, Verber, & Tian, 2010).

Although contradictory, both studies show acute cerebrovascular changes following exercise, therefore, it is likely that following 1-week of intensive training, changes could be observed within 24 hours following a week of intensive training. The direction of effects, however, is less predictable given the small existing literature on acute exercise in young adults. The duration of training needed to see longer-term brain health and behaviourally relevant changes is beyond the scope of this intervention; the main aim here was to investigate whether a 1-week ET intervention leads to measurable changes in physiological parameters frequently used as indices of overall brain health. We examined changes in the same parameters as Part 1; CBF_0, CVR, CBVcap, OEF_0 and absolute $CMRO_2$ before and after 1-week of mixed cardiovascular and high intensity resistance training in addition to normal physical activities.

5.2 Methods

5.2.1 Participants

15 healthy males aged 23-43 (mean 29.8±6) were recruited from advertisements placed around Cardiff University. The study was approved by the Cardiff University School of Psychology Research Ethics Committee and performed in accordance with the guidelines stated in the Cardiff University Research Framework (version 4.0, 2010).

5.2.2 Screening Visit

Eligibility was assessed for MRI, exercise participation and respiratory manipulations in the initial screening visit. The Physical Activity Readiness Questionnaire (PAR-Q) and American College of Sports Medicine (ACSM) checklist were used for exercise eligibility screening. The International Physical Activity Questionnaire (IPAQ) Short Form was completed at screening by all volunteers to estimate AF. Based on answers to this questionnaire, the researchers were satisfied that there would be an adequate spread of fitness levels in the study.

Volunteers then completed a respiratory gas manipulation session which was identical to the experimental procedure in a mock MR scanner in the presence of a qualified anaesthetist. This

allowed volunteers to become accustomed to the procedure prior to the scan sessions and reduce the likelihood of adverse events.

5.2.3 Estimation of $\dot{V}O_2$max

$\dot{V}O_2$max was estimated from a submaximal fitness test, therefore, when referring to the $\dot{V}O_2$max data from this study, it is estimated $\dot{V}O_2$max. Prior to the test, participants were required to fast for 12 hours overnight and tests were conducted between 7.30am and 11am. Participants were also instructed to abstain from alcohol and exhaustive exercise for 24 hours prior to the test. The fitness test began with a 1-minute warm up at 25 watts on a Lode cycle ergometer (Lode, Groningen, Netherlands). The test began at 50 watts and was increased by 15 watts every 60 seconds while participants maintained a target constant RPM of 70. The test was terminated if RPM dipped below 60 for >10 seconds. Borg ratings of perceived exertion (RPE) for legs and breathing were recorded every minute using the CR10 scale (Borg & Kaijser, 2006). Capillary blood lactate and haemoglobin levels (Hb) were measured from the earlobe at rest and at the point of test termination (100% exertion) as described in Chapter 4. Blood pressure (BP) and heart rate (HR) were recorded at baseline, at the end of each test step and at test termination using the MEDRAD system (MEDRAD, Pittsburgh, PA) and Polar FT1 heart rate monitors (Polar, UK) respectively. Participants were encouraged to cycle until heart rate exceeded 95% of the age predicted maximum, however, tests were terminated upon volitional exhaustion. Fitness tests were only conducted at baseline as $\dot{V}O_2$max was not expected to change in one week based on previous work showing no change in $\dot{V}O_2$max with moderate intensity training for 8 weeks (Helgerud et al., 2007).

5.2.4 Imaging Data Acquisition

Participants were scanned at baseline (Scan 1) and the day following the fifth exercise training session (Scan 2) at the same time each day. Scan sessions were scheduled for 2pm or 4pm and participants were required to fast and abstain from caffeine for 6 hours prior to the scan.

All images were acquired on a Siemens 3T Prisma full-body scanner (Siemens, Erlangen, Germany) using a 32 channel receive head coil. A phase contrast scan of the neck was acquired to allow optimal placement of the PCASL labelling plane; TR/TE=40.65/5.60, FOV=240mm, 60 slices, slice thickness 1.3mm, flip angle=10°, GRAPPA=2.

Functional data were acquired on a 3T Siemens Prisma MRI system using a 32-channel head coil (Siemens, Erlangen, Germany). A dual-calibrated dual-excitation PCASL sequence lasting approximately 18 minutes (249 volumes) was used; TR1/TR2/TE1/TE2=3600/800/10/30ms, TI/post-label delay= 1500/1500ms, 3.4x3.4x7mm voxels with 1mm gap, 16 slices, FOV=220mm, GRAPPA=3, flip angle=90°. Two nonselective adiabatic inversion pulses were applied 950 ms and 300 ms prior to image acquisition for background suppression. This sequence was developed in house by Dr. Michael Germuska. A PCASL calibration scan to calculate M_0 of CSF for absolute quantification of CBF was acquired with identical parameters to the dual-excitation scan, except the TR which was 6000ms to allow full relaxation of the signal. A high-resolution T1-weighted magnetization-prepared rapid gradient-echo (MPRAGE) scan was also acquired for creation of individual GM masks; TR/TE/= 2100/3.19/ms, 1.2mm resolution.

5.2.5 Respiratory Modulation Protocol

$P_{ET}CO_2$ and $P_{ET}O_2$ traces were recorded during scanning through a sampling line connected to a facemask which attached to a gas analyser system running Labchart software (both ADInstruments, Bella Vista, Australia). The breathing circuit used for delivery of gas mixtures is shown in figure 5.1 and was adapted from the circuit described by Tancredi, Lajoie, & Hoge (2014). The respiratory protocol has been described previously by Merola et al. (2017). Briefly, to achieve mild hypercapnia, fixed inspired (FI) levels of gas mixtures containing 5% CO_2 (balance air) were administered, and to achieve hyperoxia 50% O_2 mixtures were delivered. To accelerate the transition to and from hyperoxia, short periods of 100% O_2 (14s) and 10% O_2 (balance N2) (40s), respectively, were used (see figure 5.2). The duration of hypoxic mixture inhalation was short enough not to induce arterial hypoxia. Mixtures were delivered at a constant total flow rate of 25 L/min to a gas mixing chamber in the MR control room and connected to the breathing circuit through a humidifier. A separate O_2 backup cylinder was connected directly to the breathing circuit in case of emergency. A laptop using MATLAB software was used to control the voltage output from a NI-DAQ AD converter (National Instruments, Austin, Texas) which were piped into 4 mass flow controllers at 25 L/min. Flow rates and end-tidal traces were monitored by a researcher throughout the experiment to ensure participant safety.

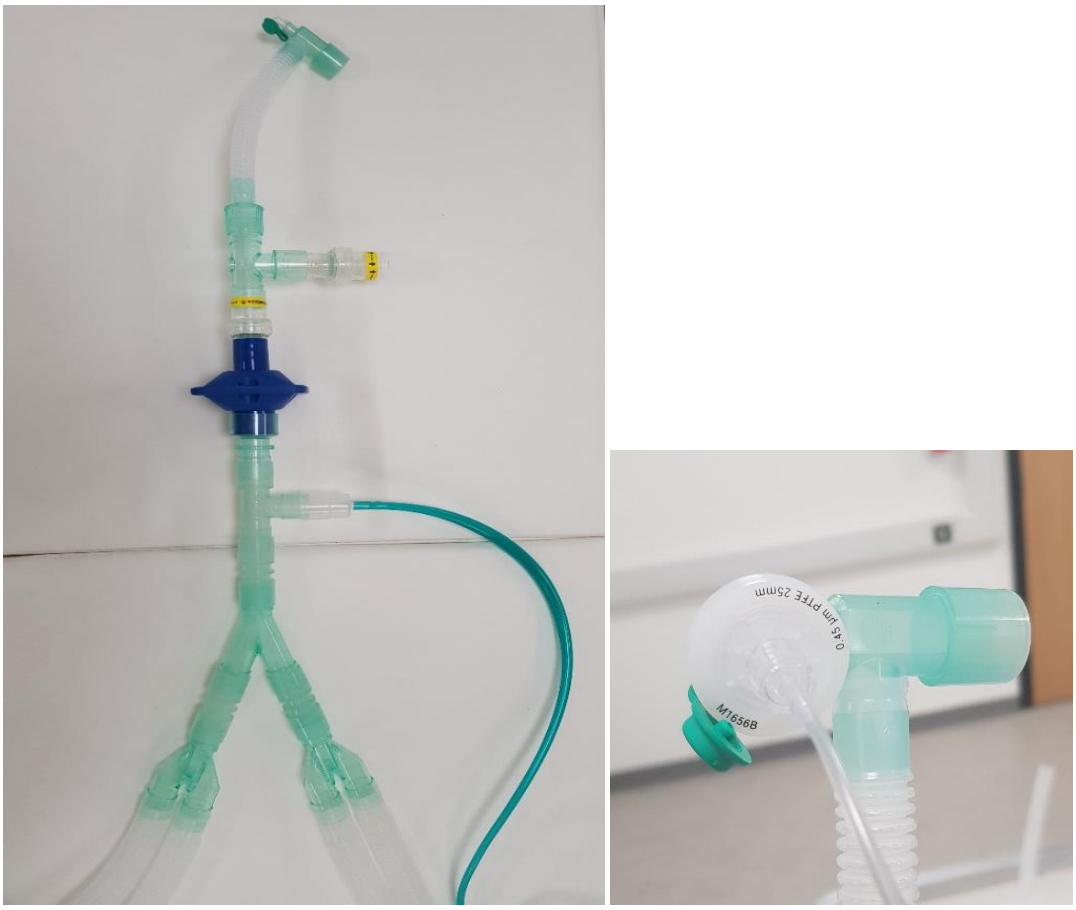

Figure 5.1 Breathing circuit (left), bacterial filter and sample line for recording end-tidal traces (right)

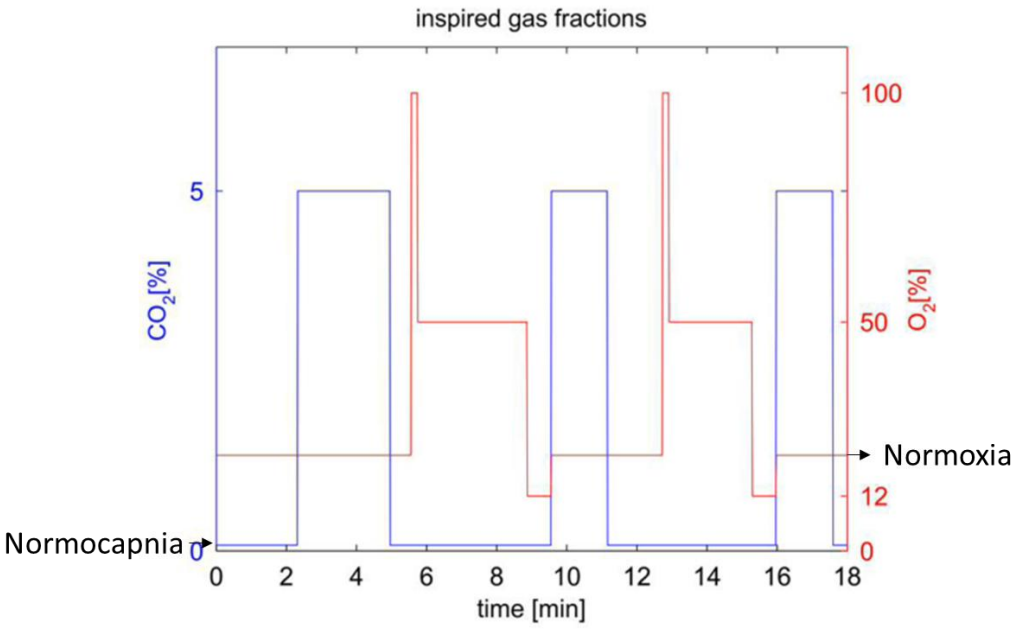

Figure 5.2 Protocol for respiratory gas manipulation, adapted from (Merola, 2016). Red line shows oxygen manipulation and blue line shows carbon dioxide manipulation.

5.2.6 Exercise Training

Volunteers completed 5 supervised exercise sessions over 7 days (table 5.1) in addition to maintaining their regular activities. Training sessions were held at lunchtime and evenings to accommodate those who participated in evening activities. The 1-week period was chosen to ensure full compliance and as a starting point for determining the timescale of exercise-induced brain changes. Each session consisted of 25 minutes of moderate intensity cycling on a Keiser M3 spin ergometer (Keiser®, Keiser M3 Indoor Cycle, Fresno, California), and on 3 of the 5 days a circuit of 5 bodyweight resistance exercises (table 5.2). Participants cycled at an RPM and resistance level of their choice which maintained heart rate at 50-75% of their age predicted maximum. In the resistance circuit, participants were asked to complete the sets as quickly as possible while maintaining the correct form. If participants completed the prescribed sets easily, they were encouraged to do additional sets within the 30-minute allocated period. While this circuit was comprised of resistance exercises, they were compound movements executed quickly, meaning that heart rate remained elevated for most of the session. Therefore, the resistance circuit was also considered cardiovascular training.

Example Testing and Training Schedule for Study Participants									
	Mon	**Tue**	**Wed**	**Thu**	**Fri**	**Sat**	**Sun**	**Mon**	**Tue**
PPT 1	Fitness Test	MRI 1							MRI 2
		C (1)	C & R (2)	C (3)	C & R (4)	-	-	C & R (5)	

Table 5.1 Example schedule for a participant. C = cardiovascular exercise, R = resistance exercise, PPT = participant. Total time commitment for the study was ~11 hours for a given participant. Supervised exercise was not carried out on weekends.

Exercise	**Sets**	**Repetitions per Set**
Squat	3	10-12
Forward Lunge	2	20 (10 per leg)
Press Up	2	10-12
Glute Bridge	2	10-12
Tricep Dip	2	20

Table 5.2 Resistance exercise circuit. Sets and repetitions are the minimum prescribed, participants were encouraged to do as many sets as they could achieve in 30 minutes.

5.3 Data Analysis

5.3.1 $\dot{V}O_2$max Estimation

$\dot{V}O_2$max was estimated using the Storer equation for males. The Storer equation estimates $\dot{V}O_2$max based on age, weight in kilograms and watts achieved (wattage for last full minute completed) using the following formula for males;

*Predicted $\dot{V}O_2$max = (10.51*watts) + (6.35*KG) - (10.49*age) + 519.3*

5.3.2 Image Preprocessing

Motion correction was carried out using FSL MCFLIRT (https://fsl.fmrib.ox.ac.uk/fsl/fslwiki/MCFLIRT) (Mark Jenkinson et al., 2002) followed by brain extraction using FSL BET (Smith, 2002). Slice timing correction was applied and data were spatially smoothed with a 6mm Gaussian kernel using SUSAN (Smith & Brady, 1997). These steps were applied to first and second excitation data.

5.3.3 Physiological Traces

Data analysis was carried out in MATLAB (Mathworks, Natick, MA, USA). $P_{ET}CO_2$ and $P_{ET}O_2$ traces were aligned to the fMRI data to remove effects of delay between the recorded traces and the BOLD and CBF data. Misaligned traces would result in errors in the calculation of the neurophysiological response to hyperoxia and hypercapnia. Physiological traces were used as input into the physiological model (see below) to constrain the model fit within the gas delivery paradigm. Second, $P_{ET}O_2$ was used to estimate the arterial blood T_1 change, as described by Germuska et al. (2016).

5.3.4 Physiological Forward Model

The parameters of interest; CBF_0, CVR, CBVcap, OEF_0 and absolute $CMRO_2$ were estimated using a forward physiological model (Germuska et al., 2016). The ASL signal was converted to absolute flow (ml/100g/min) using a PCASL kinetic model described previously (Heijtel et al., 2014). Changes in CBF and BOLD signal, calculated using the optimised BOLD signal model described by Wise et al. (2013a), along with changes in the fraction of deoxyhaemoglobin ([dHb]) were used as inputs to the forward physiological model. A value of 0.2 was assigned to α, which describes the relationship between CBV and CBF, and 1.3 for β to explain the effect of [dhb] changes on the signal relaxation rate, R2* (Gauthier & Hoge, 2012). Additional fixed input parameters were; the convolved $P_{ET}CO_2$ and $P_{ET}O_2$ traces, Hb, the post-label delay, tagging duration of arterial blood and the BOLD echo time (TE2). Haemoglobin concentration,

affects the measured BOLD signal as activation-related signal changes are dependent on absolute deoxyhaemoglobin levels, and therefore baseline Hb concentration (Levin et al., 2001). Individual subject Hb was incorporated into the model rather than assuming a default value in order to improve the accuracy of OEF_0 and CBV estimates.

The framework then finds the parameter values which minimise the error between the model predictions (priors) and the data. To ensure the output values for each parameter are realistic estimates, the model search space is restricted within an established physiological range.

The fixed model inputs were used to solve for 5 unknown parameters; CBVcap, CBF_0, the calibration parameter *K* (Germuska et al., 2016), OEF_0 and CVR. Absolute baseline $CMRO_2$ was determined by multiplying OEF by O_2 delivery, which was calculated as the product of; CBF_0*CaO_2 (the arterial O_2 content) (Lajoie, Tancredi, & Hoge, 2016). A constant $CMRO_2$ was assumed across periods of normocapnia/normoxia, hypercapnia and hyperoxia.

Voxelwise maps were calculated for each parameter using non-linear least squares fitting with L2 parameter regularisation[5] to determine the best fit to the data. Regularisation was applied only to CBVcap and CVR as these parameters are the main sources of potential instability in the model. The CBVcap prior was set at 1.3 ml/100g as values are approximately 2 ml/100g in GM and 0.3 ml/10g in white matter (WM). Therefore 1.3 gives a good approximation where GM maps are thresholded at 0.5 GM probability. CBVcap is then estimated from CBF, OEF_0 and mean transit time (MTT). CVR was given a prior of 2.5%, again an intermediate value based on known GM and WM values. These priors were used to guide the model fit within known physiological values. In this model, *K* is analogous to the BOLD calibration parameter *M* used in calibrated fMRI experiments, but is renamed in this model as OEF_0 can be factored out of the calculation as all parameters are estimated in one step. *K* is not given a prior but estimated directly from the data.

In a change from the original model (Germuska et al., 2016) where OEF_0 was assigned a mean prior of 0.35, here OEF was modelled using the an assumed value for the MTT of tagged blood, incorporating known physiological constants describing the oxygen concentration in blood and

[5] L2 regularisation is used to reduce model over-fitting and stabilise the model. Regularisation simplifies the model to improve prediction accuracy. Least squares regression minimises the residual sum of squares increasing potential instability of the model. Andale. (2017, July 29). Statistics How To. Retrieved August 8, 2017, from http://www.statisticshowto.com/regularization/

the ratio of tissue oxygen concentration to arterial plasma oxygen concentration (Zheng et al., 2002). Finally, CBF_0 was assigned a non-informative prior of 60 ml/100g/min to provide a uniform probability distribution. Unlike previous models (Gauthier & Hoge, 2013; Wise, Harris, Stone, & Murphy, 2013), BOLD and CBF data are analysed simultaneously with each time-series informing the other to improve stability of parameter estimates.

Note, in this model, estimated CBVcap is only true CBVcap where the oxygen tension of tissue (ptO_2) remains constant, which in this model is an average of 15mmHg across tissue (Leithner & Royl, 2013b). Therefore should this vary between subjects, or not represent true ptO_2, assumed CBVcap, is not a true reflection of blood volume but is a product of variation in ptO_2. This is addressed in the discussion in relation to the results.

5.3.5 Spatial Maps

Segmentation of the T1-weighted structural images into GM, WM and CSF was carried out using FSL FAST (https://fsl.fmrib.ox.ac.uk/fsl/fslwiki/FAST). T1-weighted GM maps were registered to subject space using FSL's FLIRT (https://fsl.fmrib.ox.ac.uk/fsl/fslwiki/FLIRT). For statistical analysis, values were extracted from masks thresholded at 50% GM probability to avoid inclusion of regions of poor SNR such as near white matter or CSF borders.

5.3.6 Statistical Analysis

First, linear multiple regression analysis was carried out using SPSS Version 20 (IBM Corp., Armonk, N.Y., USA) to assess whether CBF_0 was predicted by age or bodyweight. These variables are known to influence CBF and it was necessary to determine whether these parameters required consideration in further analysis.

Correlation analysis with permutation testing (1000 permutations per comparison, 95% CIs) was conducted to examine relationships between $\dot{V}O_2max$ and cerebrovascular parameters at baseline and post-intervention using GM ROI values. Permutation testing was used as an alternative to Bonferroni to correct for multiple comparisons as described in Chapter 4. To test whether there was an effect of the intervention on cerebrovascular function, paired t-tests with bootstrapping (1000 samples, 95% CI) of the baseline and post-intervention data were conducted.

Non-parametric, permutation-based voxelwise analysis of GM was conducted using FSL's Randomise as described in Chapter 4, including both positive and negative contrasts. Significance threshold for clusters was set at $z = 2.3$, $p < 0.05$ and threshold-free cluster enhancement (TFCE) was applied (Smith & Nichols, 2009).

5.4 Results

Subject Characteristics	Mean ± SD
Est. Vo_2max l/min	3.28 ± 0.53
Est. VO_2max ml/kg/min	40.01 ± 5.59
Age	29.86 ± 5.9
Weight (kg)	82.8 ± 10.7
IPAQ – Time Sitting (min)	540 ± 165
IPAQ – Time Active (min	4737 ± 8419
Baseline Lactate (mmol/L)	0.92 ± 0.37
Peak Lactate	10.44 ± 2.17
Baseline HR (BPM)	78.26 ± 18.31
Peak HR	186.4 ± 11.24
Baseline Hb (g/L)	155.35 ± 10.56
Baseline MAP	96.2 (9.2)
Peak MAP	111 (15.5)
Peak Hb	156.03 ± 45.03
Baseline Borg (Breathing)	0.13 ± 0.35
Baseline Borg (Legs)	0.1 ± 0.28
Peak Borg (Breathing)	8.4 ± 2.55
Peak Borg (Legs)	9.66 ± 0.61
Watts Achieved	243 ± 44

Table 5.3 Group characteristics and physiological measures from the fitness test. MAP = mean arterial pressure, Hb = haemoglobin, Borg ratings are out of a maximum score of 10.

Table 5.3 provides an overview of resting and post fitness test characteristics. 15 volunteers completed the study, however baseline dual-calibrated PCASL data was not collected for 2 subjects due to timing (n=1) and equipment (n=1) issues leaving n=13 for the pre-post intervention comparison. Baseline Hb was not obtained for 1 subject, therefore an estimated value of 150 g/L (Bulte et al., 2012) was used in the forward model.

Multiple regression analysis showed that CBF at baseline was not predicted by age or bodyweight; adjusted $F(2, 10) = 1.486$, $p = 0.272$ with an $R^2 = 0.075$. Subjects' CBF was 0.028 ml/100g/min higher for each year increase in age and was 0.008 ml/100g/min lower per kg increase in weight. These variables were not considered necessary to include as covariates in further analysis.

Out of 15 subjects, 14 achieved a peak lactate > 8 mmol/L and 11 achieved a peak HR which exceeded 95% of the age predicted maximum, all 15 exceeded 90% of the age-predicted maximum. All subjects reported peak Borg ratings > 9 for heaviness of legs and >8 for breathing, out of a maximum rating of 10.

5.4.1 Cross-Sectional Relationship between $\dot{V}O_2$max and Cerebrovascular Function

5.4.1.1 GM ROI Analysis

In GM, correlation analysis did not reveal significant associations between $\dot{V}O_2$max and cerebrovascular parameters at baseline (n=13 subjects). However, in the post-intervention data, there were significant inverse correlations between $\dot{V}O_2$max and CBVcap, OEF_0 and $CMRO_2$ before corrections. No correlations survived multiple comparison corrections (see table 5.4).

Correlation Analysis Between $\dot{V}O_2$max and Cerebrovascular Function				
	Baseline		**Post-Intervention**	
	Pearson's R	**p-value (uncorrected/ corrected)**	**Pearson's R**	**p-value (uncorrected/ corrected)**
CBF_0	0.06	0.85/0.996	0.25	0.38/0.818
CVR	-0.51	0.08/0.195	-0.24	0.38/0.825
CBVcap	-0.54	0.06/0.154	-0.51	0.05*/0.212
OEF	-0.47	0.10/0.259	-0.53	0.04*/0.173
$CMRO_2$	-0.53	0.06/0.169	-0.51	0.05*/0.204

Table 5.4 Reported values based on 100,000 permutations per test, * denotes significant correlations at $p < 0.05$.

5.4.1.2 GM Voxelwise Analysis

The voxelwise analysis showed that $\dot{V}O_2$max was not correlated with any of the 5 parameters of interest at baseline. An exploratory analysis at $p < 0.1$, did not reveal any clusters approaching statistical significance. In the post-intervention measures, there was a significant

correlation between $\dot{V}O_2$max and OEF in the left precentral gyrus (Figure 5.3) and between $\dot{V}O_2$max and CBVcap in the left precentral gyrus, left precuneus, bilateral anterior and posterior cingulate gyrus, left intracalcarine cortex and left lateral occipital cortex (Figure 5.4). For CBF, CVR and $CMRO_2$, there were no strong associations with $\dot{V}O_2$max.

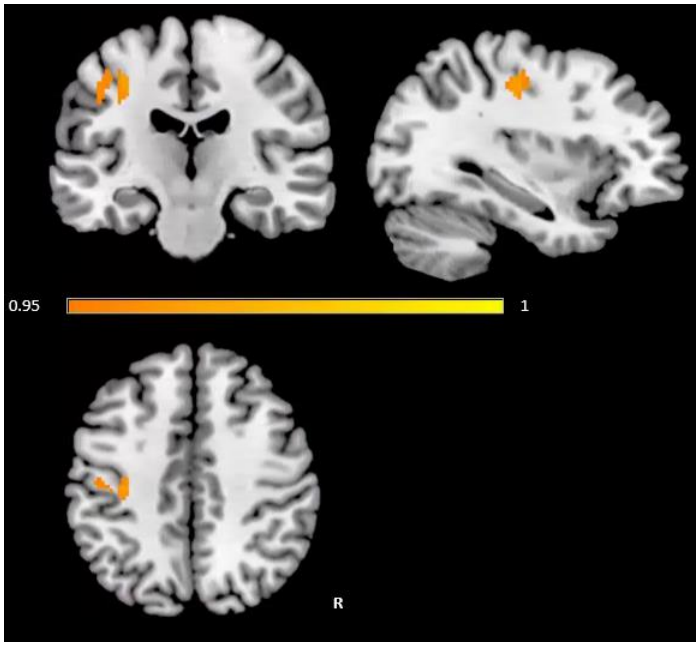

Figure 5.3 OEF_0 in the left precentral and postcentral gyri was significantly lower in subjects with greater $\dot{V}O_2$max. Analysis was conducted using FSL Randomise, with a z-threshold of 2.3, $p < 0.05$, FDR corrected.

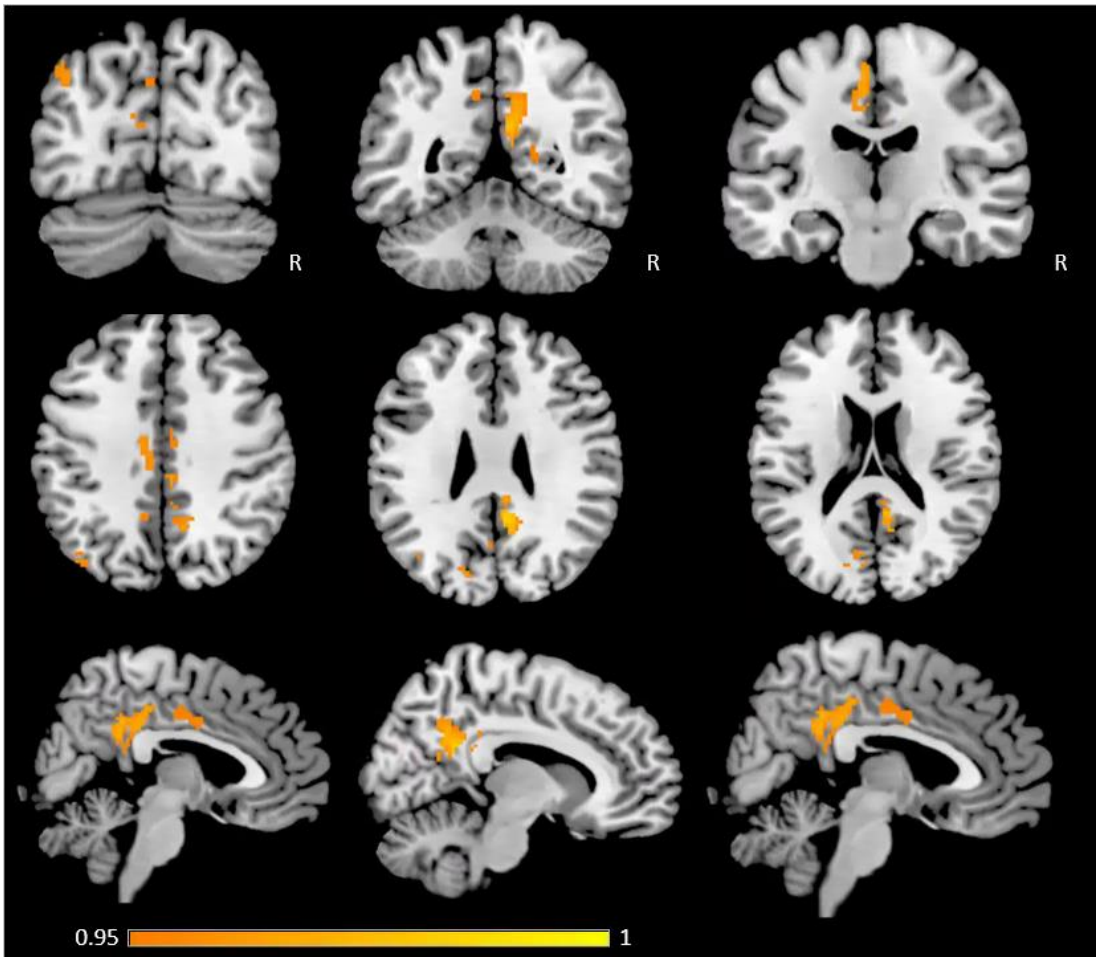

Figure 5.4 CBVcap was significantly lower in subjects with greater $\dot{V}O_2$max in regions of the left precentral gyrus (M1), bilateral precuneus, posterior and anterior cingulate, as well as left lateral occipital and intracalcarine cortices.

5.4.2 Effects of the Exercise Training Intervention on Cerebrovascular Function

5.4.2.1 GM ROI Analysis

Comparisons were based on 13 subjects for which full baseline and post-intervention data was collected. Pre- and post-intervention data are shown in Figure 5.5 for each parameter. Paired t-tests for GM CBF_0, CVR, CBVcap, OEF_0 and $CMRO_2$ did not reveal any notable changes following the intervention in an ROI analysis (Table 5.5). Further, there was no correlations between $\dot{V}O_2$max and percentage changes in any parameter following the intervention (Table 5.6).

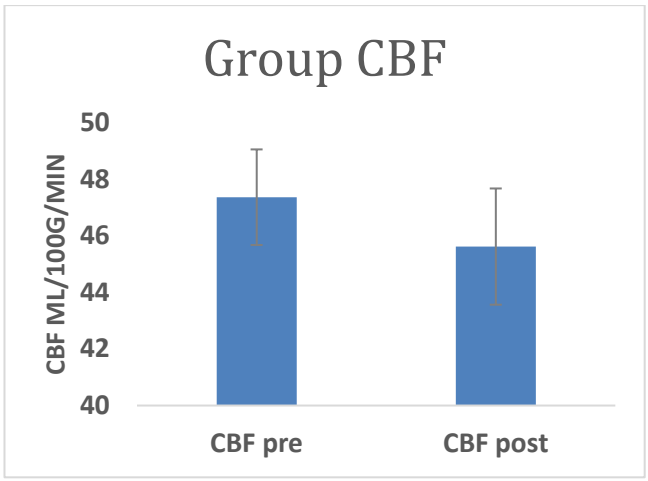
Group CBF
CBF ML/100G/MIN
50
48
46
44
42
40
CBF pre
CBF post

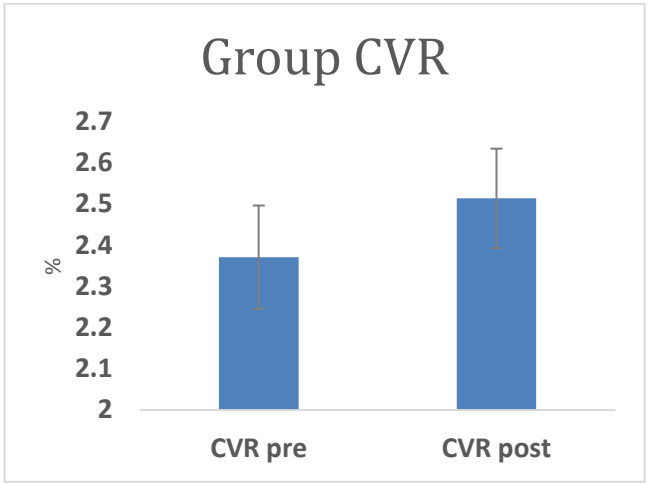
Group CVR
%
2.7
2.6
2.5
2.4
2.3
2.2
2.1
2
CVR pre
CVR post

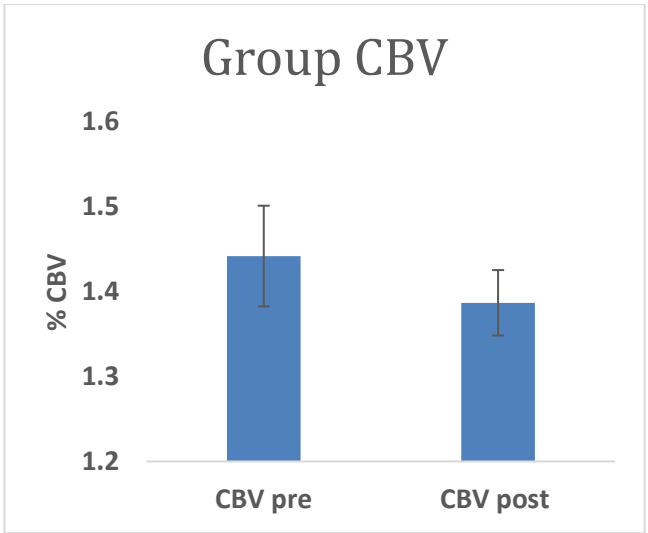
Group CBV
% CBV
1.6
1.5
1.4
1.3
1.2
CBV pre
CBV post

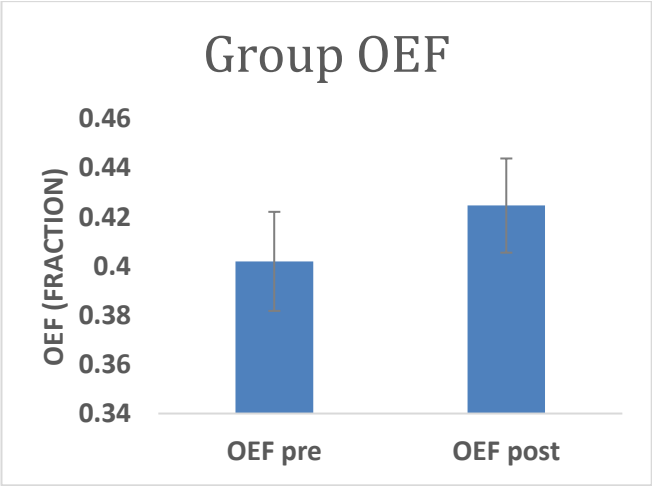

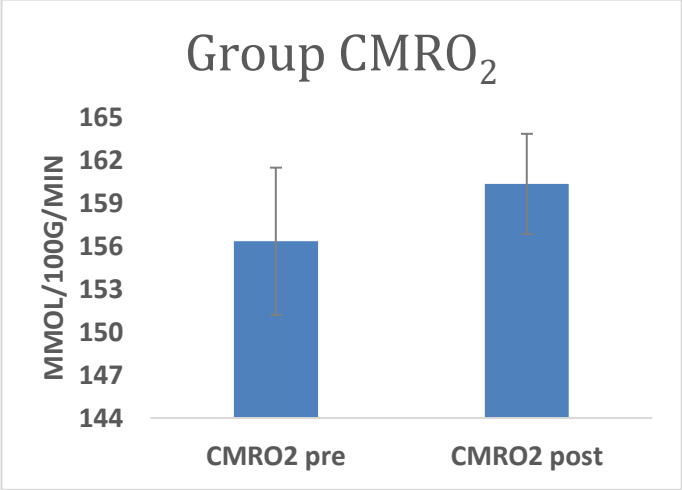

Figure 5.5 Changes (mean and SEM) in physiological parameters following the 1-week intervention.

Pre and Post Intervention Neurophysiological Measures					
	Baseline	**Post-Intervention**	**T-statistic**	**p-value**	**95% CIs**
CBF_0 ml/100g/min	47.4 (1.7)	45.7 (2)	-0.869	.402	-1.9-4.5
CVR %	2.4 (0.1)	2.5 (0.1)	1.488	.163	-0.4-0.08
CBVcap %	1.4 (0.05)	1.4 (0.02)	0.950	.361	-0.1-0.05
OEF_0	0.4 (0.02)	0.38 (0.02)	1.689	.117	-0.04-0.005

Pre and Post Intervention Neurophysiological Measures					
	Baseline	**Post-Intervention**	**T-statistic**	**p-value**	**95% CIs**
$CMRO_2$ µmol/100g/min	156.7 (5.1)	157.6 (3.7)	0.596	.562	-10.6-6

Table 5.5 Average (mean ± SEM) values for each parameter. Paired t-tests (uncorrected) showed no significant changes following the training intervention.

Correlation between $\dot{V}O_2$max and % Change Following the Intervention			
	%ΔPre-Post	**Pearson's R**	**p-value**
CBF_0 ml/100g/min	0.09 (2.73)	0.197	0.519
CVR %	1.68 (4.1)	-0.070	0.820
CBVcap %	0.4 (3)	0.157	0.608
OEF_0	0.91 (3)	0.042	0.981
$CMRO_2$ µmol/100g/min	1.08 (2.42)	0.236	0.438

Table 5.6 Group results (mean ± SEM) of correlation analysis between $\dot{V}O_2$max and % change in parameters of interest following the intervention (uncorrected p values shown).

5.4.2.2 GM Voxelwise Analysis

Voxelwise paired t-tests for each parameter of interest were conducted using FSL Randomise. No significant effects of the exercise intervention on cerebrovascular parameters were observed, nor were any notable trends seen in the data at an uncorrected threshold.

5.4.3 Results Summary

This study examined the relationship between $\dot{V}O_2$max and indices of cerebral vascular and metabolic function, namely resting CBF, CBVcap, CVR, OEF_0, and $CMRO_2$. Secondly, we investigated whether 1 week of intensive exercise lead to changes in the parameters of interest. In this cohort, $\dot{V}O_2$max was not significantly correlated with CBF_0 or CVR in whole brain GM in baseline or post-intervention data. In the post-intervention data only, inverse correlations with $\dot{V}O_2$max were observed for CBVcap, OEF_0 and $CMRO_2$, however, these correlations did not survive corrections. In the voxelwise analysis of GM OEF_0 and CBVcap, but not $CMRO_2$, were significantly negatively correlated with fitness.

The extremely short duration is likely to be the main reason for the lack of observed changes. Values changed only marginally in most cases, and not in a consistent direction for all subjects, therefore, we conclude that 1 week of intensive exercise is not sufficient to induce cerebrovascular adaptations.

5.5 Discussion

The results from part 1 of this study are not in agreement with the work reported in Chapter 4 where higher AF was associated with lower CBF and greater CVR in GM. There are several possible reasons for the discrepancy between the two studies. First, there was a narrower spread of estimated fitness levels despite a range of activity levels in the IPAQ scores (see table 5.3) which was suggestive of a larger than observed variation in $\dot{V}O_2$max. It is possible that fitness did not vary enough to see CBF and CVR differences. However, within this sample, OEF_0, CBVcap, and $CMRO_2$ correlated with $\dot{V}O_2$max in the post-intervention data, meaning that either the fitness range was large enough to detect differences, or certain vascular and metabolic processes show greater adaptation with ET. Second, this study was conducted on a different scanner, using an EPI-based dual-excitation PCASL scheme rather than spiral dual-echo PASL as in Chapter 4. In addition, multi-inversion time ASL was used previously, whereas the dual-calibrated paradigm necessitated single inversion time imaging as simultaneous BOLD data was needed to estimate OEF_0 and CBVcap. In the previous study, normocapnic MTI data was acquired over 7 minutes, from which an average perfusion map was created for CBF quantification. In the current study, baseline flow is calculated within the forward model using the full 18-minute timeseries, rather than creating an average perfusion map from a constant resting normocapnic scan. Differences in the acquisition and analysis approach, most notably the use of single rather than multiple inversion time ASL in the current study, may explain the lack of a relationship between CBF and $\dot{V}O_2$max. However, if a strong relationship between the variables was present, it is unlikely that the use of single inversion time ASL would not have revealed a significant relationship between the two variables. It is believed that MTI acquisitions analysed using a 2-compartment model yield the most accurate estimates of CBF (Michael A. Chappell et al., 2010; Wong, 2014), however, this was not possible in the dual-calibrated experiment as explained above. Additional MTI acquisitions for baseline CBF quantification would be useful in future studies to provide a gold-standard estimate of brain perfusion.

We identified an interesting result in the cross-sectional data whereby $\dot{V}O_2$max was inversely correlated with CBVcap, OEF_0 and $CMRO_2$ in the GM ROI analysis before multiple comparison

corrections, and with CBVcap and OEF_0 in voxelwise analyses of GM. These results were only observed in the post-intervention data and are probably due to either, small cerebrovascular changes post-intervention which led to statistically significant correlations with $\dot{V}O_2max$, or the slightly larger sample size (n=15) in the post-intervention data compared to baseline (n=13).

The following discussion focuses on potential explanations for the statistically significant relationship between CBVcap, OEF_0 and $\dot{V}O_2max$ in the voxelwise data. The direction of the correlations between CBVcap and $\dot{V}O_2max$, and OEF and $\dot{V}O_2max$ were the opposite of what was expected. Studies in humans and animals such as that of Pereira et al. (2007) have reported increased regional total CBV following exercise training, with CBV increases in humans related to the degree of improvement in $\dot{V}O_2max$ following a 3-month ET intervention. In rodents, increases in angiogenesis, which translates to increased CBV, has been reported following exercise in a number of brain regions including motor cortex (R. . Swain et al., 2003), hippocampus (Klauke & Borght, 2009) and cerebellum (Black, Isaacs, Anderson, Alcantara, & Greenough, 1990). The consistent findings that ET is associated with higher CBV, and increased angiogenesis in animals raises the question of whether the current data reflects a true CBVcap reduction. While it is possible that there is regional heterogeneity in the effects of fitness on the brain, as this has been described previously for CVR data by Gauthier et al. (2015), a number of methodological factors must be considered when interpreting the results. Due to model assumptions about flow and oxygen kinetics, it is possible that the CBVcap and OEF_0 reductions in subjects with a greater $\dot{V}O_2max$ in reality reflect differences in tissue oxygen tension (ptO_2) and/or capillary transit time heterogeneity (CTTH).

PO_2 is typically 35-50mmHg in capillaries, decreasing as it diffuses through the extravascular compartment to meet local energy requirements. In the forward model, an average ptO_2 of 15mmHg was assumed across the tissue, an accepted literature value for an assumed average OEF_0 of 0.3, flow rate of ~60ml/100g/min and mean transit time (MTT) of 1.4s (Angleys et al., 2015; Jespersen & Østergaard, 2012; Leithner & Royl, 2013b). Model constants *g* and *k* which represent the ratio of tissue O_2 concentration to plasma O_2 concentration, and the rate of O_2 transfer across the capillary respectively, are assigned values based on the assumed average ptO_2 and MTT and used in the estimation of OEF_0. If ptO_2 and MTT are similar across all participants, then the apparent CBVcap and OEF_0 values likely reflect true reductions in subjects with a greater $\dot{V}O_2max$. The OEF_0 reduction would occur as MTT would be shorter where CBV is lower, making oxygen extraction more difficult. However, it is also possible that the parameter representing CBVcap reflects some combination of CBVcap and ptO_2

differences, as an increase in ptO_2 would lead to a reduced CBVcap estimate by the forward model, as OEF_0 is assumed to be constant across subjects.

Model parameters are estimated in one step and are therefore interdependent. For example, CBVcap, which could be more appropriately termed apparent CBVcap, may reflect additional physiological processes such as ptO_2 and CTTH, and if this is the case, estimates of OEF_0 and $CMRO_2$ will also be affected as OEF_0 relies on accurate MTT estimation, which in turn is estimated from CBV. $CMRO_2$ is calculated outside of the forward model, but is calculated using OEF_0. Lower blood volume in capillaries leaves less oxygen available in tissue, hence the lower measured OEF_0, and does not facilitate any obvious cerebrovascular health benefits. At present, it is not clear whether a true CBVcap was observed and if so, what this means in terms of the effect of higher $\dot{V}O_2$max on brain health. Greater Hb in subjects with a higher $\dot{V}O_2$max could have explained lower CBVcap, as the brain would have to compensate for a higher haemoglobin mass, potentially by lowering CBVcap. This would also equate to less oxygen availability for tissue, thereby reducing OEF_0 and $CMRO_2$. Trained athletes have a higher circulating Hb mass, and therefore greater oxygen carrying capacity, in comparison to inactive individuals (Mairbäurl, 2013), however, in this study $\dot{V}O_2$max and Hb did not correlate, nor did CBVcap and Hb (data not shown) as subjects were not trained to the level of typical athletes.

As ptO_2 depends on several factors including vascular geometry, capillary density and capillary oxygenation (Leithner & Royl, 2013), it is possible that $\dot{V}O_2$max does influence oxygen tension gradients, which lead to an apparent CBVcap reduction. As factors such as ptO_2, MTT and CTTH could not be measured in the current study, the model relies on assumed values in healthy populations, and the accuracy of output parameters relies on these unknown variables.

Changes in ptO_2 gradients in tissue may represent an additional means of regulating oxygen supply, for example, in hypoxia (Jespersen & Østergaard, 2012) to maintain oxygen availability, therefore increased ptO_2 may represent greater oxygen availability in those with higher $\dot{V}O_2$max which is not reflected by the current forward model. Unfortunately, it is not possible to conclusively attribute the apparent CBVcap reduction in those with a higher $\dot{V}O_2$max to differences in ptO_2 or CBV, but it is a finding that warrants further investigation to determine whether the observed effects can be replicated, and to identify whether there is an effect of $\dot{V}O_2$max on ptO_2. It is not possible to directly measure brain ptO_2 in humans non-invasively, however, fMRI techniques exploiting the T1-signal relaxation rate (R1), could be used to determine tissue oxygen tension in the brain (Muir et al., 2016).

An alternative but related explanation for the inverse association between CBVcap and $\dot{V}O_2$max is the possibility of CTTH increases across participants related to fitness, leading to a lower measured CBVcap. CTTH is a determinant of oxygen delivery to brain tissue and its increase, seen in conditions such as Alzheimer's disease, is associated with reduced OEF efficacy for a given CBF rate (Gyldensted et al., 2017). Homogenous capillary transit time is believed to indicate a healthy vascular system (Østergaard et al., 2016) and recent model simulations have shown that CTTH reduction improves tissue oxygenation by counteracting the inherent reduction in OEF as CBF increases (Angleys et al., 2015). Studies in humans have reported increased OEF and longer MTT, along with reduced flow heterogeneity in the quadriceps of trained subjects compared to untrained subjects during exercise, although no significant differences at rest were observed (Kalliokoski et al., 2001). Although, higher OEF and MTT are suggestive of greater CBV, no differences were observed between the groups, either at rest or during exercise in the study by Kalliokoski et al. (2001).

Although comparatively greater CTTH is believed to limit oxygen delivery to tissue, Heinonen et al. (2015) in a review paper on the effects of heterogeneity of ratios of oxygen delivery to VO_2 in muscle, suggested that rather than higher CTTH being a definitive indicator of poor tissue oxygenation, factors such as local energy demands and haemodynamics along with oxygen diffusion (DO_2) capacity should be considered. It is possible that where capillary blood flow and MTT are not compromised, CTTH may improve the flexibility of the system, allowing for a greater capacity to maintain an efficient oxygen supply across a range of oxygen supply and consumption ratios. Simulation studies show that CTTH varies in proportion to MTT in healthy micro-vascular networks at rest (Rasmussen et al., 2015) and this covariance is crucial for the maintenance of optimal oxygen extraction in tissue (Eskilden et al., 2017). MTT is longer where capillary density is greater as there is a greater volume of blood to pass through and diffusion of oxygen is hindered, therefore CTTH may also vary across the brain depending on the regional capillary density. At present this theory is highly speculative and has not been systematically investigated, but accounting for CTTH may be an important modification to the forward model in future work investigating $\dot{V}O_2$max and brain function, as well as disease populations where greater CTTH is expected.

As CTTH is not factored into the forward model, homogenous capillary transit times are intrinsically assumed. Elevated CTTH, associated with compromised oxygen delivery and availability was not expected in this sample, and its omission from the model was not considered to be a potential limitation at the outset. However, CTTH affects tissue perfusion and blood volume, O_2 availability, and the maximum OEF and $CMRO_2$ (Jespersen & Østergaard,

2012). If $\dot{V}O_2$max does increase CTTH, as indicated by the lower apparent CBVcap, this will have biased parameters estimated by the forward model. Future studies using methods capable of measuring transit time distributions across the brain, such as velocity-selective ASL (van Osch et al., 2017) will provide additional model input and reduce the reliance on average values across a group.

In the previous study described in Chapter 4, lower CBF in subjects with higher AF was identified in the thalamus, brainstem, precuneus visual cortex (V1) and lingual gyrus. Here, lower CBV was observed in the precuneus, M1 and ACC and lower OEF_0 also in M1 and supplementary cortex. Both studies have found an effect of either training or detraining on the precuneus, a component of the default mode network (DMN) and an area sensitive to the effects of ageing on the brain (V. J. Williams et al., 2017). Further, Chapman et al. (2013) reported CBF increases in the left precuneus with cognitive training in healthy older adults, and this CBF increase correlated with cognitive gains. Thomas et al., (2013) have also reported higher precuneus and posterior cingulate CBF in Masters Athletes vs. sedentary controls, and Alfini et al. (2013) found detraining related CBF reductions in the precuneus in Masters Athletes. The hippocampus is capable of lifelong neurogenesis and studies have shown CBF (Chaddock-Heyman et al., 2016), microstructural (Kleemeyer et al., 2015) and volumetric (Erickson et al., 2011) correlations with AF in this region in young and older adults. There is less of a rationale for a localised effect of AF in other brain regions, yet studies consistently show regional effects rather than whole brain effects, with the precuneus being a region identified as showing AF-related CBF changes in response to both cognitive training and physical fitness. This study and the work reported in Chapter 4, both report lower estimates of vascular parameters (CBF, CBVcap and OEF_0) with increased AF although CVR, an index of vascular reserve was positively associated with fitness. As discussed in the previous chapter, there may be age-dependent effects of AF on the brain, which are not yet understood.

Regarding the intervention, although no cerebrovascular or metabolic changes were observed within the 1-week training period, there is evidence showing rapid CBF reductions when ET ceases. Alfini et al., (2016) reported significant CBF reductions in Masters Athletes (over 50 years old) in areas including the hippocampus, cerebellum, inferior temporal gyrus (ITG), lingual gyrus and precuneus following 10 days of restriction from all ET. While this suggests that very rapid detraining effects occur, it appears that training effects may occur more gradually, at least in younger adults and longer term interventions are needed to determine the effects of ET in young adults.

5.5.1 Limitations

A main limitation in this study was the low spread of fitness levels, despite differences in physical activity levels evidenced by the IPAQ (table 5.3). The ratings of perceived exertion, peak heart rates and lactate levels suggest that participants did exercise to exhaustion. It appears that a number of subjects participating in regular organised exercise still had very poor or poor fitness levels according to American College of Sports Medicine (ACSM) classifications (see Supplementary table 5.10), and in future reported levels of physical activity should not be used as an indicator of fitness level when the study aim is to recruit a range of fitness levels.

Related to the above point, the fitness test protocol used in this study provides an estimate of $\dot{V}$O2max only. The equipment needed to record inspired and expired breathing gases and calculate ventilation, which is necessary to calculate actual $\dot{V}$O2max was not available for this study. However, the Storer method (Storer et al., 1990) has been widely used in exercise testing (Malek, Berger, Housh, Coburn, & Beck, 2004; Jung, Nieman & Kernodle, 2001) and shows high correlation with the gold-standard approach of calculating the maximal volume of oxygen utilised per minute, during exhaustive exercise (ACSM's Health-Related Physical Fitness Assessment Manual, 2013). While the estimation of $\dot{V}$O2max could be considered a limitation, it is believed to be a close approximation of true values as lactate and HR thresholds reached by almost all participants satisfy secondary $\dot{V}$O2max criteria (Midgley & Carroll, 2009), although it has also been shown that these thresholds can be reached at ~70% of $\dot{V}$O2max (Poole et al., 2008). In sum, if ventilation measures are available they should be used, however the Storer equation and secondary criteria should provide good estimates of fitness and capture relative differences between subjects.

A third limitation, which may have had a meaningful impact on the results, is that CTTH was not factored into the estimation physiological parameters in the forward model. As discussed above, CTTH variation has implications for OEF_{max} and $CMRO_{2max}$ as does potential differences in pto_2 (Jespersen & Østergaard, 2012).

Another unavoidable limitation is that Hb was measured peripherally and is known to vary within the capillary network and to be significantly lower in the brain than systemically (Levin & Ausman, 1969; Pries, Fritzsche, Ley, & Gaehtgens, 1920). Although central and peripheral values differ, peripheral variability between participants could be assumed to also reflect central variability. Therefore, including individual Hb measures in the forward model is preferable to assuming a value across all subjects, as the model output will more closely reflect each subject's physiology.

5.5.2 Conclusions

Studies such as the work reported here are important as the timescale of ET related brain changes must be established in order to prescribe effective guidelines for exercise aimed at maintaining or improving brain health. The results of the intervention suggest that cerebrovascular changes do not occur as rapidly as 1-week. While a lack of observable changes after 1-week is not wholly unexpected, it is necessary to identify the point at which brain benefits are achieved through ET, and determine the nature of initial neurophysiological adaptations. The obvious samples to recruit in studies looking at associations between AF and brain health are elite athletes and sedentary controls. However, athletes are a minority group; most people will not train at the level of an athlete regardless of the potential lifelong benefits. It is important to study normal population variance in fitness to determine whether moderate levels of regular physical training is enough to obtain neuroprotective benefits of AF. In addition, the intervention suggests that sustained cerebrovascular adaptations due to AF occur over longer periods of time, and are independent of acute cerebral responses to exercise such as those observed by Macintosh et al. (2014).

While there is a growing literature showing that AF preserves CBF in older adults (Ainslie et al., 2008; Bailey et al., 2013; Gauthier et al., 2015; Thomas et al., 2013), we still do not know what effect AF has on the brain's vascular and metabolic function in early adulthood. From the two studies presented in this thesis, the effects are not clear. While Chapter 4 suggests that higher $\dot{V}O_2$peak is associated with lower CBF in a number of regions including precuneus, thalamus and brainstem, and higher CVR in whole brain GM, the current results are not in agreement, as results do not show similar trends. Still, the novel finding that apparent CBVcap and OEF_0 is lower regionally, in subjects with higher $\dot{V}O_2$max warrants further investigation in a larger sample with a greater spread of $\dot{V}O_2$max scores. Both studies suggest AF does impact cerebrovascular function in young adults, however, additional studies are needed to clarify the true direction of changes and the relevance to metabolic and cognitive health. The effect sizes observed for each parameter suggest that $\dot{V}O_2$max may have a greater effect on metabolic processes such as OEF_0 and $CMRO_2$ as well as CBV. In young adults, CBF may not be the most informative index of effects of AF on cerebrovascular function, as the healthy brain can maintain optimal CBF, especially at rest. In early adulthood, underlying processes involving oxygen availability and metabolism may be improved through chronic AF, leading to improved haemodynamics in later life. In future studies, in addition to dual-calibrated PCASL, techniques which are optimised for measurement of CBV such as VASO (Lu et al., 2013) could be used

alongside T1 relaxation mapping to determine cerebral Hb and oxygen tension to provide additional physiological information not available with the dual-calibrated data alone.

Finally, the power analysis calculated using mean effect sizes across all parameters, to calculate sample sizes for future studies, suggest a sample of 33 for cross-sectional comparisons and 90 for the intervention to achieve a power of 0.8. Collaborative or multi-centre studies may therefore be a more feasible way to achieve the required sample sizes, due to the high costs and time resources required.

Chapter 5 Supplementary Information

Baseline $\dot{V}O_2$max and Dual-Calibrated FMRI Grey Matter Estimates						
Participant	**Estimated VO2max**	**CBF ml/100g/min**	**% CVR**	**% CBVcap**	**OEF**	**$CMRO_2$ µmol/100g/min**
Participant 1	35.0	34.5	2.89	1.8	0.55	161.7
Participant 2	38.92	45.3	3.30	1.2	0.37	145
Participant 3	45.05	57.3	2.28	1.3	0.32	159.1
Participant 4	40.68	n/a	n/a	n/a	n/a	n/a
Participant 5	48.89	44.1	2.9	1	0.32	120.4
Participant 6	38.75	46.5	2.0	1.5	0.44	168.7
Participant 7	33.11	51.7	2.3	1.6	0.41	181
Participant 8	40.89	52.	2.2	1.4	0.38	166.2
Participant 9	44.85	46.2	1.6	0.9	0.28	116.4
Participant 10	39.66	47.4	1.9	1.6	0.44	171.7
Participant 11	40.5	47.9	2.6	1.66	0.45	180.3
Participant 12	50.9	n/a	n/a	n/a	n/a	n/a
Participant 13	31.8	50	2.6	1.25	0.35	149.8
Participant 14	36.7	36.7	2.4	1.55	0.50	153.8
Participant 15	34.5	56	1.8	1.28	0.34	158.3
Mean ± SD	40 ± 5	47.3 ± 6.5	2.4 ± 0.5	1.4 ± 0.25	0.4 ± 0.07	156.3 ± 19.9

Table 5.7 Average (median) parameter estimates for grey matter

Post-Intervention Dual-Calibrated FMRI Grey Matter Estimates					
Participant	**CBF ml/100g/min**	**CVR %**	**CBVcap %**	**OEF (fraction)**	**$CMRO_2$ µmol/100g/min**
Participant 1	34.6	2.9	1.7	0.55	159.6
Participant 2	45.7	3	1.4	0.41	159.5
Participant 3	59.3	2.2	1.4	0.35	173.7
Participant 4	32.4	2.8	1.6	0.55	148.6
Participant 5	47.3	3.3	1.1	0.32	128.9
Participant 6	41.9	2.4	1.3	0.41	147.4
Participant 7	49.9	2.5	1.5	0.42	173.7
Participant 8	42.2	2.4	1.4	0.44	155.9
Participant 9	47.3	1.6	1.1	0.34	138.5
Participant 10	40.5	2.8	1.5	0.48	156.9
Participant 11	54.3	2.5	1.6	0.40	182.2
Participant 12	53	1.8	1.2	0.33	149.5
Participant 13	55.4	2.4	1.4	0.36	169.5
Participant 14	35.2	2.2	1.5	0.50	147.2
Participant 15	45.42	2.9	1.6	0.45	169
Mean ± SD	45.6 ± 8	2.5 ± 0.4	1.4 ± 0.1	0.42 ± 0.07	157.4 ± 14.5

Table 5.8 Average (median) GM estimates post-intervention

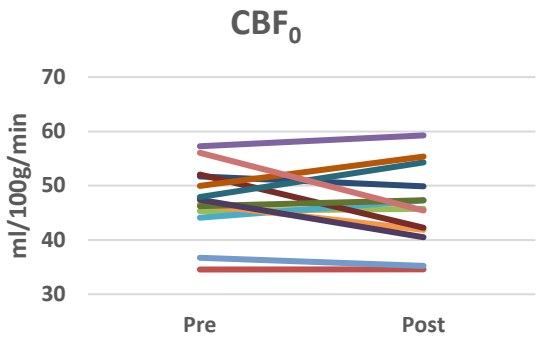
CBF0
70
60
50
40
30
ml/100g/min
Pre
Post

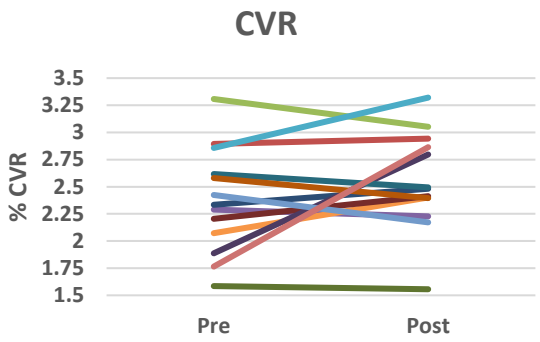
CVR
3.5
3.25
3
2.75
2.5
2.25
2
1.75
1.5
% CVR
Pre
Post

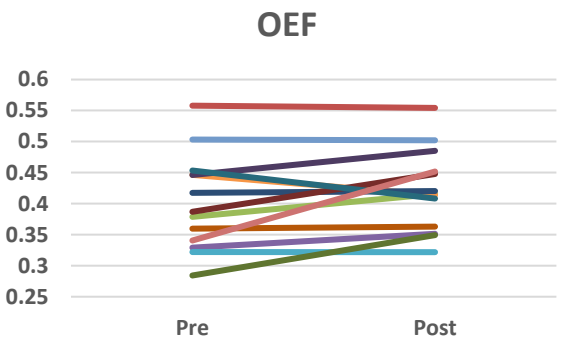
OEF
0.6
0.55
0.5
0.45
0.4
0.35
0.3
0.25
Pre
Post

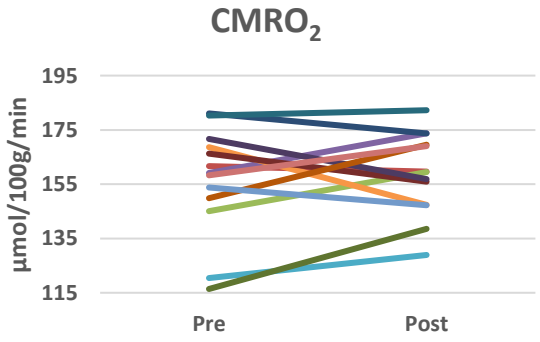
CMRO2
195
175
155
135
115
µmol/100g/min
Pre
Post

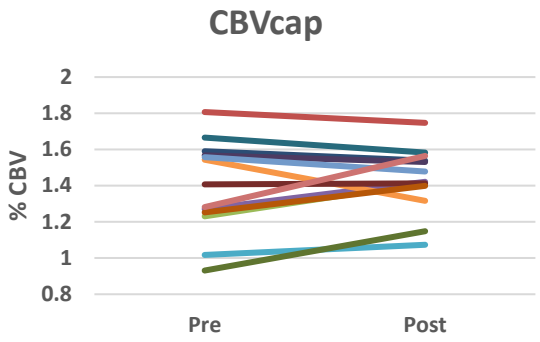

Figure 5.6 Baseline and post-intervention GM values for each subject.

Power Analysis for Future Studies			
Post-Intervention Correlations with $\dot{V}O_2max$	**Effect Size (r)**	**Required Sample Size (based on observed power)**	**Required Sample Size (predicted)**
OEF	0.53	23	33
CBV	0.67	12	33
CVR	0.24	131	33
CBF	0.25	120	33
CMRO2	0.56	26	33
Pre-Post Paired T-tests	**Effect Size (d_z)**	**Required Sample Size (observed power)**	**Required Sample Size (predicted)**
OEF	0.47	38	90
CBV	0.26	119	90
CVR	0.39	54	90
CBF	0.22	165	90
CMRO2	0.17	274	90

Table 5.9 Power analyses conducted for each parameter, for the cross-sectional correlation data and differences between pre- and post-intervention. All calculations are based on a required power of 0.8, $p < 0.05$, two-tailed tests. For the predicted sample size calculation, an effect size of 0.45 was chosen for the correlation analysis and 0.3 for the paired t-tests. These values were chosen as they represent the mean observed effect sizes.

ACSM Categorisation of $\dot{V}O_2$max Scores per Subject		
	Estimated VO2max	**ACSM Fitness Classification**
Sub01	35.0	Very poor
Sub02	38.92	Poor
Sub03	45.05	Good
Sub04	40.68	Poor
Sub05	48.89	Very good
Sub06	38.75	Poor
Sub07	33.11	Very poor
Sub08	40.89	Poor
Sub09	44.85	Fair
Sub10	39.66	Poor
Sub11	40.50	Poor
Sub12	50.91	Excellent
Sub13	31.82	Very poor
Sub14	36.67	Very poor
Sub15	34.46	Very poor

Table 5.10 ACSM fitness classifications (Hwang, Castelli, & Gonzalez-lima, 2017) for each subject.

Chapter 6

Overview of FMRI Studies on Motor Plasticity

Abstract

The next part of this thesis investigates the cerebrovascular and metabolic mechanisms underlying motor plasticity. This chapter provides a brief overview of relevant imaging studies which have demonstrated the functional networks involved in motor learning, along with a small number of existing studies which have used quantitative fMRI (qfMRI), to investigate the neural energetics of motor learning. The goal of the experiments in Chapters 7 and 8 was to test the feasibility of using quantitative techniques to characterise energetic processes underlying motor learning in the healthy brain. The results will be used to inform future studies in people with MS where the aim is to establish the contribution of cerebrovascular changes to clinical features of the disease which often include motor, and learning and memory impairments. An improved understanding of the neurobiological mechanisms which influence functional plasticity will help to identify the potential for adaptive plasticity which may be linked to cerebrovascular health. In addition, this knowledge may be used to implement effective treatment strategies which could involve interventions to improve cerebrovascular function.

6.1 Introduction

The adult brain retains structural and functional plasticity to adapt to new experiences as well as to repair and reorganise function following injury. Motor skill training leads to rapid neural adaptations across the motor cortex and functionally connected regions including sensorimotor cortex, cerebellum, prefrontal, superior temporal and visual cortices (Hardwick, Rottschy, Miall, & Eickhoff, 2013; Ungerleider, Doyon, & Karni, 2002). Measurable behavioural adaptations in the form of improved response accuracy and reaction times, mean that learning-specific neural changes can be discriminated from activity related to simple motor execution. As a result, motor and visuomotor learning paradigms are widely used models of brain plasticity. However, the cerebrovascular and metabolic processes underlying plasticity which facilitate reorganisation of structure and function in the healthy brain are not well understood. In a clinical context, neurological patients retain variable degrees of plasticity, and understanding key processes promoting and limiting this plasticity will inform appropriate interventions and treatment. Following injury, the brain can reorganise functional networks so that new regions can take over the function of a damaged area (Zeller & Classen, 2014) which serves to reduce the level of disability, at least temporarily in the presence of disease.

Early positron emission tomography (PET) investigations measuring regional cerebral blood flow (rCBF) changes during motor learning, to identify the anatomical networks involved in motor execution and motor learning (Seitz & Roland, 1991) and network involvement differences with implicit and explicit learning (Honda et al., 1998). To date, motor learning investigations, more recently using mainly BOLD fMRI (Doyon & Benali, 2005), have placed much focus on the correlation between behavioural markers of learning and anatomical location of activation changes during the task. Much less consideration has been given to the underlying neurobiological mechanisms facilitating motor plasticity, both in the activated state and in the resting brain. An adequate supply of blood and capacity to utilise energy in the form of oxygen and glucose is necessary for both motor execution and motor skill learning. FMRI studies have shown that with training, functional brain adaptations occur as behavioural performance improves, in the form of altered BOLD activation patterns. However, the complexity of the BOLD signal, which arises from changes in CBF, cerebral blood volume (CBV) and the cerebral metabolic rate of oxygen consumption ($CMRO_2$) means that is not possible to identify specific processes underlying plasticity using BOLD contrast alone. Understanding the nature of vascular and metabolic changes which occur during learning-induced plasticity is important if we are to make the best use of the capacity for plasticity in neurological rehabilitation. Advanced fMRI techniques now allow us to non-invasively quantify normal and

pathological brain responses to motor learning. Studies using quantitative imaging will help to elucidate energetic deficits which affect behaviours such as motor learning in neurological disorders including Multiple Sclerosis (MS) where plasticity can facilitate recovery following bouts of acute inflammation (Tomassini, Matthews, et al., 2012).

The following experimental chapters use arterial spin labelling (ASL) calibrated fMRI to quantify CBF and relative $CMRO_2$ changes during motor learning (Chapter 7). As a follow-up study, sustained changes in CBF and resting state functional connectivity (RSFC) are investigated following motor sequence learning in Chapter 8. This chapter first provides a brief overview of relevant imaging studies which have demonstrated the functional networks involved in motor learning, along with a small number of existing studies which have used quantitative calibrated fMRI, to quantify energetic changes during motor learning. The goal of the experiments in Chapters 7 and 8 was to test the feasibility of using quantitative techniques to characterise energetic processes underlying motor learning in the healthy brain. The results will be used to inform future studies in people with MS where the aim is to establish the contribution of cerebrovascular changes to clinical features of the disease which often include motor, and learning and memory impairments. An improved understanding of the neurobiological mechanisms which influence functional plasticity will help to identify the potential for adaptive plasticity which may be linked to cerebrovascular health. In addition, this knowledge may be used to implement effective treatment strategies which could involve interventions to improve cerebrovascular function.

6.2 Imaging Motor Plasticity in Healthy Cohorts

Although neuroplasticity affects both structure and function, this brief overview will focus on functional plasticity in response to motor and visuomotor skill learning. For a comprehensive review on brain structural changes following motor learning see Draganski & May (2008). The following experimental chapters use a visuomotor sequence learning task, the serial reaction time (SRT) task (Nissen & Bullemer, 1987), to investigate brain vascular and energy metabolism changes which accompany functional plasticity in the healthy brain. The SRT is a visuomotor task which involves implicit or explicit learning, where participants repeat a sequence of finger movements or button box responses following visual cues. These repeated movement sequences are often interspersed with pseudorandom (control) task blocks or runs where identical component movements are performed. Control tasks are used to separate activity due to simple motor performance from sequence-specific learning and identify networks involved in the acquisition and coordination of skilled movement with visual input, as well as learning and memory. The SRT task can be modified in length and difficulty to suit the research

question and the subject group of interest making it a widely used motor learning task. While the SRT is relatively simple to perform, it requires rapid communication between multiple brain regions making it an excellent task to probe cognitive function and communication between brain regions. Due to fast neural and behavioural adaptations, the SRT task is especially useful in fMRI paradigms to study the neural substrates of motor learning over time and between groups.

Performance speed and accuracy on motor tasks can be improved over very short timescales, from as little as 3 minutes (Fernandez-Seara et al., 2009). This speed of adaptation makes it possible to study the healthy brain and assess motor learning in patients where scan duration is often limited. Frequently used tasks other than the SRT include paradigms which require guided coordination of movement (bimanual movement patterns) (Puttemans, Wenderoth, & Swinnen, 2005) or response adaptation based on changes in task demands (Shannon, Neil, Vlassenko, Shimony, & Rutlin, 2016).

Beyond initial performance improvements, longer neural adaptation occurs. Karni et al. (1995), in an early fMRI study of motor plasticity, demonstrated BOLD signal changes during two phases of motor sequence learning. Participants practised a finger tapping sequence (A or B) for 20 minutes daily for 5 weeks without visual cues. Participants were scanned once a week over 4-6 weeks where sets of the trained sequence were alternately performed along with the control (non-trained) sequence. The study allowed the authors to identify two phases of learning which has been replicated in subsequent studies (Bonzano et al., 2011; Kleim et al., 2004; Korman, Raz, Flash, & Karni, 2003). In pre-training scans, primary motor cortex (M1) activation was similar for the two sequences. In early sets (alternate presentation of sequences A and B) of the first scan session, there was an effect of sequence order, whereby the first executed sequence within a set (either A or B) elicited a greater M1 activation extent. This effect reversed by the end of session 1 so that the second sequence executed within a set elicited greater M1 activation. The authors attributed this switch in the order effect to an initial fast learning phase, supported by behavioural data which showed gains in speed and accuracy over the course of the first session. By the fourth session, where subjects had had three weeks of daily practice, regardless of the order of presented sequences the trained sequence elicited greater M1 activation extent. This was believed to represent slow learning where consolidation of the increase in behavioural skill occurred. This pattern of activation overriding the order effect, which evolved gradually with longer-term practice, persisted 21 weeks after maximum performance was achieved (~5 weeks) without continued training. The authors concluded that this persistent change in M1 activation during sequence performance indicated increased

representation in M1 for the trained sequence which may support long term memory of the specific motor skill.

The above study by Karni et al. (1995) and follow-up work (Korman, Raz, Flash, & Karni, 2003; Karni et al., 1998) demonstrate that neural changes underlying functional motor plasticity evolve through several stages involving initial fast learning followed by more gradual changes reflecting consolidation and retention of skilled performance of the motor task. These studies restricted the ROI to M1, however, it is now well established that there is a spatially diverse network of regions involved in motor sequence learning, including primary somatosensory cortex (S1) and pre-motor areas, basal ganglia (BG), fronto-parietal and fronto-cerebellum circuits which are recruited under different conditions of awareness, timescale of learning and task complexity (Doyon & Ungerleider, 2002). In addition to these areas, the visual cortex, thalamus, putamen and superior parietal lobule (SPL) have also repeatedly shown recruitment during visuomotor learning (Hardwick et al., 2013). The contribution of multiple brain components reflects the multiple processes occurring to support motor learning and highlights the usefulness of motor learning tasks in identifying subtle brain changes or deficits in patient groups.

As well as neural adaptations over several weeks, visuomotor plasticity has been demonstrated within a single scan session. Floyer-Lea & Matthews (2004) used a 12 minute visuomotor tracking task to show two stages of functional changes associated with task learning; initial fast learning was associated with greater task activity in prefrontal, sensorimotor and parietal regions, bilaterally and ipsilateral cerebellum and caudate nucleus. Second, with performance improvement, activity decreased in these regions. The timescale of decreases was approximately halfway through the task, at the stage where performance was no longer increasing. The authors identified the clinical potential of motor learning tasks to investigate pathological processes associated with motor learning deficits. Importantly, for clinical applications, functional changes could be observed in a matter of minutes, without the need for weeks of daily training. Whether these changes represent true plasticity, or alternatively a long term depression (LTD) like process associated with repeated stimulus exposure is not clear. It is possible that these short-term changes represent the initial stages leading to sustained functional and potentially structural adaptations to support behavioural performance.

Structure and function are closely linked, adaptations in functional responses, e.g. changes in neuronal excitability and inhibition, may drive structural plasticity, which in turn may lead to sustained changes in metabolic demand. For example, one week of training on a visuomotor

rotation task led to increased cortical volume in contralateral M1, and an increase in white matter fractional anisotropy (FA) in a region immediately beneath M1 (Landi, Baguear, & Della-Maggiore, 2011). The increase in grey matter concentration predicted task performance (readaptation speed) at 1 year post training suggesting persistent functional adaptation as a result of training. This study was a follow-up from earlier work (Della-Maggiore & Mcintosh, 2005) using the same task where increases in functional connectivity between the cerebellum, superior temporal gyrus and motor areas were demonstrated at 1 month post training. Taken together these studies suggest both structural and functional plasticity occur following motor training. Given the likely importance of energy supply in plasticity, vascular and metabolic health may predict the capacity for both, therefore it is important to extend this work to investigate i) baseline CBF and ii) CBF and $CMRO_2$ changes during and following motor training. This will allow researchers to link structural and functional adaptations, and changes in the magnitude of task responses to the underlying neurobiology and cerebrovascular health.

6.2.1 Functional Connectivity Changes following Motor Training

Resting state networks (RSNs) are thought to play an important role in supporting the active brain during initiation and execution of behaviour (Miall & Robertson, 2006). This has led to a body of research investigating the effect of motor learning on RSFC to understand how skill training alters the resting brain. Many studies investigating functional plasticity focus on changes in the activated state, but altered baseline or resting activity may actually drive changes seen during task performance (Xiong et al., 2009).

Changes in BOLD RSFC have been reported following motor training. Albert et al. (2009) demonstrated learning specific changes in RSFC following a single 11-minute motor training session on a joystick adaptation task where one group performed a version requiring adaptation to a moving target (motor learning), and a control group where adaptation was not required. Using probabilistic ICA to investigate RSN changes over 10 minutes of resting BOLD data collected before and after training, a fronto-parietal RSN (Damoiseaux et al., 2006) was identified where functional connectivity strength was increased following the motor learning task only. In addition, the cerebellum exhibited increased resting signal following training, although this region was not identified as a resting network in baseline data across the training and control groups. However, the cerebellum is known to be involved in motor learning and coordination, it is possible that signal fluctuations are only evident following activities where cerebellum engagement occurs.

Sami & Miall, (2013) reanalysed the data reported by Albert et al. (2009) adding data from two groups training on either an implicit or explicit SRT task for ~15 minutes, again with 10 minutes

of resting state BOLD recorded before and after training. Rather than using traditional seed-based or ICA connectivity analysis, the authors employed graph theory analysis to map connectivity network changes due to motor training across each group. In each group functional connectivity (FC) strength was measured across 116 anatomical points. To summarise, all 3 tasks with a learning component resulted in connectivity strength changes in various brain regions depending on the task. Of greatest relevance to the current work are the SRT tasks, which showed greater global and local FC strength, defined as the connection density of each region, in frontal and visual regions and these changes were greatest in the explicit learning condition. The degree of connectivity, defined as the number of nodes connected to each point, was also measured and increases were noted again only in the 3 tasks with a learning component. Increases were greatest in frontal and visual areas for the explicit learning SRT task followed by visuomotor rotation where the amygdala and left hippocampus showed increased FC strength. For the implicit SRT condition, increases in the degree of FC were observed for the superior parietal gyrus, in addition to frontal and visual areas, but these FC increases were lower than the other 2 learning tasks. The authors also investigated changes in network efficiency across the tasks. Network efficiency increases for the implicit SRT condition were found in the left precentral gyrus, SMA and thalamus, and in the frontal-orbital, right angular gyrus and medial temporal cortex for the explicit condition. However for the visuomotor rotation task, efficiency increases were observed in the right cerebellum, let caudate nucleus and hippocampus. These selected results highlight the specificity of changes which occur in the brain in response to very similar tasks.

The changes in RSFC described in this study, were measured over 10 minutes following motor task performance, and do not necessarily reflect long term plasticity. To investigate whether RSFC adaptations persist, Sami, Robertson, & Miall (2014) measured RSFC immediately, 30 minutes, and 6 hours after training on implicit and explicit versions of the SRT task. The authors demonstrated different patterns of increased FC between implicit and explicit conditions, and across RSNs, however, an overall picture of two learning phases emerged similar to other studies. Immediately post-training, for the implicit learning condition, sensorimotor and cerebellar networks exhibited peak increases in a sensorimotor network, whereas a cerebellar network encompassing the thalamus and basal ganglia, showed peak activity at 30 minutes at a later phase moving towards consolidation. Activity in both networks decreased by 6 hours post training where a medial temporal (MTL) network showed greater connectivity strength than at previous timepoints. Further, this MTL network exhibited increasing connectivity to the right hippocampus at 30 minutes and 6 hours. The MTL and hippocampus are not typically

recruited in short motor-learning tasks, but may reflect longer-term learning induced plasticity. To verify this, later follow up sessions are needed, such as the 1-month follow up conducted by Della-Maggiore et al. (2005).

Functional adaptations in resting brain connectivity have also been studied over longer timescales. RSFC in the motor network was investigated over 4 weeks of daily sequential finger opposition training (Ma, Narayana, et al., 2011). The authors used ICA to identify changes related to early and late learning stages. From baseline to week 2 there was an increase in FC strength between right postcentral gyrus and right supramarginal gyrus, and from week 2 to week 4 a decrease in FC strength between these regions. Further, left supramarginal gyrus showed a linear increase in FC across the 4 week period. The authors proposed that an initial increase in connectivity is observed during skill acquisition, followed by reductions as consolidation of the skill is complete and less neural resources are recruited to perform the task. This is supported by behavioural data showing increases in performance from baseline to week 2, where no further improvement with additional performance was noted. Interestingly, connectivity of M1 and the supplementary motor area did not change over the 4 weeks, despite the significance of these regions in motor learning and consolidation (Dayan & Cohen, 2011). The authors suggested differences in the neurobiology of task and resting activity may explain this result, but given the nature of the BOLD data acquisition, differences in vascular and metabolic activity driving the signal could not be identified.

The majority of fMRI studies to date, including those discussed above, investigating motor learning related changes in RSFC and task responses have used changes in BOLD signal to infer adaptive plasticity. These studies have shown adaptations in RSFC following training (Albert et al., 2009) and changes from early to late phases of task performance (Doyon & Benali, 2005). While these studies demonstrate an effect of training on the brain, the BOLD signal is an indirect measure of the neuronal response to a stimulus which results from interactions between cerebral blood flow (CBF), volume and the cerebral metabolic rate of oxygen consumption ($CMRO_2$). This complex signal makes it difficult to interpret the nature of the physiological changes observed. As a result the vascular and metabolic adaptations facilitating presumed changes at the cellular level during and following motor learning are less clear. However, with alternatives to BOLD fMRI such as arterial spin labelling (ASL), quantification of energy supply and metabolism, in the form of CBF and $CMRO_2$, can be performed and is a promising method to advance the field of plasticity research. Several groups have investigated the cerebral metabolic processes which facilitate motor learning using ASL, in addition to quantitative studies using PET.

6.3 Quantitative FMRI and Plasticity

An early PET study (Grafton, Hazeltine & Ivry, 1995) demonstrated rCBF increases from baseline in a network of frontal, motor, occipital regions and the putamen proportional to sequence learning during a modified SRT task. The SRT was performed with and without attentional interference from a concurrent task. Without interference from the second task, most participants gained awareness of the sequence. Sequence awareness correlated with greater rCBF in bilateral parietal, temporal and right premotor areas recruited by the task as well as decreasing activity with sequence learning in areas including the right hippocampus, left premotor and temporal cortex, operculum and caudate. In subjects without sequence awareness, activity increases during the task were confined to the insula and superior temporal cortex. Grafton et al. (1995) demonstrated patterns of increasing and decreasing rCBF in during learning on an SRT task, with distinctly different patterns of activity between subjects who were and were not aware of the presence of a sequence. Other studies such as that of Seitz & Roland (1991) where both increases and decreases in rCBF were observed as subjects learned a finger movement sequence, are in agreement with BOLD fMRI studies. BOLD and rCBF increases in initial task stages, followed by reductions over time. Linear flow metabolism coupling has been reported in response to visual stimulation (Hoge et al., 1999; Uludag et al., 2004), however it is not known whether similar flow-metabolism coupling occurs during learning. Vafaee & Gjedde (2004) used PET to measure CBF and $CMRO_2$ during a finger tapping task, where subjects tapped the thumb against each of the 4 fingers in turn. The results showed generally linear flow-metabolism coupling in motor areas, however this was not the case for the right putamen which showed an increase in $CMRO_2$ without the expected increase in CBF, and the cerebellum where the opposite trend was observed. Therefore, it is possible that linear CBF-$CMRO_2$ coupling does not always occur, but is dependent on the task complexity and particular regions recruited. This task, essentially a motor learning task, may reflect regional uncoupling during motor learning and requires further investigation to determine whether this is a consistent pattern which occurs during motor learning.

A second study which measured both CBF and $CMRO_2$ was that of Shannon et al. (2016) where fMRI and PET scans were conducted before and after training on a visuomotor rotation task or control tracking task without rotation. The aim of this study was to i) determine the relationship between regional metabolic changes in oxygen and glucose consumption following task training and ii) whether assumed task-induced synaptic plasticity would be

reflected by changes in post-task aerobic glycolysis[6]. BOLD signal changes during task performance in visual, motor and attention-related areas commonly recruited during visuomotor tasks were reported. The most notable finding in this study, however, in terms of metabolic changes, was the role of Brodmann area 44 (BA44) of the frontal cortex, an area believed to play a role in execution of complex motor tasks (Shannon et al., 2016). This region was one of many recruited during task performance, and BOLD signal was modulated by the degree of learning. BA44 was the only region to show increased aerobic glycolysis, and reduced $CMRO_2$, assessed using PET, following task performance. This aerobic glycolysis increase was attributed to a reduction in $CMRO_2$ and an increase in glucose metabolism following motor learning and the opposite trend was observed in the control group on a task without a learning component. Task accuracy was highly correlated with the level of aerobic glycolysis and altered BOLD functional connectivity between BA44 and primary visual cortex (V1) after the task in different ways; subjects who made less errors had greater aerobic glycolysis and subjects who made more errors showed greater reductions in connectivity. This study adds extremely valuable information about the role of aerobic glycolysis and $CMRO_2$ changes in BA44 in relation to the level of task adaptation. This paper also demonstrates the strength of multi-modal imaging in studying motor plasticity as converging PET and fMRI results give greater confidence in results. Further, aerobic glycolysis is thought to support the expression of genes which regulate synaptic development (Goyal, Hawrylycz, Miller, Snyder, & Raichle, 2015) and the positive correlation between aerobic glycolysis increases and task performance in the study by Shannon et al. (2016) supports this outlook. aerobic glycolysis is highest during development, a time of high synaptic growth and pruning. The increased aerobic glycolysis in BA44, may therefore reflect synaptic plasticity resulting from covert learning of a complex motor task. The greater reduction in FC between BA44 and V1 in subjects with poorer task performance is interesting; generally activity reductions are associated with learning. The authors explain this result by suggesting that where visual input failed to result in motor learning, resulting in repeated incorrect responses, communication between BA44 and V1 was reduced. Behaviourally this may have been caused by disengagement with the task due to

[6] Aerobic glycolysis is the non-oxidative process through which glucose is broken down into a series of enzymes, despite the presence of sufficient oxygen. aerobic glycolysis is highest during development when synaptic growth is at its peak. aerobic glycolysis is associated with expression of genes associated with neural plasticity and synaptic remodelling and may therefore brain development and reorganisation (Goyal et al., 2015). In Shannon et al. (2016) aerobic glycolysis is computed from the rate of glucose and oxygen consumption.

negative feedback visual feedback on responses, or lack of cognitive challenge if effort was low. This could have leading to LTD like processes which were detected as reductions in connectivity with BOLD fMRI.

Xiong et al. (2009) also used PET and fMRI to study neural adaptations during task performance and in the resting state over 4 weeks of daily training on a motor sequence task previously descried by Karni et al. (1995). In task vs. rest analysis, BOLD fMRI data showed increases from baseline at week 2 in motor and somatosensory cortices, followed by reductions to within baseline levels by week 4.

PET, conducted at baseline and week 4 showed activation in M1 and S1 which was not significantly different from baseline at week 4 in a task vs. rest activation comparison. Both PET and fMRI data showed that activity returned to baseline levels after 4 weeks, which is initially suggestive of an absence of sustained functional plasticity and does not agree with findings of Karni et al. (1995, 1998) where M1 activity continued to increase past 4 weeks of training. Studies such as that of Hlustik et al. (2004) have shown decreasing trends after several weeks of training but may not capture the results seen by Xiong et al. (2009) due to shorter follow-up times. However, the resting and task performance rCBF data showed significantly higher rCBF in right M1 in the task and resting state. Left M1 did not show this increase, as expected given the left hand training task. The right supplementary motor area (SMA) also showed increased rCBF in both states but this was not significant. FMRI power spectral analysis for right and left M1 revealed an increase in spontaneous firing frequency in right M1 in the low frequency bandwidth of 0.08 Hz at 2 weeks and 4 weeks. These low frequency fluctuations are important markers of the strength of brain activity and may reflect increases in functional connectivity at rest. Left M1 did not show this change. The study by Xiong et al. (2009) very nicely illustrates the limitations of using BOLD fMRI alone to study motor plasticity, as well as effects that are not detectable in traditional task vs. rest contrasts. Investigating absolute changes in a quantitative manner, during task performance and at rest, could reveal much more information about metabolic adaptations with motor learning.

Xiong et al. (2009) suggests three potential mechanisms for the increase in rCBF with 4 weeks of motor training. The first is that synaptogenesis occurs as a result of repetitive localised neuronal excitation, leading to greater energy consumption in the resting state. As CBF and $CMRO_2$ are coupled at rest, the increased CBF seen following motor training reflects greater energetic demand due to the increased number of synapses. Second, angiogenesis is potentially increased through motor training, leading to greater rCBF and cerebral blood volume. This may be driven by neural adaptations leading to increased energy demand. Xiong

et al. (2009) referred to studies which reported angiogenesis following aerobic exercise training (Pereira et al., 2007; R. . Swain et al., 2003) and suggested motor training may have similar results. Third, cytochrome oxidase activity has been shown to be upregulated in rodent studies of learning (Sakata, Crews, & Gonzalez-Lima, 2005) and motor coordination is negatively affected by its reduction (Lalonde et al., 1999). This enzyme is closely linked to neuronal activity through its involvement in oxidative phosphorylation, the main energy synthesising pathway in the brain. Cytochrome oxidase has been implicated in increased metabolic capacity in the brain following skill training which, like synaptic formation, would increase $CMRO_2$ in regions critical for motor learning, and therefore rCBF would also be increased to supply the additional energy required.

The use of PET to study plasticity is extremely informative regarding metabolic processes involved in learning, however, it is costly, invasive and not widely available, especially for basic research. Therefore, quantitative fMRI is a more practical alternative which can still provide measures of CBF, blood volume and oxygen consumption during and following learning. Given the evidence pointing to changing energy demands following motor training, quantitative fMRI is a promising technique to further investigate learning-induced neural adaptations.

Moving away from PET, Olson et al. (2006) used single-echo ASL to measure learning related continuous perfusion and BOLD signal changes over three 15-minute SRT training sessions, each session proceeded by a 5-minute transfer task where a new sequence was presented. Unlike previous work, no regions of BOLD or CBF changes reached significance at a map wise level and it was only through reducing the statistical significance threshold and conducting ROI analysis that correlations were found between CBF reductions and reaction time, the measure of performance improvement over the session, in premotor cortex, inferior parietal lobule (IPL) and superior temporal gyrus (STG). The authors attributed the results to low SNR and statistical power and even at the uncorrected level, no BOLD signal changes related to learning were detected. This may be explained by the long task duration, as BOLD signal suffers from drift over longer timescales whereas perfusion is stable. The study by Olson et al. (2006), was however, an important step in moving towards quantitative investigation of functional plasticity. The benefits of ASL in this context are that changes can be detected over seconds or minutes and unlike BOLD, quantification of CBF means that changes can be compared to other subjects or groups without having to consider potential baseline differences. Third, greater spatial specificity of the perfusion signal over traditional BOLD fMRI (Chiarelli et al., 2007; Raoult, Petr, Bannier, Stamm, & Gauvrit, 2011) makes the technique more suited to identifying the location of learning related functional brain adaptation. Olson et al. (2006) suggest low

SNR and the continuous task design as explanations for the absence of significant signal changes with learning in many regions typically reported in BOLD studies. In typical block design experiments, spikes associated with block onsets may explain much of the task-related activity. The continuous nature of this task may have led to a more gradual neural adaptation not detected in the analysis due in part to low statistical power.

In a block design experiment by another group, Fernandez-Seara et al. (2009) used ASL to investigate CBF changes during two 6-minute explicit learning tasks where a different pattern of sequential finger movements was trained in each task. Even on this short timescale, a pattern resembling early and intermediate phases of learning emerged. Performance improved quickly within the first 2 minutes of task performance and perfusion increases were observed in M1 and secondary motor cortex (M2), premotor cortex and pre-SMA. Widespread activity was also detected in dorsolateral prefrontal cortex (DLPFC) and visual cortex as well as the ACC, insula, IPL, SPL and temporal cortex. Sub-cortical perfusion increases were also observed in the thalamus, putamen, caudate and globus pallidus. To investigate learning-related changes, 3 learning phases were defined representing early to intermediate learning. CBF decreases normalised to resting CBF were reported bilaterally for most regions recruited during task performance, and perfusion reached levels comparable to baseline by the final task block. Decreases were significantly correlated with reductions in RT, demonstrating learning related perfusion changes. In addition to these results, CBF increased from the early to late phase of learning. These increases were noted in S1, the posterior insula and putamen, cingulate cortex and left hippocampus, and were inversely associated with RT. Although the task duration was considered too short to achieve the late consolidation phase of learning, the initial increases in perfusion followed by decreases over time with performance improvement is similar to training studies which took place over weeks (Hlustik et al., 2004; Laguna & Cognitive, 1995; Xiong et al., 2009). This study by Fernandez-Seara et al. (2009) provides evidence firstly that ASL can in fact be used to detect group-level maps of activity associated with motor learning. Second, it was shown that learning-related perfusion changes occur over very short timescale so that plasticity can be studied without the cost to data quality that occurs with long paradigms, for example, related to excessive head motion. Employing calibrated fMRI to study plasticity over a short time scale, as described in Chapter 7, can extend the neurobiological understanding of the changes reported by Fernandez-Seara et al. (2009) by investigating the nature of metabolic changes accompanying CBF alterations during motor learning.

Krieger et al. (2014) conducted a methodological evaluation of calibrated fMRI (PCASL) at 7 Tesla to test the within and between session reproducibility of BOLD, CBF and $CMRO_2$ measurements during a complex visuo-motor task. In the task, participants had to learn to identify changes in movement patterns using a joystick to maintain the target position of a vertical bar and were scanned 3 times over 7 days. The aim of this study was to measure the reliability of BOLD and quantitative imaging parameters for studying plasticity, rather than primarily considering the biological significance of changes in flow and metabolism during learning. Results showed that intra and inter-subject variability was high across all 3 parameters and ROIs (grey matter, M1 and visual cortex), with $CMRO_2$ being the most stable and BOLD having the greatest variability. This variability was present despite accounting for the expected decrease in signal due to performance improvements (Ungerleider et al., 2002). Despite the variability, the authors concluded that calibrated fMRI is a promising solution for increasing signal specificity and achieving quantitative neurophysiological measures in imaging studies of cognition. The reason, despite low signal stability across sessions, is the promise of $CMRO_2$ as a marker of neural activity and learning-related neuronal changes. $CMRO_2$ had lower variability across sessions, subjects and regions, making it a preferable marker of plasticity due to it being a closer correlate of neuronal activity than CBF or BOLD, and being more easily interpreted from a neurobiological perspective due to greater signal stability. This study measured relative $CMRO_2$ ($rCMRO_2$) changes, which are dependent on BOLD and CBF stimulus responses and, for accuracy, noise-free estimations of the calibration parameter *M*. While the use of $rCMRO_2$ measures are reliable and informative, absolute CBF and $CMRO_2$ are closer correlates of the underlying stimulus-evoked neural signal. Whittaker et al. (2016) used a block design visual stimulus and hypercapnia challenge to modulate baseline and task-evoked CBF. The absolute CBF response to visual stimulation was preserved across different baseline states which translated to a lower fractional change in CBF to visual stimulation when preceded by a hyperperfused baseline. This would have a significant effect on BOLD and $rCMRO_2$ responses and potentially underestimate the true response, or change over time with training, in the case of motor learning. Although absolute quantification of $CMRO_2$ is not always feasible, this effect should be taken into consideration in the interpretation of results.

An earlier study by Mohtasib et al. (2012) used calibrated fMRI during a Stroop task to investigate age-effects on neuronal and vascular responses to the task. While this study was not aiming to study motor learning plasticity, it demonstrates a rare application of calibrated fMRI in studying neural correlates of cognitive performance, and the importance of going

beyond reliance on BOLD signal alone in ageing studies. During Stroop performance the BOLD response showed a linear relationship with age, and non-significant inverse associations with accuracy and reaction time. However, the CBF response did not show an effect of age, meaning that an overall reduction in $CMRO_2$ with age was evident. This is suggestive of a reduction in neural activity with age. Further analysis showed that the age-related BOLD and $CMRO_2$ changes were due to a low-performing sub-group of the older adults. The authors examined regional effects of age and found age-related BOLD increases to be greatest in bilateral M1 and the medial frontal gyrus (MFG), and age effects on $CMRO_2$ were also most pronounced in the M1 and left MFG. Had BOLD alone been measured during the task, the increased BOLD in older adults would likely have been attributed to an increase in neural activity, perhaps attributed to greater neural resources required to perform the task. It should also be noted that changes in end-tidal CO_2 and O_2 values with age are known to affect fMRI signal and $CMRO_2$ estimation (De Vis et al., 2015). However, when the data were analysed within a tight range of end-tidal O_2 values, the reduction in $CMRO_2$ with age was still present.

6.4 Imaging Plasticity in Patients

As well as studies of ageing, calibrated fMRI should be employed where cerebrovascular alterations are present, or suspected. In investigating neural markers of learning, or learning impairment in patients, calibrated fMRI, unlike BOLD alone, can reveal the nature of vascular and metabolic alterations which may underlie learning deficits. In MS, acute bouts of inflammation, referred to as relapses, can impair motor, visual and cognitive function as well as mood disturbances. Treatment of impairments generally involves psychological and physical rehabilitation which in a proportion of patients has a high degree of efficacy, yet others do not respond to these therapeutic interventions (Lipp & Tomassini, 2015). This suggests that non-drug treatments can enhance plasticity, but, that patients greatly vary in their capacity for adaptive plasticity. One possibility for heterogeneity in treatment responses where structural imaging does not reflect the level of disability (Barkhof, 2002), is that regional cerebrovascular and metabolic deficits are present in these patients (Ge et al., 2012; Marshall et al., 2014b) and limit the brain's ability to repair and/or reorganise function. Ge et al. (2012) used a global measurement of OEF and $CMRO_2$, and demonstrated $CMRO_2$ reductions in RRMS patients. $CMRO_2$ was inversely correlated with expanded disability status scale (EDSS) scores and lesion load. The results suggest that hypometabolism of oxygen occurs in MS and suggests a mechanism of progressive dysfunction and tissue damage characteristic of the disease. Calibrated fMRI could provide more sensitive regional identification of metabolic dysfunction at rest and during task performance. In early MS, subtle vascular and metabolic alterations

may be more apparent in the activated state, for example during motor learning. Quantification of $CMRO_2$ changes motor learning may indicate location and extent of disease-related damage as well as the current capacity for plasticity. Whether altered metabolism during learning reflects permanent damage, or reversible changes with appropriate treatment, remains to be determined and quantitative fMRI will be a key technique in future studies addressing this question.

Behavioural studies such as that of Tacchino et al. (2014) and (Deroost, Smetcoren, Vandenbossche, & Hooghe, 2014) have used the SRT task to show motor learning capabilities at different disease stages. Tacchino et al. (2014) recruited patients with minimal disability (EDSS < 2) who performed the SRT under explicit and implicit conditions. In blocks of a random sequence patients improved performance similar to controls. However, performance impairment was observed for sequence learning on both explicit and implicit conditions, with performance on the implicit learning condition lowest overall. This suggests that simple motor performance is preserved in early MS, however implicit motor learning, and to a lesser extent explicit learning, appears to be affected even at early stages.

Deroost et al. (2014) studied patients with more advanced MS (mean EDSS = 5.5), both relapsing remitting MS (RRMS) and progressive MS. In this study, patients were also tested in implicit and explicit learning conditions. In contrast to Tacchino et al. (2014), explicit learning was more affected than implicit, and as expected, was more pronounced in patients with progressive MS. Taken together, it could be concluded either that different learning systems are affected to a degree dependent on disease duration, or that there is extreme heterogeneity in MS symptoms and impairments. These studies relied on behavioural measures alone; qfMRI studies using these tasks would determine the nature of underlying neurophysiological impairments leading to these behavioural differences.

A sizeable number of studies have investigated motor activation in MS patients (see review by Pantano, Mainero & Caramia (2006)) but few have investigated motor learning and plasticity during fMRI. Morgen et al. (2004) looked at BOLD activation patterns over 8 minutes before and after 30 minutes of training on direction-specific thumb movements in 9 MS patients (mean EDSS = 2.2) and matched controls. Pre-training, patients exhibited greater pre-motor activation, which suggests additional neural resource recruitment is needed for patients to perform the task. With training, controls training led to BOLD signal reductions in M1, S1 and bilateral parietal association cortex. Patients however did not demonstrate any significant signal reductions despite comparable performance across the two groups. The results suggest patients retain the ability to perform guided motor patterns, but either do not exhibit similar

neural adaptation to the task as healthy controls, or require longer training periods to do so. In this study, pre-training activation did not correlate with lesion load, EDSS or task performance and post-training associations with these measures were not reported. It is apparent from this study however, that even in patients with a low EDSS, CBF and/or oxygen metabolism is altered during motor performance, potentially hindering neural adaptation with learning.

In contrast to the results of Morgen et al. (2004), Mancini et al. (2009), in a multi-centre study involving 56 patients (mean EDSS = 2.25) and 55 controls looked at activation patterns during a cued finger tapping task, which was repeated in a subset at 1 year (26 patients and 33 controls). Over 4 runs of the task both patients and controls showed comparable linear adaptation in the form of BOLD response reductions in M1, S1, SMA and the cerebellum. The same trends were recorded at the 1 year follow up. This task was a motor execution task rather than a motor learning task, and it is possible that simple motor execution is preserved in patients and this task was not sufficiently demanding to detect subtle changes in MS patients.

A study by Tomassini et al., (2016) investigated the effect of inflammation on visuomotor plasticity. Patients were scanned twice before and once after treatment with Interferon-Beta (IFN-beta), during which two runs of a visually cued finger-thumb flexion task were performed, separated by 25 minutes of practice. BOLD response changes within-session were used as the main indicator of plasticity. Compared to controls, patients showed a greater BOLD reduction in the cerebellum and visual cortex pre-treatment, suggesting a greater adaptation effect in patients, potentially driven by altered plasticity due to inflammation. Post-treatment with IFN-beta, which significantly reduced the presence of lesions in patients, within-session changes were reduced, which was interpreted as restoration of functional plasticity with IFN-beta treatment. While this reduction in response differences between runs could have been attributed to practice effects in the post-treatment session, a second pre-treatment session was included to control for this. If signal changes were primarily driven by practice effects, the greatest between-run differences would be expected between session 1 and session 2. The greater difference between sessions 3 and 2 are suggestive of a drug effect. This study demonstrates a potentially therapeutic effect of IFN-beta on visuomotor plasticity. However, without quantitative measures of brain function, such as CBF or $CMRO_2$ during rest and task performance before and after treatment, it is difficult to interpret the underlying neurophysiological mechanisms underlying the BOLD signal changes between runs and sessions. Future studies employing quantitative imaging, would provide additional information

on both the effect of treatments on haemodynamics, and the nature of brain changes believed to reflect plasticity.

In MS, additional studies are needed to characterise motor learning ability, and neural correlates of task the presence or absence of task learning. Quantitative measures such as CBF and $CMRO_2$ would be more informative than BOLD alone, as these indices of vascular health would elucidate potential mechanisms underlying motor plasticity in MS.

6.5 Cellular and Molecular Mechanisms of Plasticity

Neuroimaging offers an indirect way to study brain plasticity, as processes at the cellular level which either drive or require metabolic adaptations cannot be directly examined. To study microscopic-level mechanisms of plasticity we often rely on animal models, for example to directly examine changes in neuronal structure and function, and from this assume similar processes occur in humans. Studies in rodents show that acrobatic motor training leads to synaptogenesis (Black et al., 1990; Jones, Chu, Grande, & Gregory, 1999) and water-maze training has been associated with upregulation of BDNF and astrocytic processes (Sagi et al., 2012).

Enriched environments have also been shown to increase neurogenesis in the dentate gyrus (DG) of the hippocampus as well as enhancing the development of new blood vessels (Black, Polinsky & Greenough, 1989). In addition to increased numbers of neurons and vessels, greater dimensions of capillaries, glia, cell nucleus and somas of neurons have also been demonstrated in animals housed in enriched environments (Vernadakis, 1996). Similar processes have been demonstrated following aerobic exercise where angiogenesis and CBV have been upregulated in the motor cortex of exercised animals (R. . Swain et al., 2003). A review by Voss et al. (2013) discusses work showing upregulation of vascular endothelial growth factor (VEGF) and insulin-like growth factor (IGF-1) and brain-derived neurotrophic factor (BDNF) in the brain of animals who have been subjected to aerobic exercise over periods of typically 10-16 weeks. These neurotrophic factors are thought to mediate exercise-related cell proliferation. BDNF especially, has been widely associated with behavioural, structural and functional plasticity, for example BDNF is also upregulated through water-maze training, a hippocampal-dependent learning and memory task (Yamada, Mizuno, & Nabeshima, 2002).

It appears that skill learning, e.g. water maze training, and aerobic training, though very different, both lead to strengthening of existing neuronal connections, and formation of new

connections through neurogenesis and dendritic spine growth (M. W. Voss et al., 2013). Aside from neuronal processes, astrocytic changes and vascular cell development support plasticity which occurs through repeated behaviours. It should also be mentioned that immune processes support learning and memory, and therefore brain plasticity. However, in the presence of diseases, including MS, upregulation of immune processes can become toxic, increasing neuronal excitability to a level that impairs neurogenesis, and reduces neurotrophic factor production. Hyper excitability of neurons during inflammation has detrimental effects on learning, memory and locomotor behaviour as plasticity is limited under these conditions (Yirmiya & Goshen, 2011). Interventions which upregulate neurotrophic factors and stimulate neurogenesis may therefore help to restore plasticity in combination with anti-inflammatory treatments such as IFN-beta (Tomassini, d'Ambrosio, et al., 2016).

In humans, prolonged training of a particular skill or sustained increase in physical activity may lead to similar brain changes, although this cannot be tested definitively. Imaging outcomes such as changes in CBV, CBF and $CMRO_2$, which is closely coupled to cellular energy consumption, are the closest markers of cellular and molecular changes in the brain it is possible to achieve in basic research. The difficulty lies in interpreting what changes in $CMRO_2$ may reflect, as it could be any number of processes including increased firing rates, neurogenesis or non-neuronal cell upregulation. Multiple measures, including CBF and CBV may help to inform conclusions about underlying changes due to short and long term functional plasticity.

6.6 Conclusions and Future Directions

While fMRI has enhanced the understanding of functional networks involved in motor learning and the pattern of changes which occur with short and long term motor training, several important questions still remain. These primarily concern the neurobiological processes which facilitate the functional plasticity required for motor learning, and the metabolic adaptations which facilitate long-term changes in neural responses both during task performance and in the resting brain.

Both aerobic exercise and task-specific motor training can improve functional outcomes in patients (Schmidt & Wonneberger, 2014; Zeller & Classen, 2014). Aerobic exercise has been shown to increase CBF and vascular reserve in older adults (Bailey et al., 2013b; B. P. Thomas et al., 2013) which may lead to the observed cognitive benefits of physical fitness in healthy adults and patients (Beier, Bombardier, Hartoonian, Motl, & Kraft, 2014; M. W. Voss et al., 2015). Much more work is needed to establish whether motor learning can bring about

sustained changes in brain vascular function, and whether this has behavioural and cognitive benefits. First though, it is necessary to develop a better understanding of neurometabolic mechanisms of motor plasticity in the healthy brain and whether training induced changes persist at rest following task performance.

The following chapters investigate the neural energetic responses to short-term motor learning, which requires functional plasticity to improve performance. The results represent the initial fast learning phase and while they do not reflect the full extent of metabolic changes underlying functional plasticity, they provide evidence for the feasibility of calibrated fMRI and CBF RSFC as techniques to study neuroplastic adaptations, as well as information on energetic changes during the initial phase of learning.

Chapter 7

Cerebral Metabolic Changes during Visuomotor Learning Assessed using Quantitative FMRI

Abstract

Most fMRI studies investigating neural adaptation during visuomotor learning only measure the blood oxygen level dependent (BOLD) response. This can be problematic in certain groups as the BOLD signal is difficult to interpret due to its modulation by both neural and vascular processes. Calibrated fMRI offers more physiologically meaningful measures of brain activity changes compared to standard BOLD fMRI but is seldom used in cognitive neuroimaging studies. In this study, we investigated the feasibility of quantifying changes in cerebral blood flow (CBF) and the relative cerebral metabolic rate of oxygen consumption ($rCMRO_2$) during a visuomotor learning task.

The main aims were to measure CBF and $rCMRO_2$ changes associated with motor learning and to determine the flow-metabolism coupling ratio in regions recruited by the task as well as changes in this ratio over time. Simultaneous BOLD and CBF data were acquired using dual-echo arterial spin labelling (ASL) fMRI during a 12-minute serial reaction time (SRT) task, followed by a reference hypercapnic calibration scan. BOLD and CBF task-related increases were observed in the motor and sensorimotor cortex, thalamus, insula, lateral occipital cortex (LOC) and cerebellum, along with increases in $rCMRO_2$. BOLD and CBF decreases over time attributed to sequence learning were identified in the left cerebellum, insula and LOC, along with a trend towards increasing $rCMRO_2$. The flow-metabolism coupling ratio increased from 1.7 at the start of the task start to 2.8 by the end in the ROI showing a mean task response. In the ROI representing the CBF and BOLD signal decrease over time, the coupling ratio dropped from 2.2 to 1.7.

The study demonstrates the feasibility of measuring changes in neural energetics during a complex cognitive task and provides novel evidence suggesting a change of coupling in CBF and oxygen metabolism during visuomotor learning. This approach provides a more detailed understanding of neural processes which occur during learning than BOLD fMRI alone, and

may be a promising tool for studying alterations in cerebrovascular function and functional plasticity in patient groups.

7.1 Introduction

As detailed in the previous chapter, the brain has a lifelong ability to rapidly adapt through learning, and in response to injury or disease related damage, a process known as functional neuroplasticity. Residual neuroplasticity in chronic diseases such as Multiple Sclerosis (MS) can be harnessed in rehabilitation strategies to promote recovery of cognitive functions. However, the degree of plasticity varies between individuals and the mechanisms that promote and limit plasticity are not fully understood. Adequate energy delivery, in the form of cerebral blood flow (CBF) carrying oxygen, glucose and other nutrients to tissue is essential for healthy neuronal function, as is the ability to metabolise this energy. In MS, there is evidence of flow (D'haeseleer et al., 2011b; Ota et al., 2013) and metabolism dysfunction (Fan et al., 2015; Ge et al., 2012; Kidd et al., 1999) which may play a central role in limiting plasticity.

The neural energetics underlying plasticity have not been fully characterised, even in the healthy brain, and a better understanding of the flow and metabolism changes during learning which facilitate plasticity is necessary. This will aid researchers and clinicians in predicting patients' capacity for plasticity and guide treatment interventions to maintain and recover function. Secondly, the relative changes in CBF and the cerebral metabolic rate of oxygen consumption ($CMRO_2$) has not been well documented outside of the visual cortex, or during complex cognitive task performance. Determining changes in the flow-metabolism coupling ratio across task-relevant regions with learning will provide novel information on the balance between CBF and oxygen metabolism in the healthy brain during visuomotor learning.

Blood oxygen level dependent (BOLD) functional magnetic resonance imaging (fMRI) is a widely-used tool in plasticity research offering greater spatial and temporal resolution than alternative imaging methods such as Transcranial Doppler (TCD) ultrasound and Near Infrared Spectroscopy (NIRS). Another advantage of BOLD is that it is non-invasive, it does not require exogenous tracers unlike Positron Emission Tomography (PET) which is still used in motor learning studies (Shannon, Neil, Vlassenko, Shimony, & Rutlin, 2016; Ma et al., 2009). However, BOLD has several limitations; it is not possible to quantify baseline activity, and the measured signal is difficult to interpret due to its modulation by both neural and vascular processes (Attwell & Iadecola, 2002, Logothetis, Pauls, Augath, Trinath, & Oeltermann, 2001). The BOLD signal depends on complex interactions between CBF, cerebral blood volume (CBV) and $CMRO_2$, making errors in signal interpretation highly likely in the presence of compromised vasculature (Iannetti & Wise, 2007b). Despite this, BOLD is often used qualitatively, to infer

indirect changes in neural activity without much consideration given to the underlying physiological processes contributing to BOLD signal changes. It should also be mentioned that BOLD spatial specificity is limited as draining veins show large signal changes downstream of the site of activation (Turner, 2002) which could be problematic when studies aim to identify changes in specific anatomical regions during motor learning.

Calibrated fMRI, which provides estimates of CBF and relative $CMRO_2$ ($rCMRO_2$) through the addition of hypercapnic calibration (Davis et al., 1998; Hoge et al., 1999), enables greater understanding of cerebrovascular and metabolic responses contributing to the BOLD signal. In addition, changes in $CMRO_2$ should more closely reflect local neuronal activity than BOLD. Calibrated fMRI can be used to obtain direct measures of CBF and estimates of relative changes in brain energy metabolism ($rCMRO_2$). The technique has potential future applications in identifying clinically relevant abnormalities in vascular function which are not visible using BOLD fMRI. These additional measures of CBF and $rCMRO_2$ are helpful for accurate interpretation of data from fMRI studies of ageing and disease where neurovascular coupling (NVC) is likely to be altered (Restom, Bangen, Bondi, Perthen, & Liu, 2008). For example, Blicher et al. (2012) demonstrated lower CBF and CBV responses to a motor task in chronic stroke patients despite non-significant BOLD increases. Blicher et al. (2012) suggested that this effect could be explained by a decrease in vascular reserve capacity and therefore oxygen supply, meaning that an adequate $CMRO_2$ increase during the task could not be achieved. In a second study Mohtasib et al., (2012) found greater BOLD responses with increasing age during a Stroop task, but a reduced $rCMRO_2$ increase in response to the task. This suggests that as CBF was unaffected by age in this cohort, the greater BOLD signal changes were due to a reduction in the $CMRO_2$ response. As $CMRO_2$ and neuronal firing are closely coupled, a decreased neural response with age is also likely. Such changes in vascular reserve and neurovascular coupling would not have been evident had the authors of both studies used BOLD alone, and the results demonstrate the value of calibrated fMRI in any study where cerebral energetics may be altered.

A second, related application of CBF and $rCMRO_2$ measurement is in the study of functional brain plasticity. This application is in its early stages and has not been widely used yet. The BOLD signal alone is not ideal for studying experience-induced plasticity as it cannot distinguish changes in CBF and oxygen metabolism to a region, nor can it reliably reveal learning-related

activity changes between groups as baseline activity is unknown. Another advantage of obtaining perfusion measurements during learning tasks is that such tasks involve slow changes in neural activity (Olson et al., 2006) and the BOLD signal drift over longer timescales presents a challenge to separate task signal from noise due to this drift.

The aim of the current study was to quantify CBF and $rCMRO_2$ changes, in addition to measuring the BOLD response, during performance of a modified serial reaction time (SRT) using dual-echo calibrated fMRI. Visuo-motor task performance can be improved over short periods of time accompanied by changes in activity in task-recruited regions, demonstrating plasticity in the adult brain (Fernández-Seara, Aznárez-Sanado, Mengual, Loayza, & Pastor, 2009; Olson et al., 2006; Shannon et al., 2016), therefore we measured the response adaptation over time attributed to learning. Previous work has demonstrated increases in BOLD and CBF in motor and visual cortex as well as prefrontal regions and the cerebellum from rest during task performance. (Ungerleider et al., 2002). Signal reductions over time, with sequence learning have also been observed within a single task training session (Fernandez-Seara et al., 2016; Floyer-Lea & Matthews, 2004). However, $rCMRO_2$ changes during visuomotor learning have not been characterised using fMRI. Therefore, we explored $rCMRO_2$ changes in brain regions recruited during task performance and where a modelled linear BOLD and CBF signal reduction was observed across task blocks. Second, we characterised flow-metabolism coupling in these regions at the beginning and end of the task.

7.2 Methods

7.2.1 Participants

20 right handed, healthy participants (10 female, mean age 25±4.6) took part in this study. All participants were non-smokers and educated to university level. The study was approved by the Cardiff University School of Psychology Research Ethics Committee and performed in accordance with the guidelines stated in the Cardiff University Research Framework (version 4.0, 2010).

7.2.2 Imaging

Imaging was performed on a whole body 3T MRI (GE Excite HDx, Milwaukee WI, USA) system using an 8-channel receive-only head coil. Simultaneous perfusion and BOLD data were acquired with a single subtraction PICORE QUIPSS II (Wong et al., 1998) pulsed arterial spin

labelling (PASL) sequence (non-commercial) with a dual-echo gradient-echo readout (Liu et al., 2002) and spiral k-space acquisition (Glover, 1999).

Imaging parameters for functional scans were; TR = 2.4s, TE1 = 2.7ms, TE2 = 29ms, TI1 = 700ms, TI2 = 1.5s (most proximal slice), FOV = 19.8cm, flip angle = 90° matrix size = 64x64, slice thickness 7mm, 1.5 mm gap, 3.2mm in plane resolution, 15 slices. Label thickness was 200mm with 10mm gap between the end of the label and the most proximal imaging slice. A separate M_0 scan was acquired using the same parameters, except TR= 4s, to measure the equilibrium brain tissue magnetisation of cerebrospinal fluid (CSF) for absolute CBF estimation. A whole brain T_1-weighted fast spoiled gradient echo (FSPGR) structural scan was acquired to facilitate registration of the functional data to the common standard space of the Montreal Neurological Institute (MNI); 176 slices, $1mm^3$ isotropic resolution, TR=7.8s, TE=3s, TI = 450ms, flip angle 20°, acquisition matrix 256x256.

Physiological monitoring was performed, a respiratory belt placed just below the ribs monitored ventilation and a pulse oximeter was used to obtain cardiac traces. A sampling line connected to a tightly fitted face mask (Quadralite Intersurgical, Wokingham, Berkshire, UK) was used to monitor and record $P_{ET}CO_2$ and $P_{ET}O_2$ concentrations. This face mask was part of the breathing circuit used to deliver gas mixtures and followed the design used by Tancredi et al. (2014). The MEDRAD system (MEDRAD, Pittsburgh, PA) was used to monitor O_2 saturation throughout the hypercapnia task.

7.2.3 Visuomotor Task

The SRT (Nissen & Bullemer, 1987) is a measure of implicit sequence learning used frequently in fMRI studies to study the neural basis of visuomotor learning in healthy subjects as well as learning deficits in patient groups such as MS, chronic stroke and Huntington's Disease (HD) (Bonzano et al., 2011; Boyd & Winstein, 2001; Knopman & Nissen, 1991). In the SRT task, repeated presentation of visual stimuli at one of four positions on a computer monitor means that subjects can learn the sequence without explicit knowledge of the sequence. The subject is instructed to respond to each cue by pressing one of four buttons on a button box, where each button corresponds to a cue position. Without explicit task knowledge the SRT is presented as a low difficulty, continuous performance task with attentional, visuospatial, and motor demands (Rauch et al., 1997). With continued performance over these repeating blocks, subjects can improve their reaction time and accuracy due to a combination of motor habituation and sequence learning.

A modified version of the SRT developed by Nissen & Bullemer (1987) was used as the visuo-motor learning task during imaging acquisition. The task was projected via a screen inside the scanner at a frame rate of 60Hz and a resolution of 1024x768. A star appeared on the screen in a sequence of 4 boxes (Figure 7.1), participants responded by pressing the corresponding button on a button box in their right hand. The 12-minute task consisted of 6 blocks of a 12-item sequence repeated 9 times with variable inter-stimulus interval (600-1000ms) interspersed with 3 blocks of a pseudorandom sequence to control for response latency decreases related to task familiarisation rather than sequence learning. Participants were not informed that there was a repeating sequence during task instructions.

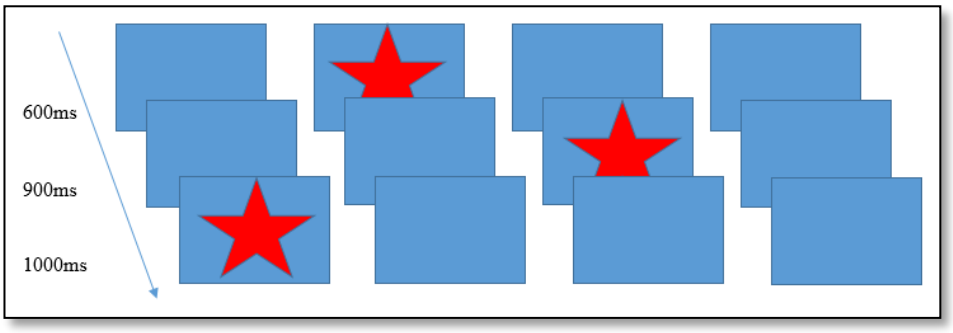

Figure 7.1 Schematic of the SRT presentation, example ISIs on the left indicate example times between trials.

7.2.4 Hypercapnic Calibration

The SRT task was followed by a hypercapnic calibration scan to obtain a measure of cerebrovascular reactivity (CVR) to CO_2 for estimation of $rCMRO_2$. Participants breathed through a tight-fitting face-mask as described above, gases were administered from gas cylinders connected to an in-house built manually controlled flow meter system. Gases were piped through a mixing chamber with three feeding lines coming in for the delivery of medical air, 5% CO_2, and medical oxygen. Medical oxygen was not administered but was connected in case of emergency. Gases were humidified for participant comfort. The scan began with a 2-minute normocapnia period during which participants breathed medical air (20.9% O_2 balance N2) with a flow rate of 30 L/min. This was followed by a rapid switch to 2 minutes of hypercapnia where an increase in $P_{ET}CO_2$ of +7 mmHg was targeted. In total, the scan consisted of 3x2 minute blocks of normocapnia and 2x2 minute blocks of hypercapnia.

7.2.5 Data Analysis

7.2.5.1 Image Preprocessing

Perfusion and BOLD weighted images were created from the first and second echo data respectively. Physiological noise correction was carried out using a modified RETROICOR technique (Glover et al., 2000) was carried out as described previously (Chapter 3). Afni software https://afni.nimh.nih.gov/afni/ was used for motion correction and processing of the image timeseries. Interpolated surround subtraction of the of the first echo tag and control image time-series was performed and surround averaging was applied to the BOLD weighted images to remove any contamination of BOLD and perfusion weighting respectively (Liu & Wong, 2005).

7.2.5.2 Task Response Modelling

One subject was excluded from the analysis due to a low task response rate. The remaining 19 subjects' BOLD and CBF task responses were modelled using a standard FEAT general linear model (GLM) (FMRIB's Software Library, www.fmrib.ox.ac.uk/fsl) with high pass filtering (cut off 80s). Functional data were registered to the high resolution T1 weighted structural image using FLIRT, FMRIB's linear image registration tool (M Jenkinson & Smith, 2001), with 6 degrees of freedom. The high-resolution images were then registered to the Montreal Neurological Institute (MNI) standard space with 12 degrees of freedom. FEAT contrasts were set up to investigate positive and negative task vs. rest activity. A second set of contrasts modelled linear response changes over time, using the task timing regressor to model the average change across the experiment as opposed to a block by block change (see supplementary figure 7.11). Cluster based thresholding was applied to define significant BOLD and CBF task responses ($z>2.3$, $p < .05$, FDR corrected). All subject's data ($n = 19$) were then entered into a higher-level FEAT analysis to help define functional ROIs for further analysis.

7.2.5.3 Definition of ROIs

2 ROIs were selected for investigation of BOLD, CBF and $rCMRO_2$ responses during SRT performance; i) the global mean task response (MR), and ii) global linear signal decrease over time (LD). Both ROIs were defined from the intersection between statistically significant BOLD and CBF responses. The ROIs were defined from positive responses only.

7.2.5.4 Calculation of Percentage BOLD and CBF Signal Changes

Percentage relative signal changes from rest and over time were calculated by dividing the appropriate FEAT contrast image by the baseline perfusion image for CBF data or mean the mean functional image for BOLD data. These changes were calculated using the average signal across the experiment from the task regressor rather than a block by block analysis. As quantitative perfusion maps cannot be incorporated into the FEAT analysis framework, CBF is reported in relative percentage changes rather than absolute ml/100g/min unit changes for the main analysis as the main aim was to determine changes in perfusion during the task rather than absolute CBF.

To estimate task BOLD and CBF signal at the start and end of the task, a linear signal change across the task was assumed. Each subject's mean linear response change across the task was calculated for each ROI. Then, to achieve an estimate of the signal at the start of the task 50% was added to the mean signal, and to estimate signal at the end of the task, 50% of the mean value was subtracted. For example, if subject 1 had a 10% CBF increase from baseline when averaging across all 6 task blocks, a 15% change from baseline would be assumed for the start of the task (block 1) and a 5% change from baseline at the end of the task (block 6).

7.2.5.5 CBF Quantification

M_0 of blood was calculated from the calibration image where equilibrium magnetisation of cerebrospinal fluid (CSF) was determined from voxels in the ventricles. M_0 of CSF was converted to M_0 blood using a blood water density scaling constant (0.87 ml/ml) (Donahue et al., 2010). A single compartment model (Wong et al., 1998) was used to estimate CBF in ml/100g/min.

7.2.5.6 BOLD and CBF CVR to CO_2

The CO_2 response was calculated using the CVR analysis method described by Bright & Murphy (2013) where the beta weight calculated for the CO_2 regressor reflects the percentage BOLD or CBF signal change caused by hypercapnia. This change is quantified in % signal change per mmHg unit increase in end-tidal CO_2. CVR was calculated using the average timeseries in each ROI used. As the timing of the haemodynamic response is not uniform across the brain and there are delays in the physiological response to CO_2, the end-tidal CO_2 regressors were shifted according to the best fit to the data, calculated from fitting 97 time shifts to the data. CVR was calculated for each ROI (as described in Chapter 3 for single inversion time CVR data).

7.2.5.7 RCMRO$_2$ Calculation

$$M = \frac{B_H - 1}{1 - F_H{}^{-(\beta-\alpha)}} \quad \textbf{A}$$

$$\mathrm{rCMR_{O2}}(t) = F(t)^{1-\alpha/\beta}\left(1 - \frac{B(t) - 1}{M}\right)^{1/\beta} \quad \textbf{B}$$

Figure 7.2 Equations from (Davis et al., 1998) for the calculation of M (A) and rCMRO$_2$ (B). B_H and F_H are BOLD and CBF CVR measures, α represents the change in CBV as a function of CBF, and β represents the relationship between blood oxygenation and the BOLD signal, F(t) = CBF at time (t), B(t) = BOLD at time (t).

The Davis model (Davis et al., 1998a) was used to calculate rCMRO$_2$ from normalised BOLD and CBF data in each ROI. The hypercapnia measurement was performed to estimate the scaling parameter M (see Figure 7.2A) which represents the estimated maximum BOLD signal response upon washout of all deoxyhaemoglobin per the calibrated fMRI equation from Davis et al. (1998). This model assumes that the targeted level of hypercapnia does not change CMRO$_2$. The values for α and β must also be assumed. In the model, α represents the change in CBV as a function of CBF, the original value of this exponential as proposed by Grubb (1974) was 0.38 to describe arterio-venous blood volume. More recently it has been established that the volume of the deoxyhaemoglobin compartment, venous CBV, is what is required to calculate M. Chen & Pike (2010) used steady-state flow and volume changes to estimate the power–law relationship between CBV and CBF and the model fit produced a coefficient of 0.18 which is comparable to simulation work from Griffeth & Buxton (2011) and values between 0.18-0.23 and are more commonly used at 3T. However, being a biological parameter, actual α values are likely to vary with age, health status and under different experimental conditions.

The parameter β which equals 1.5 in the original equation is a constant representing the relationship between blood oxygenation and the BOLD signal. As relaxivity is field dependent an optimised value of 1.3 tends to be used at 3T (Bulte et al., 2012; Mark, Fisher, & Pike, 2011). Values of α = 0.20 β =1.3 were used in this study in line with Bulte et al. (2012). These values were input into the model for calculation of M and rCMRO$_2$ changes.

7.2.6 Statistical Analysis

All statistical comparisons were carried out using SPSS Version 20 (IBM Corp., Armonk, N.Y., USA). Paired t-tests were corrected using Bonferroni corrections for multiple comparisons where relevant and significant at $p < 0.05$ using two-tailed tests. Normality was assessed using the Shapiro-Wilk test, all variables were >.05 indicating normality.

7.3 Results

7.3.1 Behavioural Data

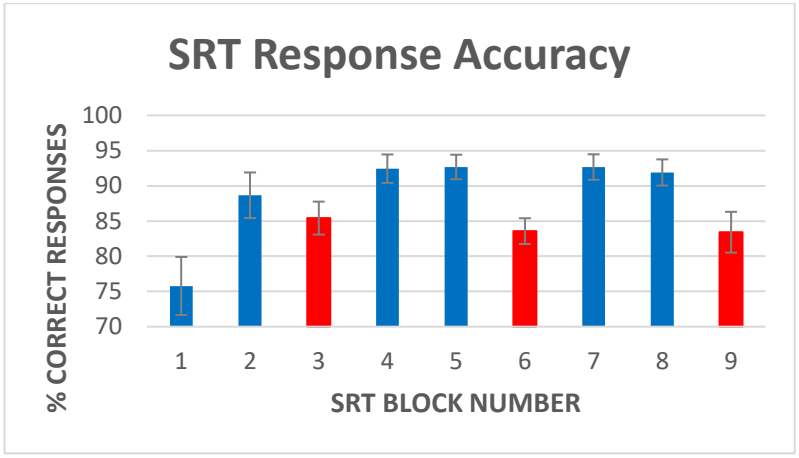

A

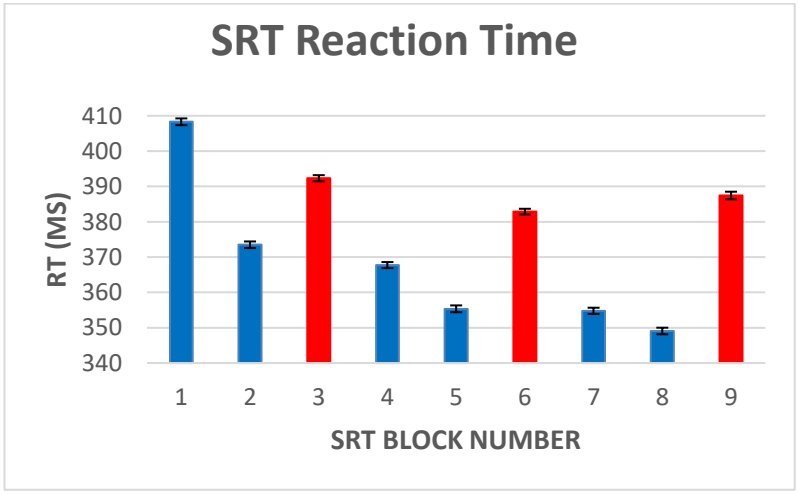

B

Figure 7.3 Average response accuracy per block (A), and average response time (B) across each task block. Error bars represent the standard error of the mean. Blocks 3, 6 and 9 (shown in red) represent pseudorandom sequence blocks.

A one-way repeated measures ANOVA was carried out to compare performance across sequence blocks. Mauchley's test for sphericity was significant with $p < 0.001$, therefore

degrees of freedom were corrected using Greenhouse-Geisser estimates of sphericity, $\varepsilon = .441$. The results showed that there was a significant effect of time on performance; response accuracy improved over time; $F(2.2, 38.3) = 12.47$, $p < 0.001$. Follow up comparisons indicated that all subsequent blocks had a significantly higher accuracy rate than block one. A direct comparison showed a 16.9±9% accuracy improvement from block 1 to block 6, $p = 0.007$. Accuracy was higher in sequence blocks than random blocks, except sequence block 1 which had the lowest performance of all blocks (Figure 7.3A). Random blocks 1 and 2 had significantly lower accuracy than sequence blocks 3-6, however random block 3 scores were only significantly lower than sequence blocks 3, 4 and 6, all $p < 0.05$. This shows that performance improvements over time can largely be attributed to sequence learning rather than motor habituation to the task.

There was a significant effect of time on reaction speed; $F(5, 85) = 27.98$, $p < 0.001$, the assumption of sphericity was met as Mauchley's test was non-significant, $p = 0.147$. Follow up comparisons showed that RT decreased by 5.1±11% from block 1 to block 6, $p < 0.001$. Random blocks had a greater response latency, except for sequence block 1 as before (Figure 7.3B). Reaction time (RT) was significantly longer in random block 1 than sequence blocks 2-6, random block 2, RT in random blocks 2 and 3 was longer than sequence blocks 3-6, all $p < 0.05$.

7.3.2 Imaging Data

7.3.2.1 Group Average CVR and Task Responses

ROI	BOLD CVR %/mmHg	CBF CVR %/mmHg	M %	% Mean BOLD	% Mean CBF	% BOLD Reduction	% CBF Reduction
Mean Response	0.18 (0.08)	2.3 (1)	7.8 (1.8)	0.26 (0.05)	6.9 (1.6)	-0.12 (-0.02)	-8.1 (1.2)
Linear Reduction	0.17 (0.09)	2.4 (1)	7.1 (1.6)	0.25 (0.05)	6.2 (1.4)	-0.21 (0.05)	-21.5 (5)

Table 7.1 Mean (SEM) CVR and M values used to calculate $rCMRO_2$ along with the mean BOLD and CBF task responses and % BOLD and CBF signal reduction over time. % Mean = Average BOLD signal change from the mean during task blocks, or CBF change from baseline. % BOLD Reduction = Average signal relative to the mean in regions showing a linear signal decrease across task blocks. % CBF Reduction = CBF signal change from the mean perfusion across the task.

7.3.2.2 Task Related BOLD and CBF Signal Changes

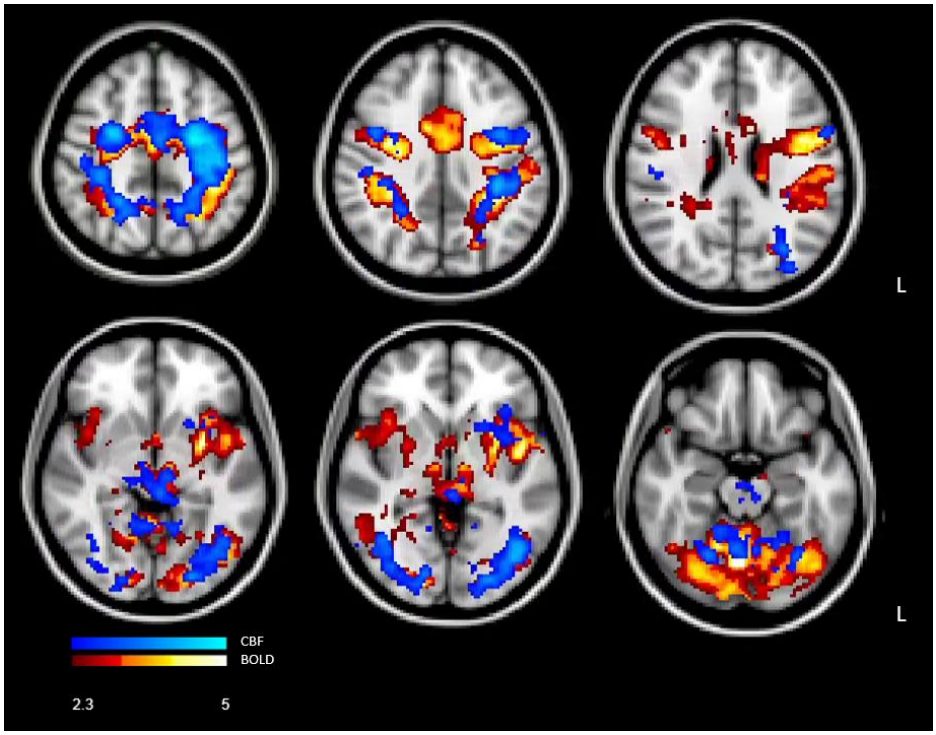

Figure 7.4 Z-score maps showing significant clusters (z= 2.3, p < 0.05, corrected) of average BOLD and CBF task-related signal increases from rest. Random blocks were not included in this analysis.

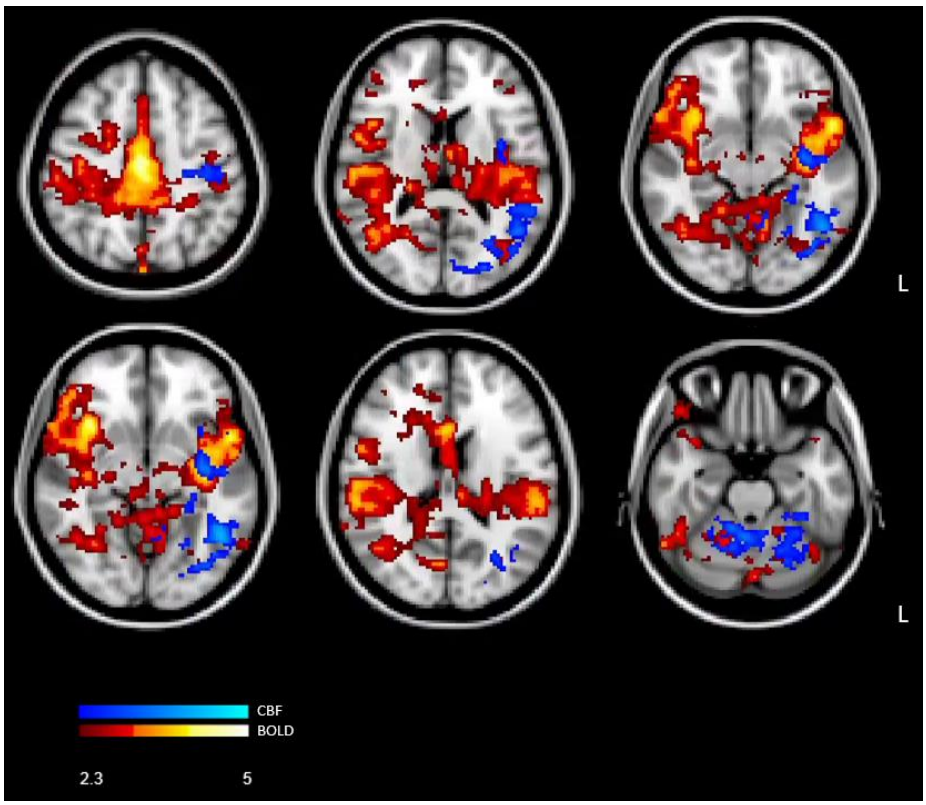

Figure 7.5 Z-score maps for Regions showing a significant (z= 2.3, p < 0.05, corrected) linear BOLD and CBF signal decrease during task blocks only over time.

Figure 7.4 shows the mean CBF and BOLD responses to the task (task vs. rest contrast). There were no areas showing signal reduction from baseline during the task. Figure 7.5 shows regions where BOLD and CBF signal displayed a linear decreasing signal trend across task blocks.

7.3.3 Flow and Metabolism Changes during Task Performance

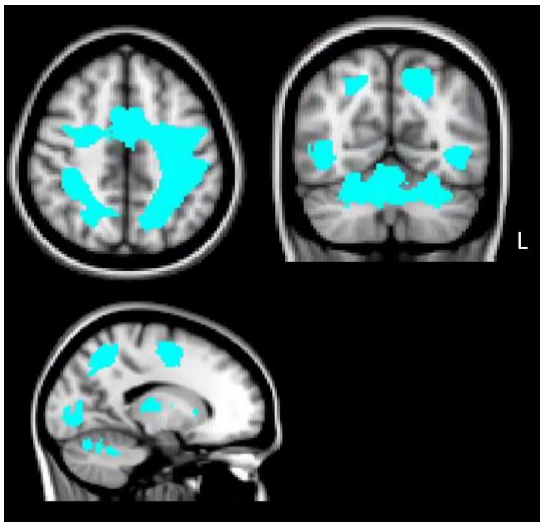

Figure 7.6 Mean Response (MR) ROI defined from the intersection of regions where both BOLD and CBF showed significant task responses (see figure 7.4 for BOLD and CBF mean task responses).

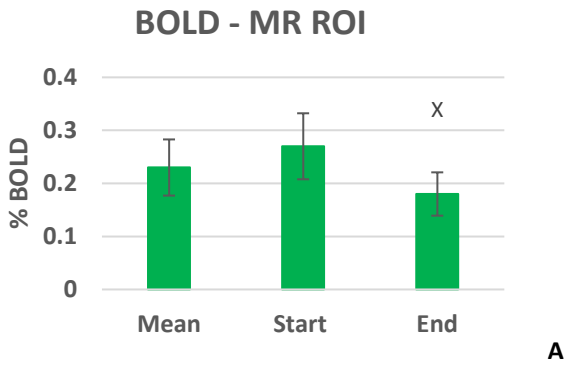

A

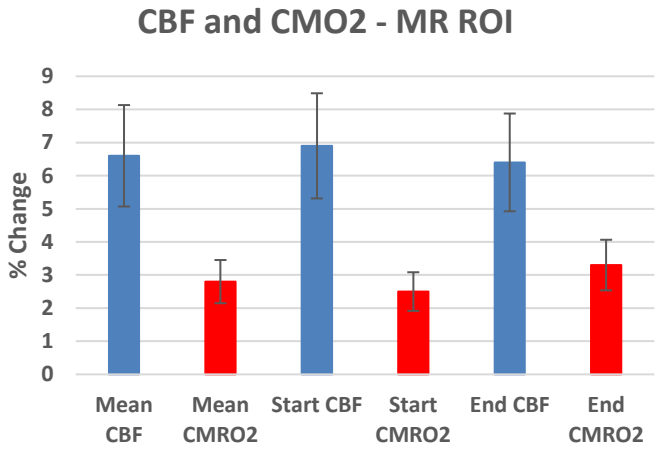

B

Figure 7.7 Mean (SEM) signal changes from the mean at the start and end of the task in the mean task response MR ROI shown in Figure 7.6. x Denotes significant difference from start values. Task mean shown for reference.

One subject was removed from analysis of the ROI shown in figure 7.7 due to a large M value of 40% which is outside of assumed physiologically plausible limits.

For the ROI shown in figure 7.6, paired t-tests showed a significant BOLD reduction from the start to end of the task; t(17)=-5.696, p< 0.001 [95% CIs, 0.05-0.12]. CBF was not significantly lower from the start at the end of the task; t(17)=1.155, p = -0.264 [95% CIs, -.4-1.4]. $RCMRO_2$ did not significantly increase from the start to end of the task; t(17)=2.068, p = 0.054 [95% CIs, -1.5-0.2] (figure 7.7).

7.3.4 Flow and Metabolism Reductions over Time

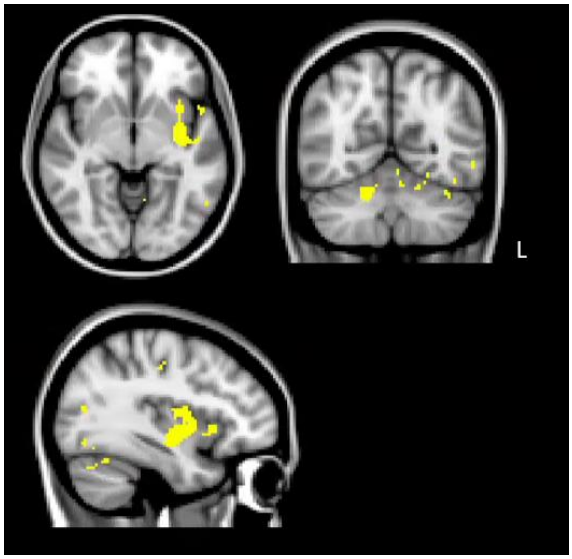

Figure 7.8 Linear decrease (LD) ROI defined from the overlap of regions where both BOLD and CBF showed a linear signal reduction over time during task performance shown in Figure 7.5.

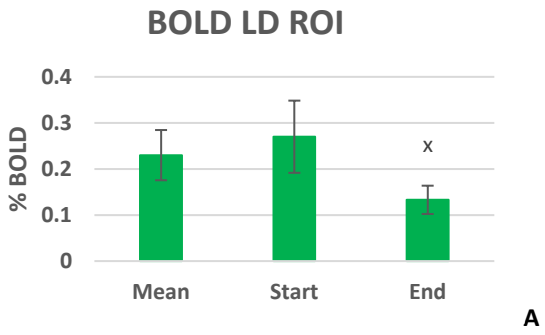

A

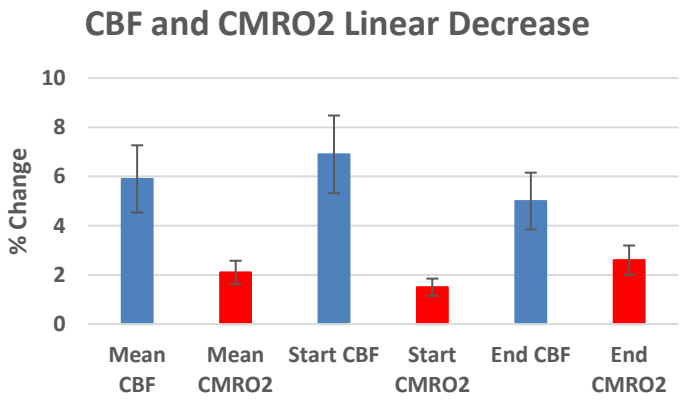

B

Figure 7.9 Group average (mean ± SEM) BOLD, CBF and $rCMRO_2$ in the ROI where a linear signal decrease was observed for BOLD and CBF across the task. ^{x} Denotes significant difference from start values. Task mean shown for reference.

For the ROI shown in figure 7.8, paired t-tests showed a significant BOLD signal reduction at the end of the task vs. the start; t(17)=-4.287, p > 0.001 [95% CIs, .10-.3]. CBF was not significantly lower at the end of the task vs. the start; t(17)=-1.846, p = 0.082 [95% CIs, -2.3-0.15]. $RCMRO_2$ as in the previous ROI, did not show a significant increase from the start to end of the task; t(17)=1.846, p = 0.082 [95% CIs, -2.3-0.15] (figure 7.9A-B).

7.3.5 Flow-Metabolism Coupling

ROI	Start	End	t-stat	p-value	95% CIs
Mean Task Response	1.7 (0.4)	2.8 (0.5)	-.671	0.511	-2.6 - 1.3
Linear Signal Reduction	2.2 (0.5)	1.7 (0.4)	0.258	0.799	-1.6 - 2

Table 7.2 Ratio of CBF and rCMRO2 task-related changes for each ROI, mean (SEM)

2 additional subjects were removed from the flow-metabolism coupling results due to large negative ratios; data from the remaining 15 subjects is reported in Table 7.2. Table 7.2 shows the coupling ratio between CBF and $rCMRO_2$ changes for each ROI. The coupling was within ranges previously reported for visual (Ances et al., 2008; Uludag et al., 2004) and motor/sensorimotor activation (Chiarelli et al., 2007; Kastrup, Kru, Neumann-Haefelin, Glover, & Moseley, 2002). The coupling ratio decreased at the end of the task compared to the start in the LD ROI, despite an overall $rCMRO_2$ increase. This reduction in the coupling ratio (greater $CMRO_2$ changes relative to CBF changes) suggests that oxygen extraction efficiency increased over the course of the task.

7.3.6 Results Summary

Using calibrated fMRI, we measured BOLD, CBF and $rCMRO_2$ changes during a 12-minute visuomotor learning paradigm; the SRT task. There were significant overlapping BOLD and CBF task responses in bilateral motor and somatosensory cortices, cerebellum, thalamus, LOC, ACC and left insular cortex. Statistically significant signal reductions over time were observed in the left insula, LOC and the bilateral cerebellum in both CBF and BOLD data. Investigations of energetic changes during task performance were confined to 2 ROIs defined from each of the response conditions; the global mean task response (MR ROI) and the global linear signal decrease (LD ROI) over time.

Across both ROIs, similar trends were observed; BOLD and CBF showed increased responses from the mean at the beginning of the task and signal reductions from the start of the task to the end. In both ROIs, $rCMRO_2$ was higher at the end of task vs. the mean and the starting values. However, these differences did not quite reach statistical significance. Flow-metabolism coupling ratios decreased over time in the LD ROI but increased in the MR ROI. The coupling decrease was driven by the CBF response decreases relative to $rCMRO_2$ response increases over time, and the increase in the MR ROI by smaller overall CBF reductions relative to $rCMRO_2$ reductions. Taken together, the results suggest an altered coupling of CBF and $rCMRO_2$ during task learning; as the task progressed, CBF and BOLD were, on average, showing signal reductions while $rCMRO_2$ increased. Increasing $rCMRO_2$ over the course of the task suggests that tissue OEF was increasing. In other words, despite less CBF being required as the task progressed, more oxygen was being extracted from blood flowing to regions involved in task-performance.

The results demonstrate the feasibility of measuring CBF and $rCMRO_2$ changes during learning and offer new information on the relationship between CBF and oxygen metabolism changes during sequence learning. This novel information about flow-metabolism coupling during complex behavioural tasks is an important step in determining regional flow and metabolism coupling in the healthy brain, which will inform the characterisation of alterations in neural energetics with ageing and disease.

7.4 Discussion

7.4.1 Energetic Changes during Task Performance

Regarding the anatomical location of task responses, activity was identified in regions typical of a visuomotor learning task, i.e. motor, visual, attention and information processing networks. Decreases over time were noted in the contralateral cerebellum, insula and LOC which can be attributed to task learning based on the improved accuracy and reaction times over task blocks. The cerebellum is critically involved in motor learning and coordination of voluntary movement, therefore decreases in this region coinciding with improved task performance may represent a shift towards automated performance of the motor task. The insula has been associated with hand to eye motor coordination, while the LOC is primarily involved in shape discrimination; signal reductions in these regions may also be attributed to increased skill and less effort required to perform the task. BOLD and CBF responses overlapped to a degree although BOLD activity in all regions was less localised than CBF. BOLD

signal has lower specificity than CBF despite higher SNR, and this study highlights the importance of including CBF measures where spatial specificity of responses is required. However, one drawback of the lower CBF SNR is that this may have reduced group level activity due to higher between-subject variation. Therefore, in studies without a pre-defined ROI, combining BOLD and CBF exploits the strengths of both techniques, allowing key ROIs to be defined from the overlap between BOLD and CBF weighted images, but also enables regional differences in BOLD and CBF responses to be identified so that potential metabolic alterations due to task demands or pathology can be investigated.

The signal reductions over task blocks observed in this study are in line with previous work showing within-session signal decreases as task-relevant skill acquisition occurs (Floyer-Lea & Matthews, 2004; Karni et al., 1995). The novelty finding of this study is that despite BOLD and CBF signal deceases from the start to end of the task, $rCMRO_2$ increased. This is somewhat counterintuitive, as CBF and $CMRO_2$ are typically shown to be positively coupled (Hoge et al., 1999; Uludag et al., 2004) during activation and deactivation. However, as $rCMRO_2$ changes over time during visuomotor learning have not been previously reported on this short timescale, it is possible that skill training leads to alterations in energy demand and the way in which the brain utilises oxygen. There is little information on changes in $CMRO_2$ during any form of learning in the calibrated fMRI and PET literature. Most quantitative fMRI studies use visual stimulation or motor tapping to probe $rCMRO_2$ changes from baseline rather than studying more complex cognitive processes and changes with task training. It is possible that typical coupling between CBF and $CMRO_2$ is altered during motor tasks, as described by Vafaee, & Gjedde (2004) or indeed during any task requiring more complex cognitive processing than passive visual stimulation or simple finger tapping. Vafaee & Gjedde (2004) used PET to compare regional CBF (rCBF) and $CMRO_2$ responses in regions activated during a thumb flexion task carried out at a range of frequencies, but did not look at changes over time. The results showed that CBF and $CMRO_2$ responses differed between regions as did the coupling between them. For example, cerebellum CBF increases were not accompanied by significant $CMRO_2$ changes, and at all frequencies (1-4 Hz) right putamen $CMRO_2$ increases were greater than CBF increases.

The current results may be true reflections of energetic changes during visuomotor learning, but require validation in future studies. In this study, we have averaged over continuous changes in neural activity due to the short task duration to calculate mean $rCMRO_2$ responses

and then calculated start and end values for BOLD, CBF and $rCMRO_2$. Continuous, or block by block $rCMRO_2$ values across the 12 minutes would build a clearer picture of the timecourse of CBF and $rCMRO_2$ changes, and coupling alterations at specific stages of sequence learning. However, with the method used here, the timeseries would simply be too noisy so that $rCMRO_2$ changes would only reflect noise in the fMRI signal. Currently, averaging over a large number of data points is needed to get reliable $rCMRO_2$ estimates. For a continuous approach to be viable, improvements in data acquisition to increase data quality are necessary, such as the use of PCASL which offers greater labelling efficiency, and background suppression which serves to reduce signal fluctuations due to physiological noise, motion and improve the stability of the signal.

Additional studies are required to validate this result, however there are several potential explanations for the observed change in coupling between CBF and $rCMRO_2$. When a task continues to be performed over a period of time, signal changes, usually reductions, in the fMRI response, it is generally attributed to an increase in neural efficiency, however, this does not explain the mechanisms driving response changes. Poldrack (2015) suggested a number of neurobiological alternatives to the catch-all neuronal efficiency explanation which are relevant to this study and may partially explain the observed changes.

The first potential mechanism for the CBF and BOLD reductions is a change in neuronal firing intensity with learning. It is possible that the same populations of neurons continue to fire during task performance, but the intensity (Hz) in certain regions critical for learning is less frequent as the task becomes less demanding. This could lead to lower energy (CBF) requirements to support cellular (neurons, glia and astrocytes) activity. However, following the same logic, a concurrent reduction in task-induced $CMRO_2$ increases would also be expected if energy demands were lower by the end of the SRT task performance.

A second explanation is that the speed of processing may increase so that neurons fire for shorter periods of time to perform the same task, resulting in lower measured fMRI responses. This explanation is unlikely given our current understanding of brain energy metabolism as $rCMRO_2$ would typically decrease if CBF demand was reduced. The only way this explanation would fit with the current results is if there was a switch in metabolic capacity with learning so that despite a reduced haemodynamic response over time there is an increase in OEF and

$rCMRO_2$. The trend towards increasing $rCMRO_2$ over time is intriguing given that Shannon et al. (2016) reported a decrease in $CMRO_2$ following visuomotor task performance. However, it is possible that $rCMRO_2$ changes observed during and following motor training depend on task difficulty and/or length of training. Skill learning may increase the metabolic capacity of the brain, perhaps even temporarily, leading to increased tissue OEF and $CMRO_2$. Xiong et al. (2009) reported rCBF increases following motor training and discussed the potential role of cytochrome oxidase (CO) in training dependent energetic changes. CO is a rate-limiting enzyme involved in oxidative phosphorylation, the major energy-synthesizing pathway used by the brain, and is up-regulated in rodents during learning, both in Pavlovian conditioning type training and spatial working memory training (Sakata et al., 2005). In these studies CO histochemistry was used to assess the metabolic history of brain regions and CO upregulation is interpreted as an increase in metabolic capacity. Xiong et al. (2009) suggested that CO upregulation in humans during motor training may lead to $rCMRO_2$ increases. If true, this could explain the $rCMRO_2$ increase despite an overall decreasing CBF. Again, more work using similar paradigms is needed to determine the validity of this result and provide evidence for this potential mechanism. Lastly, these results must be interpreted with caution as the $rCMRO_2$ increases were not statistically significant and this trend may have emerged due to noise-related variability across the group.

The high variability of responses between subjects requires further investigation. It is possible that inter-subject variation in functional brain activity is high during learning, however, the variability may also be due to data quality or low SNR as discussed above. There were a number of negative BOLD signal average task responses, which are unlikely to occur in this type of task. As $rCMRO_2$ changes are calculated from BOLD and CBF this potential inaccuracy will propagate through the model leading to inaccurate estimations. However, as BOLD signal is calculated as a percentage change from the mean in this case, it is possible that there was a signal true reduction and to class this data as outliers may be inappropriate.

Obtaining accurate estimates of $rCMRO_2$ using the Davis model can be difficult due to its simplicity. While the model has held up under many experimental conditions and is still widely used 20 years almost following the publication of the method, any noise in the CVR or task BOLD and CBF is problematic, as demonstrated.

In a task such as the SRT, with highly variable responses over time it is difficult to determine the repeatability of results without comparable studies. However, studies such as that by

Vafaee & Gjedde (2004) show that different regions recruited by the same task produce non-uniform changes in BOLD, CBF and $rCMRO_2$. Second, Krieger et al., (2014) showed that BOLD and CBF responses during a motor learning task had high inter and intra-subject variability, suggesting that individual response variability may be high during visuomotor learning, but also that typical imaging sequences and paradigms may not be refined enough to reliably measure continuous learning-related BOLD and perfusion responses. However, the authors concluded that $CMRO_2$ was more stable and repeatable than BOLD and CBF, suggesting that the magnitude of relative BOLD and CBF changes may be preserved as $rCMRO_2$ depends on both parameters. So although absolute values differ across subjects and sessions, relative changes may be reliable and $rCMRO_2$ could be a robust marker of learning-related changes in brain activity. In summary, we report promising results in using this technique to quantify brain changes during a learning task, but it is also clear that attention must be paid to sources of variability between subjects and over time in future work.

7.4.2 Flow-Metabolism Coupling

The central mechanism behind BOLD imaging is that CBF increases much more than $CMRO_2$ upon neural activation so that blood oxygenation increases with brain activity (Ogawa et al., 1993). For example, during visual stimulation CBF increases by approximately twice the $CMRO_2$ increase with much smaller increases in BOLD, ~0.05% of CBF (Hoge et al., 1999). More recently, Uludag et al. (2004) reported CBF changes 2.2 times greater than $CMRO_2$ changes during visual stimulation. Both Hoge et al. (1999) and Uludag et al. (2004) found strong linear coupling between the CBF and $CMRO_2$ increases under graded visual stimulation. In contrast, somatosensory stimulation responses do not follow the same coupling ratio. Fox & Raichle (1986), reported only a 5% $CMRO_2$ increase for a 29% CBF increase in the somatosensory cortex, meaning that CBF increased nearly 6 times that of $CMRO_2$. Motor tasks such as finger movement show coupling ratios ranging from 1.24 to 3 (Chiarelli et al., 2007; Kastrup et al., 2002) and this variation may be due to differences in the type of stimulation or task used. The degree of coupling between CBF and $CMRO_2$ in other brain regions has not been clearly established, nor is it clear how processes such as learning affect the flow-metabolism coupling. Uludag et al. (2004) reported that activation and deactivation trends vary in a similar fashion in visual cortex, but it is not clear if this trend is uniform across the brain and under different levels of cognitive load. The current results show CBF-$CMRO_2$ coupling within previously reported ranges (see table 7.2) for both ROIs for task mean, start and end values. In the LD ROI, the ratio of CBF to $rCMRO_2$ changes decreased from the start to end of the task showing

that as task adaptation or learning occurred, the slope between CBF and $CMRO_2$ task responses was reducing, in line with the BOLD reductions and $rCMRO_2$ increases observed across task blocks. As discussed above, this could indicate an increase in metabolic capacity, or efficiency, i.e. increased oxygen extraction fraction (OEF) with task learning, so that more energy is being extracted from less blood.

Future work using dual-calibrated FMRI, such as in Chapter 5, could provide additional insight into the nature of metabolic changes during tasks such as the SRT, by measuring OEF and absolute $CMRO_2$ changes during learning. Additionally, a longer task duration, or multiple imaging sessions would allow us to identify when $CMRO_2$ increases and CBF deceases level off and whether flow-metabolism coupling changes again during the late learning or consolidation periods.

7.4.3 Limitations

The study had several limitations. Previous work studying cerebrovascular changes during cognitive tasks have used much longer paradigms than the 12-minute task used here. Only 6 sequence blocks were included here due to time limitations within the scan session, meaning that SNR was relatively low for the purposes of looking at individual 45 second block activity. For this reason, we chose to assume BOLD and CBF responses at the beginning and end of the task based on the mean response. While this is an imperfect approach, it allowed us to estimate response adaptation over time. In future, calculating responses on a block-by-block basis would yield more accurate estimations.

Also, using a block-by-bock approach and including additional task blocks, would allow 'chunking' of the data into early, intermediate and late blocks to examine differences between the 3 stages of learning with increased SNR. For example, Olson et al. (2006) incorporated three 20 minute SRT blocks in their protocol which served to dilute the effects of transient anomalies in activity and build a more reliable picture of average group responses. While the 12-minute task is useful for measuring short term learning differences between patients and controls and to limit head motion and fatigue effects, to quantitatively assess neural adaptation to learning, longer paradigms should be used along with larger sample sizes to establish whether the variability observed in this study is due to real individual differences or simply noise in the data.

Secondly, it is important to mention that there is evidence suggesting hypercapnia may not be isometabolic and $CMRO_2$ can decrease by up to 13% using a 5% CO_2 mixture (F. Xu et al., 2011). Bulte et al. (2012) tested the effect of metabolism reduction due to hypercapnia on oxygen extraction fraction (OEF), which would directly affect CBF, and found that it had very little effect overall (< ±0.04 fractional OEF). We have not factored potential metabolism reductions into the model in this instance, based on Bulte et al's (2012) conclusions.

7.4.4 Conclusions

This study shows BOLD and CBF reductions over time during a visuomotor learning task, alongside increases in $rCMRO_2$. In keeping with this trend the flow-metabolism coupling ratio decreased over time in regions where a mean task response was identified, and decreased where there was a mean signal decrease over task blocks. The results demonstrate the application of calibrated fMRI to study energetic changes in the brain during learning, and the results suggest change in coupling between CBF and oxygen metabolism during task performance that suggests a more efficient oxygen extraction with learning (higher OEF). High inter-subject variability means that further research is warranted to validate the findings using similar paradigms and understand the effects of learning on the brain's metabolic capacity and changes in energetic demands as skill acquisition occurs.

Chapter 7 Supplementary Information

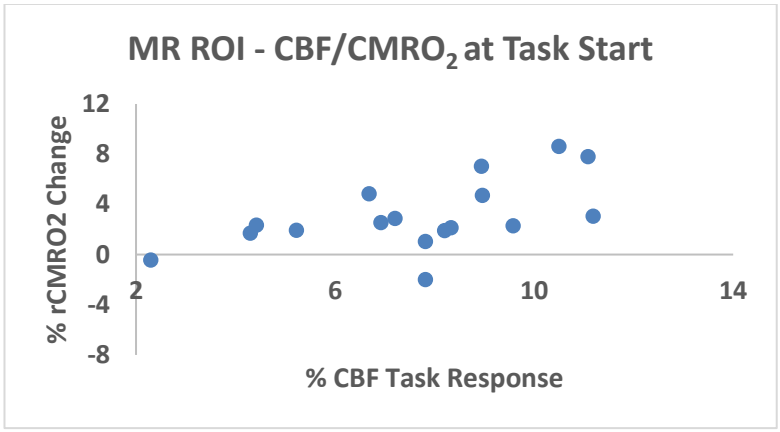

A

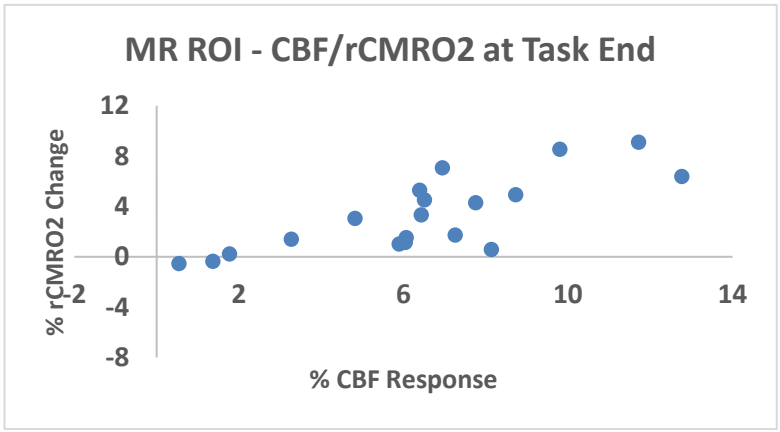

B

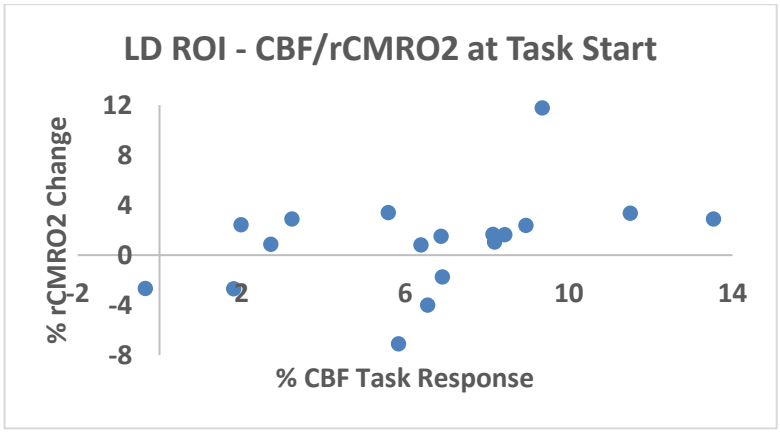

C

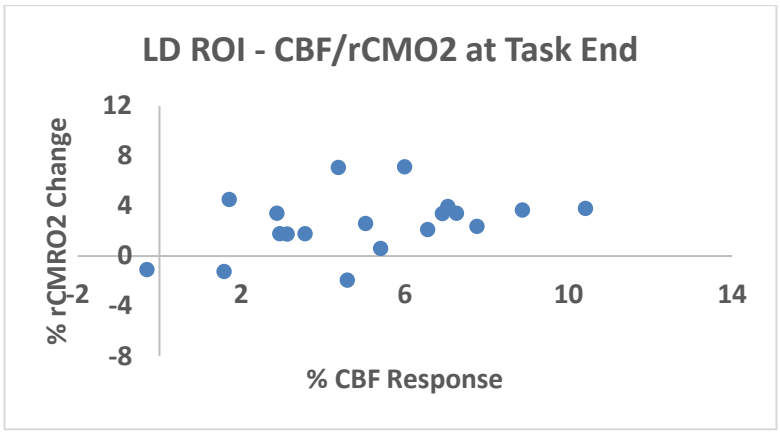

D

Figure 7.10 Relationship between CBF task responses and rCMRO2 changes at the start and end of the task in both ROIs for each subject.

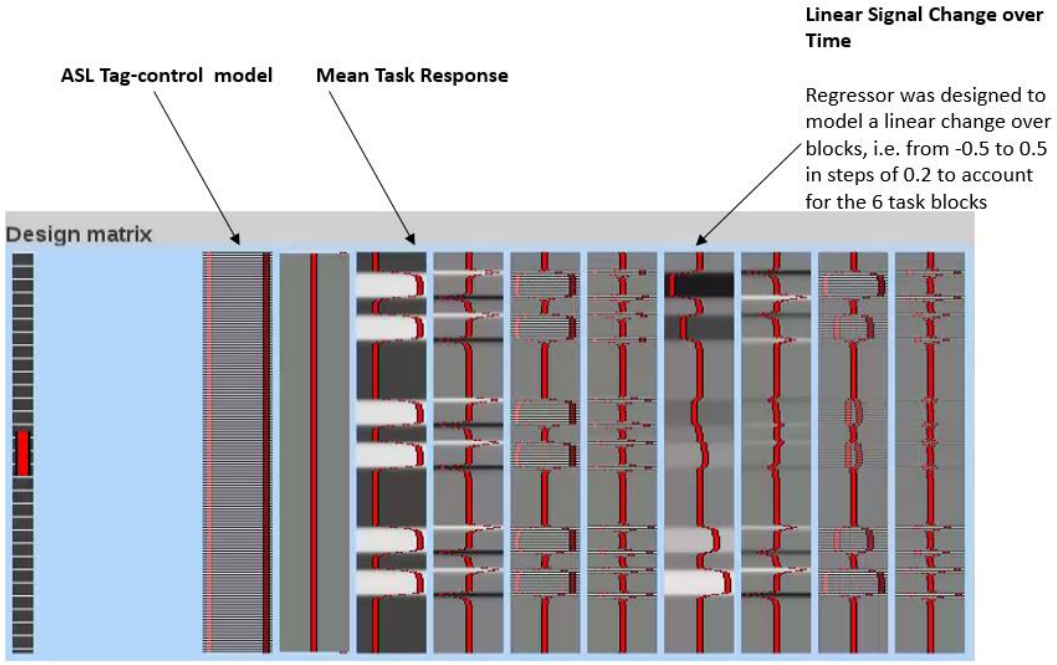

Figure 7.11 FEAT model set up showing the regressors used to model the mean task response and linear signal change over time

Chapter 8

Resting CBF Changes Following a Single Session of Visuomotor Training

Abstract

Introduction: When studying processes which involve functional neuroplasticity such as visuomotor learning, what happens in the resting brain is potentially as important as activity during tasks. Changes in the baseline state following task training may represent metabolic adaptations involved in skill acquisition and learning which are not evident during task performance. This study had several aims; to quantify resting state CBF before and after performance of a single session of an SRT and pseudorandom (PR) sequence task and to investigate RSFC of M1 before and after task training to identify potential task-related metabolic alterations underlying changes in connectivity. **Methods:** 22 young adults were scanned twice using a dual-excitation PCASL sequence for simultaneous BOLD and CBF acquisition. In one session participants completed a 10-minute SRT where 10 minutes of resting PCASL data was acquired before and after. In a separate session, participants performed a control motor task consisting of a pseudorandom task matched in component movements. We examined CBF differences following performance of both task conditions focusing on i) regions showing a mean task response, and ii) regions displaying a linear signal reduction over time during the task. CBF was also compared before and after task performance in areas showing differential M1 BOLD and CBF RSFC pre- and post-task.

Results and Discussion: Resting CBF was not significantly different following SRT task performance in regions showing a mean task response or in regions showing a mean signal decrease across task performance. However, greater pre-SRT training relative to post-training RSFC with M1 was identified in the right planum polare and temporal pole, and in the LOC and lingual gyrus post-training M1 RSFC was greater than pre-training. Again, resting CBF did not significantly change in these areas following SRT performance. Analysis of the PR task data showed that resting CBF was significantly higher post training in the mean task response ROI. In the ROI representing the linear signal reduction over task blocks, resting CBF was significantly lower post PR task performance. The results suggest that task-specific metabolic

adaptations occur following visuomotor task performance, however, further work is needed to clarify the nature of quantitative CBF changes in task-relevant regions.

8.1 Introduction

When studying processes which involve functional neuroplasticity such as motor learning, what happens in the resting brain is potentially as important as activity during task performance (Albert et al., 2009). Changes in the baseline state following task training may represent metabolic adaptations involved in skill acquisition and learning which are not evident during task performance. Non-invasive imaging studies, i.e. without contrast agent, measuring functional brain plasticity have, for the most part, relied on BOLD fMRI and studied task response adaptations within-session (Floyer-Lea & Matthews, 2004) or over several weeks (Hlustik, Solodkin, Noll, & Small, 2004) during task performance (see chapter 6 for additional details on these studies), although within-session CBF changes during task performance have been reported (Fernandez-Seara et al., 2009). These studies have revealed initial BOLD or CBF response increases, followed by signal reductions with task practice, characteristic of visuomotor learning (Doyon & Benali, 2005; Ungerleider et al., 2002). However it is necessary to determine the specific energetic changes underlying plasticity, both to understand how healthy brain physiology changes with learning, and to exploit the brain's capacity for plasticity in disease (Lipp & Tomassini, 2015; Tomassini, Matthews, et al., 2012; Zeller & Classen, 2014).

Xiong et al. (2009), using PET, showed that baseline CBF increases in the resting state likely explained the reduced task activation after 4 weeks of motor training. This important study

provided a degree of mechanistic explanation for the functional changes observed during motor learning, by showing altered baseline CBF after 4 weeks of training. In the study reported in this chapter, we were interested in whether sustained cerebral blood flow (CBF) changes could be observed after a single session of motor task training as BOLD resting state functional connectivity (RSFC) changes have been reported on this timescale, but without any investigation of sustained flow or metabolism alterations in task or resting state networks (RSNs).

For example, Albert et al. (2009) reported fronto-parietal and cerebellar BOLD RSFC network changes following a short, 11-minute sequence learning task (SRT) and these changes did not occur with a motor performance control task without a learning component. Sami et al. (2014) in a later study from this group, recorded BOLD RSFC for 10-minutes immediately, 30 minutes and 6 hours following either implicit or explicit SRT performance. In the explicit condition,

frontal and cerebellar networks showed enhanced connectivity along with visual areas immediately following training. At 30 minutes, cerebellum connectivity to the thalamus and basal ganglia (BG) was increased, and at 6 hours sensory-motor RSFC was greater. In the implicit condition, there was increased connectivity in primary motor cortex (M1) and sensory-motor areas following the task, at 30 minutes a similar cerebellar-thalamic-BG network showed greater connectivity, and at 6 hours, there was increased connectivity in medial temporal cortex, but lower RSFC in M1 and sensory-motor regions.

These studies show time-dependent RSFC changes related to motor learning, and may reflect different stages of processing and consolidation related to skill learning. However, using BOLD fMRI alone does not identify the nature of vascular and metabolic adaptations in the resting state underlying motor learning. Using quantitative methods to measure cerebral blood flow (CBF), and the cerebral metabolic rate of oxygen consumption ($CMRO_2$) where possible, can clarify whether sustained metabolic changes occur in areas recruited during task performance, and in areas where rapid task response reductions occur. Further, determining whether CBF changes occur in areas where connectivity differences are observed pre and post training, would allow greater interpretation of the metabolic basis for RSFC changes following motor learning.

Almost all RSFC studies use BOLD fMRI due to its high SNR and wide availability. Second, there is a belief that task-independent BOLD may provide clearer information on mechanisms of motor learning than task-based BOLD where changes from an unknown baseline are measured (Ma, Narayana, et al., 2011). Inability to quantify the BOLD signal still limits the understanding of the neurophysiological basis of changes where the resting vasculature is abnormal, as does the fact that it is not possible to separate CBF, CBV and $CMRO_2$ changes contributing to the measured BOLD change. In addition, the BOLD signal suffers from signal drift over long scan times (Olson et al., 2006), greater susceptibility artefacts and lower spatial specificity than perfusion measures obtained with ASL (Chen, 2015). An alternative to BOLD RSFC is perfusion-based RSFC using ASL. Viviani et al. (2011) demonstrated statistically significant correlations between BOLD and CBF connectivity of the default mode network (DMN) in a large sample (n = 265), but found that baseline CBF did not predict the strength of functional connectivity, suggesting the two measures represent independent sources of biological differences. Jann et al. (2015) comparing BOLD and ASL RSFC, showed moderate to high levels of overlap between BOLD and CBF connectivity, but more reliable between session and between scanner reproducibility with BOLD imaging. In the study by Jann et al. (2015), regional CBF was found

to correlate positively with core hubs of ASL and BOLD RSFC networks, in line with similar findings by Liang et al., (2013) in the default mode network. This finding suggests that ASL can be used to assess baseline metabolism, not just in studies of connectivity networks, but also to assess the effects of an intervention, such as motor training, on resting metabolism. Perfusion imaging may therefore be well-suited to investigations of resting state vascular and metabolic alterations underlying motor plasticity. Further, there is strong correlation between ASL and PET resting state and task-based metrics (Cha et al., 2013; Kilroy et al., 2013) allowing quantification of metabolic processes without the need for exogenous contrast agents.

Finally, lack of statistical power is a problem in many fMRI studies and increases the likelihood of type I and type II errors (Button et al., 2013). Power analyses can be difficult to conduct a priori where the expected effect size is not known, or where the aims are exploratory, such as in validating new methods or investigating a relatively new area without pilot data or similar published work. Also, sample sizes are often limited by practical considerations such as funding allocation for scan costs reducing the motivation to conduct power analyses. Although, effect sizes and observed power can be calculated from most published studies, reporting the results of a post-hoc power analysis can aid interpretation of the results, as well as providing an accessible guide for future studies using similar designs.

This study had several aims;

- To quantify resting state CBF before and after performance of a single session of an SRT and pseudorandom (PR) sequence task. We were interested in sustained CBF changes following task performance in regions showing a mean task response, and regions where activity was decreasing throughout the task.
- Use ASL to investigate RSFC of M1 before and after task training to identify potential task-related metabolic alterations underlying changes in connectivity
- Conduct a post-hoc power analysis of the main statistical comparisons to inform related future studies and to provide a measure of confidence in the results.

8.2 Methods

8.2.1 Participants

22 healthy right-handed individuals (14 female, mean age = 22±3) were recruited from posters placed around Cardiff University. The study was approved by the Cardiff University School of Psychology Research Ethics Committee and performed in accordance with the guidelines

stated in the Cardiff University Research Framework (version 4.0, 2010). All participants were non-smokers.

8.2.2 Experimental Paradigm

The aim of the study was to measure CBF changes attributed to sequence learning and not motor execution. For this reason, participants were scanned twice on separate days. In one session participants performed a repeated 8-item sequence (SRT condition) and in the other session, pseudorandom non-repeating number sequences (PR condition). The order of task and random sessions was counterbalanced across subjects. Both block design tasks lasted 10 minutes and consisted of 13 blocks of 32 items. Each block was separated by rest periods of varying durations from 13-30 seconds. Rest durations were identical in sequence and random task sessions. 10 minutes of resting state data was acquired either side of the task presentation within the same functional run to ensure all subjects data was acquired on exactly the same timescale.

Before each session participants were informed that they would be asked to respond using a button box to the location of circles on the screen and to respond as quickly and as accurately as possible. This was considered an implicit learning task as participants were not told that a repeating sequence was present in the SRT condition. A modified version of the task used in Chapter 4 was used, the same visual stimuli and set up was used, the only changes being task duration, inter-stimulus interval (ISI) (variable from 400-800ms) and the number sequence. The sequence used was 1 2 1 4 2 3 4 3, corresponding to the first 8 cues of Curran's (1997) second order predictive sequence where a cue can only be predicted using the previous two cues. The sequence contains two reversals, 121 and 343. In a random sequence, the probability of a reversal is 1/3*6 when repeating stimuli is not allowed. Vaquero et al. (2006) demonstrated slowed response times for reversals, hence it is important to match the number of reversals to expected occurrence frequency in a random sequence. This is needed when performance on predefined sequences is being compared to that on random or pseudorandom sequences where the number of reversals is of a statistically expected level.

In the random task session, subjects were presented with blocks of a 32 item ‘sequence’ to match the duration of the sequence learning blocks. Stimuli were matched for reversals and no repeating stimuli were allowed as before. Participants did not see or practice the task before the scan sessions.

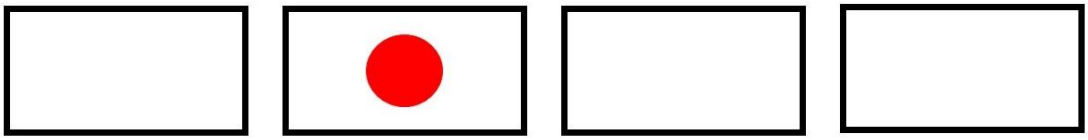

Figure 8.1 Schematic of the SRT task presentation. The red circle appeared in each of the four boxes in the specified repeating or pseudorandom motor task (PR).

8.2.3 Image Acquisition

Acquisition of functional data was carried out using a 2D gradient echo dual-excitation pseudocontinuous ASL (PCASL) sequence with EPI readout, PICORE Q2TIPS, GRAPPA 3, 16 slices, 3.4x3.4x7mm voxel size with 1mm gap, TR1/TR2=3600/800ms, TE1/TE2=3/30/ms, TI=1500ms, tagging duration=1500ms, FOV=220mm, matrix size 64x64, in-plane resolution ~3.4mm^2, flip angle 90°, bandwidth=2298 Hz/pixel, EPI factor 64, echo spacing= 0.54ms, phase encode direction A>>P. Two nonselective adiabatic inversion pulses were applied 950 ms and 300 ms prior to image acquisition for background suppression. A time-of-flight (TOF) angiogram was performed to select the tagging region for the PCASL acquisition; TR/TE = 40.65/5.60ms, FOV =240, slice thickness 1.3mm, bandwidth 300 hz/pixel, transversal orientation R>>L phase encode direction. A calibration image was acquired to determine M_0 of blood quantification of CBF data; TR1 = 6000ms, all other parameters identical to the functional acquisition.

A T1-weighted 3D MPRAGE was acquired for registration of functional data; TR/TE/TI = 2300/2.96/900ms, slice thickness/gap 1.2/0.6mm, FOV 256mm, 176 slices, bandwidth 240 Hz/pixel.

Physiological monitoring and recording of CO_2 and O_2 end-tidal traces was carried out using a nasal cannula connected through a sampling line to a gas analyser system (ADInstruments, Bella Vista, Australia).

Figure 8.2 Schematic of the functional imaging run excluding preparation scans. SRT = Sequence Learning Task, PR = pseudorandom motor task.

8.2.4 Data Analysis

Custom Matlab (Mathworks Inc., MA, USA) scripts were used to separate the data into CBF and BOLD timeseries. Motion correction was performed using FSL MCFLIRT (Motion Correction FMRIB's Linear Image Registration Tool), slice timing correction and spatial smoothing (FWHM = 5mm) was applied. The first four volumes of the BOLD and CBF timeseries were removed to ensure the signal had reached a steady state. A GLM was then fit to the full BOLD and CBF-weighted timeseries for each subject for the SRT and PR task runs using FILM (FMRIB's Improved Linear Model) (https://fsl.fmrib.ox.ac.uk/fsl/) a nonparametric estimation algorithm. Prewhitening was applied to correct for autocorrelation between timepoints. The GLM was performed to determine regions of interest (ROIs) for SRT and PR task responses, and signal decreases across task blocks. These ROIs were identified to quantify CBF in task-relevant regions before and after task performance.

FLIRT (FMRIB's Linear Image Registration Tool) was used to perform linear image registration of functional data to standard space via individual subject T1-weighted images for subsequent group-level analysis. T1-weighted images were first brain extracted using BET (Brain Extraction Tool) to delete non-brain tissue.

8.2.5 ROI Definition from Task Responses

Group-level analysis of BOLD and CBF responses was conducted to identify regions recruited by the SRT and PR tasks. ROIs were created from the overlap between BOLD and CBF positive task responses, thresholded at $z > 2.3$, $p < 0.05$, FDR corrected. Separate ROIs were created for the SRT and PR task runs. ROIs were defined from the intersection of BOLD and CBF task responses. Group-level ROIs were transformed to individual subject space via the T1-weighted image using FLIRT for creation of individual subject ROI masks.

8.2.6 CBF Quantification

M_0 of blood was calculated from the calibration image where equilibrium magnetisation of cerebrospinal fluid (CSF) was determined from voxels in the ventricles (Lu, Clingman, Golay, & Van Zijl, 2004). A single compartment PCASL kinetic model described by (Jiongjiong Wang et al., 2005) with labelling efficiency of 0.85 and T1blood = 1.65s, was then applied to the first-excitation data to convert perfusion to units of ml/100g/min.

8.2.7 Resting State Functional Connectivity

A seed-based analysis was conducted. The intersection between M1, anatomically defined using the Harvard-Oxford Cortical Atlas (within FSL), and areas of M1 where task responses

were reducing over task blocks in both BOLD and CBF data, was selected as the connectivity seed. The filtered CBF and surround averaged BOLD timeseries, were extracted for the M1 seed for each subject and used as regressors in a second GLM analysis. CBF was quantified in areas showing both BOLD and CBF RSFC differences before and after task performance.

8.2.8 Statistical Analysis

All statistical comparisons were carried out using SPSS version 20 (IBM Corp., Armonk, N.Y., USA). Paired t-tests were conducted using bootstrapping (1000 samples, 95% CIs). All reported ANOVA results are reported following Bonferroni corrections and all group data reported as mean ± SEM unless stated otherwise.

2x2 repeated measures ANOVAs were conducted to investigate a) CBF before and after task performance in regions showing an overall positive task response and b) CBF differences due to task condition (SRT or PR). This CBF analysis was carried out twice; with and without normalisation for resting $P_{ET}CO_2$ as arterial CO_2 fluctuations can have substantial effects on the resting state signal (Murphy, Birn, & Bandettini, 2013b; Wise et al., 2004). CBF was normalised by dividing CBF in each ROI by the mean $P_{ET}CO_2$ value cross the rest period. This was considered appropriate as the CBF- $P_{ET}CO_2$ is linear within small $P_{ET}CO_2$ changes (F. B. Tancredi & Hoge, 2013).

A power analysis was conducted using G*Power, version 3.1.9.2 (Faul, Erdfelder, Buchner, & Lang, 2009; Faul, Erdfelder, Lang, & Buchner, 2007) to determine observed power in the current study, and the required sample size in future studies to detect an effect of task training on resting CBF. For ANOVAs, effect sizes are reported as partial eta squared (n^2p). T-test effect sizes were calculated using the Cohen's d_z formula which is the mean change score divided by the standard deviation of change. Both Cohen's d_z and n^2p values were calculated using Lakens (2013) effect size calculator. These values were input into G*Power to determine the effect size *f,* observed power and sample size required for a two-way test with power of 0.8 and 95% confidence intervals (CIs).

8.3 Results

8.3.1 Behavioural Results

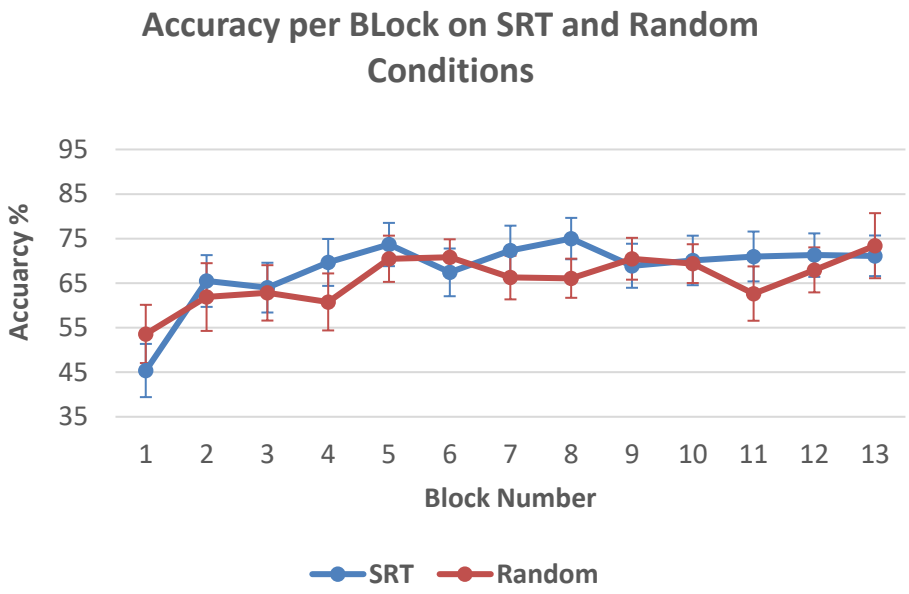

Figure 8.3 Mean ± SEM accuracy across the group for the SRT and pseudorandom sequence tasks.

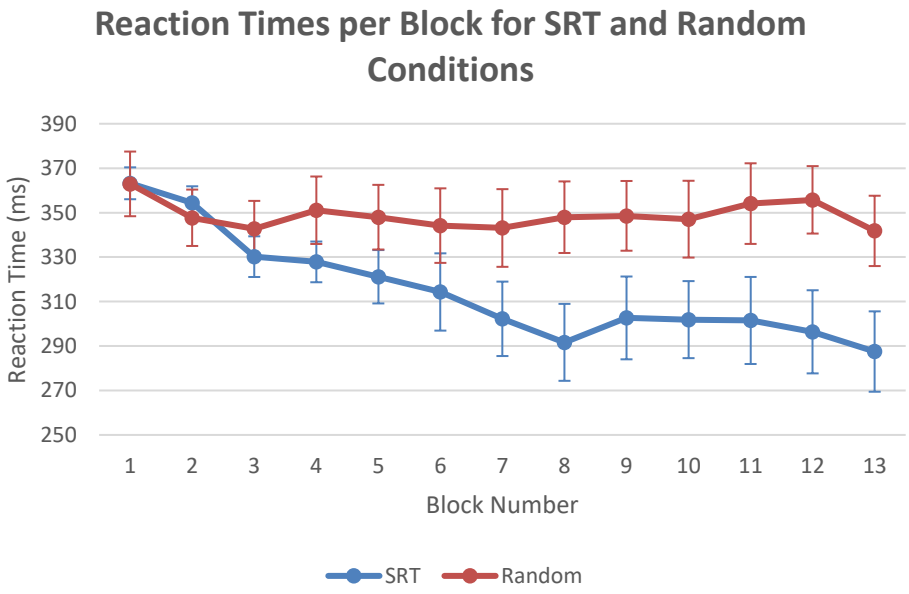

Figure 8.4 Reaction times (mean ± SEM) per block for the SRT and pseudorandom task conditions.

One subject was excluded from the analysis as they did not complete the study. As expected, reaction times were faster overall for the SRT learning task along with higher response accuracy (Figures 8.3 & 8.4). Paired t-tests were used to identify accuracy and reaction time (RT) differences between the first and last task blocks, and between the SRT and PR conditions. There were significant improvements in accuracy from block 1 to block 13 for the SRT condition; $t(20)=4.787$, $p < 0.001$, and the PR condition; $t(20)=3.231$, $p = 0.004$. Accuracy was not significantly different between the SRT and PR conditions for block 1; $t(20)=1.142$, $p = 0.268$, or block 13; $t(20)=.441$, $p = 0.664$. For RT, there was a significant reduction from block 1 to block 13 for the SRT; $t(20)=4.014$, $p = 0.001$, but not the PR condition; $t(20)=1.951$, $p = 0.067$. RT was not significantly different between the SRT and PR conditions in block 1; $t(20)=0.188$, $p = 0.853$, but RT was significantly shorter in the SRT condition by block 13; $t(20)=3.476$, $p = 0.003$. The behavioural data demonstrates gains in reaction time in the SRT condition, reflective of motor sequence learning.

8.3.2 Resting CBF in Task-Recruited Regions

Paired t-tests revealed a significant decrease in $P_{ET}CO_2$ at rest following SRT training. $P_{ET}CO_2$ decreased from a group mean of 34.64 (0.8) mmHg pre-training to 33.7 (0.9) mmHg post-training; $t(20)=2.745$, $p=0.012$ [95% CIs, 0.2-1.5]. This was not observed for the random task condition where $P_{ET}CO_2$ was 33.8 (0.7) mmHg pre-task and 33.2 (0.6) mmHg post-task; $t(20)=0.824$, $p=0.420$ [95% CIs,-0.4-1].

CBF data for each ROI was therefore analysed with and without $P_{ET}CO_2$ normalisation to explore effects of $P_{ET}CO_2$ differences on CBF. The GLM analysis identified BOLD and CBF task responses in bilateral primary motor (M1) and supplementary motor cortex (SMA), lateral occipital cortex (LOC) and cerebellum (all $z = 2.3$, $p < 0.05$) for the SRT and PR task conditions (see figure 8.5).

In the analysis without $P_{ET}CO_2$ normalisation, the repeated measures ANOVA showed that there was not a significant interaction between time (pre and post training) and condition (SRT or PR task), $F(1, 20)=0.238$, $p=0.638$. There was also not a significant main effect of time, $F(1, 20)=2.435$, $p=0.134$ [95% CIs, -.28-1.95], or condition, $F(1, 20)=0.366$, $p=0.366$ [95% CIs, -.2-5.3].

When this data was reanalysed with $P_{ET}CO_2$ normalisation, a significant interaction effect emerged; $F(1, 20)=5.080$, $p=0.036$, but no main effect of time; $F(1, 20)=2.806$, $p=0.109$, or condition; $F(1, 20)=0.127$, $p=0.725$. Follow-up paired tests of simple main effects revealed that

CBF was significantly higher post-training in the PR condition only; t(20)=3.031, p = 0.007 [95% CIs, 0.01-0.07] (figure 8.6). No other CBF changes were approaching significance.

Group-level voxelwise comparison of SRT and PR task runs was carried and no significant task response differences between the SRT and PR runs were identified.

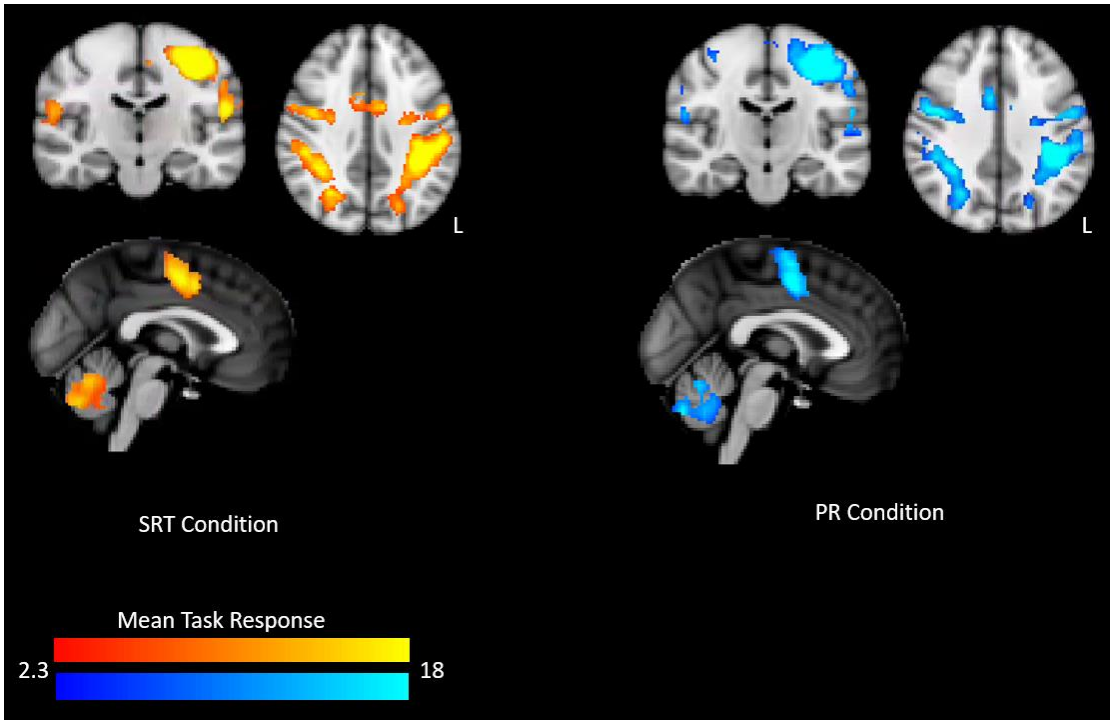

Figure 8.5 Group-level SRT and PR task responses, (z > 2.3, p < 0.05). SRT = Serial Reaction Time task, PR = pseudorandom sequence task. ROI was defined from regions showing both a BOLD and CBF significant task responses.

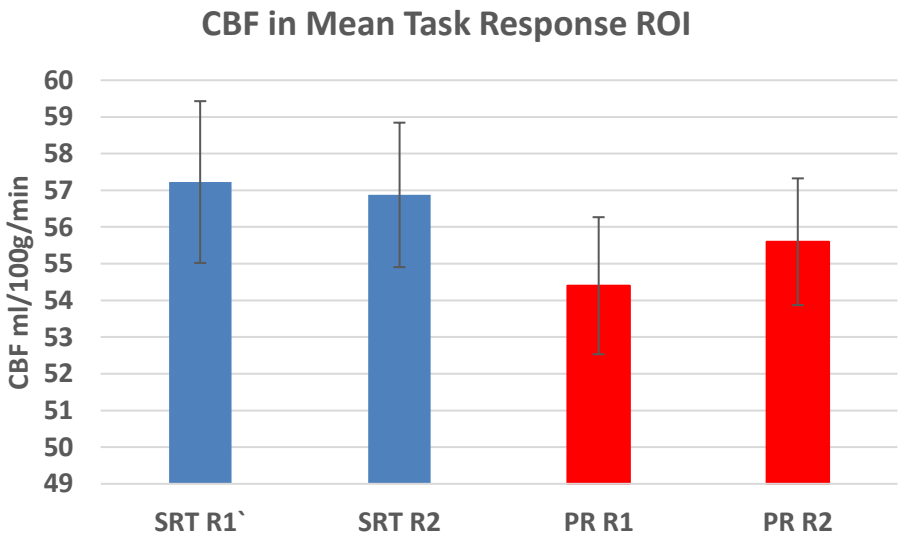

A

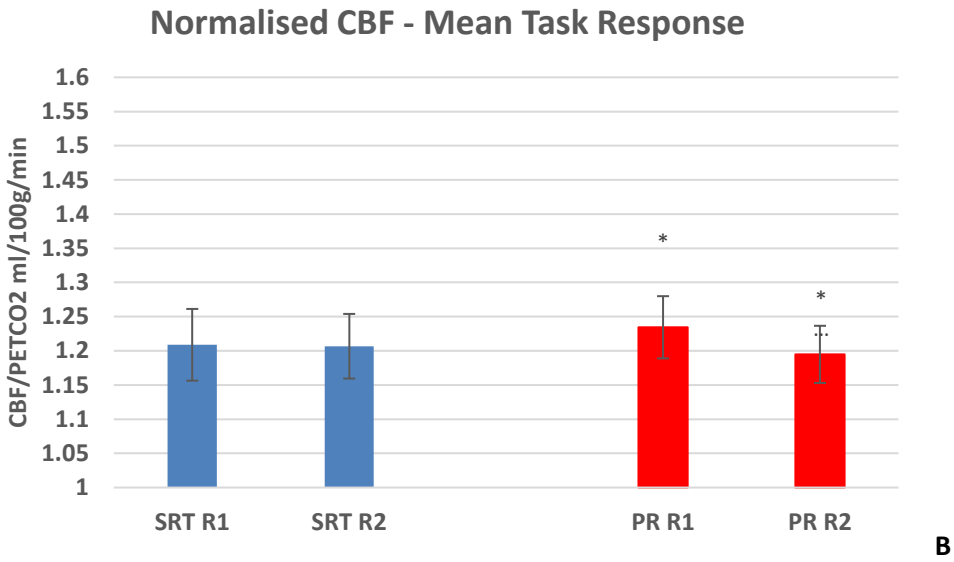

Figure 8.6 Mean ± SEM CBF pre- and post-training in the ROI defined from the mean SRT and PR task responses (A) and the same data following $P_{ET}CO_2$ normalisation (CBF/ $P_{ET}CO_2$) (B). R1= Rest 1, R2 = Rest2. * denotes significant difference between R1 and R2 group CBF at $p < 0.05$.

8.3.3 Linear Signal Reductions across Task Blocks

Linear reductions in BOLD and CBF responses over the duration of the task runs were identified in the right M1, superior parietal lobule (SPL), angular gyrus, supramarginal gyrus (SMG), anterior cingulate cortex (ACC) and cuneal cortex for the SRT. For the PR task, reductions were identified in the right M1, SMG, inferior frontal gyrus (IFG) and bilateral ACC. The overlap between BOLD and CBF linear signal reductions over time for the SRT and PR tasks were defined as ROIs for CBF quantification (see figure 8.7). A repeated measures ANOVA was conducted as above. In the analysis without $P_{ET}CO_2$ normalisation there was a significant interaction effect between time and condition; $F(1, 20)=10.457$, p=0.004. There was not a significant main effect of condition; $F(1, 20)=0.058$, p=0.816. However, there was a main effect of time; $F(1, 20)=7.609$, p=0.014. Follow up comparisons of simple main effects revealed that CBF was significantly lower post PR task performance; t(20)=3.592, p = 0.002 [95% CIs, -0.07-1.6]. No other comparisons were approaching significance.

With $P_{ET}CO_2$ normalisation there was also a significant interaction effect; $F(1, 20)=16.474$, p = 0.001. As before there was not a main effect of condition; $F(1, 20)=0.273$, p = 0.607, but there was a main effect of time; $F(1, 20)=8.060$, p = 0.010. Follow-up tests to look at simple main effects revealed the same effect as the previous analysis; CBF was significantly lower post PR task performance; t(20)=4.066, p=0.001 [95% CIs, 0.08-0.25], with no other comparisons nearing statistical significance (figure 8.8). Average CBF reductions of 6.3 ± 1.7 ml/100g/min and 0.16 ± 0.04 (CBF/CO_2) were observed for the original and normalised CBF for the PR task

condition respectively. For the SRT condition, average CBF was higher post-task; 1.2 ± 1.4 and 0.04 ± 0.01 for original and normalised data.

Group-level comparisons of the CBF and BOLD SRT and PR task decreases over time revealed no significant differences between task responses reduction over time.

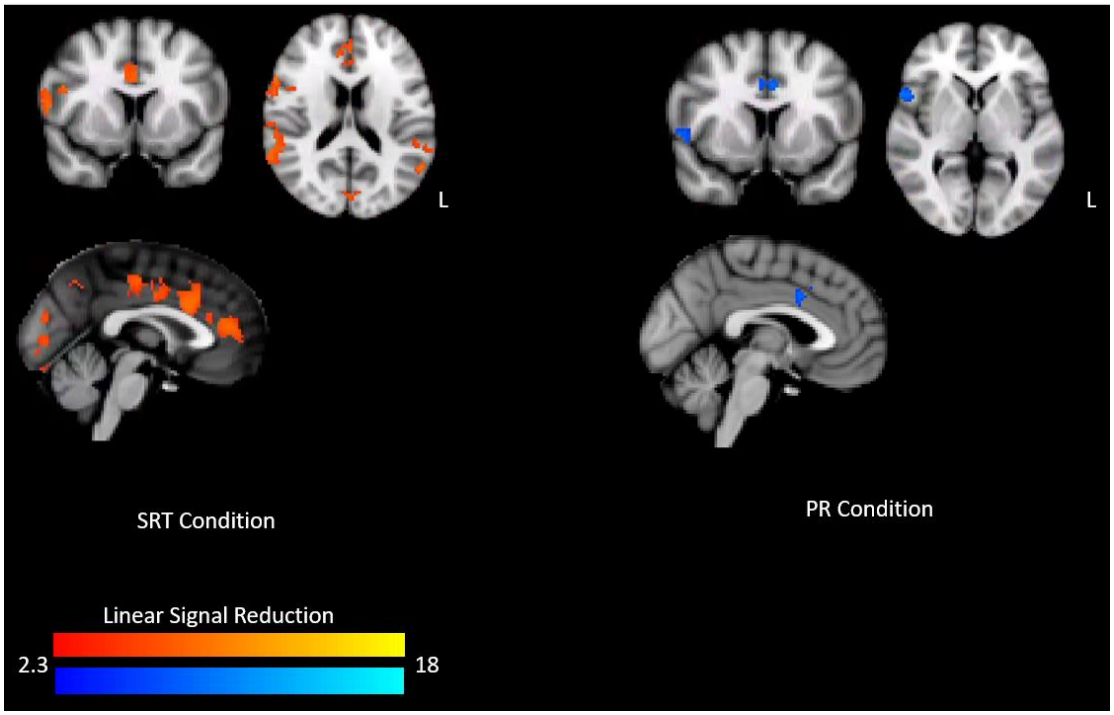

Figure 8.7 Group-level linear signal reduction across task blocks for SRT (left) and PR (right) task conditions.

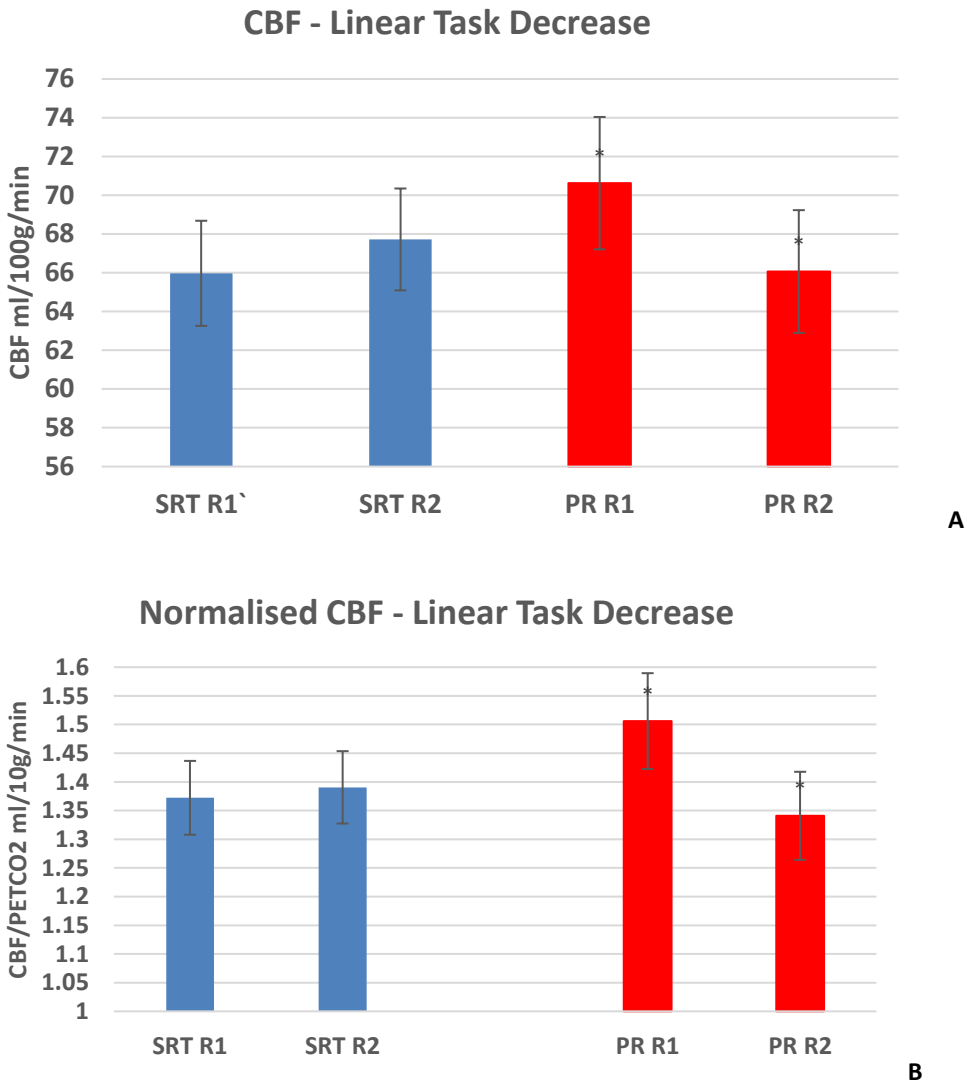

Figure 8.8 Mean ± SEM CBF pre- and post-training in the ROI defined from the linear signal decreases during SRT and PR task performance (A) and the same data following $P_{ET}CO_2$ normalisation (B). R1= Rest 1, R2 = Rest2. * denotes significant difference between R1 and R2 group CBF at $p < 0.05$

8.3.4 Resting Motor Network CBF Changes

M1 seed (figure 8.9) RSFC differences before and after SRT and PR task performance were investigated. In the PR task session, there were no statistically significant differences in BOLD or CBF RSFC between baseline and post-task. For the SRT there were significant CBF RSFC differences only, therefore CBF was quantified in these regions only as no overlap with BOLD was observed.

In M1 regions showing a significant BOLD and CBF task response decrease over time, higher CBF RSFC with the right planum polare and temporal pole was detected pre-training (figure

8.10). Following SRT training, the same M1 seed showed greater connectivity with the right LOC and lingual gyrus (figure 8.11).

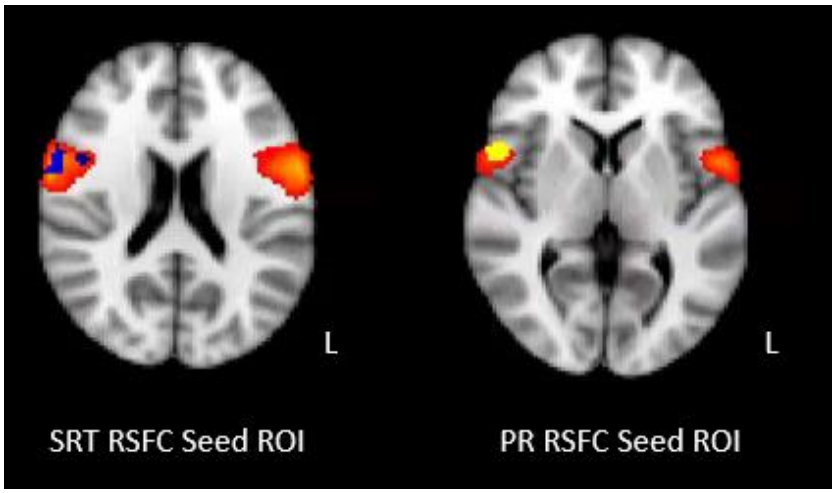

Figure 8.9 Seed regions for the RSFC analysis. M1 as defined by the Harvard-Oxford Cortical Atlas shown in red. On the left the SRT task seed is shown in blue and on the right the PR task seed is shown in yellow.

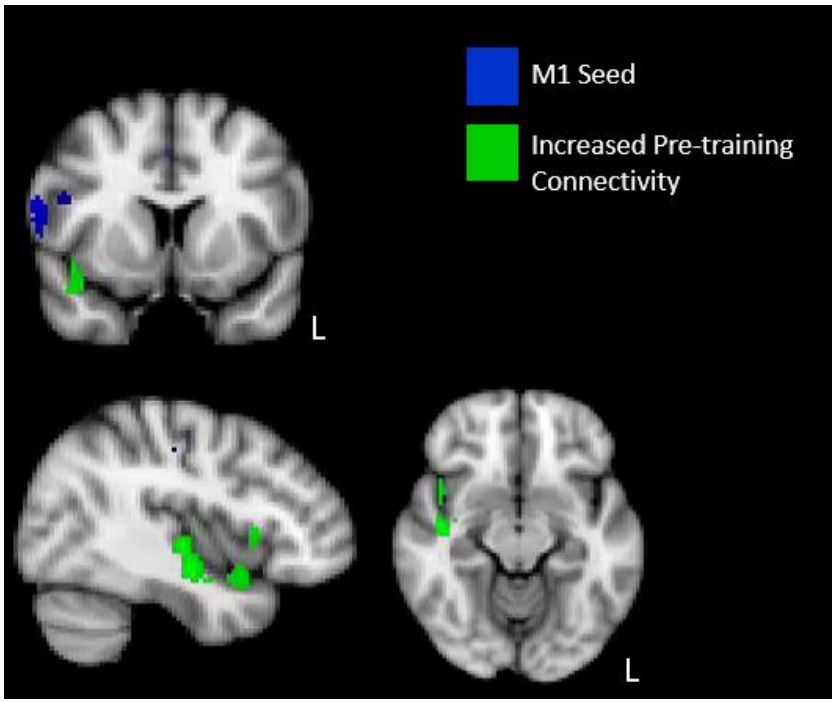

Figure 8.10 Higher M1 connectivity pre-SRT training in the planum polare and temporal pole.

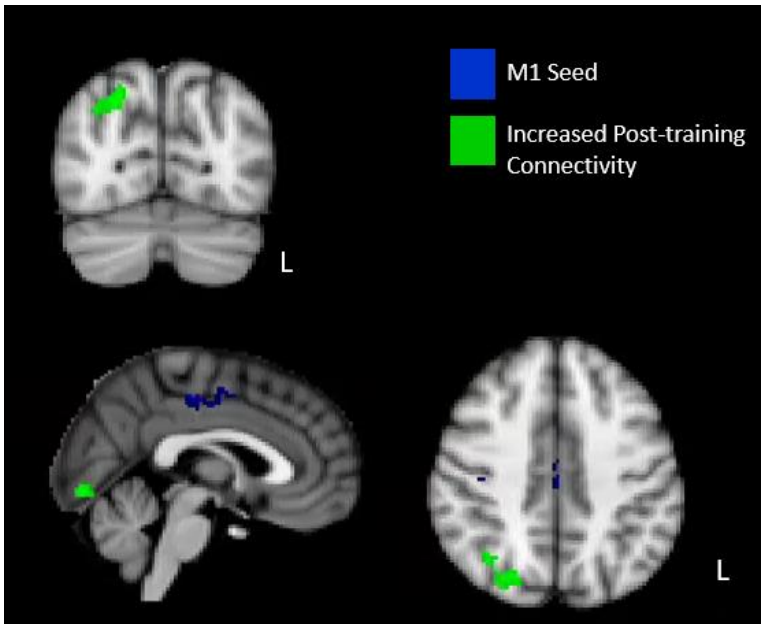

Figure 8.11 Increased M1 connectivity post-SRT training in the lateral occipital cortex and lingual gyrus.

CBF was quantified for the ROIs showing increased connectivity before and after SRT training. There was not a significant change in CBF for the ROI showing increased RSFC before training; $t(20)=1.833$, $p = 0.082$ (figure 8.12A), nor was there a significant change in the ROI showing increased RSFC following training; $t(20)=1.901$, $p = 0.072$ (figure 8.12B).

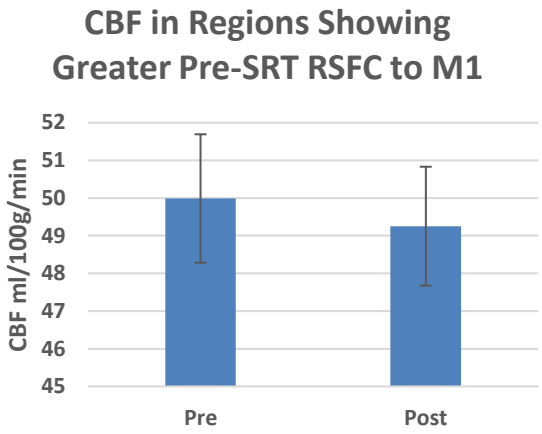

A

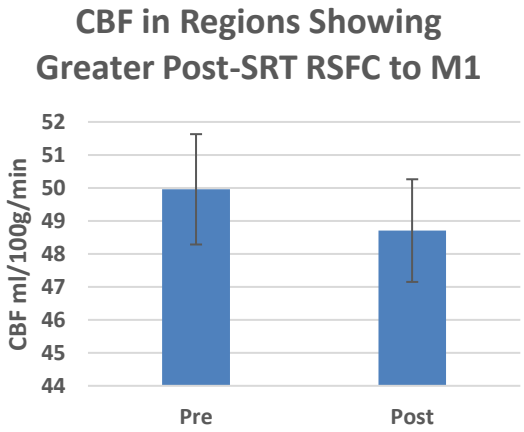

B

Figure 8.12 CBF (without normalisation) pre- and post SRT task performance in the ROIs shown in figures 8.10 and 8.11 (mean ± SEM).

8.3.5 Power Analysis for Future Studies

A post-hoc power analysis was conducted based on the interaction effect size for the normalised and non-normalised ANOVAs investigating CBF differences pre and post task. In addition, power was assessed for the comparison of CBF in regions showing increased RSFC pre and post training (table 8.1).

Power Analysis			
***F* Tests**	**Effect Size η^2p**	**Observed Power**	**Required *n* for power of 0.8**
Mean Response ROI	0.11	0.3	69
Mean Response ROI (CO_2 norm)	0.2	1	22

Power Analysis			
Linear Decrease ROI	.35	1	4
Linear Decrease ROI (CO_2 norm)	.45	1	5
***T* Tests**	**Effect Size d_z**		
SRT Pre-Training RSFC	0.4	0.41	52
SRT Post-Training RSFC	0.41	0.43	49

Table 8.1 A power analysis was conducted for the main statistical comparisons to inform sample size considerations in future studies.

8.4 Discussion

8.4.1 Summary of Main Results

The main aim of this study was to quantify CBF changes in the resting brain following performance of a visuomotor learning task, the SRT, and a pseudorandom sequence response task, to investigate metabolic adaptations underlying motor system plasticity. We examined CBF differences following performance of both task conditions focusing on i) regions showing a mean task response, and ii) regions displaying a linear signal reduction over time. CBF was also compared before and after task performance in areas showing differential M1 CBF RSFC pre- and post-task. Results showed that resting CBF was not significantly different following SRT task performance in regions showing a mean task response, or in regions showing a mean signal decrease across the 13 task blocks. However, greater pre-SRT training RSFC with M1 was identified in the right planum polare and temporal pole, and greater post-training CBF was identified in the LOC and lingual gyrus. Again, resting CBF did not significantly change in these areas following SRT performance. Analysis of the PR task data showed that resting CBF was significantly higher post training in the mean task response ROI. In the ROI representing the linear signal reduction over task blocks, resting CBF was significantly lower post PR task performance. There was not a statistically significant difference in RSFC of M1 with any region before or after task performance.

A post-hoc power analysis revealed that follow-up studies would benefit from larger samples as small to medium effect sizes were observed for each of the main CBF comparisons in this study (table 8.1).

8.4.2 CBF in Task-Relevant Areas

BOLD and CBF task responses were observed in the motor network including M1, premotor cortex and primary somatosensory cortex (S1), cerebellum, and visual regions typical of visuomotor tasks (Miall & Robertson, 2006; Ungerleider, Doyon, & Karni, 2002). Spatially, there was little difference between the SRT and PR task responses. Of note, activity was not detected in the cortico-striatal loop and frontal regions frequently associated with the early phase of motor learning (Doyon & Benali, 2005). This may be due to susceptibility-induced signal distortion in frontal and temporal regions, a common drawback of EPI (G. Xu et al., 2011). The use of 3D or spiral acquisitions can partially overcome such artifacts, however neither options were available at the time of data acquisition.

In line with previous work (Fernandez-Seara et al., 2009; Floyer-Lea & Matthews, 2004; Seitz & Roland, 1991), signal reductions over task blocks were observed within the session and signal decreases were more widespread for the SRT than the PR task condition (see figure 8.7) which may reflect more similar neural energy demands across all blocks of the PR task than the SRT, as evidenced by the lack of a significant RT decrease by the end of the PR task.

In this study, we were interested in identifying markers of metabolic adaptations following performance of a motor learning task. Short-term motor learning is an indicator of motor system plasticity (Doyon & Benali, 2005) which is reflected by neural response adaptations with repeated performance of a motor sequence. To overcome the limitations of interpreting BOLD changes during or following task performance, we quantified CBF in the resting brain, before and after performance of the SRT task and control PR task to identify whether greater CBF changes would occur following motor learning compared to motor performance (Albert et al., 2009). Unexpectedly, significant resting CBF increases post-task were observed for the PR condition only. At rest, in areas which had shown mean signal decrease across the PR task, a significant CBF reduction was detected. In the mean response ROI, this effect was only observed following CBF normalisation for $P_{ET}CO_2$ changes, which demonstrates the importance of correction for effects of physiological fluctuations.

Non-neuronal physiological processes such as arterial CO_2 ($PaCO_2$) fluctuations can affect the resting BOLD and ASL signal, especially in occipital and temporal grey matter (Golestani, Chang, & Chen, 2015; Grubb, Raichle & Eichling, 1974; Wise, Ide, Poulin, & Tracey, 2004), therefore it is important to account for these effects to correctly interpret resting-state data. Task performance can alter breathing patterns, and this may have continued at rest. In the current study, $P_{ET}CO_2$ which is believed to reflect $PaCO_2$ was sampled throughout the study and

included as a regressor in the GLM analyses to minimise the effect of fluctuations on measured task responses and RSFC. Overall, the results with and without $P_{ET}CO_2$ normalisation displayed the same trends, however, in the mean response ROI the increase in CBF post PR task performance was not evident before normalisation. While a statistically significant $P_{ET}CO_2$ reduction was noted only in the SRT condition, the CBF-normalised data did not reveal any task-effects masked by CO_2 differences. However, in the PR condition the slight reduction in $P_{ET}CO_2$ appeared to hide the post-task CBF change in the mean task response ROI. It can be concluded that $P_{ET}CO_2$ alterations can mask task-related CBF changes, and motor learning studies should include $P_{ET}CO_2$ measures in analysis.

Previous work (Olson et al., 2006), did not find group level motor learning effects in BOLD or CBF data, potentially due to low SNR and insufficient power. Another reason may be that the data was acquired using a single echo, meaning that the necessary trade-off between BOLD and CBF-weighted images may have resulted in low sensitivity to both perfusion and BOLD changes. Alternative data acquisition methods, such as the dual-excitation PCASL sequence used in the current study have improved simultaneous BOLD and CBF acquisitions to enable identification of motor learning adaptations as observed in this study during task performance. This study aimed to extend existing work, which has reported changes in resting state BOLD connectivity following motor learning (Albert et al., 2009; Saber Sami et al., 2014), by identifying sustained CBF changes following motor learning. However, evidence for metabolic adaptations in areas involved in motor learning was not observed. Instead, CBF changes following performance of a motor execution task, without a learning component were identified. As the order of task conditions per subject was counterbalanced and the PR task matched in duration, and component movements, this effect was unlikely to be due to order effects or differences in motor execution difficulty.

The reduction in resting CBF in the PR condition where linear CBF and BOLD reductions were observed over task blocks is suggestive of altered metabolic demand in portions of right M1, SMG, IFG and the ACC following the task. In contrast, for the linear decrease ROI in the SRT condition, mean CBF was non-significantly higher overall in right M1, SPL, angular gyrus, SMG, ACC and cuneal cortex. It is possible that differences in task demand (motor learning vs. motor execution) underlie the different effects seen in the two task conditions. However, the reduction in CBF was expected in the SRT condition where the task becomes relatively easier to perform as the sequence is learned. In the PR condition, task difficulty stays the same as a new sequence is presented in each block. At present, the reason for this result is not easily

explained and would benefit from further exploration in future studies investigating metabolic changes following motor learning and motor execution tasks.

8.4.3 Resting State Functional Connectivity

A seed-based RSFC analysis was chosen as we were specifically interested in metabolic changes in regions functionally connected to M1 due to its role in motor learning. RSFC analysis is based on the assumption that functionally associated brain regions have measurable temporally correlated fluctuations (Biswal, Yetkin, Haughton, & Hyde, 1995). As M1 is critical to motor performance and motor learning, if sustained SRT task-related metabolic adaptations occur over short timescales, these are likely to occur in areas showing altered RSFC to M1. Unexpectedly, BOLD RSFC appeared not to change following SRT performance. Increases in CBF RSFC of the right lingual gyrus and LOC were observed following the SRT task and M1 RSFC was greater pre-task in the right temporal pole and planum polare. No changes were evident for the PR task, which may reflect the absence of a task learning component and therefore a lack of motor network adaptation. The spatially distinct areas of greater CBF RSFC before and after the SRT task, may reflect a degree of motor learning. The LOC, which showed greater post-task M1 connectivity is related to object perception and recognition (Grill-spector, Kourtzi, & Kanwisher, 2001) and the lingual gyrus is linked to processing of complex visual information and analysis of logical conditions and event order (Goel & Dolan, 2004; Machielsen, Rombouts, Barkhof, Scheltens, & Witter, 2000). The temporal pole and planum polare which were more highly connected to M1 pre-SRT task, have been linked to processing of emotional information and language processing respectively (Binder et al., 1997; Olson & Plotzker, 2007). The lingual gyrus has previously shown increased CBF during the early phase of motor learning (Fernandez-Seara et al., 2009) and resting state activation of the LOC has also been found following implicit motor learning (Saber Sami et al., 2014). These RSFC increases post-SRT training may therefore reflect sustained metabolic alterations, however the small CBF difference pre- and post-task does not clarify the nature of these changes. Further, the power analysis suggests the study was not powered to detect a real effect with this comparison, therefore further work in a much larger sample is needed to determine the directional change in CBF in regions displaying altered RSFC with M1 following visuomotor learning.

It could be argued that a single session may not be long enough to see connectivity changes in motor-basal ganglia and motor-cerebellar networks as observed by Ma et al., (2010) following 4 weeks of training, for example. However, Albert et al. (2009) and Sami et al. (2014) reported

altered BOLD RSFC in sample sizes of 9 and 29 respectively, following performance of a motor learning task and these changes were attributed to increases in metabolic demand related to memory consolidation of previously acquired skills occurring in the so-called resting state. In this study, changes in BOLD M1 RSFC were not observed, the only M1 RSFC differences exceeding the statistical threshold were noted in the CBF data before and after the SRT task, but not the motor execution task in line with Albert et al., (2009) who reported motor-learning specific effects. Data quality or choice of sequence may have influenced results. Data were inspected for excessive head motion, which can decrease functional connectivity strength (Dijk et al., 2010). The output of MCFLIRT motion correction revealed all subjects absolute head motion was < 0.8mm. Further, CO_2 fluctuations were accounted for by adding the $P_{ET}CO_2$ traces as a regressor in the analysis. Although some cardiac and respiratory noise may have been present due to the absence of these recordings, it is unlikely to explain the absence of BOLD RSFC changes.

The use of the dual excitation sequence necessitated a long (4.4s) effective TR in order to achieve full brain coverage, but also to facilitate an optimal labelling duration and post-label delay time established during piloting. This meant that the TR used was not optimal for BOLD which may have led to lower sensitivity to detect small fluctuations in the resting state, despite being adequate to detect motor task responses. Typical TRs for BOLD are between 2-3s, although longer TRs have been used successfully, although infrequently, in BOLD functional connectivity studies (Horn, Jann & Federspiel et al., 2012). Dual-acquisition sequences with long TRs have elsewhere been shown to affect BOLD temporal SNR, resulting in lower t-scores on activation maps and lower number of activated voxels (Fernández-Seara, Rodgers, Englund, & Wehrli, 2016). Although dual-excitation sequences can be optimised for both ASL and BOLD in terms of TE, the inversion time and tagging duration must be long enough to label an adequate amount of blood and ensure it reaches the tissue before images are acquired to minimise arterial contributions in ASL data. Dual-excitation sequences may not be the most optimal approach for BOLD RSFC studies; future studies aiming to quantify CBF changes following motor learning should perhaps use CBF RSFC only to achieve the best data quality, or combine multiband multi-echo acquisitions (Cohen, Nencka, Lebel, & Wang, 2017) to improve resolution and image distortion in both BOLD and ASL data.

Seed based analysis is reliant on the seed being unaffected by noise and representative of the process of interest. Motor and visual tasks tend to provide sufficiently robust responses from which to define a seed area (Beckmann, Deluca, Devlin, & Smith, 2005) due to the typical response magnitude. However, unlike ICA, where connectivity metrics are data-driven, seed-

connectivity analysis is based on a-priori assumptions about regional connectivity, or in this case, where task-related changes will occur. While it is sensible to predict motor network connectivity changes following a visuomotor task, and use a seed defined from the task activity, it is possible that with motor learning, plasticity occurs outside of the site of task activation and may be dependent on pre-training motor experience or skill (Adkins, Boychuk, Remple, & Kleim, 2006). Further analysis of known networks involved in motor learning, such as cortico-striatal and cortico-cerebellar loops, could be investigated as sites of altered RSFC and metabolism following visuomotor task performance.

ASL has long been suggested as a more powerful tool than BOLD for group analysis when using low frequency tasks or long paradigms (Jiongjiong Wang et al., 2003), however low sensitivity to small flow changes has hampered its widespread application in cognitive and clinical research. Recent hardware and pulse sequence optimisation, such as the use of background suppression, has improved SNR, spatial coverage and ASL can provide quantitative measures of baseline perfusion, task activation and functional connectivity (Chuang et al., 2009). Baseline or resting perfusion is associated with RSFC strength (Liang, Zou, He, & Yang, 2013; Jann et al., 2015) providing a neurophysiological basis for resting network connectivity. Repeated practice of a particular skill is thought to induce Hebbian like learning processes where long term potentiation and depression (LTP and LTD) are altered due to synaptic remodelling following skill acquisition (Shannon et al., 2016). Metabolic changes reflective of synaptic plasticity can be quantified using ASL and used to characterise learning processes in the healthy brain as well as identifying pathological changes affecting learning in disease.

8.4.4 Limitations

In this study cardiac and respiratory traces were not regressed from the fMRI data due to an equipment failure and some degree of physiological noise may have been present in the data. While we are aware of the importance of physiological noise regression (Bright & Murphy, 2013b) it was not possible in this case and is therefore a limitation of the study.

Global signal regression (GSR) of the resting state timeseries is a controversial technique and there is no general consensus on whether it should be incorporated into the processing of resting data (Murphy & Fox, 2017). The main reason for the conflicting opinions on the use of GSR, is that the global signal includes some neuronal as well as physiological fluctuations (Chen et al., 2012). GSR can potentially introduce spurious negative or anti-correlations with the timeseries of the seed region. As we were interested in both positive and negative RSFC in this study we did not carry out GSR. However, GSR can also improve specificity of positive

correlations and remove cardiac and respiratory noise and may have improved the detection of true RSFC changes following task performance.

Doyon & Benali (2005) stated that to understand the mechanisms of functional plasticity occurring during learning and automatization of motor skills, methods including functional connectivity analysis to detect changes in network communication were necessary. We believe that in addition to traditional BOLD RSFC analysis, quantification of CBF and $CMRO_2$ in regions critical for motor skill learning, especially in areas showing dynamic changes at different learning phases, can provide detailed information on the metabolic changes facilitating plasticity.

8.4.5 Future Research

An alternative technique to ASL, with applications in plasticity research, is vascular space occupancy (VASO) imaging of blood volume (Lu et al., 2013) which can be used to measure task activity in specific cortical layers. This technique has been demonstrated using motor paradigms (Huber, Goense, et al., 2015) and provides a high-resolution quantitative alternative to BOLD and CBF imaging. More suitably powered studies, ideally with training and follow-up imaging on the order of weeks or months are needed to determine whether sustained metabolic changes occur following motor learning. However, in future methods such as VASO could be used as a sensitive measure of changes in learning-related connectivity within and between cortical layers. In addition, quantitative CBV measures obtained using VASO could be used as a marker of angiogenesis. Angiogenesis is increased following physical exercise training (Pereira et al., 2007) but it is not known if motor skill learning has similar effects in humans, although vascular plasticity has been shown to be critical for learning and memory in rodents (Kerr, Steuer, Pochtarev, & Swain, 2010).

Chapter 8 Supplementary Data

8.5 Individual Subject CBF

SRT Task Condition						
Mean Response ROI				**Linear Decrease ROI**		
	Pre-Task	**Post-Task**	**ΔCBF ml/100g/min**	**Pre-Task**	**Post-Task**	**% ΔCBF ml/100g/min**
sub01	58.6	56.9	-1.7	67.0	69.4	2.4
sub02	42.7	43.2	0.5	49.9	49.5	-0.3
sub03	74.2	72.9	-1.3	79.9	88.8	9
sub04	58.1	58.8	0.7	65.9	63.1	-2.8
sub06	75.3	71.7	-3.6	91	86.7	-4.3
sub07	57.2	58.7	1.5	77.8	70.5	-7.2
sub08	64.4	64	-0.4	73.9	68.9	-5
sub09	52	50.3	-1.7	56.4	53.8	-2.6
sub10	52.7	51.3	-1.4	60.5	53.7	-6.9
sub11	54.1	54.7	0.6	59.7	60.2	0.5
sub12	71.9	66.8	-5.1	83.1	79.9	-3.2
sub13	67.9	58.6	-9.3	75.7	69.7	-6
sub14	65.4	71.5	6.1	75.9	76.7	0.8
sub15	38.5	41.3	2.8	40.5	47.8	7.3
sub16	59.9	56.1	-3.8	69	67.7	-1.3
sub17	54.1	57.1	3	66	77.4	11.4
sub18	50.1	52.9	2.8	56.2	60	3.8
sub19	62	57.7	-4.3	65.1	63	-2.1

SRT Task Condition						
sub20	55.2	55.3	0.1	64	71	7
sub21	50.7	51.3	0.6	56.9	57.3	0.4
sub22	42.3	42.2	-0.1	48.1	46.8	-1.3
Mean ± SEM	**57.5 ± 2.2**	**56.8 ± 2**	**-0.7 ± 0.7**	**65.8 ± 2.7**	**65.7 ± 2.6**	**-0.03 ± 1.1**

Table 8.2 Individual subject mean CBF for each ROI and ΔCBF post-task. Subject 5 was removed as both scan sessions were not completed.

PR Task Condition						
Mean Response ROI				**Linear Decrease ROI**		
	Pre-Task	**Post-Task**	**% ΔCBF ml/100g/min**	**Pre-Task**	**Post-Task**	**% ΔCBF ml/100g/min**
sub01	47.2	48.6	1.4	72.7	66.1	-6.6
sub02	41.5	43.2	1.7	70.6	67.6	-3
sub03	70.1	66.8	-3.	77.3	67.9	-9.4
sub04	66	66	0	86.2	86.8	0.6
sub06	54	54	0	62.1	59.8	-2.3
sub07	59.2	56.5	-2.7	86	83.1	-2.9
sub08	59	58.8	-0.1	74.2	80.7	6.5
sub09	66.6	64	-2.4	91.9	79	-12.9
sub10	51.5	51.4	-0.1	66.1	41.5	-24.6
sub11	59.2	58.4	-0.8	81.3	66.5	-14.8
sub12	54.4	55.6	1.2	54.3	48.6	-5.7

PR Task Condition						
sub13	71.3	63.5	-7.8	103.9	86.3	-17.6
sub14	56.9	60	3.1	62.3	52.9	-9.4
sub15	44.9	41.1	-3.8	76.7	72	-4.7
sub16	52.5	50.4	-2.1	52.3	55.7	3.4
sub17	47.8	43.7	-4.1	58.5	50.3	-8.2
sub18	53	52	-1	55.8	60.1	4.3
sub19	68.3	66.8	-1.5	81.5	74.9	-6.6
sub20	55.6	58.1	2.5	41	44.9	3.9
sub21	51.7	50.6	-1.1	49.4	43	-6.4
sub22	46.4	46.2	-0.2	61.6	52.1	-9.5
Mean ± SEM	**56 ± 1.9**	**55 ± 1.7**	**-1.1 ± 0.55**	**69.8 ± 3.4**	**63.7 ± 3.2**	**-6 ± 1.7**

Table 8.3 Individual subject mean CBF for each ROI and ΔCBF post-task.

8.6 G*Power Output

Mean Response ANOVA

F tests – ANOVA: Repeated measures, within factors

Analysis:	Post hoc: Compute achieved power		
Input:	Effect size f	=	0.1102078
	α err prob	=	0.05
	Total sample size	=	21
	Number of groups	=	1
	Number of measurements	=	4
	Corr among rep measures	=	0.7
	Nonsphericity correction ϵ	=	1
Output:	Noncentrality parameter λ	=	3.4008126
	Critical F	=	2.7580783
	Numerator df	=	3.0000000
	Denominator df	=	60.0000000
	Power (1−β err prob)	=	0.2904289

Mean Response ANOVA

F tests - ANOVA: Repeated measures, within factors

Analysis:	A priori: Compute required sample size		
Input:	Effect size f	=	0.1102078
	α err prob	=	0.05
	Power (1−β err prob)	=	0.8
	Number of groups	=	1
	Number of measurements	=	4
	Corr among rep measures	=	0.7
	Nonsphericity correction ϵ	=	1
Output:	Noncentrality parameter λ	=	11.1740984
	Critical F	=	2.6488634
	Numerator df	=	3.0000000
	Denominator df	=	204
	Total sample size	=	69
	Actual power	=	0.8023706

Mean Response ANOVA (CO_2 normalised)

F tests - ANOVA: Repeated measures, within factors

Analysis:	Post hoc: Compute achieved power		
Input:	Effect size f	=	0.5046832
	α err prob	=	0.05
	Total sample size	=	21
	Number of groups	=	1
	Number of measurements	=	4
	Corr among rep measures	=	0.7
	Nonsphericity correction ϵ	=	1
Output:	Noncentrality parameter λ	=	71.3174371
	Critical F	=	2.7580783
	Numerator df	=	3.0000000
	Denominator df	=	60.0000000
	Power (1−β err prob)	=	1.0000000

Mean Response ANOVA (CO_2 normalised)

F tests - ANOVA: Repeated measures, within factors

Analysis:	A priori: Compute required sample size		
Input:	Effect size f	=	0.5046832
	α err prob	=	0.05
	Power (1−β err prob)	=	0.8
	Number of groups	=	1
	Number of measurements	=	4
	Corr among rep measures	=	0.7
	Nonsphericity correction ϵ	=	1
Output:	Noncentrality parameter λ	=	16.9803422
	Critical F	=	3.4902948

	Numerator df	=	3.0000000
	Denominator df	=	12.0000000
	Total sample size	=	5
	Actual power	=	0.8461089

Linear Decrease ANOVA

F tests – ANOVA: Repeated measures, within factors

Analysis:	Post hoc: Compute achieved power		
Input:	Effect size f	=	0.7225441
	α err prob	=	0.05
	Total sample size	=	21
	Number of groups	=	1
	Number of measurements	=	4
	Corr among rep measures	=	0.7
	Nonsphericity correction ϵ	=	1
Output:	Noncentrality parameter λ	=	146.1796
	Critical F	=	2.7580783
	Numerator df	=	3.0000000
	Denominator df	=	60.0000000
	Power (1−β err prob)	=	1.0000000

Linear Decrease ANOVA

F tests – ANOVA: Repeated measures, within factors

Analysis:	A priori: Compute required sample size		
Input:	Effect size f	=	0.7225441
	α err prob	=	0.05
	Power (1−β err prob)	=	0.8
	Number of groups	=	1
	Number of measurements	=	4
	Corr among rep measures	=	0.7
	Nonsphericity correction ϵ	=	1
Output:	Noncentrality parameter λ	=	27.8437321
	Critical F	=	3.8625484
	Numerator df	=	3.0000000
	Denominator df	=	9.0000000
	Total sample size	=	4
	Actual power	=	0.9547112

Linear Decrease ANOVA (CO_2 normalised)

F tests – ANOVA: Repeated measures, within factors

Analysis:	Post hoc: Compute achieved power		
Input:	Effect size f	=	0.9081946
	α err prob	=	0.05
	Total sample size	=	21

	Number of groups	=	1
	Number of measurements	=	4
	Corr among rep measures	=	0.7
	Nonsphericity correction ϵ	=	1
Output:	Noncentrality parameter λ	=	230.9489
	Critical F	=	2.7580783
	Numerator df	=	3.0000000
	Denominator df	=	60.0000000
	Power (1−β err prob)	=	1.0000000

Linear Decrease ANOVA (CO_2 normalised)

F tests – ANOVA: Repeated measures, within factors

Analysis:	A priori: Compute required sample size		
Input:	Effect size f	=	0.9081946
	α err prob	=	0.05
	Power (1−β err prob)	=	0.8
	Number of groups	=	1
	Number of measurements	=	4
	Corr among rep measures	=	0.7
	Nonsphericity correction ϵ	=	1
Output:	Noncentrality parameter λ	=	32.9926973
	Critical F	=	4.7570627
	Numerator df	=	3.0000000
	Denominator df	=	6.0000000
	Total sample size	=	3
	Actual power	=	0.9395918

RSFC CBF Change, Pre-training ROI

t tests – Means: Difference between two dependent means (matched pairs)

Analysis:	Post hoc: Compute achieved power		
Input:	Tail(s)	=	Two
	Effect size dz	=	0.4
	α err prob	=	0.05
	Total sample size	=	21
Output:	Noncentrality parameter δ	=	1.8330303
	Critical t	=	2.0859634
	Df	=	20
	Power (1−β err prob)	=	0.4150032

RSFC CBF Change, Pre-training ROI

t tests – Means: Difference between two dependent means (matched pairs)

Analysis:	A priori: Compute required sample size		
Input:	Tail(s)	=	Two
	Effect size dz	=	0.4
	α err prob	=	0.05

	Power (1−β err prob)	=	0.8
Output:	Noncentrality parameter δ	=	2.8844410
	Critical t	=	2.0075838
	Df	=	51
	Total sample size	=	52
	Actual power	=	0.8077878

RSFC CBF Change, Post-training ROI

t tests − Means: Difference between two dependent means (matched pairs)

Analysis:	Post hoc: Compute achieved power		
Input:	Tail(s)	=	Two
	Effect size dz	=	0.41
	α err prob	=	0.05
	Total sample size	=	21
Output:	Noncentrality parameter δ	=	1.8788560
	Critical t	=	2.0859634
	Df	=	20
	Power (1−β err prob)	=	0.4320424

RSFC CBF Change, Post-training ROI

t tests − Means: Difference between two dependent means (matched pairs)

Analysis:	A priori: Compute required sample size		
Input:	Tail(s)	=	Two
	Effect size dz	=	0.41
	α err prob	=	0.05
	Power (1−β err prob)	=	0.8
Output:	Noncentrality parameter δ	=	2.8700000
	Critical t	=	2.0106348
	Df	=	48
	Total sample size	=	49
	Actual power	=	0.8029445

Table 8.4 Output from G*Power for each of the power calculations presented in table 8.1.

8.7 M1 Resting State Functional Connectivity

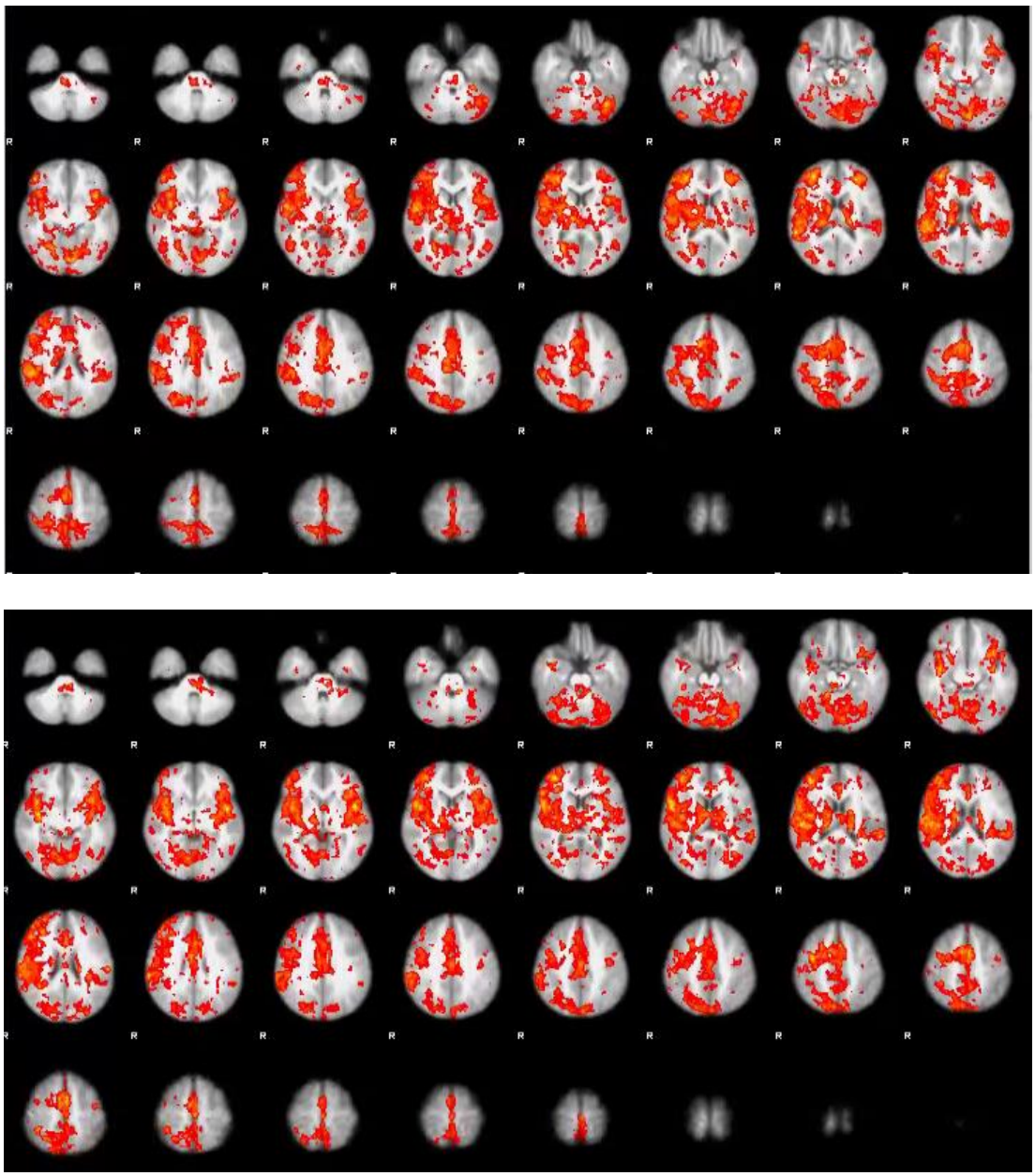

Figure 8.13 M1 BOLD RSFC before (top) and after (bottom) SRT task performance, z-stat 4-6.9, $p < 0.05$.

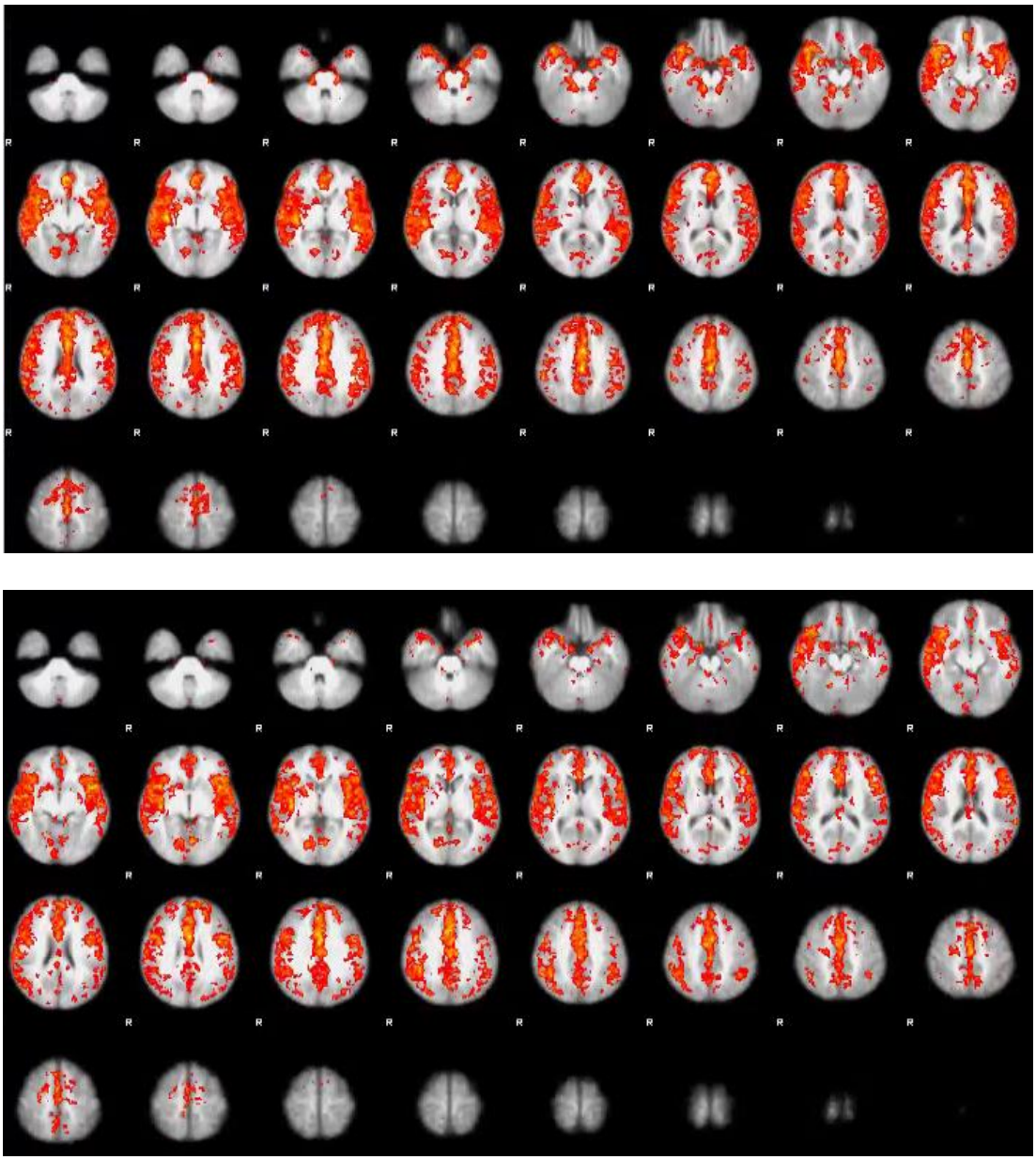

Figure 8.14 M1 CBF RSFC before (top) and after (bottom) SRT task performance, z-stat 4-7, $p < 0.05$.

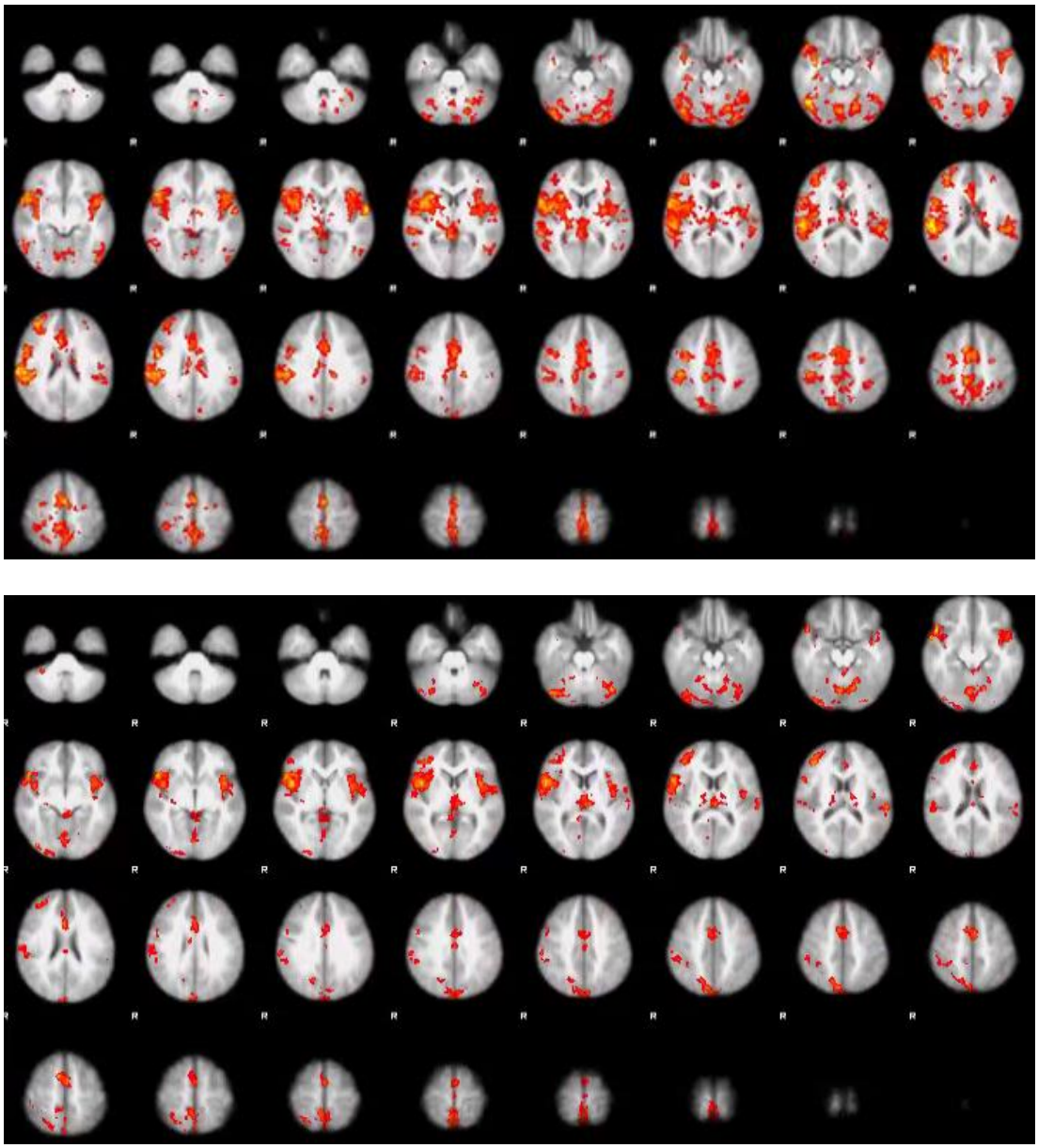

Figure 8.15 M1 BOLD RSFC before (top) and after (bottom) PR task performance, z-stat 4-5.9, $p < 0.05$.

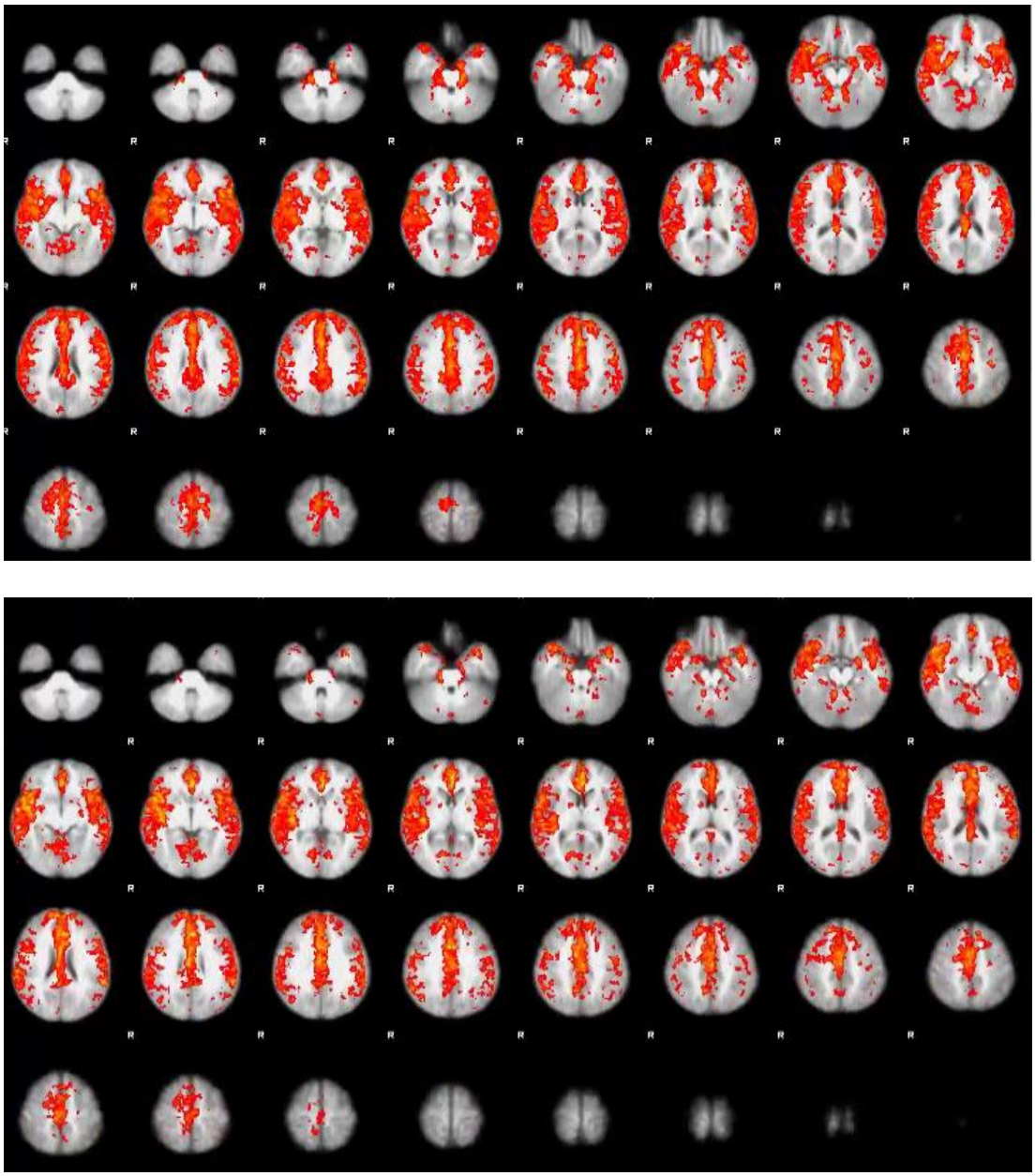

Figure 8.16 M1 CBF RSFC before (top) and after (bottom) PR task performance, z-stat 4-7.8, $p < 0.05$.

Chapter 9

Characterising Vascular and Metabolic Dysfunction in Multiple Sclerosis: Pilot Data

Abstract

It is now accepted that there is a vascular component to Multiple Sclerosis (MS) which contributes to brain damage and cognitive dysfunction (D'haeseleer et al., 2011a)**. The current project, which is ongoing, will build on existing work, quantifying regional CBF, CVR, capillary cerebral blood volume (CBVcap), baseline OEF and absolute $CMRO_2$ in 20 patients with relapsing-remitting MS (RR-MS) and matched healthy controls using dual-excitation, dual-calibrated PCASL fMRI.**

The preliminary results demonstrate the application of the dual-calibrated PCASL acquisition and forward physiological model used in healthy controls in Chapter 5, in a clinical population. Here, the MS group showed significantly reduced grey matter $CMRO_2$ (p=0.008), baseline OEF (p=0.009), and CBVcap (p=0.013). Previous investigations have used either quantitative but global estimates of metabolism (Ge et al., 2012) or regional but relative estimates of $CMRO_2$ (Hubbard et al., 2017). The current approach permits regional, quantitative measures which in planned future analysis will be used to investigate the relationship between baseline metabolic function and motor plasticity.

9.1 Introduction

Multiple Sclerosis (MS) is the most common cause of neurological dysfunction in young adults worldwide aside from traumatic brain injury (TBI) (Kingwell et al., 2013). The Multiple Sclerosis Foundation estimates that the prevalence of MS is around 2.5million people worldwide, with rates increasing further away from the equator. Symptoms of MS include, but are not limited to; cognitive, motor and balance impairments, loss of vision due to optic neuritis, fatigue, depression and bladder problems (Kister et al., 2013), all of which reduce independence and quality of life.

Although the cause of MS is not known, the autoimmune model of MS, experimental autoimmune encephalomyelitis (EAE) suggests that the disease is a consequence of T cell attacks on myelin. This autoimmune response is thought to be triggered by viral infections such as Epstein Barr, a herpes virus and one of the most common viruses in humans. The EAE model has proved a very useful model to study the pathogenic processes of MS in non-human animals and informed pharmaceutical treatment in humans targeting autoimmune responses. EAE models have demonstrated how viruses trigger inflammation which over time leads to demyelination, axonal injury and progressive neurodegeneration.

A diagnosis of MS requires objective evidence of two separate inflammatory lesions in the CNS (brain, spinal cord, optic nerves) or objective evidence of one lesion with reasonable historical evidence of a prior attack, according to the revised McDonald MS Diagnostic Criteria (Polman et al., 2011). In addition to grey natter (GM) and white matter (WM) lesions caused by inflammation, demyelination, axonal injury and gliosis are characteristic in MS along with brain atrophy at later disease stages.

MS can develop at any stage of life but is most commonly diagnosed between 20-40 years of age and is almost twice as common in women as men. Most patients are diagnosed with relapsing-remitting MS (RR-MS), which is characterised by acute periods of increased inflammation, or relapses, followed by periods of recovery. The frequency and severity of relapses varies greatly between patients. Symptoms are also heterogeneous and the course of disease progression is often unpredictable. Further, clinical disability is frequently not reflected in traditional structural imaging protocols, which suggests that, additional factors such as blood flow and oxygen availability may be compromised leading to metabolic dysfunction, prior to significant lesion presence or atrophy. However, these processes are not detected by traditional clinical imaging techniques which tend to focus on brain structure.

It is now accepted that there is a vascular component to MS which contributes to brain damage and cognitive dysfunction (D'haeseleer et al., 2011a). A growing number of studies show cerebrovascular and metabolic alterations in RR-MS. Decreased global and regional CVR to CO_2 has been demonstrated using PCASL in two studies, (Marshall, Chawla, Lu, Pape, & Ge, 2016; Marshall et al., 2014) and correlations with lesion load and atrophy suggest that vascular dysfunction may contribute to neurodegeneration in MS. As well as CVR decreases, in RR-MS hypoperfusion has been reported in deep GM (Debernard et al., 2014), although increased perfusion in white matter attributed to metabolic dysfunction has also been reported (Rashid, Thompson & Miller et al., 2004). It is thought that hypoperfusion leads to an energy crisis in MS which contributes to lesion development and atrophy (De Keyser, Steen, Mostert, & Koch, 2008; Juurlink, 2013). While perfusion reductions could be attributed to reduced energy demand, diffusion tensor imaging (DTI) has demonstrated mean diffusivity (MD) reductions in WM tracts during acute hypoperfusion (Saindane, Law, Ge, Johnson, Babb, & Grossman, 2007). This suggests that perfusion reductions may occur prior to axonal loss. MD would be expected to increase with axonal loss, leading to reduced energy demand and reduced perfusion (Paling, Golay, & Miller, 2011). However, the inverse MD and perfusion correlation suggests initial perfusion decreases lead to neuronal loss.

More focus must be given to understanding early dysfunction in energy supply and metabolism to inform the development of new treatments which reverse or prevent further metabolic dysfunction (D'haeseleer et al., 2013) before significant irreversible GM and WM damage occurs. Such treatments may help to slow disease progression.

Several groups have studied metabolic function in RR-MS, and results have revealed absolute $CMRO_2$ and OEF reductions. In a study by Ge et al., (2012), higher global venous oxygenation was reported along with reduced $CMRO_2$, despite CBF being comparable to controls, which suggests hypometabolism of oxygen in tissue. Venous oxygenation was positively correlated with Expanded Disability Severity Scale (EDSS) scores and lesion load, whereas lesion load and EDSS were inversely correlated with $CMRO_2$. The downside of the method used by Ge et al. (2012) is that only global measurements were permitted, meaning that focal areas of dysfunction were not identified. More recently, Fan et al., (2015) assessed the repeatability of OEF measurements using phase contrast MRI at 7T using pial veins in the sensorimotor, parietal and prefrontal cortical regions. OEF was found to be highly reproducible, with OEF significantly lower than controls across all region. Further, OEF correlated positively with information processing speed in patients. Taken together, these studies show reductions in

oxygen extraction and $CMRO_2$, which relate to disease status, memory and lesion load.

A recent study by Hubbard et al. (2017) used calibrated BOLD during a visual stimulation task, and DTI to investigate relationships between WM integrity and metabolic activity. Interesting results were reported, whereby radial diffusivity (RD) of the occipital tract was inversely correlated with BOLD signal but positively correlated with CBF and relative changes in $CMRO_2$. Further $CMRO_2$ changes predicted fatigue scores on the Modified Fatigue Impact Scale (MFIS), but were not related to lesion burden. The opposite direction of BOLD compared to CBF and $CMRO_2$ correlations with WM RD, may reflect failures in normal neurovascular coupling (Iannetti & Wise, 2007a), potentially through altered baseline $CMRO_2$, which as Hubbard et al. (2017) suggested, may explain the increased $CMRO_2$ during visual stimulation. The study demonstrates that some perturbation of cerebral oxygen metabolism during stimulation is present, however, conclusions are limited due to the measurement relative rather than absolute changes and lack of control data.

The current project, which is ongoing, will build on this existing work, quantifying regional CBF, CVR, capillary cerebral blood volume (CBVcap), OEF_0 and absolute $CMRO_2$ in patients with RR-MS and matched healthy controls. The preliminary results demonstrate the application of the dual-calibrated PCASL technique used in healthy controls in Chapter 5, in a clinical population, an approach which combines the strengths of quantitative (Ge et al., 2012) and regional (Hubbard et al., 2017) investigations of metabolism in MS.

The main aim of the study is to characterise cerebrovascular and metabolic dysfunction in MS, and relate imaging outcomes to functional motor plasticity, using a modified version of the SRT task from Chapter 8. As mentioned above, the results presented here should be considered preliminary and demonstrate GM metabolic differences between 7 RR-MS patients and 12 (unmatched) controls.

The full study once completed, will include investigation of regional metabolism in areas including the thalamus, putamen, frontal and motor cortices, areas where perfusion abnormalities have been previously detected (Debernard et al., 2014; Rashid, Thompson & Miller, 2004). Secondly, the relationship between baseline energetics and motor plasticity, will be investigated, using lesion data, EDSS, and behavioural measures (walking ability, executive function) to provide an improved understanding of the contribution of metabolic dysfunction

to disease presentation.

9.2 Methods

9.2.1 Participants

Ethical approval was granted by the Cardiff University School of Psychology Research Ethics Committee as well as a local NHS Research Ethics Committee and Research and Development department of Cardiff and Vale University Health Board. The study is conducted in accordance with Good Clinical Practice guidelines. 20 patients with RR-MS (EDSS < 6) will be recruited from the Helen Durham Neuroinflammatory Centre, Department of Neurology at the University of Wales. Age and gender matched controls will be recruited from the Cardiff University Community Panel and poster advertisement within Cardiff University.

Note: the control data for the results reported here come from baseline data from subjects in the Chapter 5 study and 2 matched controls for the current study.

9.2.2 Imaging Protocol

All imaging was performed on a 3T Siemens Prisma MRI system using a 32-channel head coil (Siemens, Erlangen, Germany). Functional data were acquired using the dual-excitation, dual-calibrated PCASL acquisition and respiratory modulation paradigm described in Chapter 5; TR1/TR2/TE1/TE2=3600/800/10/30ms, TI/post-label delay= 1500/1500ms, 3.4x3.4x7mm voxels with 1mm gap, 16 slices, FOV=220mm, GRAPPA=3, flip angle=90°. Two nonselective adiabatic inversion pulses were applied 950 ms and 300 ms prior to image acquisition for background suppression. A T1-weighted MPRAGE was acquired for registration of functional data; TR/TE/= 2100/3.19/ms, 1mm isotropic resolution.

A second dual-excitation scan, without gases, using identical parameters as the calibrated scan was carried out during performance of an implicit learning serial reaction time (SRT) task, as described in Chapter 8. A slight modification was made to include 3 blocks of a pseudorandom sequence to control for response latency decreases related to task familiarisation rather than sequence learning as in Chapter 7. Additional scans to characterise the presence of inflammatory lesions were; a 3D FLAIR; TR/TE=5000/388ms, FOV=256mm, slice thickness=1mm, partial Fourier 7/8, bandwidth 751 Hz/px and dual-echo T2/proton density weighted scan; 41 slices, TR/TE1/TE2= 4050/11/90ms, slice thickness 3mm, FOV256mm, flip angle= 160°.

Data from the SRT and structural scans are not reported here, but will be used in planned analysis of the full set of patients and controls were processed and analysed using the same forward physiological model (Germuska et al., 2016) described in Chapter 5. Independent t-tests to assess group differences were carried out using SPSS version 20 (IBM Corp., Armonk, N.Y., USA). All t-tests were conducted with bootstrapping (1000 samples, 95% CIs) and examined for normality using the Shapiro-Wilk test.

9.3 Results

Interim results from 7 patients (1 male) and 12 controls (11 male) are presented in table 9.1. EDSS scores were not available for patient numbers 5 and 6, however they were known to be <4 as assessed by a nurse. All patients were characterised as having RR-MS.

Participant Characteristics and Neurophysiological Data		
	RR-MS	**Controls**
Age	39 ± 1.1	29 ± 1.8
EDSS	3 ±1.1	n/a
Disease Duration (years)	11 ± 2.3	n/a
Baseline CBF	51.6 ± 2.2	50 ± 1.2
CBVcap	1.2 ± 0.09	1.4 ± 0.04
Baseline OEF	0.32 ± 0.02	0.38 ± 0.01
Absolute CMRO2	130 ± 8.8	160 ± 3.4
CVR	2.1 ± 0.2	2.3 ± 0.2

Table 9.1 Mean ± SEM group characteristics and grey matter values for all cerebrovascular parameters of interest.

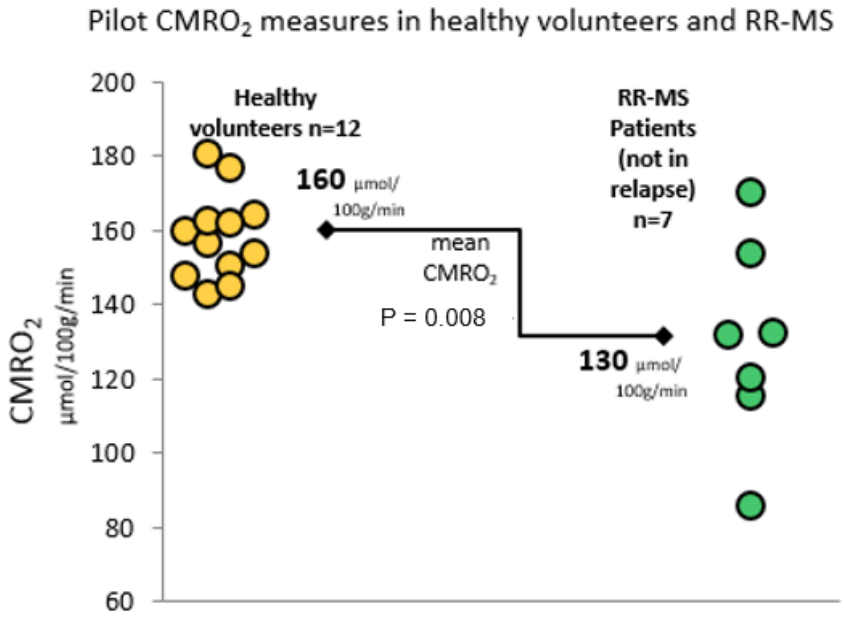

Figure 9.1 Comparison of mean GM values for each parameter of interest between patients and controls

Normal group variances were observed for patients and controls. Results of independent t-tests revealed RR-MS had significantly lower absolute $CMRO_2$; t(17)=3.015, p=0.008, OEF_0; t(17)=2.964, p=0.009, and CBVcap; t(17)=2.775, p=0.013. CBF_0 was not significantly different between patients and controls; t(17)=0.845, p = 0.435, nor was CVR; t(17)=1.473, p=0.159.

Figure 9.1 shows the absolute $CMRO_2$ differences between patients and controls. RR-MS patients had significantly lower $CMRO_2$, despite similar CBF (see supplementary table 9.2), which along with lower OEF_0 in the patient group (figure 9.2) suggests a failure of oxygen utilisation in GM.

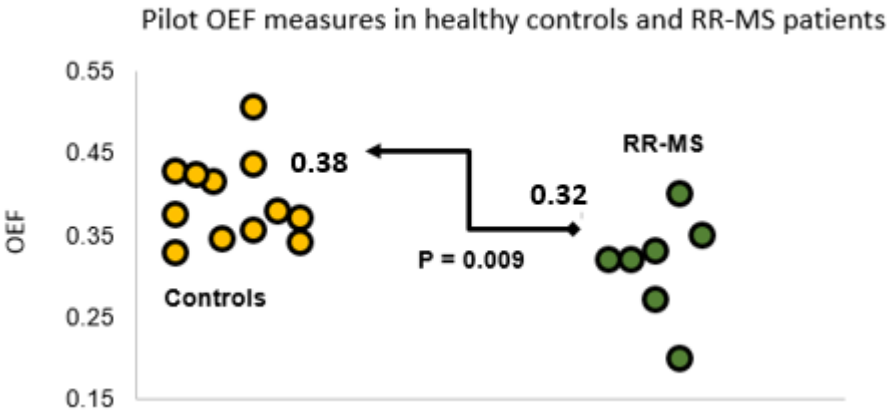

Figure 9.2 Mean GM OEF was significantly lower in patients vs. controls. Fractional OEF values are reported.

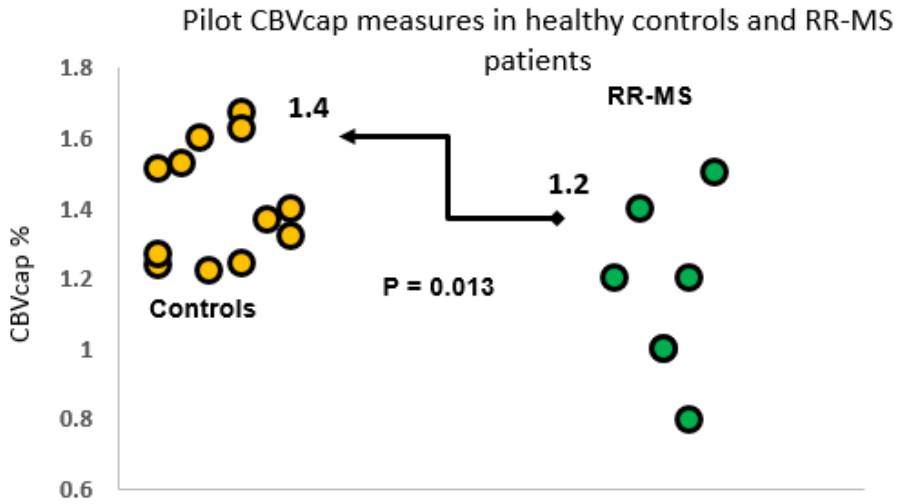

Figure 9.3 Mean GM CBVcap (%) was also significantly lower in patients

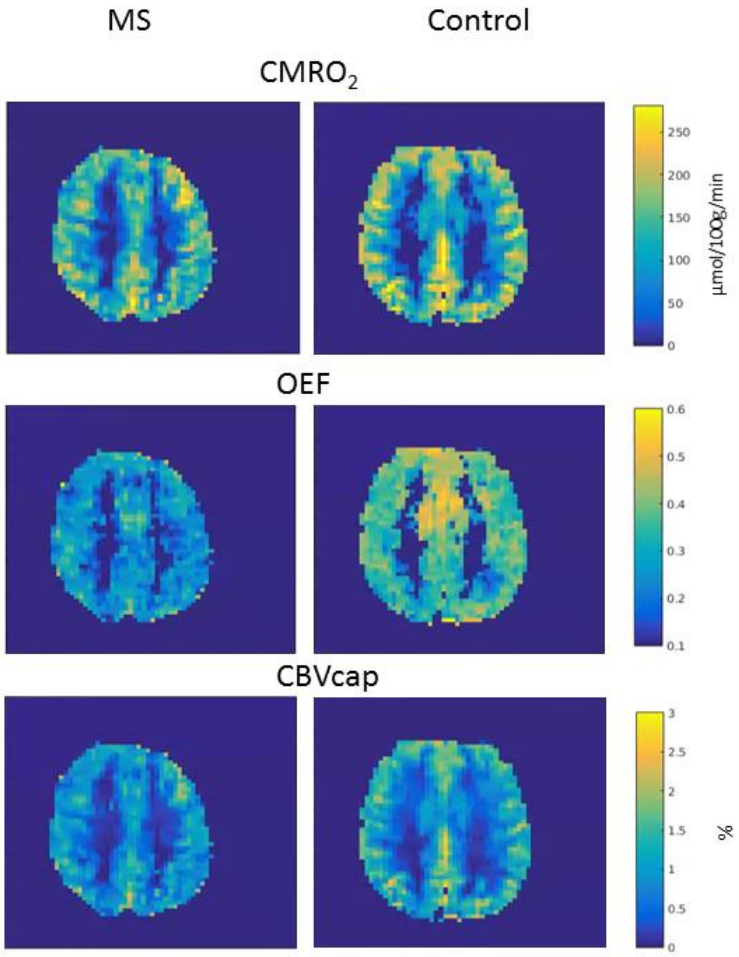

Figure 9.4 Sample GM maps from a representative MS patient and control subject.

9.4 Discussion and Future Work

This is an ongoing study and results must be interpreted with caution for several reasons. First, the control group was not fully matched to patients as recruitment and testing is still in progress. Second, patient group is small with only 7 patients, and at present, unmatched controls. Still, this pilot data in in agreement with the work of Ge et al. (2012) who showed that global CBF was unchanged between MS patients and controls, however $CMRO_2$ and OEF was significantly lower in patients. Additional work by Fan et al. (2015) also shows OEF reductions in people with MS. The current data shows again absolute $CMRO_2$ and OEF reductions in an analysis of whole GM, demonstrating that this effect is not driven by WM abnormalities alone. In other words, while WM lesions and demyelination may be present, along with metabolic changes in WM, disease-related abnormalities are clearly present in GM tissue. How $CMRO_2$ and OEF_0 relate to disability and structural integrity will be investigated in the full study, however, based on previous work by Ge et al. (2012) and Fan et al (2015) it is predicted that hypometabolism will be inversely related to EDSS and positively related to behavioural function. It is also expected that regional metabolism will depend on the presence and type of lesions observed, but inverse relationships between lesions and metabolism is predicted based on the work of Fan et al. (2015).

In addition, the current data suggest that CBVcap are also significantly lower in patients. Unlike Marshall et al. (2014) a significant reduction in CVR was not observed in patients although there was a trend towards this effect. Reductions in CBVcap have not previously been demonstrated using fMRI without contrast. Increases in CBV have been reported prior to blood-brain-barrier (BBB) breakdown in MS in the rat brain, (Broom et al., 2005), and in contrast enhancing lesions (Ge et al., 2005), however reductions in CBV have also been observed in deep grey matter in progressive MS (thalamus, putamen, caudate) (Inglese, Park, Johnson, Babb, & Miles, 2017). CBV reductions are thought to be the result of edema following BBB breakdown. Blood volume measures, may therefore be sensitive markers to inflammatory damage and the state of the BBB. However, as discussed in Chapter 5, our estimate of CBVcap does not account for differences in tissue oxygen pressure (ptO_2) and capillary transit time heterogeneity (CTTH) which may be affected due to microvascular abnormalities in MS.

While CBF was not different between the groups, evidence of hypoperfusion, or regional hyperperfusion (Juurlink, 2013) may emerge in the planned full group analysis of individual

cortical regions known to be affected in MS including visual cortex, thalamus and other deep GM structures. Similarly, CVR, which requires high SNR and will benefit from additional data, may be altered in patients, but is not visible in this small sample. Additional processing steps, namely correction or partial volume effects and the appearance of lesions, will be conducted on the full sample as atrophy will affect all measures of flow and metabolism.

As discussed in the introduction, the effect of baseline flow and metabolism on short-term motor plasticity will be investigated; it is predicted that patients with greater flow and metabolism reductions at baseline will show less of a performance gain during motor training. However, the effect of baseline function on task-responses, and adaptation over time is less clear. It is expected that hypometabolism in task-relevant areas may lead to reduced overall responses and less functional adaptation, however task $CMRO_2$ will depend on baseline flow, CBVcap and OEF_0. The relationship between these parameters during behavioural tasks is not clear at present, either in healthy controls or patients. This study will shed light on the effect of vascular and metabolic dysfunction in MS on motor plasticity, and characterise compensatory activity during task performance.

In future, interventions which help to promote vascular and metabolic health, such as AF interventions, may be used in conjunction with anti-inflammatory pharmacological treatments to maximise plasticity and functional recovery in MS.

Chapter 9 Supplementary Data

Individual Participant Grey Matter Values								
	Sex	**Age**	**EDSS**	**CBF_0**	**CBVcap**	**OEF_0**	**CMRO2**	**CVR**
P01	F	43	4	46.2	1	0.3	125	2.1
P02	M	40	6	56.5	1	0.3	126.1	1.1
P03	F	45	3	51.5	1.2	0.3	134.4	2.6
P04	F	31	0	62.2	1.5	0.3	173.7	2.4
P05	F	39	n/a	41	1.2	0.4	133.3	1.6
P06	F	22	n/a	49.3	1.4	0.3	154.8	1.9
P07	F	35	1	57.1	0.8	0.2	100.8	2.7
C01	M	31	n/a	45.1	1.2	0.4	143.4	3.4
C02	M	23	n/a	57.2	1.2	0.3	156.7	2.4
C03	M	32	n/a	45.7	1.5	0.4	162.9	2.1
C04	M	31	n/a	52.1	1.6	0.4	180.8	2.5
C05	M	40	n/a	52.7	1.2	0.3	150.7	2.6
C06	M	25	n/a	46.7	1.5	0.4	164.5	1.9
C07	M	26	n/a	47.7	1.7	0.4	177.1	2.7
C08	M	28	n/a	49.3	1.2	0.4	145.2	2.6
C09	M	36	n/a	36.2	1.6	0.5	154.2	2.2
C10	M	26	n/a	51.9	1.4	0.4	162.3	2.2
C11	F	43	n/a	50.5	1.3	0.4	150.2	2.1
C12	F	28	n/a	59	1.4	0.3	164.5	2.0

Table 9.2 Individual subject data for each parameter of interest. P = patient, C = control.

Chapter 10

General Discussion

Overall health and behavioural function is dependent on optimal CBF and O_2 metabolism. Although cerebrovascular dysfunction is not the only consequence of ageing and disease processes, without adequate energy supply to the brain, rehabilitation and treatment will not be effective. Therefore, efforts to maintain, or ideally improve, brain vascular and metabolic health are extremely important and could reduce the burden of ill health in many populations. This includes not only those with neurological disorders such as MS and mild cognitive impairment (MCI) but also groups who develop cerebrovascular damage as secondary disease complications such as in diabetes (Østergaard et al., 2015) and HIV (Ances, Vaida, Benson, Smith, & Ellis, 2010).

Exercise training (ET), based on the literature in older adults, promotes healthy brain function across the lifespan and may strengthen vascular reserve helping to protect the brain against functional decline when it becomes vulnerable to the effects of ageing and disease (Davenport, Hogan, Eskes, Longman, & Poulin, 2012). One of the most damaging effects of functional decline is the loss of brain plasticity, which impairs the ability of the brain to adapt and repair itself leading to a loss of behavioural and cognitive capabilities. ET may therefore promote brain plasticity helping to reduce the functional decline in vulnerable groups.

To further the understanding of these two areas, this thesis used quantitative fMRI techniques to investigate the effects of AF on brain function in the healthy brain (Chapters 4 and 5), and the vascular and metabolic changes that occur during tasks requiring motor system plasticity (Chapters 7 and 8). Then, the ASL techniques used to quantify CBF and O_2 metabolism at rest and during motor learning were applied to map the same parameters in a group of MS patients (Chapter 9).

Below, the main findings from the work presented in this thesis are summarised followed by a discussion of methodological considerations and areas for future research aimed at improving brain energetics and plasticity in MS and other diseases.

10.1 Aerobic Fitness and Brain Health

Chapters 4 and 5 suggest that AF does influence brain haemodynamics and O_2 metabolism in young adults. However, the results do not show a consistent and clear relationship between AF and brain function. In Chapter 4, higher AF was inversely correlated with CBF and positively with CVR. For CBF, this effect was statistically significant only in a voxelwise analysis, not in the ROI analysis, and the opposite was true of CVR. The voxelwise analysis of CBF showed that subjects with a higher VO_2peak had lower CBF in portions of the thalamus, brainstem, visual cortex, precuneus and cerebellum.

In Chapter 5, AF was negatively correlated with CBVcap, OEF_0 and $CMRO_2$ before multiple comparison corrections in the ROI analysis. In a voxelwise analysis, CBVcap was negatively correlated with estimated $\dot{V}O_2$max in left primary motor cortex (M1), left precuneus, bilateral anterior and posterior cingulate gyrus, left intracalcarine cortex and left lateral occipital cortex. For OEF, the negative correlation with $\dot{V}O_2$max was confined to the left M1 and supplementary motor areas.

As these studies were conducted on different scanners the CBF and CVR results from the two studies are not directly comparable. The results from Chapter 4 are likely more accurate estimations of CBF as data were acquired using MTI ASL and analysed using a dual-compartment model which fits a macro and microvascular compartment. This reduces the risk of perfusion overestimation which can occur with single compartment models. Lower resting GM CBF together with a greater CVR to CO_2 was thought to indicate greater functional efficiency in subjects with higher AF, whereby greater extraction of O_2 reduced CBF demand, yet the capacity to respond to a physiological stimulus was enhanced in some way as a result of physical training.

The results from Chapter 5 did not support this hypothesis, as both baseline OEF and $CMRO_2$ were negatively correlated with fitness as was CBVcap. Further, there was no strong directional trend between CBF or CVR and fitness. As discussed in Chapter 5, due to the assumptions of the forward physiological model, the apparent reduction in CBVcap and metabolic parameters may be due to underlying differences in ptO_2 and CTTH, rather than true blood volume and metabolic reductions. This is highly speculative at present and new methods which are capable of measuring CTTH and ptO_2 noninvasively are needed to reduce the need for these model assumptions.

The ET intervention reported in Chapter 5 did not lead to measurable brain changes over 1-week. Most studies assess the effects of ET on brain and/or behaviour following 12 weeks (Chapman et al., 2013; Murrell et al., 2013) or longer 1-year periods (Erickson et al., 2011). The very short-term effects of ET were not known, and a better understanding of the timescale of vascular and metabolic adaptations to ET will help to elucidate the mechanisms driving ET adaptations in humans.

Interesting work in cardiac muscle in pigs (White et al., 1998), has shown that the greatest capillary density increases occurred only 3 weeks after training. Further training reduced capillary density to control levels, however larger arterioles and then arteries increased at 8 and 16 weeks of training. At 8 weeks, not 16 weeks, the greatest coronary blood flow increase was recorded. Therefore, should a study show no effect, or an unexpected effect, changes which cannot be measured non-invasively but may affect results, such as capillary density and the diameter of arterioles or arteries, should be considered. While White et al. (1998) investigated cardiovascular changes, similar step-wise changes (Bloor, 2005) may occur in the brain. This study provides useful information for future intervention studies of similar duration in humans. Imaging of capillary and total blood volume at multiple time-points during an intervention may show differential initial and long-term adaptations which could provide useful mechanistic information on how exercise and AF increases affect brain physiology and the changes necessary to induce cognitive or behavioural benefits.

Current understanding is that physical training upregulates neurotrophic factors which stimulate cell and vessel development (M. W. Voss, Vivar, Kramer, & van Praag, 2013), and training may also preserve aortic elasticity, which facilitates the transport of nutrients to the brain (Claudine Joëlle Gauthier et al., 2015). In addition, as AF is associated with greater Hb concentration (Mairbäurl, 2013), blood can transport more O_2 to cells which may be of particular benefit in groups with a lower absolute CBF.

In the healthy brain, not facing age-related decline, it is possible that AF does not lead to measurable benefits in the presence of already healthy vessels and adequate energy supply, as the system is already functioning optimally. It may be that only small or selective effects are seen in younger adults for this reason, for example, greater CVR as reported in Chapter 4. A greater extent of cerebrovascular benefits of AF may only become apparent when the system becomes vulnerable to the loss of vessel elasticity, declines in stroke volume from the heart, and therefore a decline in energy delivery to the brain. Fitness may preserve cerebral energy

delivery and mitochondrial function, and the upregulation of factors such as BDNF, VEGF and IGF-1 may facilitate this effect.

Research investigating neurological disorders and rehabilitation therapies rarely assesses the contribution of cardiovascular problems to neurological disorders, despite known increased cardiovascular risk in many brain conditions (Christiansen et al., 2010; Firoz et al., 2015; Stampfer, 2006). Efforts to improve brain vascular function and metabolism will not be successful if cardiovascular health is not also targeted in treatment strategies. Using MRI, comprehensive investigations of the peripheral and central vasculature can be conducted which would improve our understanding of the relationship between cardiovascular and brain health. An integrated approach would allow for the development of therapeutic interventions which act to maintain, or even improve, overall physiological function which would enhance quality of life in many neurological disorders. AF is long known to reduce cardiovascular risk; therefore, ET interventions are likely to have systemic benefit given the growing literature on cerebral benefits. In addition, assessing the capacity of the cardiovascular system to adapt with ET, may help to predict the potential for cerebrovascular benefits to be gained from such interventions.

10.2 Functional Neuroplasticity of the Motor System

The aim of Chapters 7 and 8 was to identify i) metabolic changes during task performance which are likely to facilitate functional motor plasticity in the healthy brain and ii) based on previous work showing sustained BOLD RSFC changes following motor learning (Albert, Robertson, & Miall, 2009; Saber Sami, Robertson, & Miall, 2014), investigate whether these changes were due to sustained CBF alterations in these regions. Persistent CBF changes following motor learning may also reflect energetic changes as a result of brain adaptation following motor sequence learning.

The results of the first plasticity study (Chapter 7) revealed that performance of the SRT task led to reductions in BOLD signal and CBF as the task progressed. Signal reductions were observed in the left cerebellum, insula and LOC, however a concurrent increase in $rCMRO_2$ that did not reach statistical significance was observed in the same regions. This study demonstrates the feasibility of using calibrated fMRI to study complex cognitive processes. The limitations of using standard BOLD imaging in studies of plasticity are also shown, as reduced BOLD signal could be interpreted as a reduction in neuronal activity in the absence of accompanying information about $rCMRO_2$. In addition, the flow-metabolism coupling ratio

decreased from the beginning to end of the task, suggesting that a greater amount of O_2 was extracted from less CBF. Although this decrease did not reach statistical significance, future studies designed specifically to investigate flow-metabolism coupling changes during learning would be useful in determining regional coupling between CBF and O_2 metabolism during cognitive task performance.

The results of a second motor plasticity study (Chapter 8) did not support the predictions of CBF alterations at rest following motor training in areas showing statistically significant BOLD and CBF signal reductions across the SRT task. Reductions in right M1, superior parietal lobule (SPL), angular gyrus, supramarginal gyrus (SMG), anterior cingulate cortex (ACC) and cuneal cortex were observed over the duration of the task. However, CBF over 10 minutes immediately post-task, was not different from the 10 minutes preceding the task. For the control motor performance task, reductions were identified in the right M1, SMG, inferior frontal gyrus (IFG) and bilateral ACC, demonstrating differences in task responses for the motor learning vs. the motor performance task. Further, M1 RSFC was altered following the SRT, but not the control task. Again, there was not a strong CBF change in these regions, or in M1, following task performance. These results suggest that sustained brain changes, reflective of functional and/or structural plasticity, likely occur over longer periods than a single session of motor task training.

In future, using this data or new data, alternative approaches to modelling of task changes may lend additional insight into task-related metabolic changes over time. The response change over time may not be linear as assumed here, a steep initial change followed by less pronounced block-by-block reductions in CBF or BOLD signal may better reflect the data. Also, exploration of RSFC changes was limited to M1 connectivity changes due to time constraints. Additional investigation of known resting state networks using ICA or seed-based analysis may reveal additional changes as a result of motor learning, as reported previously in frontal-cerebellar and cerebellar-basal ganglia networks (Albert et al., 2009; Saber Sami et al., 2014; S Sami & Miall, 2013).

It should also be mentioned that aerobic glycolysis is increased during neuronal activation but its contribution to plasticity cannot be investigated using ASL. Aerobic glycolysis is the upregulation of glucose metabolism in the presence of sufficient O_2, and although its cellular function is not well known, it is a phenomenon that has been observed in many rodent studies

of learning, memory acquisition and consolidation (Dienel & Cruz, 2016). Recently increases in aerobic glycolysis with motor learning have been reported in healthy subjects (Shannon, Neil, Vlassenko, Shimony, & Rutlin, 2016) and its role in plasticity both in health and disease may be overlooked in an area of research primarily using fMRI. Imaging of glucose utilisation requires PET imaging, therefore in ASL studies, only a portion of energy metabolism can be investigated. To fully investigate plasticity, combined fMRI and PET imaging would be ideal, especially for investigating mechanisms limiting plasticity in neurological patients.

Finally, with 7T now becoming more widely available it is possible to study intra-cortical layer-specific plasticity, with sub-millimetre resolution (~0.8mm). While this is not possible with ASL, BOLD imaging at extremely high resolution could be conducted during motor learning to identify the specific regions and layers which show adaptation with learning. Additional scans before and after task performance using VASO, could quantitatively assess changes in CBV following task training. CBV changes peak in deeper cortical layers than the BOLD or CBF signal and therefore measure activity closer to the site of neuronal and metabolic activity (Huber, Goense, et al., 2015). Given the results in Chapter 8, longer motor-training paradigms, or inter-session training may also be necessary in these studies to observe changes reflecting functional plasticity. Yu & Koretsky (2014) used layer-specific fMRI to study brain reorganisation and sensory input following denervation in rats. Given that factors limiting plasticity in humans are still relatively unknown, ultra high-resolution investigations could provide information on metabolic activity in different cortical layers e.g. afferent or efferent signal dysfunction in disease.

10.3 Multiple Sclerosis

The MS patient study reported in Chapter 9 demonstrates the application of previous methods used to quantify brain function in healthy controls (Chapter 5) in a clinical population.

This project is ongoing, however, metabolic changes in GM are evident in patients despite the small sample (n=7), with lower $CMRO_2$, OEF_0 and CBVcap observed. These results are in agreement with previous quantitative methods which have used sagittal sinus (Ge et al., 2012) or pial artery measurements (Fan et al., 2014) to estimate global CBF and metabolism. The current results add supporting evidence that global measures are reliable indicators of cortical function, however the regional mapping method which will be used in the ongoing study may identify areas specifically vulnerable to inflammatory damage. Secondly, dual-calibrated PCASL acquisitions in conjunction with structural imaging of lesions and cortical integrity may help to

determine whether vascular and metabolic changes are secondary to chronic inflammatory damage, or occur prior to loss of cortical and subcortical tissue. OEF and $CMRO_2$ may both be more sensitive markers of brain health than CBF as metabolic changes could indicate at risk tissue which could be preserved with effective treatments.

In optimising methods from Chapter 7, absolute $CMRO_2$ and OEF_0 changes during task performance can be investigated as the dual-calibrated PCASL data is acquired in the same session immediately before SRT task performance. This will enable more accurate quantification of metabolism during cognitive task performance than standard calibrated fMRI as baseline $CMRO_2$ is known to be altered in this MS group. The use of dual-calibrated fMRI to study plasticity in patient groups represents a step forward in this area of research as BOLD fMRI is often used despite known vascular and metabolic changes in MS (Pantano, Mainero & Caramia, 2006; Prosperini, Piattella, & Giannì, 2015). In fact, in the review by Prosperini et al. (2015) the appropriateness of BOLD for investigating plasticity was questioned, due to the heterogeneity of MS which makes group level responses to rehabilitation difficult to detect (Rasova et al., 2006). Quantitative baseline measures of $CMRO_2$ and OEF may provide an indication of likely treatment response, as well as more meaningful measures of treatment outcome which could explain the lack of measured BOLD changes in motor rehabilitation interventions (Rasova et al., 2015)

10.4 Methodological Considerations and Limitations

Most limitations have been mentioned in the relevant chapters, however a few may be highlighted here for consideration in future studies.

First, it is, unsurprisingly, difficult to recruit sedentary participants to exercise studies. Due to time limitations for completing studies, it was not possible to recruit an even number of active and sedentary subjects. Although both fit and sedentary subjects were recruited, samples had a lower spread of fitness levels than planned which has obvious limitations for detecting fitness-related brain differences. Given that participants were paid for their time, money does not appear to be an incentive for inactive people to take part. In future, targeting people who are currently inactive but intending to improve their fitness may be a more successful way of recruiting sedentary individuals.

Equipment for recording respiratory and cardiac traces was not available at the time of data collection in the new imaging centre, meaning that physiological noise correction could not be carried out on data reported in Chapters 5, 8 and 9. The effects of $P_{ET}CO_2$ fluctuations were controlled for where necessary (see normalisation of CBF in Chapter 8), cardiac and respiratory variability are also known to confound fMRI signals (Golestani, Chang, & Chen, 2015; Murphy, Birn, & Bandettini, 2013b). As a result, some non-neuronal signal may have been interpreted as part of the task-response in Chapter 8. However, in Chapters 5 and 9, where the hypercapnia and hyperoxia response is global, physiological fluctuations present less of a problem. As discussed in the introduction, physiological noise correction also removes neuronal signal as noise may be coupled to neuronal fluctuations. There is no perfect solution to data clean-up, and the most appropriate method depends on the questions being addressed. However, where correction is not carried out, either purposefully or due to lack of resources, it is important to be aware of potential non-neuronal contributions.

The power analyses conducted to inform future studies suggest, in many cases, that larger samples are necessary due to small effect sizes. FMRI is expensive and time-consuming, and many studies including those presented in this thesis, are limited by time and funding constraints. For example, the study presented in Chapter 5 required an 11-hour time commitment for each participant, with each hour also requiring the time of at least 2 researchers. As a result, 15 participants was a feasible and affordable sample size. Ideally, studies would not be designed around practical considerations, but that is often necessary at a cost to statistical power. As previously suggested, the best way to overcome this problem is coordinated research efforts across centres to increase total sample sizes.

In small samples, individual variability has a considerable effect on data, and this may explain why the significant correlations between CBVcap and OEF and fitness were only observed in the post-intervention data in Chapter 5 which had an additional 2 participants.

The eligibility criteria for respiratory challenges using gases is stringent, and this means that the RR-MS patient cohort is disproportionately healthy in comparison to the general population of people with MS. As the aim of the study is to look at MS-related vascular dysfunction, those with other common comorbidities, e.g. bipolar disorder, asthma, were not eligible. While this means that we can look at true dysfunction due to MS, the results may not generalise to more severely impaired patients. Future studies which include those with comorbidities which do not present a safety risk will provide a more representative picture of vascular and metabolic dysfunction in MS.

10.5 Translation of Findings: Improving Brain Plasticity in Disease

Exercise training in rodents has been shown to improve subsequent learning and memory (Berchtold, Castello, & Cotman, 2010) and recently it has been suggested that aerobic exercise in Parkinson's disease may promote motor skill learning as a result of molecular, synaptic and metabolic changes which occur with ET and help to improve motor control, learning and memory (Petzinger et al., 2013). Figure 10.1 outlines this hypothesis, and provides a framework for future research efforts to increase neuroplasticity and improve rehabilitation outcomes.

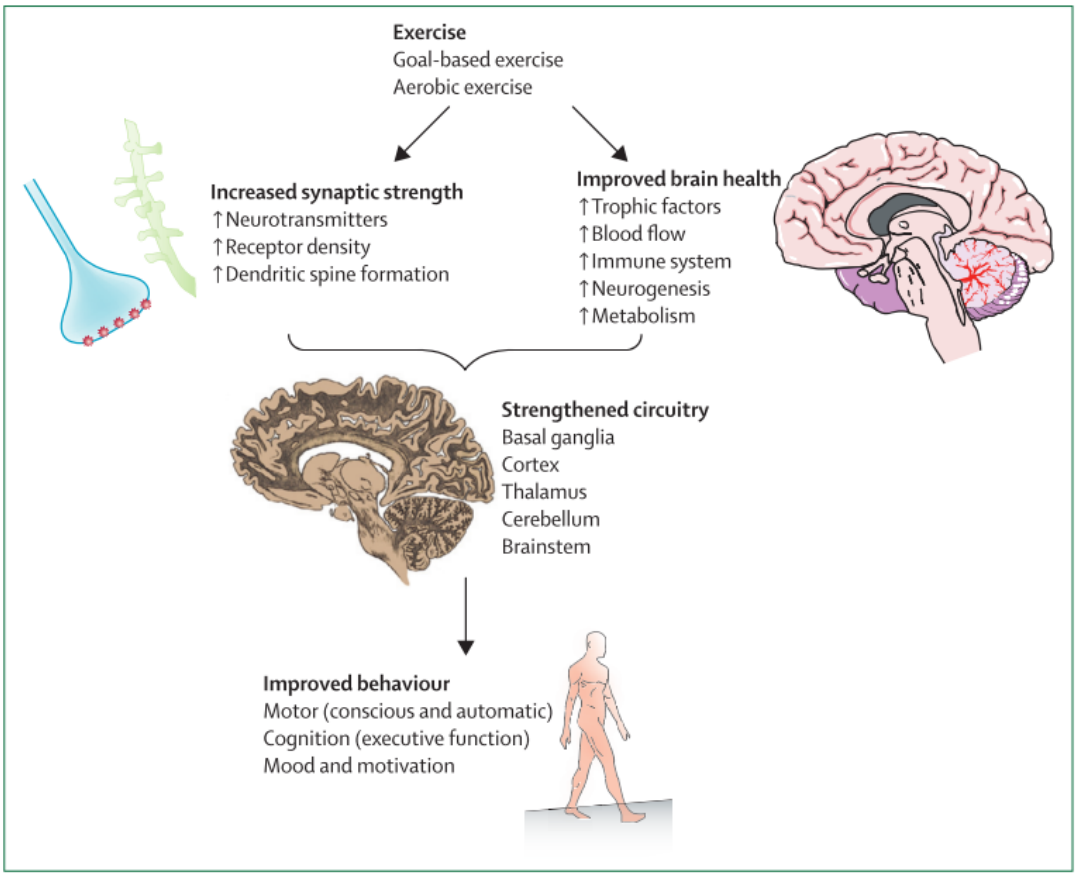

Figure 10.1 Image taken from Petzinger et al. (2013). This diagram outlines the likely mechanisms through which aerobic exercise can increase brain plasticity and improve motor and cognitive function in disease.

A combination of aerobic ET and goal-directed training, e.g. motor sequence learning, may strengthen synaptic connections (Adkins, Boychuk, Remple, & Kleim, 2006), vascular health (Ainslie et al., 2008; Pereira et al., 2007; B. P. Thomas et al., 2013), and upregulate BDNF and other neurotrophic factors involved in learning and memory formation (Cotman & Berchtold,

2002). Multi-dimensional interventions encompassing both aerobic and motor skill training may provide the greatest potential for clinically relevant improvements in plasticity and functional ability, in MS and other diseases.

The results of Chapters 4 and 5 suggest that AF may have differential effects on the healthy brain and those facing decline, which has been suggested elsewhere (V. J. Williams et al., 2017). It may be that there are limited measurable differences in optimally functioning young adults, however results are suggestive of greater vascular reserve, and potentially metabolic efficiency, which warrants further exploration. This thesis clearly demonstrates the application of quantitative fMRI and physiological modelling (Davis, Kwong, Weisskoff, & Rosen, 1998b; Germuska et al., 2016) to investigate CBF and O_2 metabolism at rest, during and following motor learning. Importantly, Chapter 9 shows that the use of calibrated fMRI to study metabolic dysfunction in MS is well-tolerated, and ongoing work will determine the role of baseline metabolic dysfunction as a limiting factor in functional brain plasticity.

The feasibility of conducting exercise interventions in MS has been demonstrated (Platta, Ensari, Motl, & Pilutti, 2016), and a recent motor training study in ~30 people with MS in our lab shows that longitudinal home-based training also has a high retention rate (Lipp, Foster et al., *in prep*). In the latter part of this thesis, it is shown that ideal imaging methods for quantitative investigations of vascular and metabolic function are suitable for imaging studies in people with MS. Going forward, studies combining both aerobic and motor training can investigate the efficacy of this rehabilitation approach in terms of improving cerebral vascular and metabolic function and behavioural outcomes in MS.

Bibliography

American College of Sports Medicine (Ed.). (2013). ACSM's health-related physical fitness assessment manual. Lippincott Williams & Wilkins.

Aanerud, J., Borghammer, P., Chakravarty, M. M., Vang, K., Rodell, A. B., Møller, A., … Gjedde, A. (2012). Brain energy metabolism and blood flow differences in healthy aging, *2*, 1177–1187. http://doi.org/10.1038/jcbfm.2012.18

Adkins, D. L., Boychuk, J., Remple, M. S., & Kleim, J. a. (2006). Motor training induces experience-specific patterns of plasticity across motor cortex and spinal cord. *Journal of Applied Physiology (Bethesda, Md. : 1985)*, *101*(6), 1776–1782. http://doi.org/10.1152/japplphysiol.00515.2006

Ahlgren, A., Wirestam, R., Petersen, E. T., Ståhlberg, F., & Knutsson, L. (2014). Partial volume correction of brain perfusion estimates using the inherent signal data of time-resolved arterial spin labeling. *NMR in Biomedicine*, *27*(9), 1112–1122. http://doi.org/10.1002/nbm.3164

Ainslie, P. N., Cotter, J. D., George, K. P., Lucas, S., Murrell, C., Shave, R., … Atkinson, G. (2008). Elevation in cerebral blood flow velocity with aerobic fitness throughout healthy human ageing, *16*, 4005–4010. http://doi.org/10.1113/jphysiol.2008.158279

Albert, N. B., Robertson, E. M., & Miall, R. C. (2009). The Resting Human Brain and Motor Learning. *Current Biology*, *19*(12), 1023–1027. http://doi.org/10.1016/j.cub.2009.04.028

Alfini, A. J., Weiss, L. R., Leitner, B. P., Smith, T. J., Hagberg, J. M., Smith, J. C., … Smith, J. C. (2016). Hippocampal and Cerebral Blood Flow after Exercise Cessation in Master Athletes, *8*(August), 1–9. http://doi.org/10.3389/fnagi.2016.00184

Ances, B. M., Leontiev, O., Perthen, J. E., Liang, C., Lansing, A. E., & Buxton, R. B. (2008). Regional differences in the coupling of cerebral blood flow and oxygen metabolism changes in response to activation: Implications for BOLD-fMRI. *NeuroImage*, *39*(4), 1510–1521. http://doi.org/10.1016/j.neuroimage.2007.11.015

Ances, B. M., Vaida, F., Benson, D., Smith, D. M., & Ellis, R. J. (2010). Resting Cerebral Blood Flow as a Biomarker of HIV in the Brain, *73*, 2009.

Andreasen, a K., Stenager, E., & Dalgas, U. (2011). The effect of exercise therapy on fatigue in multiple sclerosis. *Multiple Sclerosis (Houndmills, Basingstoke, England)*, *17*(9), 1041–54. http://doi.org/10.1177/1352458511401120

Angleys, H., Østergaard, L., & Jespersen, S. N. (2015). The effects of capillary transit time heterogeneity (CTH) on brain oxygenation, (December 2014), 806–817. http://doi.org/10.1038/jcbfm.2014.254

Antonio, S., Case, L., Harman, C., & Lacey, J. (1987). Attentional Requirements of Learning : Performance Measures Evidence from, *32*.

Aslan, S., Xu, F., Wang, P. L., Uh, J., Yezhuvath, U. S., Osch, M. Van, & Lu, H. (2010). Estimation of Labeling Efficiency in Pseudocontinuous Arterial Spin Labeling, *771*, 765–771. http://doi.org/10.1002/mrm.22245

Asllani, I., Borogovac, A., & Brown, T. R. (2008). Regression Algorithm Correcting for Partial Volume Effects in Arterial Spin Labeling MRI, *1371*, 1362–1371.

http://doi.org/10.1002/mrm.21670

Attwell, D., & Iadecola, C. (2002). The neural basis of functional brain imaging signals. *Trends in Neurosciences*, *25*(12), 621–625. http://doi.org/10.1016/S0166-2236(02)02264-6

Bailey, D. M., Marley, C. J., Brugniaux, J. V, Hodson, D., New, K. J., Ogoh, S., & Ainslie, P. N. (2013a). Elevated aerobic fitness sustained throughout the adult lifespan is associated with improved cerebral hemodynamics. *Stroke; a Journal of Cerebral Circulation*, *44*(11), 3235–8. http://doi.org/10.1161/STROKEAHA.113.002589

Bailey, D. M., Marley, C. J., Brugniaux, J. V, Hodson, D., New, K. J., Ogoh, S., & Ainslie, P. N. (2013b). Elevated aerobic fitness sustained throughout the adult lifespan is associated with improved cerebral hemodynamics. *Stroke; a Journal of Cerebral Circulation*, *44*(11), 3235–8. http://doi.org/10.1161/STROKEAHA.113.002589

Barkhof, F. (2002). The clinico-radiological paradox in multiple sclerosis revisited, 239–245.

Barnes, J. N., Taylor, J. L., Kluck, B. N., Johnson, C. P., & Joyner, M. J. (2013). Cerebrovascular reactivity is associated with maximal aerobic capacity in healthy older adults. *Journal of Applied Physiology (Bethesda, Md. : 1985)*, *114*(10), 1383–7. http://doi.org/10.1152/japplphysiol.01258.2012

Barnes, J. N., Taylor, J. L., Kluck, B. N., Johnson, C. P., Joyner, M. J., Jn, B., … Mj, J. (2013). Cerebrovascular reactivity is associated with maximal aerobic capacity in healthy older adults, 1383–1387. http://doi.org/10.1152/japplphysiol.01258.2012

Baym, C. L., Khan, N. A., Pence, A., Raine, L. B., Hillman, C. H., & Cohen, N. J. (2011). Aerobic Fitness Predicts Relational Memory but Not Item Memory Performance in Healthy Young Adults, 2645–2652. http://doi.org/10.1162/jocn

Beckmann, C. F., DeLuca, M., Devlin, J. T., & Smith, S. M. (2005). Investigations into resting-state connectivity using independent component analysis. *Philosophical Transactions of the Royal Society B: Biological Sciences*, *360*(1457), 1001-1013.

Beier, M., Bombardier, C. H., Hartoonian, N., Motl, R. W., & Kraft, G. H. (2014). Improved physical fitness correlates with improved cognition in multiple sclerosis. *Archives of Physical Medicine and Rehabilitation*, *95*(7), 1328–34. http://doi.org/10.1016/j.apmr.2014.02.017

Berchtold, N. C., Castello, N., & Cotman, C. W. (2010). Exercise and time-dependent benefits to learning and memory. *Neuroscience*, *167*(3), 588–97. http://doi.org/10.1016/j.neuroscience.2010.02.050

Bherer, L., Erickson, K. I., & Liu-ambrose, T. (2013). A Review of the Effects of Physical Activity and Exercise on Cognitive and Brain Functions in Older Adults, *2013*.

Binder, J. R., Frost, J. A., Hammeke, T. A., Cox, R. W., Rao, S. M., & Prieto, T. (1997). Human Brain Language Areas Identified by Functional Magnetic Resonance Imaging, *17*(1), 353–362.

Biswal, B., Zerrin Yetkin, F., Haughton, V. M., & Hyde, J. S. (1995). Functional connectivity in the motor cortex of resting human brain using echo-planar mri. *Magnetic resonance in medicine*, *34*(4), 537-541.

Black, J. E., Isaacs, K. R., Anderson, B. J., Alcantara, A. A., & Greenough, W. T. (1990). Learning causes synaptogenesis , whereas motor activity causes angiogenesis , in cerebellar cortex

of adult rats 00OcOO (OOOO, *87*(July), 5568–5572.

Black, J. E., Polinsky, M., & Greenough, W. T. (1989). Progressive failure of cerebral angiogenesis supporting neural plasticity in aging rats. *Neurobiology of aging*, *10*(4), 353-358.

Blicher, J. U., Stagg, C. J., O'Shea, J., Ostergaard, L., MacIntosh, B. J., Johansen-Berg, H., … Donahue, M. J. (2012). Visualization of altered neurovascular coupling in chronic stroke patients using multimodal functional MRI. *Journal of Cerebral Blood Flow and Metabolism*, *32*(11), 2044–2054. http://doi.org/DOI 10.1038/jcbfm.2012.105

Blockley, N. P., Griffeth, V. E. M., Simon, A. B., & Buxton, R. B. (2013). A review of calibrated blood oxygenation level-dependent (BOLD) methods for the measurement of task-induced changes in brain oxygen metabolism. *NMR in Biomedicine*, *26*(8). http://doi.org/10.1002/nbm.2847

Bloor, C. M. (2005). Angiogenesis during exercise and training. *Angiogenesis*, *8*(3), 263–271. http://doi.org/10.1007/s10456-005-9013-x

Bonzano, L., Tacchino, A., Roccatagliata, L., Sormani, M. P., Mancardi, G. L., & Bove, M. (2011). NeuroImage Impairment in explicit visuomotor sequence learning is related to loss of microstructural integrity of the corpus callosum in multiple sclerosis patients with minimal disability, *57*, 495–501. http://doi.org/10.1016/j.neuroimage.2011.04.037

Boraxbekk, C.-J., Salami, A., Wåhlin, A., & Nyberg, L. (2015). Physical activity over a decade modifies age-related decline in perfusion, gray matter volume, and functional connectivity of the posterior default-mode network—A multimodal approach. *NeuroImage*. http://doi.org/10.1016/j.neuroimage.2015.12.010

Borg, E. (2014). A Comparison Between Two Rating Scales For Perceived Exertion, (April).

Borogovac, A., & Asllani, I. (2012). Arterial Spin Labeling (ASL) fMRI: advantages, theoretical constrains, and experimental challenges in neurosciences. *International Journal of Biomedical Imaging*, *2012*, 818456. http://doi.org/10.1155/2012/818456

Bouvier, J., Detante, O., Tahon, F., Attye, A., Perret, T., Chechin, D., … Krainik, A. (2014). Reduced CMRO2 and cerebrovascular reserve in patients with severe intracranial arterial stenosis: A combined multiparametric qBOLD oxygenation and BOLD fMRI study. *Human Brain Mapping*, *0*(October), 1–12. http://doi.org/10.1002/hbm.22657

Boyd, L. A., & Winstein, C. J. (2001). Implicit motor-sequence learning in humans following unilateral stroke : the impact of practice and explicit knowledge, *298*, 65–69.

Brackley, K. J., Ramsay, M. M., Pipkin, F. B., & Rubin, P. C. (1999). The effect of the menstrual cycle on human cerebral blood flow : studies using Doppler ultrasound, 52–57.

Bright, M. G., & Murphy, K. (2013a). Reliable quantification of BOLD fMRI cerebrovascular reactivity despite poor breath-hold performance. *NeuroImage*, *83*, 559–568. http://doi.org/10.1016/j.neuroimage.2013.07.007

Bright, M. G., & Murphy, K. (2013b). Removing motion and physiological artifacts from intrinsic BOLD fluctuations using short echo data. *NeuroImage*, *64*(1), 526–537. http://doi.org/10.1016/j.neuroimage.2012.09.043

Bright, M. G., & Murphy, K. (2015). NeuroImage Is fMRI " noise " really noise ? Resting state nuisance regressors remove variance with network structure. *NeuroImage*, *114*, 158–

169. http://doi.org/10.1016/j.neuroimage.2015.03.070

Brookes, M. J., Morris, P. G., Gowland, P. A., & Francis, S. T. (2007). Noninvasive Measurement of Arterial Cerebral Blood Volume Using Look-Locker EPI and Arterial Spin Labeling, *54*, 41–54. http://doi.org/10.1002/mrm.21199

Brooks, J. C. W., Faull, O. K., Pattinson, K. T., & Jenkinson, M. (2013). Physiological noise in brainstem FMRI. *Frontiers in human neuroscience*, *7*, 623.

Broom, K. A., Anthony, D. C., Blamire, A. M., Waters, S., Styles, P., Perry, V. H., & Sibson, N. R. (2005). MRI reveals that early changes in cerebral blood volume precede blood – brain barrier breakdown and overt pathology in MS-like lesions in rat brain, 204–216. http://doi.org/10.1038/sj.jcbfm.9600020

Brown, A. D., McMorris, C. a., Longman, R. S., Leigh, R., Hill, M. D., Friedenreich, C. M., & Poulin, M. J. (2010). Effects of cardiorespiratory fitness and cerebral blood flow on cognitive outcomes in older women. *Neurobiology of Aging*, *31*(12), 2047–2057. http://doi.org/10.1016/j.neurobiolaging.2008.11.002

Brown, M. M., Wade, J. P. H., & Marshall, J. (1985). Fundamental importance of arterial oxygen content in the regulation of cerebral blood flow, (September 2017), 81–93.

Bulte, D., Chiarelli, P., Wise, R., & Jezzard, P. (2007). Measurement of Cerebral Blood Volume in Humans Using Hyperoxic MRI Contrast, *i*, 894–899. http://doi.org/10.1002/jmri.21096

Bulte, D. P., Kelly, M., Germuska, M., Xie, J., Chappell, M. a., Okell, T. W., … Jezzard, P. (2012a). Quantitative measurement of cerebral physiology using respiratory-calibrated MRI. *NeuroImage*, *60*(1), 582–591. http://doi.org/10.1016/j.neuroimage.2011.12.017

Bulte, D. P., Kelly, M., Germuska, M., Xie, J., Chappell, M. a, Okell, T. W., … Jezzard, P. (2012b). Quantitative measurement of cerebral physiology using respiratory-calibrated MRI. *NeuroImage*, *60*(1), 582–91. http://doi.org/10.1016/j.neuroimage.2011.12.017

Button, K. S., Ioannidis, J. P. A., Mokrysz, C., Nosek, B. A., Flint, J., Robinson, E. S. J., & Munafò, M. R. (2013). Power failure: why small sample size undermines the reliability of neuroscience, *14*(May). http://doi.org/10.1038/nrn3475

Buxton, R. B., & Diego, S. (2015). HHS Public Access, *76*(9). http://doi.org/10.1088/0034-4885/76/9/096601.

Buxton, R. B. (2009). *Introduction to functional magnetic resonance imaging: principles and techniques*. Cambridge university press.

Buxton, R. B., & Frank, L. R. (1997). A Model for the Coupling Between Cerebral Blood Flow and Oxygen Metabolism During Neural Stimulation, 64–72.

Buxton, R. B., Frank, L. R., Wong, E. C., Siewert, B., Warach, S., & Edelman, R. R. (1998). A General Kinetic Model for Quantitative Perhsion Imaging with Arterial Spin Labeling, (19), 383–396.

Cahill, L. S., Bishop, J., Gazdzinski, L. M., Dorr, A., Stefanovic, B., Sled, J. G., & Region-of-interest, R. O. I. (2017). Altered cerebral blood flow and cerebrovascular function after voluntary exercise in adult mice. *Brain Structure and Function*, *0*(0), 0. http://doi.org/10.1007/s00429-017-1409-z

Cantin, S., Villien, M., Moreaud, O., Tropres, I., Keignart, S., Chipon, E., … Krainik, a. (2011). Impaired cerebral vasoreactivity to CO2 in Alzheimer's disease using BOLD fMRI.

NeuroImage, *58*(2), 579–87. http://doi.org/10.1016/j.neuroimage.2011.06.070

Carro, E., Trejo, J. L., Busiguina, S., & Torres-Aleman, I. (2001). Circulating insulin-like growth factor I mediates the protective effects of physical exercise against brain insults of different etiology and anatomy. *Journal of Neuroscience*, *21*(15), 5678–5684. http://doi.org/21/15/5678 [pii]

Cha, Y. K., Jog, M. A., Kim, Y., Chakrapani, S., Kraman, S. M., & Wang, D. J. J. (2013). Regional correlation between resting state FDG PET and pCASL perfusion MRI, *33*(12), 1909–1914. http://doi.org/10.1038/jcbfm.2013.147

Chaddock-Heyman, L., Erickson, K. I., Chappell, M. A., Johnson, C. L., Kienzler, C., Knecht, A., … Kramer, A. F. (2016). Aerobic fitness is associated with greater hippocampal cerebral blood flow in children. *Developmental Cognitive Neuroscience*, *20*, 52–58. http://doi.org/10.1016/j.dcn.2016.07.001

Chalela, J. A., Alsop, D. C., Gonzalez-Atavales, J. B., Maldjian, J. A., Kasner, S. E., & Detre, J. A. (2000). Magnetic resonance perfusion imaging in acute ischemic stroke using continuous arterial spin labeling. *Stroke.31(3):680-7,* (UNITED STATES PT-Journal Article PT-Research Support, Non-U.S. Gov't PT-Research Support, U.S. Gov't, P.H.S NO-NS02079 (United States NINDS NIH HHS) LG-English).

Chapman, S. B., Aslan, S., Spence, J. S., Defina, L. F., Keebler, M. W., Didehbani, N., & Lu, H. (2013). Shorter term aerobic exercise improves brain, cognition, and cardiovascular fitness in aging. *Frontiers in Aging Neuroscience*, *5*(November), 75. http://doi.org/10.3389/fnagi.2013.00075

Chappell, M. A., Groves, A. R., Macintosh, B. J., Donahue, M. J., Jezzard, P., & Woolrich, M. W. (2011). Partial Volume Correction of Multiple Inversion Time Arterial Spin Labeling MRI Data, *C*, 1173–1183. http://doi.org/10.1002/mrm.22641

Chappell, M. A., Groves, A. R., Whitcher, B., & Woolrich, M. W. (2009). Variational Bayesian Inference for a Nonlinear Forward Model, *57*(1), 223–236.

Chappell, M. A., MacIntosh, B. J., Donahue, M. J., G??nther, M., Jezzard, P., & Woolrich, M. W. (2010). Separation of macrovascular signal in multi-inversion time arterial spin labelling MRI. *Magnetic Resonance in Medicine*, *63*(5), 1357–1365. http://doi.org/10.1002/mrm.22320

Chen, J. J. (2015). Characterizing Resting-State Brain Function Using Arterial Spin Labeling Characterizing Resting-State Brain Function, (July). http://doi.org/10.1089/brain.2015.0344

Chen, J. J., & Pike, G. B. (2009). BOLD-specific cerebral blood volume and blood flow changes during neuronal activation in humans, (May). http://doi.org/10.1002/nbm.1411

Chiarelli, P. A., Bulte, D. P., Gallichan, D., Piechnik, S. K., Wise, R., & Jezzard, P. (2007). Flow-Metabolism Coupling in Human Visual , Motor , and Resonance Imaging, *547*, 538–547. http://doi.org/10.1002/mrm.21171

Christiansen, C. F., Christensen, S., Farkas, D. K., Miret, M., Sørensen, H. T., & Pedersen, L. (2010). Risk of arterial cardiovascular diseases in patients with multiple sclerosis: A population-based cohort study. *Neuroepidemiology*, *35*(4), 267–274. http://doi.org/10.1159/000320245

Chuang, K., Gelderen, P. Van, Merkle, H., Bodurka, J., Vasiliki, N., Koretsky, A. P., … Talagala, S.

L. (2009). NIH Public Access, *40*(4), 1595–1605.

Chodzko-Zajko, W. J., & Moore, K. A. (1994). Physical fitness and cognitive functioning in aging. *Exercise and sport sciences reviews*, *22*(1), 195-220.

Cohen, A. D., Nencka, A. S., Lebel, R. M., & Wang, Y. (2017). Multiband multi-echo imaging of simultaneous oxygenation and flow timeseries for resting state connectivity, 1–23. http://doi.org/10.1371/journal.pone.0169253

Colcombe, S. J., Kramer, A. F., Erickson, K. I., Scalf, P., McAuley, E., Cohen, N. J., … Elavsky, S. (2004). Cardiovascular fitness, cortical plasticity, and aging. *Proceedings of the National Academy of Sciences of the United States of America*, *101*(9), 3316–21. http://doi.org/10.1073/pnas.0400266101

Collett, J., Dawes, H., Meaney, A., Sackley, C., Barker, K., Wade, D., … Buckingham, E. (2011). Exercise for multiple sclerosis: a single-blind randomized trial comparing three exercise intensities. *Multiple Sclerosis Journal*, *17*(5), 594–603. http://doi.org/10.1177/1352458510391836

Cooney, J. K., Moore, J. P., Ahmad, Y. a, Jones, J. G., Lemmey, A. B., Casanova, F., … Thom, J. M. (2013). A simple step test to estimate cardio-respiratory fitness levels of rheumatoid arthritis patients in a clinical setting. *International Journal of Rheumatology*, *2013*, 174541. http://doi.org/10.1155/2013/174541

Cotman, C. W., & Berchtold, N. C. (2002). Exercise: a behavioral intervention to enhance brain health and plasticity. *Trends in Neurosciences*, *25*(6), 295–301. Retrieved from http://www.ncbi.nlm.nih.gov/pubmed/12086747

Cotman, C. W., Berchtold, N. C., & Christie, L.-A. (2007). Exercise builds brain health: key roles of growth factor cascades and inflammation. *Trends in Neurosciences*, *30*(9), 464–72. http://doi.org/10.1016/j.tins.2007.06.011

Craig, C. L., Marshall, A. L., Sj??str??m, M., Bauman, A. E., Booth, M. L., Ainsworth, B. E., … Oja, P. (2003). International physical activity questionnaire: 12-Country reliability and validity. *Medicine and Science in Sports and Exercise*, *35*(8), 1381–1395. http://doi.org/10.1249/01.MSS.0000078924.61453.FB

Curran, T. (1989). Higher-Order Associative Learning i n Amnesia Evidence from the Serial Reaction Time Task, 522–533.

D'haeseleer, M., Cambron, M., Vanopdenbosch, L., & De Keyser, J. (2011a). Vascular aspects of multiple sclerosis. *The Lancet Neurology*, *10*(7), 657–666. http://doi.org/10.1016/S1474-4422(11)70105-3

Damoiseaux, J. S., Rombouts, S. A. R. B., Barkhof, F., Scheltens, P., Stam, C. J., Smith, S. M., & Beckmann, C. F. (2006). Consistent resting-state networks, (2).

Daulatzai, M. A. (2017). Review Cerebral Hypoperfusion and Glucose Hypometabolism : Key Pathophysiological Modulators Promote Neurodegeneration , Cognitive Impairment , and Alzheimer ' s Disease, *972*(February 2016), 943–972. http://doi.org/10.1002/jnr.23777

Davenport, M. H., Hogan, D. B., Eskes, G. a, Longman, R. S., & Poulin, M. J. (2012). Cerebrovascular reserve: the link between fitness and cognitive function? *Exercise and Sport Sciences Reviews*, *40*(3), 153–8. http://doi.org/10.1097/JES.0b013e3182553430

Davis, T. L., Kwong, K. K., Weisskoff, R. M., & Rosen, B. R. (1998a). Calibrated functional MRI: mapping the dynamics of oxidative metabolism. *Proceedings of the National Academy of Sciences of the United States of America*, *95*(4), 1834–1839. http://doi.org/10.1073/pnas.95.4.1834

Davis, T. L., Kwong, K. K., Weisskoff, R. M., & Rosen, B. R. (1998b). Calibrated functional MRI: mapping the dynamics of oxidative metabolism. *Proceedings of the National Academy of Sciences of the United States of America*, *95*(4), 1834–9. http://doi.org/10.1073/pnas.95.4.1834

Dayan, E., & Cohen, L. G. (2011). Review Neuroplasticity Subserving Motor Skill Learning. *Neuron*, *72*(3), 443–454. http://doi.org/10.1016/j.neuron.2011.10.008

De Keyser, J., Steen, C., Mostert, J. P., & Koch, M. W. (2008). Hypoperfusion of the cerebral white matter in multiple sclerosis: possible mechanisms and pathophysiological significance. *Journal of Cerebral Blood Flow & Metabolism*, *28*(10), 1645–1651. http://doi.org/10.1038/jcbfm.2008.72

De Vis, J. B., Hendrikse, J., Bhogal, a., Adams, a., Kappelle, L. J., & Petersen, E. T. (2015). Age-related changes in brain hemodynamics; A calibrated MRI study. *Human Brain Mapping*, (July), n/a-n/a. http://doi.org/10.1002/hbm.22891

Debernard, L., Melzer, T. R., Van Stockum, S., Graham, C., Wheeler-Kingshott, C. a., Dalrymple-Alford, J. C., … Mason, D. F. (2014). Reduced grey matter perfusion without volume loss in early relapsing-remitting multiple sclerosis. *Journal of Neurology, Neurosurgery & Psychiatry*, *85*(5), 544–551. http://doi.org/10.1136/jnnp-2013-305612

Della-Maggiore, V., Mcintosh, A. R., & Mcintosh, A. R. (2005). Time Course of Changes in Brain Activity and Functional Connectivity Associated With Long-Term Adaptation to a Rotational Transformation, 2254–2262. http://doi.org/10.1152/jn.00984.2004.

Deng, W., Aimone, J. B., & Gage, F. H. (2010). NIH Public Access, *11*(5), 339–350. http://doi.org/10.1038/nrn2822.New

Derdeyn, C. P., Videen, T. O., Yundt, K. D., Fritsch, S. M., Carpenter, D. A., Grubb, R. L., & Powers, W. J. (2002). Variability of cerebral blood volume and oxygen extraction : stages of cerebral haemodynamic impairment revisited.

Desjardins, A. E., Kiehl, K. A., & Liddle, P. F. (2001). Removal of Confounding Effects of Global Signal in Functional MRI Analyses 1, *758*, 751–758. http://doi.org/10.1006/nimg.2000.0719

Detre, J. A., & Wang, J. (2002). Technical aspects and utility of fMRI using BOLD and ASL, *113*, 621–634.

Dienel, G. A., & Cruz, N. F. (2016). Aerobic glycolysis during brain activation: adrenergic regulation and influence of norepinephrine on astrocytic metabolism. *Journal of Neurochemistry*, 14–52. http://doi.org/10.1111/jnc.13630

Dijk, K. R. A. Van, Hedden, T., Venkataraman, A., Evans, K. C., Lazar, S. W., & Buckner, R. L. (2010). Intrinsic Functional Connectivity As a Tool For Human Connectomics : Theory , Properties , and Optimization, *2138*, 297–321. http://doi.org/10.1152/jn.00783.2009.

Donahue, M. J., Sideso, E., MacIntosh, B. J., Kennedy, J., Handa, A., & Jezzard, P. (2010). Absolute arterial cerebral blood volume quantification using inflow vascular-space-occupancy with dynamic subtraction magnetic resonance imaging. *Journal of Cerebral*

Blood Flow and Metabolism, *30*(7), 1329–1342. http://doi.org/10.1038/jcbfm.2010.16

Douaud, G., Smith, S., Jenkinson, M., Behrens, T., Johansen-Berg, H., Vickers, J., … James, A. (2007). Anatomically related grey and white matter abnormalities in adolescent-onset schizophrenia. *Brain*, *130*(9), 2375–2386. http://doi.org/10.1093/brain/awm184

Doyon, J., & Benali, H. (2005). Reorganization and plasticity in the adult brain during learning of motor skills. *Current Opinion in Neurobiology*, *15*(2), 161–167. http://doi.org/10.1016/j.conb.2005.03.004

Draganski, B., & May, A. (2008). Training-induced structural changes in the adult human brain, *192*, 137–142. http://doi.org/10.1016/j.bbr.2008.02.015

Driver, I. D., Wise, R. G., Murphy, K., & Driver, I. D. (2017). Graded Hypercapnia-Calibrated BOLD : Beyond the Iso-metabolic Hypercapnic Assumption, *11*(May), 1–9. http://doi.org/10.3389/fnins.2017.00276

Dubois, R. L. M., & Eyer, C. S. J. (1999). Motor coordination and spatial orientation are affected by neurofilament maldistribution : correlations with regional brain activity of cytochrome oxidase, 223–224.

Duckles, S. P., & Krause, D. N. (2007). Cerebrovascular effects of oestrogen: multiplicity of action. *Clinical and experimental pharmacology and physiology*, *34*(8), 801-808.

Dupuy, O., Gauthier, C. J., Fraser, S. a, Desjardins-Crèpeau, L., Desjardins, M., Mekary, S., … Bherer, L. (2015). Higher levels of cardiovascular fitness are associated with better executive function and prefrontal oxygenation in younger and older women. *Frontiers in Human Neuroscience*, *9*(February), 66. http://doi.org/10.3389/fnhum.2015.00066

Erickson, K. I., Voss, M. W., Prakash, R. S., Basak, C., Szabo, A., Chaddock, L., … Kramer, A. F. (2011). Exercise training increases size of hippocampus and improves memory. *Proceedings of the National Academy of Sciences of the United States of America*, *108*(7), 3017–22. http://doi.org/10.1073/pnas.1015950108

Eskildsen, S. F., Gyldensted, L., Nagenthiraja, K., Nielsen, R. B., Hansen, M. B., Dalby, R. B., ... & Lund, T. E. (2017). Increased cortical capillary transit time heterogeneity in Alzheimer's disease: a DSC-MRI perfusion study. *Neurobiology of aging*, *50*, 107-118.

Etnier, J. L., Nowell, P. M., Landers, D. M., & Sibley, B. A. (2006). A meta-regression to examine the relationship between aerobic fitness and cognitive performance. *Brain Research Reviews*, *52*(1), 119–130. http://doi.org/10.1016/j.brainresrev.2006.01.002

Fan, A. P., Govindarajan, S. T., Kinkel, R. P., Madigan, N. K., Nielsen, a S., Benner, T., … Mainero, C. (2014). Quantitative oxygen extraction fraction from 7-Tesla MRI phase: reproducibility and application in multiple sclerosis. *Journal of Cerebral Blood Flow and Metabolism : Official Journal of the International Society of Cerebral Blood Flow and Metabolism*, *35*(July), 1–9. http://doi.org/10.1038/jcbfm.2014.187

Faul, F., Erdfelder, E., Buchner, A., & Lang, A.-G. (2009). Statistical power analyses using G*Power 3.1: Tests for correlation and regression analyses. *Behavior Research Methods*, *41*(4), 1149–1160. http://doi.org/10.3758/BRM.41.4.1149

Faul, F., Erdfelder, E., Lang, A.-G., & Buchner, A. (2007). G*Power: A flexible statistical power analysis program for the social, behavioral, and biomedical sciences. *Behavior Research Methods*, *39*(2), 175–191. http://doi.org/10.3758/BF03193146

Fernández-Seara, M. A., Aznárez-sanado, M., Mengual, E., Loayza, F. R., & Pastor, M. A. (2009). NeuroImage Continuous performance of a novel motor sequence leads to highly correlated striatal and hippocampal perfusion increases. *NeuroImage*, *47*(4), 1797–1808. http://doi.org/10.1016/j.neuroimage.2009.05.061

Fernandez-Seara, M. A., Mengual, E., Loayza, F., Superior, E., Es, L., & Pastor, M. A. (2016). Continuous performance of a novel motor sequence leads to highly correlated striatal and hippocampal perfusion increases, (June 2009). http://doi.org/10.1016/j.neuroimage.2009.05.061

Fernández-seara, M. A., Rodgers, Z. B., Englund, E. K., & Wehrli, F. W. (2016). NeuroImage Calibrated bold fMRI with an optimized ASL-BOLD dual-acquisition sequence. *NeuroImage*, *142*, 474–482. http://doi.org/10.1016/j.neuroimage.2016.08.007

Ferré, J.-C., Bannier, E., Raoult, H., Mineur, G., Carsin-Nicol, B., & Gauvrit, J.-Y. (2013). Arterial spin labeling (ASL) perfusion: techniques and clinical use. *Diagnostic and Interventional Imaging*, *94*(12), 1211–23. http://doi.org/10.1016/j.diii.2013.06.010

Firoz, C. K., Jabir, N. R., Khan, M. S., Mahmoud, M., Shakil, S., Damanhouri, G. A., … Kamal, M. A. (2015). An overview on the correlation of neurological disorders with cardiovascular disease. *Saudi Journal of Biological Sciences*, *22*(1), 19–23. http://doi.org/10.1016/j.sjbs.2014.09.003

Floyer-Lea, A., & Matthews, P. M. (2004). Changing brain networks for visuomotor control with increased movement automaticity. *Journal of Neurophysiology*, *92*, 2405–2412. http://doi.org/10.1152/jn.01092.2003

Franke, B., Stein, J. L., Ripke, S., Anttila, V., Hibar, D. P., van Hulzen, K. J. E., … Medland, S. E. (2016). Genetic influences on schizophrenia and subcortical brain volumes: large-scale proof of concept. *Nature Neuroscience*. http://doi.org/10.1038/nn.4228

Fraum, T. J., Ludwig, D. R., Bashir, M. R., & Fowler, K. J. (2017). Gadolinium-Based Contrast Agents : A Comprehensive Risk Assessment. http://doi.org/10.1002/jmri.25625

Gallichan, D., & Jezzard, P. (2009). Variation in the Shape of Pulsed Arterial Spin Labeling Kinetic Curves across the Healthy Human Brain and Its Implications for CBF Quantification, *695*(January), 686–695. http://doi.org/10.1002/mrm.21886

Gauthier, C. J., & Hoge, R. D. (2013). A generalized procedure for calibrated MRI incorporating hyperoxia and hypercapnia. *Human Brain Mapping*, *34*(5). http://doi.org/10.1002/hbm.21495

Gauthier, C. J., & Hoge, R. D. (2013). A Generalized Procedure for Calibrated MRI Incorporating Hyperoxia and Hypercapnia, *1069*(January 2012), 1053–1069. http://doi.org/10.1002/hbm.21495

Gauthier, C. J., Lefort, M., Mekary, S., Desjardins-Crépeau, L., Skimminge, A., Iversen, P., … Hoge, R. D. (2015). Hearts and minds: linking vascular rigidity and aerobic fitness with cognitive aging. *Neurobiology of Aging*, *36*(1), 304–14. http://doi.org/10.1016/j.neurobiolaging.2014.08.018

Ge, Y., Law, M., Johnson, G., Herbert, J., Babb, J. S., Mannon, L. J., & Grossman, R. I. (2005). Dynamic Susceptibility Contrast Perfusion MR Imaging of Multiple Sclerosis Lesions : Characterizing Hemodynamic Impairment and Inflammatory Activity, (July), 1539–1547.

Ge, Y., Zhang, Z., Lu, H., Tang, L., Jaggi, H., Herbert, J., … Grossman, R. I. (2012). Characterizing

brain oxygen metabolism in patients with multiple sclerosis with T2-relaxation-under-spin-tagging MRI. *Journal of Cerebral Blood Flow & Metabolism*, *32*(3), 403–412. http://doi.org/10.1038/jcbfm.2011.191

Germuska, M., Merola, A., Murphy, K., Babic, A., Richmond, L., Khot, S., … Wise, R. G. (2016). NeuroImage A forward modelling approach for the estimation of oxygen extraction fraction by calibrated fMRI. *NeuroImage*, *139*, 313–323. http://doi.org/10.1016/j.neuroimage.2016.06.004

Girouard, H., & Iadecola, C. (2006). Regulation of the Cerebral Circulation Neurovascular coupling in the normal brain and in hypertension , stroke , and Alzheimer disease, *10021*, 328–335. http://doi.org/10.1152/japplphysiol.00966.2005.

Gjedde, A., Vafaee, M. S., & Gjedde, A. (2004). Vafaee MS & Gjedde A . Spatially dissociated flow-metabolism coupling in brain activation . Spatially dissociated flow-metabolism coupling in brain activation, (March). http://doi.org/10.1016/j.neuroimage.2003.10.003

Glover, G. H. (2013). Spiral Imaging in fMRI, *62*(2), 706–712. http://doi.org/10.1016/j.neuroimage.2011.10.039.Spiral

Glover, G. H., & Lee, A. T. (1995). Motion artifacts in fMRI: comparison of 2DFT with PR and spiral scan methods. *Magnetic Resonance in Medicine*, *33*(5), 624-635.

Glover, G. H., Li, T., & Ress, D. (2000). Image-Based Retrospective Correction of Noise. *167*(March), 162–167.

Goel, V., & Dolan, R. J. (2004). Differential involvement of left prefrontal cortex in inductive and deductive reasoning, *93*. http://doi.org/10.1016/j.cognition.2004.03.001

Golestani, A., Chang, C., & Chen, J. J. (2015). Mapping the end-tidal CO2 response function in the resting-state BOLD fMRI signal : Spatial specificity , test – retest reliability and ... *NeuroImage*, *104*(January), 266–277. http://doi.org/10.1016/j.neuroimage.2014.10.031

Gomes, V. A., Casella-filho, A., Chagas, A. C. P., & Tanus-santos, J. E. (2008). Nitric Oxide Enhanced concentrations of relevant markers of nitric oxide formation after exercise training in patients with metabolic syndrome. *Nitric Oxide*, *19*(4), 345–350. http://doi.org/10.1016/j.niox.2008.08.005

Good, C. D., Johnsrude, I., Ashburner, J., Henson, R. N., Friston, K. J., & Frackowiak, R. S. (2001). Cerebral asymmetry and the effects of sex and handedness on brain structure: a voxel-based morphometric analysis of 465 normal adult human brains. *NeuroImage*, *14*(3), 685–700. http://doi.org/10.1006/nimg.2001.0857

Goyal, M. S., Hawrylycz, M., Miller, J. A., Snyder, A. Z., & Raichle, E. (2015). HHS Public Access, *19*(1), 49–57. http://doi.org/10.1016/j.cmet.2013.11.020.Aerobic

Grafton, S. T., Hazeltine, E., & Ivry, R. (1995). Functional mapping of sequence learning in normal humans. *Journal of Cognitive Neuroscience*, *7*(4), 497-510.

Green, D. J., Maiorana, A., O'driscoll, G., & Taylor, R. (2004). Effect of exercise training on endothelium-derived nitric oxide function in humans. *Journal of Physiology*, *561*(Pt 1), 1–25. http://doi.org/10.1113/jphysiol.2004.068197

Greif, D. M., & Eichmann, A. (2014). Vascular biology: brain vessels squeezed to death. *Nature*, *508*(7494), 50-51.

Griffeth, V. E. M., & Buxton, R. B. (2011). A theoretical framework for estimating cerebral

oxygen metabolism changes using the calibrated-BOLD method: Modeling the effects of blood volume distribution, hematocrit, oxygen extraction fraction, and tissue signal properties on the BOLD signal. *NeuroImage*, *58*(1), 198–212. http://doi.org/10.1016/j.neuroimage.2011.05.077

Grill-spector, K., Kourtzi, Z., & Kanwisher, N. (2001). The lateral occipital complex and its role in object recognition, *41*, 1409–1422.

Grubb, B. Y. R. L., Raichle, M. E., Eichling, J. O., & Ph, D. (1974). The Effects of Changes in Paco 2 on Cerebral Blood Volume , Blood Flow , and Vascular Mean Transit Time, *11059*(5).

Hardwick, R. M., Rottschy, C., Miall, R. C., & Eickhoff, S. B. (2013). A quantitative meta-analysis and review of motor learning in the human brain. *NeuroImage*, *67*, 283–297. http://doi.org/10.1016/j.neuroimage.2012.11.020

Haskell, W. L., Lee, I., Pate, R. R., Powell, K. E., & Blair, S. N. (2007). Physical Activity and Public Health : Updated Recommendation for Adults From the American College of Sports Medicine and the American Heart Association, *39*, 1423–1434. http://doi.org/10.1249/mss.0b013e3180616b27

Hayes, S. M., Alosco, M. L., & Forman, D. E. (2014). The Effects of Aerobic Exercise on Cognitive and Neural Decline in Aging and Cardiovascular Disease, 282–290. http://doi.org/10.1007/s13670-014-0101-x

Hayes, S. M., Forman, D. E., & Verfaellie, M. (2014). Cardiorespiratory Fitness Is Associated With Cognitive Performance in Older But Not Younger Adults, 1–8. http://doi.org/10.1093/geronb/gbu167

Heijtel, D. F. R., Mutsaerts, H. J. M. M., Bakker, E., Schober, P., Stevens, M. F., Petersen, E. T., … Nederveen, a J. (2014). Accuracy and precision of pseudo-continuous arterial spin labeling perfusion during baseline and hypercapnia: a head-to-head comparison with ^{15}O H_2O positron emission tomography. *NeuroImage*, *92*, 182–92. http://doi.org/10.1016/j.neuroimage.2014.02.011

Heinonen, I., Koga, S., Kalliokoski, K. K., Musch, T. I., & Poole, D. C. (2015). Heterogeneity of muscle blood flow and metabolism: influence of exercise, aging and disease states. *Exercise and sport sciences reviews*, *43*(3), 117.

Helgerud, J. A. N., Ydal, K. H. K., Wang, E., Karlsen, T., Simonsen, T., Helgesen, C., … Hoff, J. A. N. (2007). Aerobic High-Intensity Intervals Improve ˙ O, (11), 665–671. http://doi.org/10.1249/mss.0b013e3180304570

Hillman, C. H., Erickson, K. I., & Kramer, A. F. (2008). Be smart, exercise your heart: exercise effects on brain and cognition. *Nature reviews neuroscience*, *9*(1), 58.

Hlus, P., Solodkin, A., Noll, D. C., & Small, S. L. (2004). Cortical Plasticity During Three-Week Motor Skill Learning, *21*(3), 1–12.

Hofstetter, S., Tavor, I., Moryosef, S. T., & Assaf, Y. (2013). Short-Term Learning Induces White Matter Plasticity in the Fornix, *33*(31), 12844–12850. http://doi.org/10.1523/JNEUROSCI.4520-12.2013

Hoge, R. D. (2012). Calibrated fMRI. *NeuroImage*, *62*(2), 930–937. http://doi.org/10.1016/j.neuroimage.2012.02.022

Hoge, R. D., Atkinson, J., Gill, B., Crelier, G. R., Marrett, S., & Pike, G. B. (1999). Linear coupling

between cerebral blood flow and oxygen consumption in activated human cortex. *Proceedings of the National Academy of Sciences USA*, *96*(August), 9403–9408.

Hoge, R. D., Atkinson, J., Gill, B., Crelier, R., Marrett, S., & Pike, G. B. (1999). Investigation of BOLD Signal Dependence on Cerebral Blood Flow and Oxygen Consumption : The Deoxyhemoglobin Dilution Model, *863*, 849–863.

Honda, M., Deiber, M., Iba, V., Pascual-leone, A., Zhuang, P., & Hallett, M. (1998). Dynamic cortical involvement in implicit and explicit motor sequence learning A PET study, 2159–2173.

Horn, H., & Federspiel, A. (2012). Semantic Network Disconnection in, 14–23. http://doi.org/10.1159/000337133

Horton, T. J., Grunwald, G. K., Lavely, J., Donahoo, W. T., Horton, T. J., Dow, S., … Lavely, J. (2011). Glucose kinetics differ between women and men , during and after exercise Glucose kinetics differ between women and men , during and after exercise, *80262*, 1883–1894. http://doi.org/10.1152/japplphysiol.01431.2005

Hubbard, N. A., Turner, M. P., Ouyang, M., Himes, L., Thomas, B. P., Hutchison, J. L., … Rypma, B. (2017). Calibrated Imaging Reveals Altered Grey Matter Metabolism Related to White Matter Microstructure and Symptom Severity in Multiple Sclerosis, *0*(February). http://doi.org/10.1002/hbm.23727

Huber, L., Goense, J., Kennerley, A. J., Trampel, R., Guidi, M., Reimer, E., … Möller, H. E. (2015). Cortical lamina-dependent blood volume changes in human brain at 7 T. *NeuroImage*, *107*(December 2014), 23–33. http://doi.org/10.1016/j.neuroimage.2014.11.046

Huber, L., Ivanov, D., Guidi, M., Turner, R., Uluda??, K., M??ller, H. E., & Poser, B. A. (2015). Functional cerebral blood volume mapping with simultaneous multi-slice acquisition. *NeuroImage*, *125*, 1159–1168. http://doi.org/10.1016/j.neuroimage.2015.10.082

Hwang, J., Castelli, D. M., & Gonzalez-lima, F. (2017). Physiology & Behavior The positive cognitive impact of aerobic fi tness is associated with peripheral in fl ammatory and brain-derived neurotrophic biomarkers in young adults. *Physiology & Behavior*, *179*(January), 75–89. http://doi.org/10.1016/j.physbeh.2017.05.011

Iadecola, C., & Nedergaard, M. (2007). Glial regulation of the cerebral microvasculature, *10*(11), 1369–1376. http://doi.org/10.1038/nn2003

Iannetti, G. D., & Wise, R. G. (2007a). BOLD functional MRI in disease and pharmacological studies : room for improvement ?, *25*, 978–988. http://doi.org/10.1016/j.mri.2007.03.018

Iannetti, G. D., & Wise, R. G. (2007b). BOLD functional MRI in disease and pharmacological studies: room for improvement? *Magnetic Resonance Imaging*, *25*(6), 978–88. http://doi.org/10.1016/j.mri.2007.03.018

Inglese, M., Park, S., Johnson, G., Babb, J. S., & Miles, L. (2017). Deep Gray Matter Perfusion in Multiple Sclerosis, *64*.

Ivey, F. M., Ryan, A. S., Hafer-macko, C. E., & Macko, R. F. (2011). Training in Hemiparetic Stroke Survivors, (18). http://doi.org/10.1161/STROKEAHA.110.607879

Jenkinson, M., Bannister, P., Brady, M., & Smith, S. (2002). Improved optimization for the robust and accurate linear registration and motion correction of brain images.

NeuroImage, *17*(2), 825–841. http://doi.org/10.1016/S1053-8119(02)91132-8

Jenkinson, M., & Smith, S. M. (2001). A global optimization method for robust affine registration of brain images. *Medical Imaging Analysis*, *5*, 143–156.

Jespersen, S. N., & Østergaard, L. (2012). The roles of cerebral blood flow , capillary transit time heterogeneity , and oxygen tension in brain oxygenation and metabolism, 264–277. http://doi.org/10.1038/jcbfm.2011.153

Jones, T. A., Chu, C. J., Grande, L. A., & Gregory, A. D. (1999). Motor Skills Training Enhances Lesion-Induced Structural Plasticity in the Motor Cortex of Adult Rats, *19*(22), 10153–10163.

Jonge, X. A. K. J. De. (2003). Effects of the Menstrual Cycle on Exercise Performance, *33*(11), 833–851.

Joyner, M. J. (2000). Effect of exercise on arterial compliance. *Circulation*, *102*, 1214–1215. http://doi.org/10.1161/01.CIR.102.11.1214

Juurlink, B. H. J. (2013). The evidence for hypoperfusion as a factor in multiple sclerosis lesion development. *Multiple Sclerosis International*, *2013*, 598093. http://doi.org/10.1155/2013/598093

Kalliokoski, K. K., Oikonen, V., Takala, T. O., Kari, K., Oikonen, V., Teemu, O., … Nuu-, P. (2001). Enhanced oxygen extraction and reduced flow heterogeneity in exercising muscle in endurance-trained men, 1015–1021.

Kastrup, A., Kru, G., Neumann-haefelin, T., Glover, G. H., & Moseley, M. E. (2002). Changes of Cerebral Blood Flow , Oxygenation , and Oxidative Metabolism during Graded Motor Activation, *82*, 74–82. http://doi.org/10.1006/nimg.2001.0916

Kerr, A. L., Steuer, E. L., Pochtarev, V., & Swain, R. A. (2010). ANGIOGENESIS BUT NOT NEUROGENESIS IS CRITICAL FOR NORMAL LEARNING AND MEMORY ACQUISITION. *NSC*, *171*(1), 214–226. http://doi.org/10.1016/j.neuroscience.2010.08.008

Khan, N. A., & Hillman, C. H. (2014). The Relation of Childhood Physical Activity and Aerobic Fitness to Brain Function and Cognition : A Review, 138–146.

Kidd, D., Barkhof, F., Mcconnell, R., Algra, P. R., Allen, I. V, & Revesz, T. (1999). Cortical lesions in multiple sclerosis, 17–26.

Kim, S.-G., & Ogawa, S. (2012). Biophysical and Physiological Origins of Blood Oxygenation Level-Dependent fMRI Signals. *Journal of Cerebral Blood Flow & Metabolism*, *32*(7), 1188–1206. http://doi.org/10.1038/jcbfm.2012.23

Kingwell, E., Marriott, J. J., Jetté, N., Pringsheim, T., Makhani, N., Morrow, S. A., … Marrie, R. A. (2013). Incidence and prevalence of multiple sclerosis in Europe : a systematic review.

Kister, I., Bacon, T. E., Chamot, E., Salter, A. R., Cutter, G. R., Kalina, J. T., & Herbert, J. (2013). Natural history of multiple sclerosis symptoms. *International Journal of MS Care*, *15*(3), 146–158. http://doi.org/10.7224/1537-2073.2012-053

Klauke, K., & Borght, K. Van Der. (2009). Physical exercise leads to rapid adaptations in hippocampal vasculature : Temporal dynamics and relationship to cell ... Physical Exercise Leads to Rapid Adaptations in Hippocampal Vasculature : Temporal Dynamics and Relationship to Cell Proliferation and, (October). http://doi.org/10.1002/hipo.20545

Kleemeyer, M. M., Kühn, S., Prindle, J., Bodammer, N. C., Brechtel, L., Garthe, A., … Lindenberger, U. (2015). Changes in fitness are associated with changes in hippocampal microstructure and hippocampal volume among older adults. *NeuroImage*. http://doi.org/10.1016/j.neuroimage.2015.11.026

Kleim, J. A., Hogg, T. M., Vandenberg, P. M., Cooper, N. R., Bruneau, R., & Remple, M. (2004). Cortical Synaptogenesis and Motor Map Reorganization Occur during Late , But Not Early , Phase of Motor Skill Learning, *24*(3), 628–633. http://doi.org/10.1523/JNEUROSCI.3440-03.2004

Knaepen, K., Goekint, M., Heyman, E. M., & Meeusen, R. (2010). Neuroplasticity - exercise-induced response of peripheral brain-derived neurotrophic factor: a systematic review of experimental studies in human subjects. *Sports Medicine (Auckland, N.Z.)*, *40*(9), 765–801. http://doi.org/10.2165/11534530-000000000-00000

Knopman, D., & Nissen, M. J. (1991). PROCEDURAL LEARNING IS IMPAIRED IN HUNTINGTON ' S DISEASE : EVIDENCE FROM THE SERIAL REACTION TIME TASK that the brain has separate learning systems has generated a great deal of controversy [12 , 22 , 29]. The neuropsychological evidence is perhaps the, *29*(3), 245–254.

Kobilo, T., Liu, Q. R., Gandhi, K., Mughal, M., Shaham, Y., & van Praag, H. (2011). Running is the neurogenic and neurotrophic stimulus in environmental enrichment. *Learning & memory*, *18*(9), 605-609.

Kodama, S., Saito, K., Tanaka, S., Maki, M., Yachi, Y., Asumi, M., … Sone, H. (2009). CLINICIAN ' S CORNER Cardiorespiratory Fitness as a Quantitative Predictor of All-Cause Mortality and Cardiovascular Events. *Journal of American Medical Association*, *301*(19), 2024–2035.

Korman, M., Raz, N., Flash, T., & Karni, A. (2003). Multiple shifts in the representation of a motor sequence during the acquisition of skilled performance.

Kramer, A. F. (2010). Basal Ganglia Volume Is Associated with Aerobic Fitness in Preadolescent Children, 249–256. http://doi.org/10.1159/000316648

Krieger, S. N., Gauthier, C. J., Ivanov, D., Huber, L., Roggenhofer, E., Sehm, B., … Egan, G. F. (2014). NeuroImage Regional reproducibility of calibrated BOLD functional MRI : Implications for the study of cognition and plasticity. *NeuroImage*, *101*, 8–20. http://doi.org/10.1016/j.neuroimage.2014.06.072

Kro, K., Fehsel, K., & Kolb-bachofen, V. (1997). Nitric Oxide : Cytotoxicity versus Cytoprotection — How , Why , When , and Where ?, *1*(2), 107–120.

Krogh, A. (1919). The number and distribution of capillaries in muscles with calculations of the oxygen pressure head necessary for supplying the tissue. *The Journal of physiology*, *52*(6), 409-415.

Laguna, L., & Cognitive, H. (1995). Karni , A . et al . Functional MRI evidence for adult motor cortex plasticity during motor skill learning . Nature 377 , 155-158, (May 2016), 155–158. http://doi.org/10.1038/377155a0

Lajoie, I., Tancredi, F. B., & Hoge, R. D. (2016). Regional Reproducibility of BOLD Calibration Parameter M , OEF and Resting-State CMRO 2 Measurements with QUO2 MRI, 1–31. http://doi.org/10.1371/journal.pone.0163071

Lakens, D. (2013). Calculating and reporting effect sizes to facilitate cumulative science : a practical primer for t -tests and ANOVAs, *4*(November), 1–12.

http://doi.org/10.3389/fpsyg.2013.00863

Landi, S. M., Baguear, F., & Della-maggiore, V. (2011). One Week of Motor Adaptation Induces Structural Changes in Primary Motor Cortex That Predict Long-Term Memory One Year Later, *31*(33), 11808–11813. http://doi.org/10.1523/JNEUROSCI.2253-11.2011

Law, M., Ge, Y., Johnson, G., Babb, J. S., & Grossman, R. I. (2007). Correlation of Diffusion Tensor and Dynamic Perfusion MR Imaging Metrics in Normal- Appearing Corpus Callosum : Support for Primary Hypoperfusion in Multiple Sclerosis.

Lee, D., Artero, E. G., Sui, X., & Blair, S. N. (2010). Mortality trends in the general population: the importance of cardiorespiratory fitness. *Journal of Psychopharmacology (Oxford, England)*, *24*(4 Suppl), 27–35. http://doi.org/10.1177/1359786810382057

Leithner, C., & Royl, G. (2013a). The oxygen paradox of neurovascular coupling, *34*(1), 19–29. http://doi.org/10.1038/jcbfm.2013.181

Leithner, C., & Royl, G. (2013b). The oxygen paradox of neurovascular coupling, *34*(1), 19–29. http://doi.org/10.1038/jcbfm.2013.181

Levin, J. M., Frederick, B. D., Ross, M. H., Fox, J. F., Von Rosenberg, H. L., Kaufman, M. J., … Renshaw, P. F. (2001). Influence of baseline hematocrit and hemodilution on BOLD fMRI activation. *Magnetic Resonance Imaging*, *19*(8), 1055–1062. http://doi.org/10.1016/S0730-725X(01)00460-X

Levin, V. A., & Ausman, J. I. (1969). Relationship of peripheral venous hematocrit to brain hematocrit. *Journal of applied physiology*, *26*(4), 433-437.

Liang, X., Connelly, A., & Calamante, F. (2013). Improved Partial Volume Correction for Single Inversion Time Arterial Spin Labeling Data, *C*, 531–537. http://doi.org/10.1002/mrm.24279

Liang, X., Zou, Q., He, Y., & Yang, Y. (2013). Coupling of functional connectivity and regional cerebral blood fl ow reveals a physiological basis for network hubs of the human brain, *110*(5), 1929–1934. http://doi.org/10.1073/pnas.1214900110

Lipp, I., Murphy, K., Caseras, X., & Wise, R. (2013). Agreement and repeatability of vascular reactivity estimates based on a breath-hold task and a resting state scan, (2001).

Lipp, I., & Tomassini, V. (2015). Neuroplasticity and motor rehabilitation in multiple sclerosis, *6*(March), 1–3. http://doi.org/10.1038/nn.3045

Liu, T. T., & Wong, E. C. (2005). A signal processing model for arterial spin labeling functional MRI. *NeuroImage*, *24*(1), 207–215. http://doi.org/10.1016/j.neuroimage.2004.09.047

Logothetis, N. K., Pauls, J., Augath, M., Trinath, T., & Oeltermann, A. (2001). Neurophysiological investigation of the basis of the fMRI signal. *Nature*, *412*(6843), 150–7. http://doi.org/10.1038/35084005

Logothetis, N. K., & Pfeuffer, J. (2004). On the nature of the BOLD f MRI contrast mechanism, *22*, 1517–1531. http://doi.org/10.1016/j.mri.2004.10.018

Lu, H., Clingman, C., Golay, X., & Van Zijl, P. C. M. (2004). Determining the longitudinal relaxation time (T1) of blood at 3.0 tesla. *Magnetic Resonance in Medicine*, *52*(3), 679–682. http://doi.org/10.1002/mrm.20178

Lu, H., Donahue, M. J., & Van Zijl, P. C. M. (2006). Detrimental effects of BOLD signal in arterial

spin labeling fMRI at high field strength. *Magnetic Resonance in Medicine*, *56*(3), 546–552. http://doi.org/10.1002/mrm.20976

Lu, H., Golay, X., Pekar, J. J., & Zijl, P. C. M. Van. (2003). Functional Magnetic Resonance Imaging Based on Changes in Vascular Space Occupancy, *274*, 263–274. http://doi.org/10.1002/mrm.10519

Lu, H., Hua, J., & van Zijl, P. C. M. (2013). Noninvasive functional imaging of cerebral blood volume with vascular-space-occupancy (VASO) MRI. *NMR in Biomedicine*, *26*(8), 932–948. http://doi.org/10.1002/nbm.2905

Lu, H., Xu, F., Rodrigue, K. M., Kennedy, K. M., Cheng, Y., Flicker, B., … Park, D. C. (2011). Alterations in Cerebral Metabolic Rate and Blood Supply across the Adult Lifespan, (June). http://doi.org/10.1093/cercor/bhq224

Ma, L., Narayana, S., Robin, D. A., Fox, P. T., & Xiong, J. (2011). NeuroImage Changes occur in resting state network of motor system during 4 weeks of motor skill learning. *NeuroImage*, *58*(1), 226–233. http://doi.org/10.1016/j.neuroimage.2011.06.014

Ma, L., Wang, B., Narayana, S., Hazeltine, E., Chen, X., Robin, A., … Xiong, J. (2011). NIH Public Access, 64–76. http://doi.org/10.1016/j.brainres.2009.12.073.Changes

Machielsen, W. C. M., Rombouts, S. A. R. B., Barkhof, F., Scheltens, P., & Witter, M. P. (2017). FMRI of visual encoding : Reproducibility of activation fMRI of Visual Encoding : Reproducibility of Activation, *193*(April 2000). http://doi.org/10.1002/(SICI)1097-0193(200003)9

MacIntosh, B. J., Crane, D. E., Sage, M. D., Rajab, a. S., Donahue, M. J., McIlroy, W. E., & Middleton, L. E. (2014). Impact of a single bout of aerobic exercise on regional brain perfusion and activation responses in healthy young adults. *PLoS ONE*, *9*(1). http://doi.org/10.1371/journal.pone.0085163

MacIntosh, B. J., Filippini, N., Chappell, M. a, Woolrich, M. W., Mackay, C. E., & Jezzard, P. (2010). Assessment of arterial arrival times derived from multiple inversion time pulsed arterial spin labeling MRI. *Magnetic Resonance in Medicine : Official Journal of the Society of Magnetic Resonance in Medicine / Society of Magnetic Resonance in Medicine*, *63*(3), 641–7. http://doi.org/10.1002/mrm.22256

Macintosh, B. J., Swardfager, W., Crane, D. E., Ranepura, N., & Saleem, M. (2014). Cardiopulmonary Fitness Correlates with Regional Cerebral Grey Matter Perfusion and Density in Men with Coronary Artery Disease, *9*(3), 3–9. http://doi.org/10.1371/journal.pone.0091251

Madsen, P. L., Hasselbalch, S. G., Hagemann, L. P., Olsen, K. S., Bülow, J., Holm, S., … Lassen, N. A. (1995). Persistent Resetting of the Cerebral Oxygen/Glucose Uptake Ratio by Brain Activation: Evidence Obtained with the Kety—Schmidt Technique. *Journal of Cerebral Blood Flow & Metabolism*, *15*(3), 485–491. http://doi.org/10.1038/jcbfm.1995.60

Mainero, C., Ph, D., & Caramia, F. (2006). Views & Reviews Functional Brain Reorganization in Multiple Sclerosis : Evidence from fMRI Studies, 104–114. http://doi.org/10.1111/j.1552-6569.2006.00029.x

Mairbäurl, H. (2013). Red blood cells in sports : effects of exercise and training on oxygen supply by red blood cells, *4*(November), 1–13. http://doi.org/10.3389/fphys.2013.00332

Malek, M. O. H. H., Berger, D. E., Housh, T. J., Coburn, J. W., & Beck, T. W. (2004). ˙ O 2max

Equations for Aerobically Validity of V Trained Males and Females, (November 2003), 1427–1432. http://doi.org/10.1249/01.MSS.0000135795.60449.CE

Mancini, L., Ciccarelli, O., Manfredonia, F., Thornton, J. S., Agosta, F., Barkhof, F., … Yousry, T. (2009). NeuroImage Short-term adaptation to a simple motor task : A physiological process preserved in multiple sclerosis. *NeuroImage*, *45*(2), 500–511. http://doi.org/10.1016/j.neuroimage.2008.12.006

Mansfield, P. (1977). Multi-planar image formation using NMR spin echoes. *Journal of Physics C: Solid State Physics*, *10*(3), L55.

Mark, C. I., Fisher, J. A., & Pike, G. B. (2011). NeuroImage Improved fMRI calibration : Precisely controlled hyperoxic versus hypercapnic stimuli, *54*, 1102–1111. http://doi.org/10.1016/j.neuroimage.2010.08.070

Mark, C. I., Mazerolle, E. L., & Chen, J. J. (2015). Metabolic and vascular origins of the BOLD effect: Implications for imaging pathology and resting-state brain function. *Journal of Magnetic Resonance Imaging*, *42*(2), 231-246.

Marshall, O., Chawla, S., Lu, H., Pape, L., & Ge, Y. (2016). Cerebral blood flow modulation insufficiency in brain networks in multiple sclerosis: A hypercapnia MRI study. *Journal of Cerebral Blood Flow & Metabolism*. http://doi.org/10.1177/0271678X16654922

Marshall, O., Lu, H., Brisset, J.-C., Xu, F., Liu, P., Herbert, J., … Ge, Y. (2014). Impaired cerebrovascular reactivity in multiple sclerosis. *JAMA Neurology*, *71*(10), 1275–81. http://doi.org/10.1001/jamaneurol.2014.1668

Martin, a J., Friston, K. J., Colebatch, J. G., & Frackowiak, R. S. (1991). Decreases in regional cerebral blood flow with normal aging. *Journal of Cerebral Blood Flow and Metabolism : Official Journal of the International Society of Cerebral Blood Flow and Metabolism*, *11*, 684–689. http://doi.org/10.1038/jcbfm.1991.121

Mathiesen, C., Caesar, K., Thomsen, K., Hoogland, T. M., Witgen, B. M., Brazhe, A., & Lauritzen, M. (2011). Activity-dependent Increases in Local Oxygen Consumption Correlate with Postsynaptic Currents in the Mouse Cerebellum In Vivo. *Journal of Neuroscience*, *31*(50), 18327–18337. http://doi.org/10.1523/JNEUROSCI.4526-11.2011

Mayhew, S. D., Macintosh, B. J., Dirckx, S. G., Domenico, G., & Wise, R. G. (2010). Coupling of simultaneously acquired electrophysiological and haemodynamic responses during visual stimulation. *Magnetic Resonance Imaging*. http://doi.org/10.1016/j.mri.2010.03.027

Merola, A. (2016). *Development of MRI methods to map cerebral metabolic oxygen consumption in humans*. Cardiff University.

Merola, A., Germuska, M. A., Warnert, E. A., Richmond, L., Helme, D., Khot, S., … Wise, R. G. (2017). Mapping the pharmacological modulation of brain oxygen metabolism: the effects of caffeine on absolute CMRO 2 measured using dual calibrated fMRI. *NeuroImage*, *155*(August 2016), 331–343. http://doi.org/10.1016/j.neuroimage.2017.03.028

Merola, A., Murphy, K., Stone, A. J., Germuska, M. A., Griffeth, V. E. M., Blockley, N. P., … Wise, R. G. (2013). Measurement of oxygen extraction fraction (OEF): an optimised BOLD signal model for use with hypercapnic and hyperoxic calibration. *NeuroImage*, (1998), 5–6. http://doi.org/10.1016/j.neuroimage.2016.01.021

Miall, R. C., & Robertson, E. M. (2006). Functional imaging: is the resting brain resting?. *Current*

Biology, *16*(23), R998-R1000.

Midgley, A. W., & Carroll, S. (2009). Emergence of the verification phase procedure for confirming 'true'VO2max. *Scandinavian journal of medicine & science in sports*, *19*(3), 313-322.

Miguel, D., Beelen, R., Fierens, Y., Cambron, M., Vanbinst, A., & Verborgh, C. (2013). Cerebral hypoperfusion in multiple sclerosis is reversible and mediated by endothelin-1. http://doi.org/10.1073/pnas.1222560110/-/DCSupplemental.www.pnas.org/cgi/doi/10.1073/pnas.1222560110

Milani, R. V, Lavie, C. J., Mehra, M. R., & Ventura, H. O. (2006). Understanding the basics of cardiopulmonary exercise testing. *Mayo Clinic Proceedings. Mayo Clinic*, *81*(12), 1603–1611. http://doi.org/10.4065/81.12.1603

Mohtasib, R. S., Lumley, G., Goodwin, J. A., Emsley, H. C. A., Sluming, V., & Parkes, L. M. (2012). NeuroImage Calibrated fMRI during a cognitive Stroop task reveals reduced metabolic response with increasing age, *59*, 1143–1151. http://doi.org/10.1016/j.neuroimage.2011.07.092

Morgen, K., Kadom, N., Sawaki, L., Tessitore, A., Ohayon, J., Mcfarland, H., … Cohen, L. G. (2004). Training-dependent plasticity in patients with multiple sclerosis, 2506–2517. http://doi.org/10.1093/brain/awh266

Motl, R. W., & Pilutti, L. a. (2012). The benefits of exercise training in multiple sclerosis. *Nature Reviews. Neurology*, *8*(9), 487–97. http://doi.org/10.1038/nrneurol.2012.136

Muir, E. R., Cardenas, D. P., Duong, T. Q., Antonio, S., Antonio, S., Antonio, S., & Antonio, S. (2017). HHS Public Access, 498–503. http://doi.org/10.1016/j.neuroimage.2016.03.040.MRI

Muoio, V., Persson, P. B., & Sendeski, M. M. (2014). The neurovascular unit – concept review, 790–798. http://doi.org/10.1111/apha.12250

Murphy, K., Birn, R. M., & Bandettini, P. A. (2013a). NeuroImage Resting-state fMRI confounds and cleanup. *NeuroImage*, *80*, 349–359. http://doi.org/10.1016/j.neuroimage.2013.04.001

Murphy, K., Birn, R. M., & Bandettini, P. A. (2013b). Resting-state fMRI confounds and cleanup. *NeuroImage*, *80*, 349–359. http://doi.org/10.1016/j.neuroimage.2013.04.001

Murphy, K., & Fox, M. D. (2017). NeuroImage Towards a consensus regarding global signal regression for resting state functional connectivity MRI. *NeuroImage*, *154*(November 2016), 169–173. http://doi.org/10.1016/j.neuroimage.2016.11.052

Murphy, K., Harris, A. D., & Wise, R. G. (2011). Robustly measuring vascular reactivity differences with breath-hold: normalising stimulus-evoked and resting state BOLD fMRI data. *NeuroImage*, *54*(1), 369–79. http://doi.org/10.1016/j.neuroimage.2010.07.059

Murrell, C. J., Cotter, J. D., Thomas, K. N., Lucas, S. J. E., Williams, M. J. a, & Ainslie, P. N. (2013). Cerebral blood flow and cerebrovascular reactivity at rest and during sub-maximal exercise: effect of age and 12-week exercise training. *Age (Dordrecht, Netherlands)*, *35*(3), 905–20. http://doi.org/10.1007/s11357-012-9414-x

Nieman, D. C., & Kernodle, M. W. (2001). Prediction of Maximal Aerobic Power in Adolescents from Cycle Ergometry, 167–172.

Nishijima, T., Torres-Aleman, I., & Soya, H. (2016). Exercise and cerebrovascular plasticity. *Progress in Brain Research*, *225*(October), 243–268. http://doi.org/10.1016/bs.pbr.2016.03.010

Nissen, M. J., & Bullemer, P. (1987). Attentional requirements of learning: Evidence from performance measures. *Cognitive Psychology*, *19*(1), 1–32. http://doi.org/10.1016/0010-0285(87)90002-8

Offenhauser, N., Thomsen, K., Caesar, K., & Lauritzen, M. (2005). Activity-induced tissue oxygenation changes in rat cerebellar cortex: interplay of postsynaptic activation and blood flow. *The Journal of Physiology*, *565*(1), 279–294. http://doi.org/10.1113/jphysiol.2005.082776

Ogawa, S., Menon, R. S., Tank, D. W., Kim, S. G., Merkle, H., Ellermann, J. M., … Ugurbil, K. (1993). Functional brain mapping by blood oxygenation level-dependent contrast magnetic resonance imaging. A comparison of signal characteristics with a biophysical model. *Biophysical Journal*, *64*(3), 803–812. http://doi.org/10.1016/S0006-3495(93)81441-3

Olson, I. R., & Plotzker, A. (2007). The Enigmatic temporal pole : a review of findings on social and emotional processing, 1718–1731. http://doi.org/10.1093/brain/awm052

Olson, I. R., Rao, H., Moore, K. S., Wang, J., Detre, J. A., & Aguirre, G. V. K. (2006). Using perfusion fMRI to measure continuous changes in neural activity with learning, *60*, 262–271. http://doi.org/10.1016/j.bandc.2005.11.010

Ookawara, T., Suzuk, K., Haga, S., Ha, S., Chung, K. S., Toshinai, K., ... & Hitomi, Y. (2002). Transcription regulation of gene expression in human skeletal muscle in response to endurance training. *Research communications in molecular pathology and pharmacology*, *111*(1-4), 41-54.Osch, M. J., Hendrikse, J., & van der Grond, J. (2007). Sensitivity comparison of multiple vs. single inversion time pulsed arterial spin labeling fMRI. *Journal of magnetic resonance imaging*, *25*(1), 215-221.

Osch, M. J. P. Van, Teeuwisse, W. M., Chen, Z., Suzuki, Y., Helle, M., & Schmid, S. (2017). Advances in arterial spin labelling MRI methods for measuring perfusion and collateral flow. http://doi.org/10.1177/0271678X17713434

Osch, M. J. P. Van, Teeuwisse, W. M., Walderveen, M. A. A. Van, Hendrikse, J., Kies, D. A., & Buchem, M. A. Van. (2009). Can Arterial Spin Labeling Detect White Matter Perfusion Signal ?, *173*(April), 165–173. http://doi.org/10.1002/mrm.22002

Østergaard, L., Engedal, T. S., Aamand, R., Mikkelsen, R., Iversen, N. K., Anzabi, M., … Rasmussen, M. (2014). Capillary transit time heterogeneity and flow-metabolism coupling after traumatic brain injury, (June), 1585–1598. http://doi.org/10.1038/jcbfm.2014.131

Østergaard, L., Engedal, T. S., Moreton, F., Hansen, M. B., Wardlaw, J. M., Dalkara, T., … Muir, K. W. (2016). Cerebral small vessel disease : Capillary pathways to stroke and cognitive decline. http://doi.org/10.1177/0271678X15606723

Østergaard, L., Finnerup, N. B., Terkelsen, A. J., Olesen, R. A., Drasbek, K. R., Knudsen, L., … Andersen, H. (2015). The effects of capillary dysfunction on oxygen and glucose extraction in diabetic neuropathy. *Diabetologia*, *58*(4), 666–677. http://doi.org/10.1007/s00125-014-3461-z

Ota, M., Sato, N., Nakata, Y., Ito, K., Kamiya, K., Maikusa, N., … Kunugi, H. (2013). Abnormalities of cerebral blood flow in multiple sclerosis: A pseudocontinuous arterial spin labeling MRI study. *Magnetic Resonance Imaging*, *31*(6), 990–995. http://doi.org/10.1016/j.mri.2013.03.016

Oxide, T. H. E. N., & Of, D. (1947). THE NITROUS OXIDE METHOD FOR THE QUANTITATIVE, (1), 476–483.

Paling, D., Golay, X., & Miller, D. (2011). Energy failure in multiple sclerosis and its investigation using MR techniques, 2113–2127. http://doi.org/10.1007/s00415-011-6117-7

Paling, D., Thade Petersen, E., Tozer, D. J., Altmann, D. R., Wheeler-Kingshott, C. A. M., Kapoor, R., … Golay, X. (2014). Cerebral arterial bolus arrival time is prolonged in multiple sclerosis and associated with disability. *Journal of Cerebral Blood Flow and Metabolism : Official Journal of the International Society of Cerebral Blood Flow and Metabolism*, *34*(1), 34–42. http://doi.org/10.1038/jcbfm.2013.161

Park, M. G., Yang, T. Il, Oh, S. J., Baik, S. K., Kang, Y. H., & Park, K. P. (2014). Multiple hypointense vessels on susceptibility-weighted imaging in acute ischemic stroke: Surrogate marker of oxygen extraction fraction in penumbra? *Cerebrovascular Diseases*, *38*(4), 254–261. http://doi.org/10.1159/000367709

Parkes, L. M. (2005). Quantification of cerebral perfusion using arterial spin labeling: Two-compartment models. *Journal of Magnetic Resonance Imaging*, *22*(6), 732–736. http://doi.org/10.1002/jmri.20456

Parkes, L. M., & Tofts, P. S. (2002). Improved Accuracy of Human Cerebral Blood Perfusion Measurements Using Arterial Spin Labeling : Accounting for Capillary Water Permeability, *41*, 27–41. http://doi.org/10.1002/mrm.10180

Paula, L., Emma, L., & Ian, D. (2015). and Brookes , Matthew Jon and Gowland , Penny A . and Francis , Susan T . (2015) The effect of isocapnic hyperoxia on neurophysiology as measured with MRI and MEG . NeuroImage , 105 . pp . 323-331 . ISSN 1053-, 323–331.

Paulson, O. B. (2002). B lood – brain barrier , brain metabolism and cerebral blood flow, *12*, 495–501.

Pereira, A. C., Huddleston, D. E., Brickman, A. M., Sosunov, A. a, Hen, R., McKhann, G. M., … Small, S. a. (2007). An in vivo correlate of exercise-induced neurogenesis in the adult dentate gyrus. *Proceedings of the National Academy of Sciences of the United States of America*, *104*(13), 5638–43. http://doi.org/10.1073/pnas.0611721104

Petcharunpaisan, S., Ramalho, J., & Castillo, M. (2010). World Journal of Radiology, *2*(10), 384–398. http://doi.org/10.4329/wjr.v2.i10.384

Petr, J., Schramm, G., Hofheinz, F., Langner, J., & Van Den Hoff, J. (2013). Partial volume correction in arterial spin labeling using a Look-Locker sequence. *Magnetic Resonance in Medicine*, *70*(6), 1535–1543. http://doi.org/10.1002/mrm.24601

Petzinger, G. M., Fisher, B. E., McEwen, S., Beeler, J. a, Walsh, J. P., & Jakowec, M. W. (2013). Exercise-enhanced neuroplasticity targeting motor and cognitive circuitry in Parkinson's disease. *The Lancet. Neurology*, *12*(7), 716–26. http://doi.org/10.1016/S1474-4422(13)70123-6

Platta, M. E., Ensari, I., Motl, R. W., & Pilutti, L. A. (2016). *Effect of Exercise Training on Fitness in Multiple Sclerosis: A Meta-Analysis*. *Archives of Physical Medicine and Rehabilitation*

(Vol. 97). Elsevier Ltd. http://doi.org/10.1016/j.apmr.2016.01.023

Poldrack, R. A. (2015). Developmental Cognitive Neuroscience Is " efficiency " a useful concept in cognitive neuroscience ? *Accident Analysis and Prevention*, *11*, 12–17. http://doi.org/10.1016/j.dcn.2014.06.001

Polman, C. H., Reingold, S. C., Banwell, B., Clanet, M., Cohen, J. A., Filippi, M., … Connor, P. O. (2011). Diagnostic Criteria for Multiple Sclerosis : 2010 Revisions to the McDonald Criteria. http://doi.org/10.1002/ana.22366

Poole, D. C., Wilkerson, Æ. D. P., & Jones, A. M. (2008). Validity of criteria for establishing maximal O 2 uptake during ramp exercise tests, 403–410. http://doi.org/10.1007/s00421-007-0596-3

Powers, W. J. (2009). PET studies of cerebral metabolism in Parkinson Disease. *Journal of Bioenergetics and Biomembranes*, *41*(6), 505–508. http://doi.org/10.1007/s10863-009-9251-5

Prakash, R. S., Patterson, B., Janssen, A., Abduljalil, A., & Boster, A. (2011). Physical activity associated with increased resting-state functional connectivity in multiple sclerosis. *Journal of the International Neuropsychological Society : JINS*, *17*(6), 986–97. http://doi.org/10.1017/S1355617711001093

Prakash, R. S., Snook, E. M., Erickson, K. I., Colcombe, S. J., Voss, M. W., Motl, R. W., & Kramer, A. F. (2007). Cardiorespiratory fitness: A predictor of cortical plasticity in multiple sclerosis. *NeuroImage*, *34*(3), 1238–1244. http://doi.org/10.1016/j.neuroimage.2006.10.003

Prakash, R. S., Snook, E. M., Motl, R. W., & Kramer, A. F. (2010). Aerobic fitness is associated with gray matter volume and white matter integrity in multiple sclerosis. *Brain Research*, *1341*, 41–51. http://doi.org/10.1016/j.brainres.2009.06.063

Pries, A. R., Fritzsche, A., Ley, K., & Gaehtgens, P. (1920). Redistribution of Red Blood Cell Flow in Microcirculatory Networks by Hemodilution.

Prosperini, L., Piattella, M. C., & Giannì, C. (2015). Functional and Structural Brain Plasticity Enhanced by Motor and Cognitive Rehabilitation in Multiple Sclerosis. *Neural Plasticity*, *2015*, 481574. http://doi.org/10.1155/2015/481574

Puttemans, V., Wenderoth, N., & Swinnen, S. P. (2005). Changes in Brain Activation during the Acquisition of a Multifrequency Bimanual Coordination Task : From the Cognitive Stage to Advanced Levels of Automaticity, *25*(17), 4270–4278. http://doi.org/10.1523/JNEUROSCI.3866-04.2005

Raichle, M. E. (1986). Focal physiological uncoupling of cerebral blood flow and oxidative metabolism during somatosensory stimulation in human subjects, *83*(February), 1140–1144.

Raichle, M. E. (1998). The acquisition of skilled motor performance : Fast and slow experience-driven changes in primary motor cortex, *95*(February), 861–868.

Raoult, H., Petr, J., Bannier, E., Stamm, A., & Gauvrit, J. (2011). NeuroImage Arterial spin labeling for motor activation mapping at 3T with a 32-channel coil : Reproducibility and spatial accuracy in comparison with BOLD fMRI. *NeuroImage*, *58*(1), 157–167. http://doi.org/10.1016/j.neuroimage.2011.06.011

Rashid, W., Parkes, L. M., Ingle, G. T., Chard, D. T., Toosy, A. T., Altmann, D. R., ... & Miller, D. H. (2004). Abnormalities of cerebral perfusion in multiple sclerosis. *Journal of Neurology, Neurosurgery & Psychiatry*, *75*(9), 1288-1293.

Rasova, K., Havrdova, E., Brandejsky, P., Zálisová, M., Foubikova, B., & Martinkova, P. (2006). Comparison of the influence of different rehabilitation programmes on clinical, spirometric and spiroergometric parameters in patients with multiple sclerosis. *Multiple Sclerosis (Houndmills, Basingstoke, England)*, *12*(January 2005), 227–234. http://doi.org/10.1191/135248506ms1248oa

Rasova, K., Prochazkova, M., Tintera, J., Ibrahim, I., Zimova, D., & Stetkarova, I. (2015). Motor programme activating therapy influences adaptive brain functions in multiple sclerosis. *International Journal of Rehabilitation Research*, *38*(1), 49–54. http://doi.org/10.1097/MRR.0000000000000090

Rauch, S. L., Whalen, P. J., Savage, C. R., Curran, T., Kendrick, A., Brown, H. D., … Rosen, B. R. (1997). Striatal recruitment during an implicit sequence learning task as measured by functional magnetic resonance imaging. *Human Brain Mapping*, *5*(2), 124–132. http://doi.org/10.1002/(SICI)1097-0193(1997)5:2<124::AID-HBM6>3.0.CO;2-5

Restom, K., Bangen, K. J., Bondi, M. W., Perthen, J. E., & Liu, T. (2008). NIH Public Access, *37*(2), 430–439.

Richiardi, J., Monsch, A. U., Haas, T., Barkhof, F., Van de Ville, D., Radü, E. W., … Haller, S. (2015). Altered cerebrovascular reactivity velocity in mild cognitive impairment and Alzheimer's disease. *Neurobiology of Aging*, *36*(1), 33–41. http://doi.org/10.1016/j.neurobiolaging.2014.07.020

Robertson, A. D., Crane, D. E., Rajab, A. S., Swardfager, W., Marzolini, S., & Shirzadi, Z. (2015). Exercise intensity modulates the change in cerebral blood flow following aerobic exercise in chronic stroke. *Experimental Brain Research*, *233*(8), 2467–2475. http://doi.org/10.1007/s00221-015-4317-6

Roque, F. R., Hernanz, R., Salaices, M., & Briones, A. M. (2013). Exercise training and cardiometabolic diseases: Focus on the vascular system. *Current Hypertension Reports*, *15*(3), 204–214. http://doi.org/10.1007/s11906-013-0336-5

Saba, L. (Ed.). (2016). *Image Principles, Neck, and the Brain*. CRC Press.

Sagi, Y., Tavor, I., Hofstetter, S., Tzur-moryosef, S., Blumenfeld-katzir, T., & Assaf, Y. (2012). Article Learning in the Fast Lane : New Insights into Neuroplasticity, 1195–1203. http://doi.org/10.1016/j.neuron.2012.01.025

Sakata, J. T., Crews, D., & Gonzalez-lima, F. (2005). Behavioral correlates of differences in neural metabolic capacity, *48*, 1–15. http://doi.org/10.1016/j.brainresrev.2004.07.017

Sami, S., & Miall, R. C. (2013). Graph network analysis of immediate motor-learning induced changes in resting state BOLD. *Frontiers in Human Neuroscience*, *7*(May), 166. http://doi.org/10.3389/fnhum.2013.00166

Sami, S., Robertson, E. M., & Miall, R. C. (2014). The Time Course of Task-Specific Memory Consolidation Effects in Resting State Networks, *34*(11), 3982–3992. http://doi.org/10.1523/JNEUROSCI.4341-13.2014

Schmidt, S., & Wonneberger, M. (2014). Long-term endurance exercise improves aerobic capacity in patients with relapsing-remitting multiple sclerosis: impact of baseline

fatigue. *Journal of the Neurological Sciences*, *336*(1–2), 29–35. http://doi.org/10.1016/j.jns.2013.09.035

Schmithorst, V. J., Hernandez-Garcia, L., Vannest, J., Rajagopal, A., Lee, G., & Holland, S. K. (2014). Optimized simultaneous ASL and BOLD functional imaging of the whole brain. *Journal of Magnetic Resonance Imaging*, *39*(5), 1104-1117.

Seitz, R. J., & Roland, P. E. (1991). Learning of Sequential Finger Movements in Man : A Combined Kinematic and Positron Emission Tomography (PET) Study, *4*(May), 154–165.

Shannon, B. J., Neil, S., Vlassenko, A. G., Shimony, J. S., & Rutlin, J. (2016). Brain aerobic glycolysis and motor adaptation learning, (26), 1–10. http://doi.org/10.1073/pnas.1604977113

Singh, M., Kim, S., & Kim, T. (2003). Correlation Between BOLD-fMRI and EEG Signal Changes in Response to Visual Stimulus Frequency in Humans, *114*, 108–114. http://doi.org/10.1002/mrm.10335

Smetcoren, S., Deroost, N., Smetcoren, S., Vandenbossche, J., & Hooghe, M. D. (2014). Implicit and Explicit Learning of Sequential Motor Skill in Multiple Sclerosis : Directions for Rehabilitation Implicit And Explicit Learning of Sequential Motor Skill in Multiple Sclerosis : Directions for Rehabilitation, (July). http://doi.org/10.17653/2374-9091.SS0001

Smith, J. C., Paulson, E. S., Cook, D. B., Verber, M. D., & Tian, Q. (2010). Detecting changes in human cerebral blood flow after acute exercise using arterial spin labeling : Implications for fMRI, *191*, 258–262. http://doi.org/10.1016/j.jneumeth.2010.06.028

Smith, S., & Brady, J. (1997). SUSAN—a new approach to low level image processing. *International Journal of Computer Vision*, *23*(1), 45–78. http://doi.org/10.1023/A:1007963824710

Smith, S. M. (2002). Fast Robust Automated Brain Extraction, *155*, 143–155. http://doi.org/10.1002/hbm.10062

Smith, S. M., & Nichols, T. E. (2009a). Threshold-free cluster enhancement : Addressing problems of smoothing , threshold dependence and localisation in cluster inference. *NeuroImage*, *44*(1), 83–98. http://doi.org/10.1016/j.neuroimage.2008.03.061

Smith, S. M., & Nichols, T. E. (2009b). Threshold-free cluster enhancement: Addressing problems of smoothing, threshold dependence and localisation in cluster inference. *NeuroImage*, *44*(1), 83–98. http://doi.org/10.1016/j.neuroimage.2008.03.061

Sperling, R., Dickerson, B., Pihlajamaki, M., Vannini, P., LaViolette, P., Vitolo, O., … Johnson, K. (2010). Functional alterations in memory networks in early Alzheimer's disease. *Neuromolecular Med*, *12*(1), 27–43. http://doi.org/10.1007/s12017-009-8109-7.Functional

Stampfer, M. J. (2006). Cardiovascular disease and Alzheimer's disease: Common links. *Journal of Internal Medicine*, *260*(3), 211–223. http://doi.org/10.1111/j.1365-2796.2006.01687.x

Storer, T. W., Davis, J. A., & Caiozzo, V. J. (1990). Accurate prediction of VO2max in cycle ergometry. *Medicine and Science in Sports and Exercise*, *22*(5), 704-712.Stroth, S., Hille, K., Spitzer, M., & Reinhardt, R. (2016). Aerobic endurance exercise benefits memory and affect in young adults, *2011*(September). http://doi.org/10.1080/09602010802091183

Swain, R. ., Harris, a. ., Wiener, E. ., Dutka, M. ., Morris, H. ., Theien, B. ., … Greenough, W. . (2003). Prolonged exercise induces angiogenesis and increases cerebral blood volume in primary motor cortex of the rat. *Neuroscience*, *117*(4), 1037–1046. http://doi.org/10.1016/S0306-4522(02)00664-4

Swain, R. A., Harris, A. B., Wiener, E. C., Dutka, M. V., Morris, H. D., Theien, B. E., … Greenough, W. T. (2003). Prolonged exercise induces angiogenesis and increases cerebral blood volume in primary motor cortex of the rat. *Neuroscience*, *117*(4), 1037–1046. http://doi.org/10.1016/S0306-4522(02)00664-4

Tacchino, A., Bove, M., Roccatagliata, L., Luigi, G., Uccelli, A., & Bonzano, L. (2014). Selective impairments of motor sequence learning in multiple sclerosis patients with minimal disability. *Brain Research*, *1585*, 91–98. http://doi.org/10.1016/j.brainres.2014.08.031

Tanaka, H., Dinenno, F. A., Monahan, K. D., Clevenger, C. M., DeSouza, C. A., & Seals, D. R. (2000). Aging, habitual exercise, and dynamic arterial compliance. *Circulation*, *102*(11), 1270–1275. http://doi.org/10.1161/01.CIR.102.11.1270

Tancredi, F. B., Gauthier, C. J., Bolar, D. S., Fisher, J. A., Wang, D. J. J., & Hoge, R. D. (2012). Comparison of Pulsed and Pseudocontinuous Arterial Spin-Labeling for Measuring CO 2 - Induced Cerebrovascular Reactivity, *0*, 1–10. http://doi.org/10.1002/jmri.23658

Tancredi, F. B., & Hoge, R. D. (2013). Comparison of cerebral vascular reactivity measures obtained using breath-holding and CO2 inhalation. *Journal of Cerebral Blood Flow and Metabolism : Official Journal of the International Society of Cerebral Blood Flow and Metabolism*, *33*(7), 1066–74. http://doi.org/10.1038/jcbfm.2013.48

Tancredi, F. B., Lajoie, I., & Hoge, R. D. (2014). A simple breathing circuit allowing precise control of inspiratory gases for experimental respiratory manipulations. *BMC Research Notes*, *7*(1), 235. http://doi.org/10.1186/1756-0500-7-235

Themanson, J. R., Pontifex, M. B., & Hillman, C. H. (2008). Fitness and action monitoring: evidence for improved cognitive flexibility in young adults. *Neuroscience*, *157*(2), 319-328.

Thomas, A. G., Dennis, A., Rawlings, N. B., Stagg, C. J., Matthews, L., Morris, M., … Johansen-Berg, H. (2015). Multi-modal characterization of rapid anterior hippocampal volume increase associated with aerobic exercise. *NeuroImage*, *i*. http://doi.org/10.1016/j.neuroimage.2015.10.090

Thomas, B. P., Yezhuvath, U. S., Tseng, B. Y., Liu, P., Levine, B. D., Zhang, R., & Lu, H. (2013). Life-long aerobic exercise preserved baseline cerebral blood flow but reduced vascular reactivity to CO2. *Journal of Magnetic Resonance Imaging : JMRI*, *38*(5), 1177–83. http://doi.org/10.1002/jmri.24090

Thomas, D. L., Lythgoe, M. F., Calamante, F., Gadian, D. G., & Ordidge, R. J. (2001). Simultaneous noninvasive measurement of CBF and CBV using double-echo FAIR (DEFAIR). *Magnetic Resonance in Medicine : Official Journal of the Society of Magnetic Resonance in Medicine / Society of Magnetic Resonance in Medicine*, *45*(5), 853–63. Retrieved from http://www.ncbi.nlm.nih.gov/pubmed/11323812

Thompson, A. J., & Miller, D. H. (2004). Abnormalities of cerebral perfusion in multiple sclerosis, 1288–1294. http://doi.org/10.1136/jnnp.2003.026021

Tomassini, V., Ambrosio, A., Petsas, N., Wise, R. G., Sbardella, E., Allen, M., … Pozzilli, C. (2016).

The Effect of Inflammation and Its Reduction on Brain Plasticity in Multiple Sclerosis : MRI Evidence, *0*(September 2015). http://doi.org/10.1002/hbm.23184

Tomassini, V., d'Ambrosio, A., Petsas, N., Wise, R. G., Sbardella, E., Allen, M., … Pozzilli, C. (2016). The effect of inflammation and its reduction on brain plasticity in multiple sclerosis: MRI evidence. *Human Brain Mapping*, *0*(September 2015), n/a-n/a. http://doi.org/10.1002/hbm.23184

Tomassini, V., Johansen-Berg, H., Jbabdi, S., Wise, R. G., Pozzilli, C., Palace, J., & Matthews, P. M. (2012). Relating Brain Damage to Brain Plasticity in Patients With Multiple Sclerosis. *Neurorehabilitation and Neural Repair*, *26*(6), 581–593. http://doi.org/10.1177/1545968311433208.Relating

Tomassini, V., Matthews, P. M., Thompson, A. J., Fuglø, D., Geurts, J. J., Johansen-Berg, H., … Palace, J. (2012). Neuroplasticity and functional recovery in multiple sclerosis. *Nature Publishing Group*, *8*(11), 635–646. http://doi.org/10.1038/nrneurol.2012.179

Turner, R. (2002). How Much Cortex Can a Vein Drain ? Downstream Dilution of Activation-Related Cerebral Blood Oxygenation Changes, *1067*, 1062–1067. http://doi.org/10.1006/nimg.2002.1082

Tuunanen, P. I., & Kauppinen, R. A. (2006). Effects of oxygen saturation on BOLD and arterial spin labelling perfusion fMRI signals studied in a motor activation task. *NeuroImage*, *30*(1), 102–109. http://doi.org/10.1016/j.neuroimage.2005.09.021

Ugurbil, K. (2016). What is feasible with imaging human brain function and connectivity using functional magnetic resonance imaging.

Uludag, K., Dubowitz, D. J., Yoder, E. J., Restom, K., Liu, T. T., & Buxton, R. B. (2004). {C}oupling of cerebral blood flow and oxygen consumption during physiological activation and deactivation measured with f{MRI}. *Neuroimage*, *23*(1), 148–155. http://doi.org/10.1016/j.neuroimage.2004.05.013

Ungerleider, L., Doyon, J., & Karni, A. (2002). Imaging brain plasticity during motor skill learning. *Neurobiol Learn Mem*, *78*, 553–564. http://doi.org/10.1006/nlme.2002.4091

Vafaee, M. S., & Gjedde, A. (2000). Model of blood–brain transfer of oxygen explains nonlinear flow-metabolism coupling during stimulation of visual cortex. *Journal of Cerebral Blood Flow & Metabolism*, *20*(4), 747-754.

Vallance, P., & Hingorani, A. (1999). Endothelial nitric oxide in humans in health and disease. *International Journal of Experimental Pathology*, *80*(6), 291–303. Retrieved from http://www.ncbi.nlm.nih.gov/pubmed/10632779%5Cnhttp://www.pubmedcentral.nih.gov/articlerender.fcgi?artid=PMC2517837

van Praag, H., Kempermann, G., & Gage, F. H. (1999). Running increases cell proliferation and neurogenesis in the adult mouse dentate gyrus. *Nature Neuroscience*, *2*(3), 266–270. http://doi.org/10.1038/6368

Vanzetta, I. (1999). Increased Cortical Oxidative Metabolism Due to Sensory Stimulation: Implications for Functional Brain Imaging. *Science*, *286*(5444), 1555–1558. http://doi.org/10.1126/science.286.5444.1555

Vaquero, J. M. M., Jim??nez, L., & Lupi????ez, J. (2006). The problem of reversals in assessing implicit sequence learning with serial reaction time tasks. *Experimental Brain Research*, *175*(1), 97–109. http://doi.org/10.1007/s00221-006-0523-6

Vernadakis, A. (1996). Glia-neuron intercommunications and synaptic plasticity. *Progress in neurobiology*, *49*(3), 185-214.

Viviani, R., Messina, I., & Walter, M. (2011). Resting state functional connectivity in perfusion imaging: correlation maps with BOLD connectivity and resting state perfusion. *PloS One*, *6*(11), e27050. http://doi.org/10.1371/journal.pone.0027050

Voss, M. W., Chaddock, L., Kim, J. S., Vanpatter, M., Matthew, B., Raine, L. B., … Kramer, A. F. (2012). NIH Public Access, 166–176. http://doi.org/10.1016/j.neuroscience.2011.10.009.Aerobic

Voss, M. W., Nagamatsu, L. S., Liu-ambrose, T., Arthur, F., Fedewa, A. L., Ahn, S., … Kramer, A. F. (2015). Exercise , brain , and cognition across the life span adults, (April 2011), 1505–1513. http://doi.org/10.1152/japplphysiol.00210.2011

Voss, M. W., Vivar, C., Kramer, A. F., & van Praag, H. (2013). Bridging animal and human models of exercise-induced brain plasticity. *Trends in Cognitive Sciences*, *17*(10), 525–44. http://doi.org/10.1016/j.tics.2013.08.001

Voss, W., Vanpatter, M., Pontifex, M. B., Raine, L. B., & Konkel, A. (2014). NIH Public Access, 172–183. http://doi.org/10.1016/j.brainres.2010.08.049.A

Walther, C., Gielen, S., & Hambrecht, R. (2004). The Effect of Exercise Training on Endothelial Function in Cardiovascular Disease in Humans, (2), 129–134.

Wang, J., Aguirre, G. K., Kimberg, D. Y., Roc, A. C., Li, L., & Detre, J. A. (2003). Arterial Spin Labeling Perfusion fMRI With Very Low Task Frequency, *802*, 796–802. http://doi.org/10.1002/mrm.10437

Wang, J., Qiu, M., & Constable, R. T. (2005). In vivo method for correcting transmit/receive nonuniformities with phased array coils. *Magnetic Resonance in Medicine*, *53*(3), 666–674. http://doi.org/10.1002/mrm.20377

Wang, J., Zhang, Y., Wolf, R. L., Roc, A. C., Alsop, D. C., & Detre, J. A. (2005). Radiology Perfusion MR Imaging with a Single Coil : Feasibility.

Warnert, E. A., Rodrigues, J. C., Burchell, A. E., Neumann, S., Ratcliffe, L. E., Manghat, N. E., ... & Paton, J. F. (2016). Is high blood pressure self-protection for the brain?. *Circulation research*, CIRCRESAHA-116.

Warnert, E. A. H., Harris, A. D., Murphy, K., Saxena, N., Tailor, N., Jenkins, N. S., … Wise, R. G. (2014). In vivo assessment of human brainstem cerebrovascular function : a multi-inversion time pulsed arterial spin labelling study, *34*(6), 956–963. http://doi.org/10.1038/jcbfm.2014.39

Warnert, E. a H., Harris, A. D., Murphy, K., Saxena, N., Tailor, N., Jenkins, N. S., … Wise, R. G. (2014). In vivo assessment of human brainstem cerebrovascular function: A multi-inversion time pulsed arterial spin labelling study. *Journal of Cerebral Blood Flow and Metabolism*, *34*(6), 956–963. http://doi.org/10.1038/jcbfm.2014.39

White, F. C., Bloor, C. M., Mckirnan, M. D., Carroll, S. M., Behnke, B. J., Ramsey, M. W., … Francis, C. (2014). Exercise training in swine promotes growth of arteriolar bed and capillary angiogenesis in heart morphology molecular mechanisms Exercise training in swine promotes growth of arteriolar bed and capillary angiogenesis in heart. *Journal of Applied Physiology*, *1*, 1160–1168.

Whittaker, J. R., Driver, I. D., Bright, M. G., & Murphy, K. (2015). The absolute CBF response to activation is preserved during elevated perfusion: Implications for neurovascular coupling measures. *NeuroImage*, *125*, 198–207. http://doi.org/10.1016/j.neuroimage.2015.10.023

Wilkinson, M., Leedale-brown, D., & Winter, E. M. (2009). Validity of a Squash-Specific Fitness Test, *4*, 29–40.

Williams, D. S., Detre, J. A., Leigh, J. S., & Koretsky, A. P. (1992). Magnetic resonance imaging of perfusion using spin inversion of arterial water. *Proceedings of the National Academy of Sciences*, *89*(1), 212-216.Williams, V. J., Hayes, J. P., Forman, D. E., Salat, D. H., Sperling, R. A., Verfaellie, M., & Hayes, S. M. (2017). NeuroImage Cardiorespiratory fi tness is differentially associated with cortical thickness in young and older adults, *146*(July 2016), 1084–1092. http://doi.org/10.1016/j.neuroimage.2016.10.033

Winkler, A. M., Ridgway, G. R., Webster, M. A., Smith, S. M., & Nichols, T. E. (2014). NeuroImage Permutation inference for the general linear model. *NeuroImage*, *92*, 381–397. http://doi.org/10.1016/j.neuroimage.2014.01.060

Wise, R. G., Harris, A. D., Stone, A. J., & Murphy, K. (2013a). Measurement of OEF and absolute CMRO2: MRI-based methods using interleaved and combined hypercapnia and hyperoxia. *NeuroImage*, *83*(0), 135–147. http://doi.org/10.1016/j.neuroimage.2013.06.008

Wise, R. G., Harris, A. D., Stone, A. J., & Murphy, K. (2013b). Measurement of OEF and absolute CMRO2: MRI-based methods using interleaved and combined hypercapnia and hyperoxia. *NeuroImage*, *83*, 135–47. http://doi.org/10.1016/j.neuroimage.2013.06.008

Wise, R. G., Harris, A. D., Stone, A. J., & Murphy, K. (2013c). Measurement of OEF and absolute CMRO2: MRI-based methods using interleaved and combined hypercapnia and hyperoxia. *NeuroImage*, *83*, 135–47. http://doi.org/10.1016/j.neuroimage.2013.06.008

Wise, R. G., Ide, K., Poulin, M. J., & Tracey, I. (2004). Resting fluctuations in arterial carbon dioxide induce significant low frequency variations in BOLD signal. *NeuroImage*, *21*(4), 1652–1664. http://doi.org/10.1016/j.neuroimage.2003.11.025

Wise, R. G., & Tracey, I. (2006). The role of fMRI in drug discovery. *Journal of Magnetic Resonance Imaging*, *23*(6), 862–876. http://doi.org/10.1002/jmri.20584

Wittenberg, J. B., & Wittenberg, B. A. (2007). Myoglobin-enhanced oxygen delivery to isolated cardiac mitochondria, 2082–2090. http://doi.org/10.1242/jeb.003947

Wong, E. C. (2014). An Introduction to ASL Labeling Techniques, *10*, 1–10. http://doi.org/10.1002/jmri.24565

Wong, E. C., Buxton, R. B., & Frank, L. R. (1998). Quantitative imaging of perfusion using a single subtraction (QUIPSS and QUIPSS II). *Magnetic Resonance in Medicine*, *39*(5), 702–708. http://doi.org/10.1002/mrm.1910390506

Xiong, J., Ma, L., Wang, B., Narayana, S., Duff, E. P., Egan, G. F., & Fox, P. T. (2009). NeuroImage Long-term motor training induced changes in regional cerebral blood flow in both task and resting states. *NeuroImage*, *45*(1), 75–82. http://doi.org/10.1016/j.neuroimage.2008.11.016

Xu, F., Ge, Y., & Lu, H. (2009). Non-invasive quantification of whole-brain cerebral metabolic rate of oxygen by MRI. *Magn Reson Med*, *62*(1), 141–148.

http://doi.org/10.1002/mrm.21994.Non-invasive

Xu, F., Uh, J., Brier, M. R., Hart Jr., J., Yezhuvath, U. S., Gu, H., … Lu, H. (2011). The influence of carbon dioxide on brain activity and metabolism in conscious humans. *J Cereb Blood Flow Metab*, *31*(1), 58–67. http://doi.org/jcbfm2010153 [pii]\r10.1038/jcbfm.2010.153

Xu, G., Rowley, H. A., Wu, G., Alsop, D. C., Dowling, M., Christian, B. T., … Hospital, M. V. A. (2011). NIH Public Access, *23*(3), 286–293. http://doi.org/10.1002/nbm.1462.Reliability

Yamada, K., Mizuno, M., & Nabeshima, T. (2002). Role for brain-derived neurotrophic factor in learning and memory. *Life Sciences*, *70*(7), 735–744. http://doi.org/10.1016/S0024-3205(01)01461-8

Yan, L., Li, C., Kilroy, E., Wehrli, F. W., & Wang, D. J. J. (2012). Quantification of arterial cerebral blood volume using multiphase-balanced SSFP-based ASL. *Magnetic Resonance in Medicine*, *68*(1), 130–139. http://doi.org/10.1002/mrm.23218

Yirmiya, R., & Goshen, I. (2011). Immune modulation of learning, memory, neural plasticity and neurogenesis. *Brain, Behavior, and Immunity*, *25*(2), 181–213. http://doi.org/10.1016/j.bbi.2010.10.015

Young, W. L., Prohovnik, I., Ornstein, E., Ostapkovich, N., & Matteo, R. S. (1991). Cerebral Blood Flow Reactivity to Changes in Carbon Dioxide Calculated Using End-Tidal versus Arterial Tensions. *Journal of Cerebral Blood Flow & Metabolism*, *11*(6), 1031–1035. http://doi.org/10.1038/jcbfm.1991.171

Yu, X., & Koretsky, A. P. (2014). Interhemispheric plasticity protects the deafferented somatosensory cortex from functional takeover after nerve injury. *Brain Connectivity*, *4*(9), 709–17. http://doi.org/10.1089/brain.2014.0259

Zeller, D., & Classen, J. (2014). Plasticity of the motor system in multiple sclerosis. *Neuroscience*, *283C*, 222–230. http://doi.org/10.1016/j.neuroscience.2014.05.043

Zheng, Y., Martindale, J., Johnston, D., Jones, M., Berwick, J., & Mayhew, J. (2002). A Model of the Hemodynamic Response and Oxygen Delivery to Brain, *637*, 617–637. http://doi.org/10.1006/nimg.2002.1078

Zhu, Y. S., Tarumi, T., Tseng, B. Y., Palmer, D. M., Levine, B. D., & Zhang, R. (2013). Cerebral vasomotor reactivity during hypo- and hypercapnia in sedentary elderly and Masters athletes. *Journal of Cerebral Blood Flow and Metabolism*, *33*(8), 1190–1196. http://doi.org/DOI 10.1038/jcbfm.2013.66

Zimmerman, B., Bradley, P., Low, K. A., Fletcher, M. A., Tan, C. H., Schneider-garces, N., … Fabiani, M. (2014). Cardiorespiratory fitness mediates the effects of aging on cerebral blood flow, *6*(April), 1–13. http://doi.org/10.3389/fnagi.2014.00059